

EMPLACEMENT OF RADIAL PYROCLASTIC DENSITY  
CURRENTS OVER IRREGULAR TOPOGRAPHY: THE  
CHEMICALLY-ZONED, LOW ASPECT-RATIO GREEN  
TUFF IGNIMBRITE, PANTELLERIA, ITALY.

Thesis submitted for the degree of  
Doctor of Philosophy  
at the University of Leicester

by  
Rebecca Williams BSc (London) MS (Buffalo)  
Department of Geology  
University of Leicester  
September 2010

---

# Emplacement of radial pyroclastic density currents over irregular topography: the chemically-zoned, low aspect-ratio Green Tuff ignimbrite, Pantelleria, Italy.

---

Rebecca Williams

Low aspect-ratio ignimbrites are thought to be emplaced by particularly hazardous, radial, high-velocity pyroclastic density currents from caldera-forming eruptions. Their circular distribution has been inferred to record simultaneous flow in all directions from source, overtopping hills, rather than passively flowing down valleys. This study aims to understand how such currents behave and evolve during an eruption by mapping out the internal chemical-architecture of a zoned, low-aspect ratio ignimbrite sheet on the island of Pantelleria, Italy. The pristine, welded Green Tuff Formation (aspect ratio  $>1:1,000$ ) was deposited during the most recent (c. 50 ka) explosive eruption on the island. The extensive flow-unit is zoned from pantellerite to trachyte, recording changes in the composition of the erupting magma with time. Detailed logging with very close-spaced sampling for chemical and petrographic analysis has distinguished an internal chemical stratigraphy that allows the brief history of the sustained current to be divided into successive time-periods. The compositional zones have been mapped around the island enabling the reconstruction of how the footprint of the sustained current shifted during the eruption as the current waxed and then waned. Furthermore, the mapped compositional zones can be used to assess how the current and its resultant deposit encountered and overtopped barriers, such as cone-shaped hills and transverse ridges. This study has revealed that the ignimbrite was not emplaced entirely radially: rather, it flowed into certain sectors before others, and that the leading edge of the current advanced and then retreated, and shifted laterally with time. Deposition was diachronous, and previously proposed lithofacies correlations within the ignimbrite are demonstrated to be incorrect. As the pyroclastic density current encroached upon topographic barriers, it was initially blocked, reflected, or deflected around the lower flanks of the barrier. As the mass-flux of the eruption increased, the current waxed and was progressively able to overtop topographic barriers.

I would like to thank Mike Branney, Tiffany Barry and Mike Norry, for conceiving the project and supervising the research. Thanks go to Mike and Tiff for the support and suggestions throughout the project. In particular, thank you to Norry for the common room chats about my geochemically weird rocks and phenocrysts. I would also like to thank Prof. Tim Druitt and Prof. Andy Saunders for stimulating discussions and suggestions which significantly improved the final version of the thesis

This project was funded by NERC (NER/S/A/2006/14156). Further funding for fieldwork, geochemical analysis, training and conference attendance was provided by the Volcanic and Magmatic Studies Group; the British Sedimentological Research Group; the Department of Geology, Leicester; the Mineralogical Society; International Association of Volcanology and Chemistry of the Earth's Interior; The International Union of Geodesy and Geophysics; Geological Society of London; Shell and Leicester Literary and Philosophical Society.

Without the help of the following people, the analytical side of this research would not have been possible: Rob Wilson (EMPA); Rob Kelly and Nick Marsh (XRF); and Sam Hammond (LA ICP MS). Further thanks to the Open University for use of their LA ICP MS. Also, thank you to Natalie Turner for all her help during the summer of 2009.

Fieldwork was made a lot easier and more sociable thanks to a plethora of field assistants and geology tourists. Namely, Richard Walker, Joanne Tudge, Adam Stinton, Mike McCurry, Rhys Langford, Leanne Gunn, Sally Smith, and Chris McDonald (the last three deserve extra thanks for phenomenal help with the rock preparation). Further thanks to all the people on Pantelleria who looked out for me and were kind enough to feed me some of the best food I've ever tasted: Laura Viviano & Benedetto Barone who I am indebted to for their hospitality; Linda & Salvatore; and Theresa & Gaspare.

Leicester has been a great place to do a PhD and thanks are due to all the academic, technical and administrative staff. Special thanks to all my fellow PhD students, past and present that have made the last four years incredibly enjoyable. A special shout-out goes to the ex-residents of Office G3: Alex, Pete and Nick. You've been awesome. Honourable mentions to Ben (advice and inspiration), Dan (gigs), Steve (robot dancing), Pablo (freehand), Simon (geochemical chatter), Andy (forever chirpy), Jawad and Mohib (pakoras), Steve (GIS), Dave & Xiaoya (for putting up with me at Bonchurch), Carys (Lazy Sunday Coffee), Rowan, Dinah, Chris, Rob S and anyone else

I've probably forgotten. A big thank you goes to Louise Anderson (cocktails) and Graham Andrews (endless advice and rheomorphism talk).

To friends of old, in particular Imogen (brownies), Ivvet, Melissa, Anna and Rosie: I thank you for always being there when I find the time to not be a geologist. To all the residents of 142 Howard Road for a brilliant first two years, especially Claire and Rebecca for their constant supply of cheese and Turkish takeaway.

A special mention goes out to Sam Cheyney, for extraordinary help, unwavering support and encouragement in the eleventh hour

Finally, but most importantly, I'd like to thank my extended family. Without you, with your constant support, encouragement and belief that I could do it, I couldn't have actually done it. Especially to Dad, Mum, and also to Melanie & Darren, Michael, and Daniel & Nicole. To my niece Isobel, and nephews Ryan & Keiran, and Harry for being adorable.

Thank you.

<b>1.</b>	<b>INTRODUCTION .....</b>	<b>1</b>
1.1.	METHODS OF STUDY.....	1
1.2.	AIMS OF PROJECT.....	2
1.3.	THESIS OUTLINE AND OBJECTIVES .....	2
1.4.	REGIONAL GEOLOGY .....	4
1.4.1.	<i>Pantelleria tectonic setting .....</i>	<i>4</i>
1.4.2.	<i>Petrogenesis.....</i>	<i>4</i>
1.5.	PANTELLERIA VOLCANIC EVOLUTION.....	8
1.5.3.	<i>Post-Green Tuff Stratigraphy .....</i>	<i>9</i>
1.5.4.	<i>Pre-Green Tuff Stratigraphy.....</i>	<i>10</i>
<b>2.</b>	<b>THE PHYSICAL VOLCANOLOGY OF THE GREEN TUFF FORMATION: A LITHOFACIES-BASED APPROACH .....</b>	<b>12</b>
2.1.	ABSTRACT .....	12
2.2.	INTRODUCTION .....	14
2.2.1.	<i>Previous work.....</i>	<i>14</i>
2.2.2.	<i>Pyroclastic density currents and the emplacement of ignimbrites .....</i>	<i>18</i>
2.2.3.	<i>Welding and rheomorphism in ignimbrites.....</i>	<i>24</i>
2.2.4.	<i>Terminology .....</i>	<i>28</i>
2.3.	LITHOFACIES OF THE GREEN TUFF FORMATION .....	30
2.3.1.	<i>Massive pumice-lapilli (mpl).....</i>	<i>30</i>
2.3.2.	<i>Cross-stratified pumice-lapilli (xspl) .....</i>	<i>33</i>
2.3.3.	<i>Massive ash (mT) .....</i>	<i>38</i>
2.3.4.	<i>Massive lapilli-tuff (mLT and emLT).....</i>	<i>40</i>
2.3.5.	<i>Diffuse stratified and cross-stratified lapilli-tuff (dsLT and dxsLT).....</i>	<i>42</i>
2.3.6.	<i>Parallel-bedded eutaxitic lapilli-tuff (/beLT).....</i>	<i>42</i>
2.3.7.	<i>Rheomorphic massive lapilli-tuff (rheomLT) .....</i>	<i>46</i>
2.3.8.	<i>Lithic breccia (lBr).....</i>	<i>48</i>
2.4.	WELDING AND RHEOMORPHISM OF THE GREEN TUFF FORMATION .....	50
2.4.1.	<i>Vitrophyres.....</i>	<i>51</i>
2.4.2.	<i>Fiamme and vesicles .....</i>	<i>53</i>
2.4.3.	<i>Lineations and foliation.....</i>	<i>54</i>
2.4.4.	<i>Folding.....</i>	<i>57</i>
2.4.5.	<i>Flow structures.....</i>	<i>58</i>
2.4.6.	<i>Post-depositional features .....</i>	<i>61</i>
2.4.7.	<i>Geochemical causes of welding in the Green Tuff Formation .....</i>	<i>63</i>
2.5.	LATERAL VARIATION .....	64

2.6.	AREAL EXTENT AND ASPECT RATIO .....	64
2.7.	GRANULOMETRY .....	66
2.8.	PHENOCRYSTS .....	67
2.9.	DISCUSSION.....	68
2.9.1.	<i>Overview of the Green Tuff Formation</i> .....	68
2.9.2.	<i>The eruption history of the Green Tuff Formation</i> .....	71
2.10.	CONCLUSIONS.....	73
<b>3.</b>	<b>THE CHEMICAL STRATIGRAPHY OF THE GREEN TUFF FORMATION: EVIDENCE FOR PROGRESSIVE TAPPING OF A SINGLE, ZONED MAGMA CHAMBER .....</b>	<b>74</b>
3.1.	ABSTRACT .....	74
3.2.	INTRODUCTION .....	74
3.2.1.	<i>Aims and objectives</i> .....	75
3.2.2.	<i>Methods</i> .....	75
3.3.	RESULTS: CHEMICAL STRATIGRAPHY OF THE GREEN TUFF TYPE SECTION .....	80
3.3.1.	<i>Trends in major elements</i> .....	80
3.3.2.	<i>Trends in trace elements and rare earth elements</i> .....	84
3.3.3.	<i>Trends in Phenocrysts</i> .....	89
3.3.4.	<i>Oxygen isotope results</i> .....	95
3.4.	DISCUSSION.....	95
3.4.1.	<i>Chemically zoned ignimbrites</i> .....	95
3.4.2.	<i>Withdrawal mechanisms for zoned magma chambers</i> .....	97
3.4.3.	<i>A zoned magma chamber</i> .....	102
3.5.	CONCLUSIONS.....	102
<b>4.</b>	<b>HOW PYROCLASTIC DENSITY CURRENTS EVOLVE WITH TIME AND SPACE I: DIACHRONOUS EMPLACEMENT OF A THIN, CIRCULAR IGNIMBRITE SHEET .....</b>	<b>105</b>
4.1.	ABSTRACT .....	105
4.2.	INTRODUCTION .....	106
4.2.1.	<i>Radial, low-aspect ratio pyroclastic density currents</i> .....	106
4.2.2.	<i>Entrachrons and their use in reconstructing ignimbrite emplacement</i> .....	107
4.2.3.	<i>Aims and hypothesis</i> .....	108
4.2.4.	<i>Methods</i> .....	109
4.3.	RESULTS AND INTERPRETATION .....	112
4.3.1.	<i>The current reconstructed through time (t)</i> .....	113
4.4.	DISCUSSION.....	115

4.4.1.	<i>Assumptions and potential problems</i> .....	115
4.4.2.	<i>Diachronous emplacement of the ignimbrite sheet</i> .....	118
4.4.3.	<i>Radial flow during times of peak flow</i> .....	118
4.4.4.	<i>Lateral shingling</i> .....	118
4.4.5.	<i>Implications for mass flux</i> .....	119
4.4.6.	<i>Lithofacies correlations as time-markers</i> .....	120
4.4.7.	<i>Possible causes of asymmetric flow</i> .....	121
4.5.	CONCLUSIONS.....	123
<b>5.</b>	<b>HOW SUSTAINED PYROCLASTIC DENSITY CURRENTS EVOLVE WITH TIME AND SPACE II: BEHAVIOR AT TOPOGRAPHIC BARRIERS</b> .....	<b>125</b>
5.1.	ABSTRACT.....	125
5.2.	INTRODUCTION.....	125
5.2.1.	<i>Previous work on density currents and topography</i> .....	126
5.2.2.	<i>Aims</i> .....	128
5.2.3.	<i>Methods</i> .....	129
5.3.	RESULTS AND INTERPRETATIONS.....	132
5.3.1.	<i>Interaction with cones</i> .....	132
5.3.2.	<i>Interaction with transverse ridges</i> .....	143
5.3.3.	<i>Interaction with palaeovalleys</i> .....	147
5.4.	DISCUSSION.....	149
5.4.1.	<i>Progressive inundation of topographic barriers</i> .....	149
5.4.2.	<i>Blocking, deflection and reflection of the current</i> .....	149
5.4.3.	<i>Implications for mass flux</i> .....	150
5.4.4.	<i>Formation of a caldera during the Green Tuff eruption</i> .....	151
5.4.5.	<i>Assumptions and potential problems</i> .....	160
5.5.	CONCLUSIONS.....	161
<b>6.</b>	<b>STRATIGRAPHY OF THE PRE-GREEN TUFF WELDED IGNIMBRITES OF NE PANTELLERIA</b> .....	<b>162</b>
6.1.	ABSTRACT.....	162
6.2.	INTRODUCTION.....	162
6.2.1.	<i>Previous Work</i> .....	163
6.3.	IDENTIFICATION OF THREE ERUPTION-UNITS.....	164
6.3.1.	<i>Field data</i> .....	164
6.3.2.	<i>Chemical data</i> .....	173
6.4.	A REVISED STRATIGRAPHY FOR THE WELDED IGNIMBRITES OF PANTELLERIA, ITALY.....	173
6.4.1.	<i>Discussion and further work</i> .....	175

---



---

6.5.	CONCLUSION .....	178
<b>7.</b>	<b>CONCLUSIONS AND FURTHER WORK.....</b>	<b>180</b>
7.1.	THE GREEN TUFF FORMATION.....	180
7.2.	THE CHEMICAL STRATIGRAPHY OF THE GREEN TUFF FORMATION.....	181
7.2.1.	<i>Further work</i> .....	181
7.3.	INTERNAL MAPPING OF THE CHEMICAL STRATIGRAPHY OF THE GREEN TUFF IGNIMBRITE.....	182
7.3.1.	<i>Further work</i> .....	183
7.4.	THE ERUPTIVE HISTORY OF PANTELLERIA, ITALY.....	183
7.4.1.	<i>Further work</i> .....	184
	<b>APPENDIX INDEX .....</b>	<b>186</b>
	<b>APPENDIX I .....</b>	<b>187</b>
	<b>APPENDIX II .....</b>	<b>193</b>
	<b>REFERENCES .....</b>	<b>206</b>

# 1. Introduction

---

This study documents the Green Tuff Formation, Pantelleria, Straits of Sicily, Italy. It first focuses on the lithofacies and then the chemical stratigraphy of the deposit. The internal chemical stratigraphy of the Green Tuff ignimbrite is used to unravel the internal architecture of the deposit. This cryptic chemical architecture is then applied to understand the emplacement of the ignimbrite over irregular topography and the evolution of the density current which deposited it through time and space.

The Green Tuff Formation was chosen as a case study due to its excellently exposed outcrops, both longitudinally from source and also laterally around the vent. It is an excellent example for this type of investigation for a number of reasons. (1) The deposit consists of a basal sub-plinian pumice- and ash-fall and an overlying ignimbrite, which is a single flow unit. The ignimbrite is not compound, and represents a fluctuating quasi-steady current. (2) The deposit is welded almost entirely and the lack of a complex welding profile or internal vitrophyres supports the lithofacies interpretation that the ignimbrite is a single flow unit. (3) The viscous nature of the pyroclasts and their agglutination style of deposition mean that deposits were left on the entire landscape, including slopes up to 90°, which means that it is unlikely that the current was able to bypass significantly large areas without leaving evidence of its passing. (4) Most importantly, the Green Tuff ignimbrite shows linear, or gradational, chemical zoning

## 1.1. Methods of study

This study is the result of over 6 months of fieldwork on the island of Pantelleria, Italy and a variety of analytical methods. Field logging and mapping of the Green Tuff Formation documented the lateral, vertical and longitudinal variations of the ignimbrite. Field sketches and photographs documented the relationship of the Formation with the varied underlying topography. A detailed sampling campaign yielded over 400 samples for bulk rock X-ray fluorescence spectrometry analysis (XRF), which forms the basis of the chemical stratigraphy used throughout this thesis. A subset of these samples from the type section was analyzed by scanning electron microscope (SEM), electron microprobe (EMPA), laser ablation- inductively coupled plasma mass spectrometry

(LA-ICP-MS) and oxygen isotope analysis to reveal further details about the chemical stratigraphy. Details of the methodologies are discussed in the relevant chapters.

Dr. Mike Branney (University of Leicester), Dr. Mike Norry (University of Leicester) and Dr. Tiffany Barry (Open University) supervised this study.

## **1.2. Aims of project**

The objective of this project is to improve the understanding of how pyroclastic density currents evolve through time and space. Our understanding of density currents is hampered by the complete lack of any instrument or object that can withstand witnessing the emplacement of a large density current. So how are we to understand how they evolve through time and space, how they react to topography and changes in source dynamics? The internal architecture of deposits from catastrophic pyroclastic density currents must be understood to provide a temporal history of the current.

In this study, the aim is to study a low aspect-ratio ignimbrite, the product of a particularly hazardous form of pyroclastic density current that erupts radially at high velocity during caldera-forming eruptions. Using the pristine, welded Green Tuff ignimbrite on the island of Pantelleria, Italy, which is zoned from pantellerite at its base to trachyte at the top, chemical mapping of the internal architecture of the deposit enables reconstruction of how the current evolved in time and space. In particular, the study aims to answer the following questions.

- Were low-aspect ratio ignimbrites with circular distributions emplaced from currents that flowed radially, simultaneously in all directions from source?
- How do sustained pyroclastic density currents behave over topography?

## **1.3. Thesis outline and objectives**

Chapter 1 outlines the objectives of the thesis and the geological history of Pantelleria, Italy.

Chapter 2 is a field-based study of the Green Tuff Formation. The main objectives were: (1) to document the range of lithofacies; (2) to interpret the lithofacies based on a progressive aggradation and flow boundary approach; (3) to document the range of rheomorphic fabrics and structures; (4) to interpret the rheomorphism based on recent

advances in this area of volcanology and assess the use of rheomorphic fabrics as kinematic indicators; (5) to use the physical volcanology of the Formation to interpret eruption style and emplacement dynamics of the ignimbrite; and (6) to define a type section for the Green Tuff ignimbrite.

Chapter 3 is an analytical study of the type section of the Green Tuff ignimbrite, defined in Chapter 2. The main objective was to investigate in detail the internal geochemical zonation of the Green Tuff ignimbrite, previously inferred by Mahood & Hildreth (1983) from three bulk rock geochemical samples and a range of size and volume of feldspar crystals observed in outcrop (Mahood & Hildreth 1986). The aims were: (1) to define the type of chemical zonation (linear/gradational, reverse, or abruptly zoned); (2) to define a proxy for the chemical zonation that would be easy to analyze for the entire ignimbrite sheet; and (3) to use the chemical zonation to reveal details about the magma chamber.

The middle part of this thesis considers the major objective of this study, which is to understand the emplacement of low-aspect ratio ignimbrites and the evolution of the behavior of density currents during a sustained eruption. Chapter 4 investigates how the internal chemical stratigraphy of the ignimbrite can be applied to understand the emplacement of a circular, low aspect ratio ignimbrite. Was it emplaced by a radial pyroclastic density current? It tests theories on whether the leading edge of a current can advance, then retreat, during a sustained density current, and whether it can shift laterally with time. Chapter 5 investigates how a sustained pyroclastic density current is emplaced over topography. The chemical stratigraphy is combined with field mapping of kinematic indicators to elucidate information on how the current behaved as it encountered and encroached upon a variety of topographic barriers.

A short-communication paper based on Chapter 4 has been prepared for submission to *Nature* or *Geology* and is included in Appendix I.

Chapter 6 concerns the pre-Green Tuff Formation stratigraphy in the NE of Pantelleria. During field work on the Green Tuff Formation for this thesis, a pilot study reviewed previous stratigraphic correlations and interpretations on the pre-50 ka eruption history. This work is a combination of fieldwork and analytical studies by the author and two undergraduate Masters theses completed under co-supervision by the author (students

were Leanne Gunn and Sally Smith). A revised stratigraphy of the ignimbrite-forming eruptions from 140 ka to 50 ka is proposed.

Chapter 7 synthesizes the study of the Green Tuff Formation and what it reveals about the emplacement of low aspect-ratio ignimbrites and identifies areas of future work.

## **1.4. Regional Geology**

The island of Pantelleria is located in the Strait of Sicily (inset, Fig. 1-1) and lies approximately 70 km east of the coast of Tunisia. It is a volcanic island with an area of approximately 80 km<sup>2</sup> and lies on a drowned continental rift. Other volcanism associated with this rift system includes the small island of Linosa and Graham Bank, which has since been submerged below sea level (Mahood & Hildreth 1986). Pantelleria is the largest island in the system, with approximately half its height above sea level.

### **1.4.1. Pantelleria tectonic setting**

Pantelleria, Linosa and other submerged volcanic edifices all developed within the Pelagian Block, a continental platform that represents a section of the African lithosphere that underwent tectonic stretching during and since Late Miocene – Early Pliocene creating NW-SE trending normal faults (Civile *et al.* 2008; Finetti 1984). This extension has resulted in a series of fault bounded depressions (the Pantelleria, Malta and Linosa graben) and an intraplate rift in the foreland of the Apennine – the Maghrebian thrust-and-fold belt (Civile *et al.*). The extension has displaced Sicily away from the African continent, causing crustal thinning to 17 km in the NW of the Pantelleria Graben (Civile *et al.* 2008; Finetti 1984). During the Quaternary, two fault systems were active causing a roughly E-W extensional regime, resulting in crustal cracking which fed the Quaternary volcanism on the island (Civile *et al.* 2008).

### **1.4.2. Petrogenesis**

Peralkaline rhyolites (where molar Na+K/Al > 1) and trachytes are common in bimodal suites in continental rift and ocean island settings (Mahood 1984). Pantelleria is typical, with mafic lavas, including transitional basalt and hawaiiite (46-49 wt. % SiO<sub>2</sub>), and felsic lavas and pyroclastic deposits including metaluminous trachyte, peralkaline trachyte and pantellerite (62-72 wt. % SiO<sub>2</sub>). Pantelleria is the type locality for

pantellerite, an iron-rich, peralkaline, silica oversaturated volcanic rock (Macdonald 1974).

The bi-modal volcanism observed on Pantelleria has been the subject of debate and in particular, the origin of the 'Daly Gap' and the relationship between the basalts, trachytes and pantellerites seen on Pantelleria and at other similar volcanic centres. The question remains on how pantellerite magmas are produced. The following models have been proposed to account for the petrogenetic relationships, the two most popular models given first (White *et al.* 2009):

1. Fractional crystallization of transitional basalt.
2. Partial melting of alkali gabbro followed by fractional crystallization.
3. Fractional crystallization of a high-silica comendite which itself is the result of anatexis (e.g. Olkaria and Eburru, Kenya; Scaillet & Macdonald 2003).
4. Volatile transfer (e.g. Eburru, Kenya; Bailey *et al.* 1975).
5. Partial melting of lower mafic crust, followed by fractional crystallization (e.g. Asela-Ziway, Ethiopia; (Trua *et al.* 1999).
6. Halogen-fluxed partial melting of continental crust (e.g. Olkaria, Kenya; Black *et al.* 1997).

Models 3-6 must be discounted for Pantelleria, as the Sr, Nd, Pb and O isotopes exclude involvement of old crust or sediment (Civetta *et al.* 1998; Mahood *et al.* 1990).

Trace and major-element modelling cannot distinguish between models 1 and 2. Low H<sub>2</sub>O content in melt inclusions in Pantellerite are not compatible with extreme fractional crystallisation of the system (Lowenstern & Mahood 1991): 94% crystallisation of an alkali basalt to produce a pantellerite would result in 8% H<sub>2</sub>O contents, but their analysis yield pre-eruptive H<sub>2</sub>O contents of only 1.4-2.1 wt.%. Furthermore, the partial melting model is supported by trace element modelling and an analysis of clinopyroxene chemical and structural differences (Avanzinelli *et al.* 2004). However, several other features are more compatible with a model that involves fractional crystallization of transitional basalts to produce the felsic end-members (Civetta *et al.* 1998): (1) the large volume of mafic rocks on the island; (2) glomerocrysts of feldspar, augite, olivine and oxides; (3) the progressive and continuous compositional trends observed from trachyte to pantellerite; and (4) the trends of composition match well with experimental data (Carmichael & MacKenzie 1963) that

suggests that pantellerites are formed through extreme fractional crystallisation of a transitional basalt. The recent work by White *et al* (2009) supports a model of fractional crystallisation of transitional basalts using major and trace element modelling and thermodynamic models. They conclude that the metaluminous trachyte was formed from 70-75% low-pressure fractional crystallisation from hydrous basalt magma. The peralkaline trachytes and pantellerites were formed from an additional 20 to 80% fractional crystallisation of an assemblage dominated by alkali feldspar from the metaluminous trachyte magma. The most evolved lavas and tuffs form from a total of 95% fractional crystallisation of transitional basalt. The H<sub>2</sub>O contents obtained by Lowenstern and Mahood (1991) were uncharacteristically low for pantellerites (e.g. 4.3-6.8 wt.%, Kovalenko *et al.* 1994) and 4.6-4.9 wt.%, Webster *et al.* 1993) and buffering of the water content of more evolved magmas by exsolution will prevent the 8 wt.% contents predicted by straight fractional crystallization, thus water content cannot be used to disprove a model of extreme fractional crystallisation.

### **Mantle Source region**

Isotopic studies for Pantelleria include O, Sr, Pb, Nd and He isotopes for the mafic and felsic rocks (Civetta *et al.* 1998; Esperanca & Crisci 1995; Korringa & Noble 1972; Mahood *et al.* 1990) as well as for volcanic fluids (Parello *et al.* 2000). Results from these studies suggest that the felsic rocks were derived from more homogeneous parents in which source-related heterogeneities were dampened by magma mixing, and that there was a close link between the felsic end members and the basalts (Mahood *et al.* 1990). The isotopic data indicates both a DMM (depleted MORB) and HIMU oceanic mantle sources, with a further enriched component, possibly of EM1-type of deep asthenospheric origin (Civetta *et al.* 1998; Esperanca & Crisci 1995). The idea of a mantle plume with a HIMU-EM1-type signature is further supported by He isotopic ratios of volcanic fluids (Parello *et al.* 2000). These show evidence for a <sup>3</sup>He-rich mantle below the rift zone.

Civetta *et al.*, (1998) suggest that the geochemical and isotopic data correlate with age of emplacement. There is evidence for distinct pre-50 ka and post-50 ka parental basaltic magmas that are derived from a heterogeneous source. However, their data for the pre-50 ka rocks are limited, so these conclusions require further investigation.

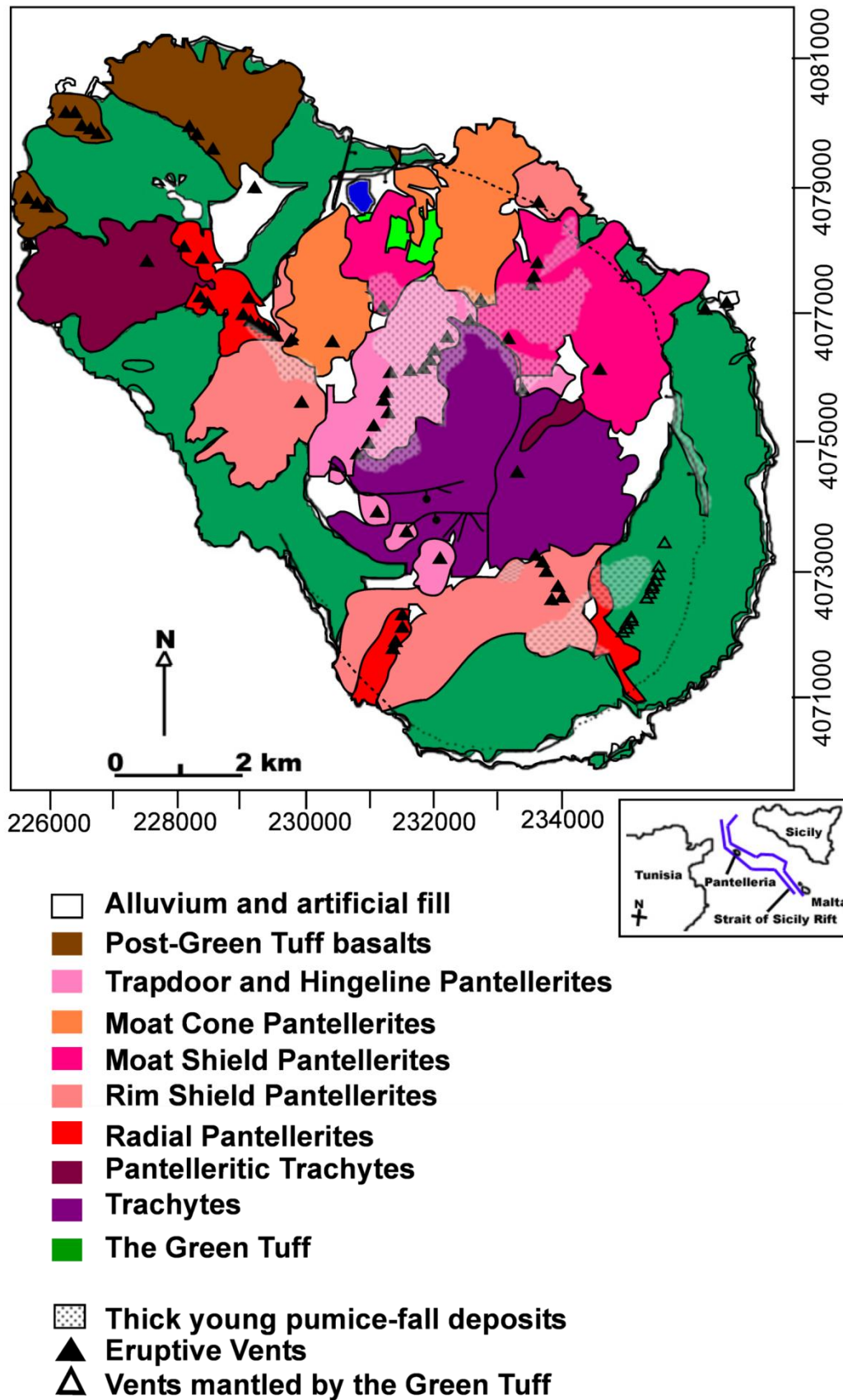


Fig. 1-1: Generalized geologic map for Pantelleria, Italy. Inset shows location in Strait of Sicily system. Bold lines indicate fault scarps. Dashed lines indicate inferred fault traces. (Adapted from Mahood & Hildreth, 1986).

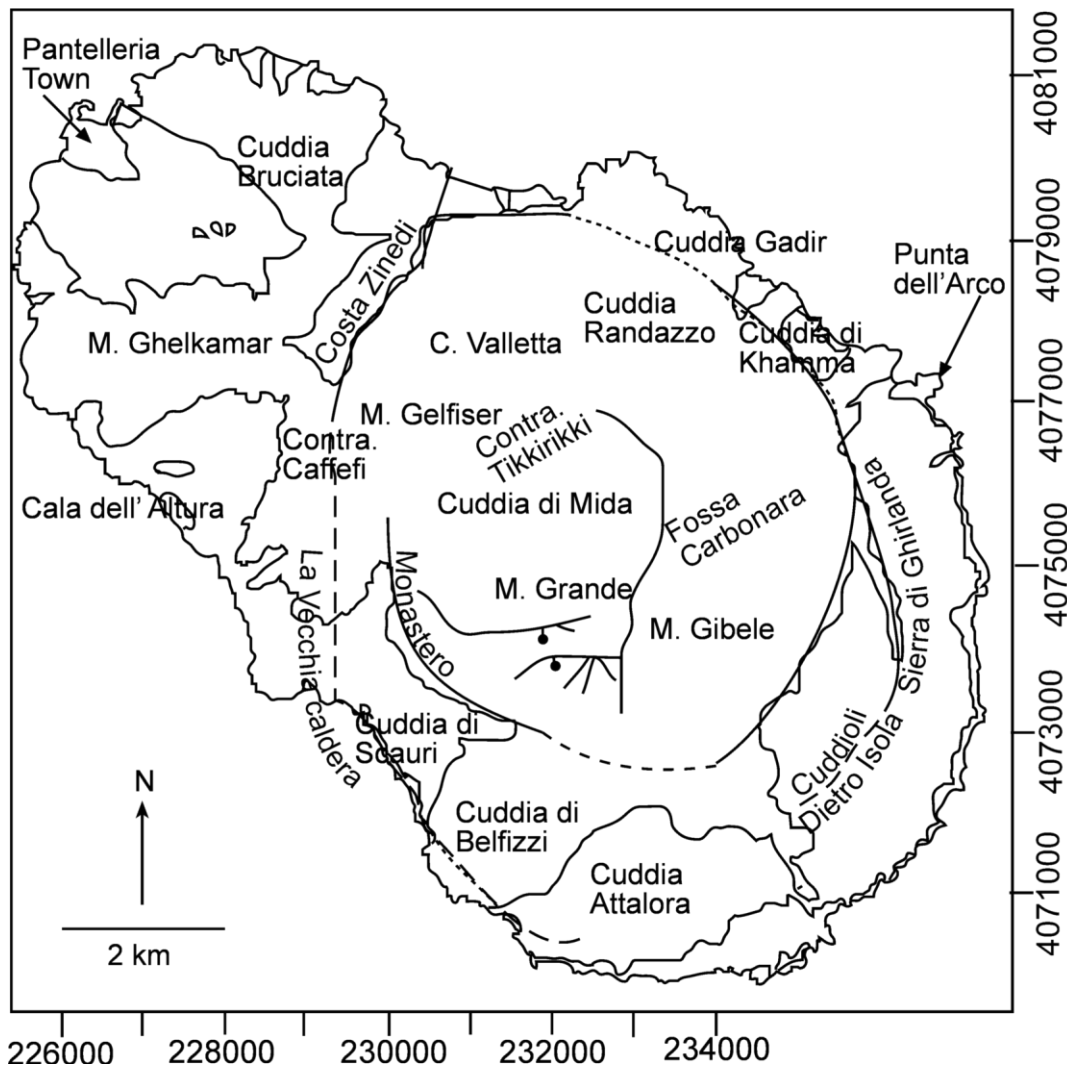


Fig. 1-2: Location map of key areas for post-Green Tuff stratigraphy.

The rare earth elements indicate that the source region of the parental magmas is in the spinel-garnet lherzolite transition zone (Civetta *et al.* 1998). Esperanca & Crisci (1995) thought that the elevated lead isotopes indicated an addition of an older component that resembles old enriched lithosphere. However,  $\delta^{18}\text{O}$  values of +5.5 to 6.6 ‰ eliminates crustal or sediment contamination (Mahood *et al.* 1990).

### 1.5. Pantelleria Volcanic Evolution

The geological history of Pantelleria can be divided into two eras, stratigraphically distinguished by the marker horizon of the Green Tuff, itself dated at 50 ka. The pre-Green Tuff stratigraphy of Pantelleria is partly hidden by the Green Tuff which was emplaced over the entire island (Fig. 1-1). This makes stratigraphic correlations between units difficult. However, attempts have been made to produce a cohesive

stratigraphy of the welded ignimbrites and lavas that outcrop along coastal section and in caldera wall scarps (Mahood & Hildreth 1986; Villari 1970, 1974; Wright 1980). The last 50,000 years, the post-Green Tuff stratigraphy has been more thoroughly studied (Civetta, 1988; Cornette *et al.* 1983; Orsi *et al.* 1991; Rotolo *et al.* 2007). It consists of lava flows and local pumice falls (Fig. 1-1) and basaltic volcanism which is restricted to the northern lobe of the island. The most recent volcanic activity was a submarine basaltic eruption that occurred 4 km NW of Pantelleria in 1891. The eruption lasted for 9 days and produced floating scoria bombs which eventually exploded and sank (Butler & Perry 1892; Washington 1909).

### 1.5.1. Post-Green Tuff Stratigraphy

The last 50 ka of silicic volcanism has been grouped into six cycles (Civetta *et al.* 1988; Orsi *et al.* 1991). These cycles are defined by age and location relationships and are dominated by local pyroclastic fall deposits likely erupted during strombolian-type activity (Orsi *et al.* 1991), beginning with explosive phases and ending with the effusion of lavas. Some debate exists in the details of this cyclic stratigraphy (Civetta *et al.* 1988; Mahood & Hildreth 1986; Orsi *et al.* 1991). The stratigraphy of Civetta *et al.*, (1988) and Orsi *et al.*, (1991) is followed here, unless stated otherwise. Stratigraphic schemes or generalised vertical sections are not published for the < 50 ka deposits and therefore are not presented here. The first silicic cycle is the Green Tuff eruption discussed in detail in Chapters 2 and 3.

The second silicic cycle consists of pantelleritic to trachytic pumice fall deposits, lava flows and lava domes were emplaced between 35 and 29 ka. These filled the southern two thirds of the caldera formed after the Green Tuff eruption (Fig. 1-1). These eruptions formed the Mt Gibeles and Cuddia Gadir centres (Fig. 1-2). The K-Ar dates for the trachyte lavas that form Mt Gibeles are indistinguishable from the Green Tuff dates, which may suggest that these eruptions are the continuing tapping of the zoned magma chamber and progressive isostatic compensation for the mass lost during the caldera-forming eruption (Mahood & Hildreth 1986). However, other dates suggest a 10,000 year repose period between the Green Tuff eruption and the intra-caldera eruptions, and therefore these may be separate eruptive episode (Civetta *et al.* 1988).

The third cycle consists of vents that are located outside the caldera depression and all cluster around a date of 22 ka. They align along NE-SW regional trends. The Mount

Gelkhamar volcano is part of this cycle as well as the small pumice cones at Contrada Caffefi (Fig. 1-2).

A ring of vents that are thought to align along the Monastero caldera rim (the Cinque Denti caldera rim of Mahood and Hildreth, 1986) makes up the fourth cycle. These vents start with an explosive phase producing pantelleritic pumice falls, and then end with an extrusion of lava between 15 and 20 ka. Mt Gelfiser is formed during this cycle (Fig. 1-2).

The fifth cycle occurred during 14 and 12 ka and is made of vents in the northern part of the island, on N-S and NW-SE alignments (Fig. 1-1). These vents also consist of pumice falls, lava domes and lava flows and are overlain by a thick red palaeosoil which acts as a marker horizon in this part of the island.

The sixth and final cycle occurred between 10 and 8 ka (18 and 3 ka, Mahood and Hildreth, 1986) and aligns along fractures related to the trapdoor uplift of the Mount Gibebe centre by 275 m to form Montagne Grande (Fig. 1-2; Mahood and Hildreth, 1986).

### **1.5.2. Pre-Green Tuff Stratigraphy**

The volcanic activity predating and including the Green Tuff eruption is dominated by a series of welded ignimbrites, with inter-dispersed pumice falls, basaltic lavas, and agglutinate shields (Table 1-1). The stratigraphy of the welded ignimbrites has also been revisited and revised as part of this thesis (see Chapter 6).

**Table 1-1: Summary of geologic history pre-Green Tuff Formation, adapted from Mahood and Hildreth, 1986. All dates are K/Ar from Mahood and Hildreth (1986) except for Eruption-unit 3. Eruption-units 1-3 are new, preliminary terms from this study (Chapter 6).**

Age (Ka)	Event
58 ± 4	Eruption of Punta dell'Arco agglutinate pile
66.9 ± 3.3	Voluminous lavas erupted along ring-fracture zone of the La Vecchia caldera at Cuddia Attalora and Cuddiolo Dietro Isola
87.9 ± 1, 87.5 ± 1.3	Eruption-unit 3 (new term, this study; previously named ignimbrites D and Z of Mahood & Hildreth, 1986). New Ar/Ar dates from La Felice et al., 2009.
101 ± 6, 105 ± 7, 110 ± 5 104 ± 14, 113 ± 5, 116 ± 5	Eruption-unit 2 (new term, this study; previously named ignimbrites F and Q of Mahood and Hildreth, 1986).
124 ± 6	Cuddia di Khamma lava shield
133 ± 5, 134 ± 6, 132 ± 6	Eruption-unit 1 (new term, this study; previously named ignimbrite P of Mahood and Hildreth, 1986).
133 – 189	Eruption of Punta Ficara lava
159 ± 8	Cala dell'Altura lava and agglutinate shield
162 ± 8, 164 ± 8, 209 ± 6	Eruption of welded tuff 'S'
172 ± 5, 178 ± 5, 169 ± 10	Eruption of welded tuff 'M'
189 ± 6	Eruption of non-welded lapilli-tuff 'T'
232 (?)	Eruption of Costa Zinedi lava cone
325-239	Eruption of voluminous pantellerite lavas in the south and east. Formation of Cuddia Scauri lava shield.

## 2. The physical volcanology of the Green Tuff Formation: a lithofacies-based approach

---

### 2.1. Abstract

The Green Tuff Formation comprises a basal pumice fall deposit, overlain by a welded, eutaxitic ignimbrite which is locally intensely rheomorphic. The Formation records the 50 ka Green Tuff eruption which was the last of at least four major ignimbrite eruptions of Pantelleria volcano to have occurred between 300 ka and 50 ka. It deposited a pumice fall deposit and a green, pantelleritic to trachytic ignimbrite sheet, typically 5 m thick and locally reaching thicknesses of up to 20 m. The pyroclastic density current which deposited the Green Tuff ignimbrite would have devastated the entire island of Pantelleria, as it covered the land with very hot glass, sterilizing over 100 km<sup>2</sup>. The majority of the pyroclastic material erupted was probably deposited in the surrounding sea. The Green Tuff Formation is excellently exposed at caldera wall sections, on extra-caldera flanks, and along sea cliffs. Detailed logging and lateral tracing of these proximal deposits has allowed detailed study of the lithofacies of the Formation and the reinterpretation of its eruptive history. The eruption began with a strombolian-scale eruption column, and changed to pyroclastic fountaining feeding an initial unsteady pyroclastic current that evolved into a more steady, sustained pyroclastic density current which spread across the entire island. The hot, sticky pyroclasts in the current agglutinated upon deposition, and underwent intense shear from the overriding current and due to gravity, causing a range of rheomorphic fabrics and structures. The ignimbrite may have continued to deform as it cooled. Absence of evidence for breaks within the ignimbrite suggests that the low-aspect ratio ignimbrite is a single flow-unit. It is compositionally zoned, with a gradual upwards increase in both the size and abundance of anorthoclase feldspar crystals.

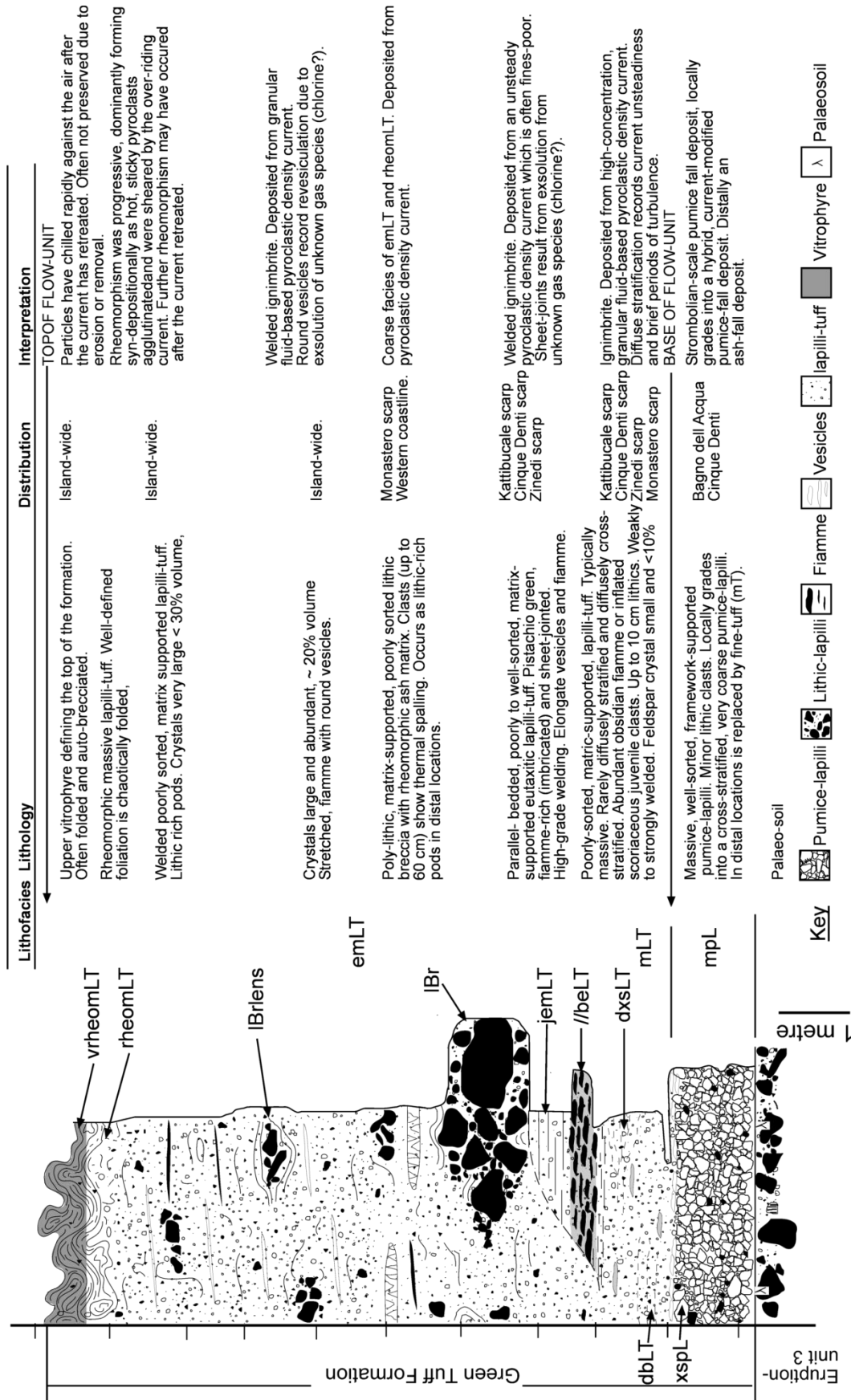


Fig. 2-1: Generalised vertical section through the Green Tuff Formation as seen at the two reference sections along the Bagno Dell Acqua caldera rim and Monastero caldera rim. Graphic log illustrates main vertical lithofacies variations. Lithofacies nomenclature adapted from Branney & Kokelaar, (2002) as stated in Table 2-2. See text for full lithological description and interpretation.

## 2.2. Introduction

This chapter defines the Green Tuff Formation (new term) based upon a lithofacies approach, summarized in Fig. 2-1. It comprises a loose pumice-lapilli layer, the Kattibucale Member (new term), here interpreted as a pumice fall deposit. This is overlain by a variably stratified, eutaxitic lapilli-tuff with local lithic breccia lenses and intensely rheomorphic in parts. This Member is here named the Green Tuff ignimbrite (new term) and it reaches thicknesses of over 20 m in palaeovalleys, but thins to less than 1 m on topographic highs and steep slopes. It is interpreted to be the deposit from a single, sustained, quasi-steady pyroclastic density current. The Green Tuff ignimbrite is defined at the Monastero scarp (Location 44; the new type locality, Fig. 2-2). The Kattibucale Member is defined at the Kattibucale scarp (Fig. 2-2). Although the Formation is often strongly welded, primary characteristics can be observed such as lithic lenses, crystal rich layers, vitroclastic textures, and pumice concentration zones, even when rheomorphic. The c. 50 ka Green Tuff Formation is a palaeosoil-bound peralkaline eruption-unit which covered the entire island of Pantelleria. The present day outcrop covers approximately 50% of the island (Fig. 2-2).

In this chapter, previous work on the Green Tuff Formation will be reviewed, particularly the lithostratigraphy presented by Orsi and Sheridan (1984). Since this work was published, significant advances have been made in the understanding of pyroclastic density currents and the sedimentation of ignimbrites. These advances, and progress in understanding rheomorphic ignimbrites in particular, will be reviewed. The Green Tuff Formation is then documented and reinterpretations upon its emplacement and eruptive history are made drawing on these new concepts.

### 2.2.1. Previous work

The Green Tuff is the youngest welded ignimbrite on Pantelleria and the first eruption in the six silicic cycles (Chapter 1; Civetta *et al.* 1988; Orsi *et al.* 1991). The Green Tuff Formation is chemically zoned from pantellerite to trachyte (Mahood 1984), on the basis of whole rock geochemistry. The matrix varies from vitrophyric (e.g. at top and base) to lithoidal with a phenocryst assemblage of anorthoclase, clinopyroxene, aenigmatite, magnetite, ilmenite, fayalite, apatite ( $\pm$  quartz in the basal vitrophyre) (Wolff & Wright 1981a). It was emplaced across the entire island, mantling all pre-existing topography including the highest peaks, leaving a deposit of about 5 m thick.

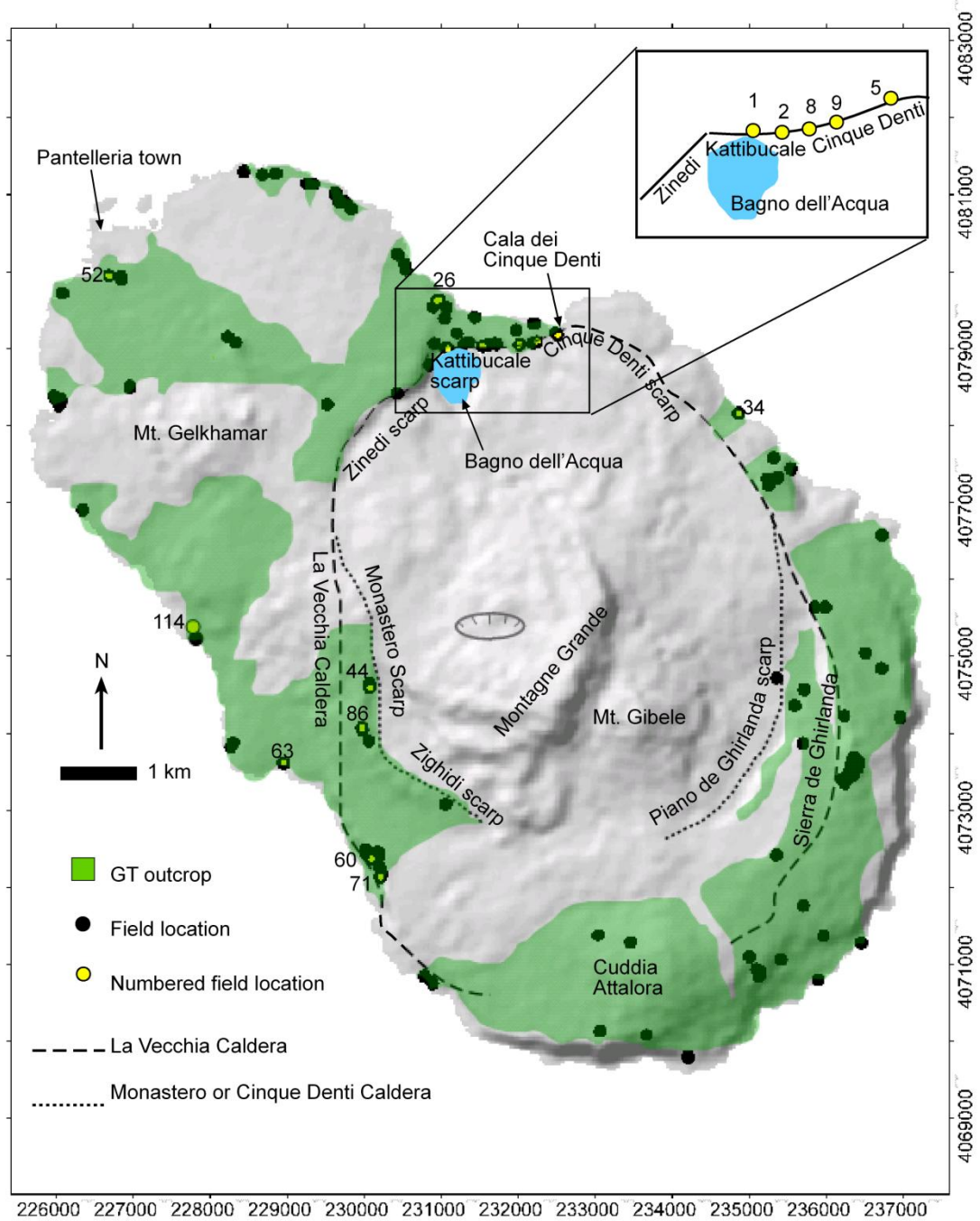


**Fig. 2-2: Location map of Pantelleria, Italy showing present day Green Tuff Formation outcrop, field locations, scarps and features discussed in this chapter. Inset shows scarps around Bagno dell'Acqua. Grid numbers are for UTM zone 32N.**

The total volume of eruptive material is difficult to determine as it was mostly deposited in the sea, but estimates are in the region of 1.5 km<sup>3</sup> to 7 km<sup>3</sup> dense rock equivalent (Wolff & Wright 1981a; Civetta *et al.* 1988). The Green Tuff ignimbrite is commonly strongly welded, with a well developed eutaxitic texture, and in places highly rheomorphic, with areas of intense folding. The folding has previously interpreted to be due to post-emplacement flow (Villari 1970; Wright 1980; Wolff & Wright 1981a, b; Mahood & Hildreth 1986) but more recently, as occurring predominantly during deposition (Catalano 2007). The strong welding has been attributed to its peralkaline chemistry (Mahood 1984) and its high magmatic temperature: 960°C by olivine-clinopyroxene (Marjorie Powell & Powell 1974); 960°C ±30 (Buddington & Lindsley 1964; Carmichael 1967); and 933°C ± 55 by Fe-Ti oxide (Wolff & Wright 1981a; Powell & Powell 1977).

Published dates for the Green Tuff Formation range from 45 to 50 ka. A Mediterranean tephra layer, 'Y6', is dated at c.45 ka (Keller *et al.* 1978) and 53.65 ± 5.69 (Margari *et al.* 2007) and has been correlated with the Green Tuff Formation on the basis of its peralkalinity (Mahood & Hildreth 1986; Wolff & Wright 1981a). K/Ar dates on feldspars from the Green Tuff Formation range from 44.5 ka to 56 ka (50.8 ± 3.6, 50.0 ± 3.5, 47.0 ± 3.2 ka, (Cornette *et al.* 1983); 56 ± 4, 54 ± 3 ka, (Mahood & Hildreth 1983); 50 ± 4, 45 ± 4 ka, (Mahood & Hildreth 1986); and 46.9 ± 2.0, 49.9 ± 2.1, 50.8 ± 2.2 ka, (Civetta *et al.* 1988).

Most authors agree that the Green Tuff eruption involved a caldera collapse, with formation of the Cinque Denti caldera (Mahood & Hildreth 1986) or the Monastero Caldera (Civetta *et al.* 1988; Orsi *et al.* 1991) as discussed in Chapter 5. For clarity, fault scarps discussed in this thesis are given local names and not named for their inferred caldera (Fig. 2-2).

The Green Tuff Formation has been the focus of several studies (Anastasakis & Pe-Piper 2006; Borsi *et al.* 1963; Korringa 1971; Mahood & Hildreth 1986; Orsi & Sheridan 1984; Villari 1970; Wolff & Wright 1981a). It has been interpreted variously as: (a) a lava (Washington 1913-1914); (b) a welded fall deposit (Mahood 1984; Wolff & Wright 1981a; Wright 1980); and (c) a welded ignimbrite plus fall deposits

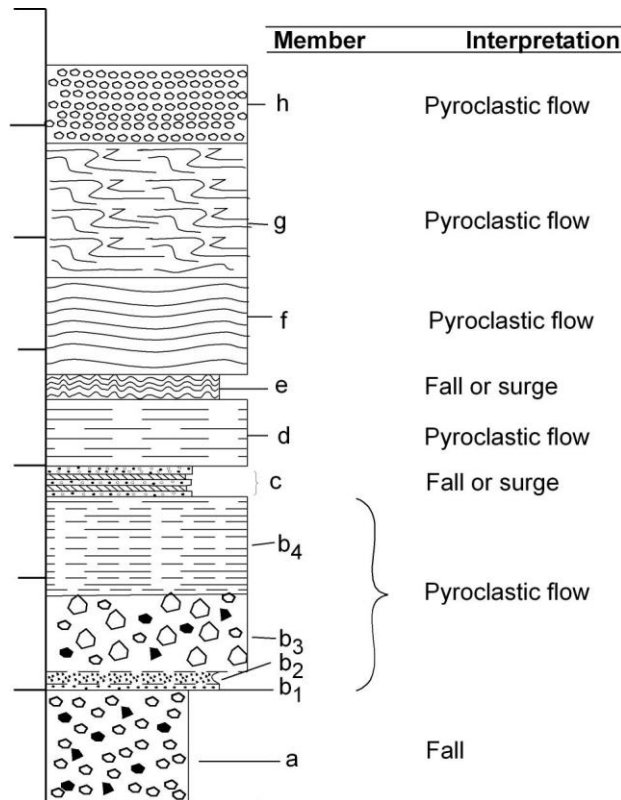


**Fig. 2-3: Orsi and Sheridan (1984) lithostratigraphy. Scale in metres. Thinly-bedded or cross-stratified horizons were interpreted to be deposited from a pyroclastic surge. Massive beds were interpreted to be deposited from a pyroclastic flow. Horizons with different characteristics (e.g. rheomorphism) were interpreted to be deposited from discrete pyroclastic density currents.**

(Borsi *et al.* 1963; Mahood & Hildreth 1986; Orsi & Sheridan 1984; Villari 1970).

These interpretations are discussed below and in Chapter 6. A lithostratigraphic scheme for the Green Tuff (Fig. 2-3), has been presented and inferred to correlate around the island (Orsi & Sheridan 1984). They subdivide the unit into eight members. Member A was interpreted to be a plinian-type pumice fall deposit at the base of the unit (Fig. 2-3), restricted to the north-eastern side of the island possibly due to an inferred westerly prevailing wind at the time of eruption. This is compatible with correlation of the Green Tuff with the Y6 ash layer found in Mediterranean drill cores to the north and east of Pantelleria. ‘Member B’ was inferred to be an ignimbrite consisting of a ‘fines depleted’ basal layer (b1), a thin ash and crystal layer (b2), a pumice and lithic rich layer (b3) and a massive, poorly-sorted layer (b4). ‘Member C’ comprised beds inferred to have been deposited by pumice fall separated by cross-bedded facies interpreted as pyroclastic ‘surge’ deposits. A ‘Member D’ was inferred to trace across the entire island, except on topographic highs, and was interpreted as a green welded ignimbrite. Their ‘Member E’

was inferred to record a widespread ‘pyroclastic surge’. ‘Member F’ was thought to be another massive, widely distributed ignimbrite, absent only from the highest peaks of the island. ‘Member G’ was inferred to be a rheomorphic ignimbrite that covered all of the highest peaks. It was lithic and crystal rich. ‘Member H’ has the highest quantity of free crystals and was inferred to cover the north-western part of the island, and showed variable welding. This stratigraphic scheme was based on correlations of characteristics of lithofacies. They assumed that every facies was a different event. For example, a cross-bedded horizon was correlated across sections and interpreted as a surge. ‘Massive’ beds were correlated and interpreted to be flow-units and rheomorphic facies were interpreted to be present only in a single flow unit. However, re-examination of this stratigraphic scheme indicates that it is tentative at best. The facies cannot be continuously, laterally traced around the island, and appear to be intergradational in the field. There is no clear evidence for separating the different facies into different flow-units.

Since the last work on the Green Tuff ignimbrite (Orsi & Sheridan 1984; Mahood & Hildreth 1986), there have been considerable advances in the understanding of ignimbrites. The physical volcanology of the Green Tuff Formation is reconsidered here in light of recent advances in our understanding of pyroclastic density currents and the emplacement and sedimentation of ignimbrites (Section 2.2.2). Furthermore, advances in the interpretation of welding and rheomorphism of ignimbrites will be reviewed (Section 2.2.3) and the fabrics and structures in the Green Tuff Formation interpreted accordingly.

### **2.2.2. Pyroclastic density currents and the emplacement of ignimbrites**

Our understanding of density currents is hampered by the lack of any instrumentation that can document the processes and conditions within pyroclastic density currents. Thus, our understanding of these currents derives from careful analysis of their deposits (e.g. Wilson 1985; Wilson & Walker 1982; Brown & Branney 2004b), laboratory experiments (Bursik & Woods 2000; McCaffrey *et al.* 2003) and theoretical modelling (Bursik & Woods 1996; Dade & Huppert 1996). In field based studies, advances have been made by adoption of a lithofacies approach (Branney & Kokelaar 2002; Bryan *et al.* 1998; Wilson 1985; Brown & Branney 2004a).

***Interpretation of deposits and development of concepts***

Historically, volcanologists have recognised two end-member types of pyroclastic density current based primarily on deposit characteristics: pyroclastic *flows* and pyroclastic *surges* (see Cas & Wright 1987; Fisher & Schmincke 1984). Massive, very poorly sorted lapilli-tuff layers were called pyroclastic flow deposits and interpreted as resulting from *en masse* deposition from a semi-fluidized plug flow that deflated during transport (Sparks 1976; Sparks *et al.* 1973; Wright *et al.* 1981; Wright & Walker 1981). The resulting deposit was interpreted to represent a proportion of thickness of the current. Less widespread, bedded and rather better sorted pyroclastic deposits were called pyroclastic surge deposits and thought to be fundamentally different in terms of their fluid dynamics. They were interpreted to have sedimented progressively from turbulent currents (Fisher 1966). However, studies of ‘veneer deposits’, which looked similar to surge deposits, suggested that they sedimented ‘layer by layer’ from turbulent currents in the tail or wake of pyroclastic flows which deposited massive deposits elsewhere (Walker *et al.* 1981b; Wilson 1985). Thus, the theory that a pyroclastic flow deposit represented a portion of the flow could not be applied. Furthermore, field studies have shown that massive lapilli-tuff layers ignimbrite (pyroclastic flow deposit) locally grade laterally into stratified facies (pyroclastic surge deposit) such as at Mt. St. Helens (Druitt 1992; Fisher 1990) and that massive deposits can be created from turbulent currents (Baer *et al.* 1997; Fisher *et al.* 1993). Thus, a simple two-fold classification was over-simplistic. With the realisation that both dilute and more particle-concentrated currents develop density stratification, and that their deposits can be variably stratified, the idea that end-members are likely to have formed through similar mechanisms which does not involve *en masse* deposition and there may be gradations between the two extremes of deposit types has evolved (Branney & Kokelaar 2002; Branney & Kokelaar 1992; Druitt 1998).

It has been proposed that pyroclastic density currents range between two-end member types (Branney & Kokelaar 2002): (1) *fully dilute pyroclastic density currents* where particle transport and support even at lower levels is dominated by turbulence of the gaseous phase; and (2) *granular fluid-based pyroclastic density currents* where particle support at lowermost levels is dominated by particle collision and/or fluid escape.

### ***Deposition from a flow-boundary zone***

Progressive aggradation is the term given to the concept that a deposit accumulates gradually by sedimentation, for example, at the base of a density current (Branney & Kokelaar 1992; Fisher 1966) or by hindered settling suspension (Druitt 1995).

Turbidites have long been considered to be assembled by progressive aggradation; for example, a Bouma sequence consists of a vertical series of layers (Bouma 1962), and the changes in grain size, sorting, stratification, etc., are interpreted to represent changes in current dynamics and boundary conditions in a simple current and not boundaries between different flow-units. A single Bouma sequence represents one flow-unit.

Incremental deposition from a sustained current can also explain features seen in pyroclastic density current deposits that contradict a model of *en masse* emplacement. Such features include gradational vertical chemical zoning, subtle diffuse stratification, lateral gradations to low angle cross-stratification, pervasive fabric development and flow structures through an entire thickness of a deposit, and changing flow directions inferred from such fabrics through a single deposit (Branney *et al.* 2004; Branney & Kokelaar 1992, 1997; Carrasco-Nunez & Branney 2005; Kneller & Branney 1995; Hughes & Druitt 1998). With progressive aggradation, the stratification and sorting within a deposit is largely controlled by conditions at the flow-boundary zone.

The concept of a depositional boundary has been considered by several authors (e.g. Branney & Kokelaar 2002; Fisher 1990; Lowe 1982; Southard 2006; Sumner *et al.* 2008) and the overview given here is based on the work of Branney & Kokelaar (2002). The depositional boundary is the interface between a current and its substrate. During sedimentation, particles from the current pass through the body and enter the deposit. It can be useful to envisage a *flow-boundary zone* (Branney & Kokelaar 2002), which encompasses the basal part of the current and the uppermost part of the aggrading deposit. The characteristics of the aggrading deposit, such as stratification and sorting, are largely created within this zone, and therefore must reflect processes and conditions in this zone, such as velocity, particle concentration and shear distribution.

Four end-member types of a flow-boundary zone have been proposed (Branney & Kokelaar 2002) controlled by particle concentration, deposition rate and shear rate. (1) *Direct-fall-out-dominated* flow boundaries involve the unhindered settling of individual particles with negligible particle interactions or lateral shear. (2) *Traction-dominated* flow boundaries involve a sharp interface between the current and the deposit. Particles

are variably supported by fluid turbulence and can be moved along the bed by traction and saltation. (3) *Granular-flow-dominated* boundary zones are where clasts are supported by grain interactions due to high particle concentrations and shear intensity. Finally, (4) *Fluid-escape-dominated* flow boundaries where upward expulsion of fluid is the predominant particle support mechanism (hindered settling).

The flow-boundary zone is not a steady feature. Rather, it can change both temporally and spatially because currents are inherently inhomogeneous. Temporal variability (or current *unsteadiness*) can include changes in velocity, competency, capacity, mass flux and particle supply, and is discussed in terms of a *waxing*, *waning* or *quasi-steady* current and is reflected in changes of lithofacies with height in a deposit. Spatial variability (or current *non-uniformity*) can include changes in slope, sedimentation, elutriation, clast and substrate interaction, and air ingestion. The down-current increase or decrease of a particular parameter can be described in terms of an *accumulative* (e.g. increased velocity/acceleration) or *depletive* (e.g. decreased competence) current, and may be recorded by lateral gradational changes within a deposit.

The concept of a variable current and its flow-boundary zone has some important implications for the interpretation of deposits of pyroclastic density currents. (1) Deposition accompanies transport, so that deposition rate may affect transport distance. (2) The thickness of the deposit is a function of the rate and duration of deposition, not the thickness of the current. (3) Vertical variations in the current record temporal changes in the current. (4) Lateral variations record spatial variations in the current. (5) The deposit records conditions at the flow-boundary zone and does not necessarily record conditions at higher levels in the current. (6) Evidence (e.g. erosion surfaces, scours, stratification, grading patterns) used previously to infer boundaries of ‘flow-units’ might in some cases be explained in terms of current unsteadiness; for example, with temporary erosion or non-deposition, within a single sustained current.

The conceptual framework of a progressively aggrading deposit and the flow-boundary zone proposed by Branney & Kokelaar (2002) have been largely accepted, with applications to a variety of current deposits (e.g. Brown & Branney 2004b; Duller *et al.* 2008; Sumner *et al.* 2008), despite a paucity of experimental and numerical modeling of this concept. However, advances are now being made in this field, as described below.

***Experimental and numerical modeling***

The development of physical models is important to test conceptual theories of current transportation and sedimentation. Such models can then be tested against real data from laboratory experiments and field observations. This overview is not exhaustive of these models (for this see Druitt, 1998) but rather a summary of important advances in our understanding of the emplacement of pyroclastic density currents.

Early models of pyroclastic density currents considered highly concentrated granular currents of a range of eruption sizes from small-scale Montserrat-style pyroclastic density currents to large-volume currents that may have formed from a rapidly condensed collapsing column or from a dense undercurrent of a suspension current. These types of currents are modelled based upon their rheological properties such as the viscoplastic and turbulent models, (e.g. Battaglia 1993), the sliding block model or the Mohr-Coloumb model, (e.g. Hayashi & Self 1992) and the rapid granular flow model (e.g. Denlinger 1987). These models do not tend to account for loss or gain of material through deposition or erosion; they assume that momentum loss is frictional, and that the current flowed as a plug flow and froze *en masse*. But, top-down *en masse* freezing has not been recorded experimentally in non-cohesive (dry) systems. However, numerical models of rapid granular flow with an upward migrating shear zone are consistent with some features of pyroclastic density current deposits (e.g. Cleary & Campbell 1993; Straub 1996).

Suspension current models are those that consider dilute, turbulent multi-phase flows (e.g. Bursik & Woods 1996; Dade & Huppert 1996; Valentine 1987) that are able to transport small clasts turbulently in suspension for long distances. Results indicate that the experimental particulate currents tend to become strongly stratified with respect to particle concentration, with an increase in bulk density towards the base of the current. Numerical models to date do not fully address this density stratification, although fully dilute, stratified density currents (Valentine 1987) and two-layer models (e.g. Doyle *et al.* 2010) have made advances in this field. Particles that reach the lower flow boundary may deposit from the suspension such that the particle concentration in the current decreases with distance, until the current ultimately becomes buoyant and lofts. The run out distance of these currents is controlled by the mass flux at source (Bursik & Woods 1996), as well as the flow geometry (channelized versus radial). Deposition from such currents can occur under three regimes (Druitt 1998), and a single current can be

gradational between these regimes (Druitt 1992). (1) *Traction sedimentation*, where particles roll, saltate or slide along the aggrading deposit before halting. Traction sedimentation can result in stratified and cross stratified deposits. (2) *Suspension sedimentation* where particles deposit directly onto the aggrading deposit without any lateral component of late-stage motion, resulting in an unstratified deposit. Grading can occur due to sorting through hindered settling or through changing flow conditions (waxing or waning flow). (3) '*Undercurrent*' formation where the particles that reach the flow-boundary zone are remobilized into a dense, highly concentrated basal flow (e.g. Middleton 1967) which in some cases may decouple from the suspension current (Doyle *et al.* 2010). At present, suspension current models typically do not consider density stratification with high particle concentrations in the lowermost levels of the current and often only model up to two particle sizes.

Geophysical currents are more likely to be a combination of these end-member models, and this is more difficult to model. Improvement to models could include density stratification in suspension current models such that basal concentrations are high enough for particle interactions to occur using poorly sorted, poly-disperse particle populations and introducing a fines-component to rapid granular models. Important advances in understanding the behaviour of pyroclastic density currents have also been made through laboratory modelling, and these advances should be incorporated into future numerical models of the emplacement and sedimentation of pyroclastic density currents. Experiments of gas-fluidized dense granular flows have shown that highly concentrated pyroclastic density currents can be described as fluid gravity currents (Roche *et al.* 2004, 2005; Roche *et al.* 2008) which may account for the high mobility observed for pyroclastic density currents, although these experiments typically use mono-disperse populations of glass beads of small grain size ranges. The use of real ignimbrite samples, with a fines component could strongly affect the outcome of these experiments. Progressive aggradation has been proven to occur in even small, high concentration flows which were modelled experimentally using real volcanic ash (Girolami *et al.* 2008; Girolami *et al.* 2010). An important implication of this work is that mathematical models of fluidized flows should include deposit aggradation, that currents can exert high shear stresses on the ground and/or deposit over which they travel, and that shear can be pervasive through an aggrading deposit. Flume experiments of turbulent suspension flows have shown that the concept of a quasi-steady current that

can wax and wane does result in variability within a deposit such as grain size grading (McCaffrey *et al.* 2003) and that inverse grading of large light particles (such as pumice blocks) does not necessarily represent flotation of these clasts to the top of the current during transport (Choux *et al.* 2004). Important implications for models of density currents arising from these studies are that geophysical currents can wax, wane and involve periods of quasi-steady flow. Strong density stratification is expected in turbulent currents, and particles can segregate rapidly within a current, thus grading in a deposit does not simply mirror grading within the current that produced it. The delayed sedimentation observed by Choux *et al.* (2004) shares features with the conceptual pumice over-passing model of Branney & Kokelaar, (2002).

### **2.2.3. Welding and rheomorphism in ignimbrites**

This section reviews some of the advances in the interpretation of welding and rheomorphism on ignimbrites as the Green Tuff Formation has been reinterpreted based upon these concepts

Welding, the adhesion of hot pyroclasts, is thought to occur through two intergradational processes: (1) load welding or compaction welding after deposition of the ignimbrite sheet (Quane & Russell 2005; Ross & Smith 1961; Russell & Quane 2005; Sheridan 1976); and (2) agglutination during deposition (Branney & Kokelaar 1992; Chapin & Lowell 1979; Freundt 1998; Mahood 1984; Pioli & Rosi 2005). Early studies, particularly those based on large welded ignimbrites in the western US, inferred that welding post-dated emplacement of an isothermal ignimbrite sheet, and was controlled by deposit thickness and cooling rates (load welding; Riehle 1973; Ross & Smith 1961). This model assumes that a hot, pyroclastic material welds by compaction due to the load of the overlying part of the cooling deposit, and it results in welding profiles with the most intense zone of welding about one third of the way up from the unit's base. However, some more intensely welded and rheomorphic ignimbrites clearly deviate from this pattern; for example, by being welded to their upper surfaces and with complex small scale-folds and lineations that show welding and early rheomorphism occurred during the sustained assembly of the ignimbrite (Andrews & Branney 2010). Experimental evidence suggests that hot pyroclastic particles can agglutinate and coalesce rapidly, without significant burial (Freundt 1998, 1999), and that this can result in a progressively aggraded welded deposit (Branney & Kokelaar 1992). The ability of a particle to agglutinate relies upon its

**Table 2-1: The welding grade continuum (Branney and Kokelaar, 1992).**

ARBITRARY DEVISIONS	EXTREMELY HIGH-GRADE	continuum			EXTREMELY LOW-GRADE
	Fountain-fed lava-flows	Lava-like ignimbrites	Rheomorphic ignimbrites	Non-rheomorphic welded ignimbrites	Non-welded ignimbrites
PROCESSES AND CONDITIONS	increase in eruption column height and consequent cooling				
	increase in temperature, decrease in particle viscosity and yield strength				
	increase in crystal fragmentation (explosivity)				
	coalescence				
	agglutination				
	welding				
	non-particulate flow accompanying emplacement				
	non-particulate flow after deposition				
	lateral particulate flow important during emplacement				
	syn- and post-emplacement vesiculation				
droplets transported laterally					
blocky or cusped shards transported					
PRODUCT CHARACTERISTICS	increase in accidental lithics, eroded from vent and ground surface				
	increase in fragmentation of crystals				
	pumice imbrication and grain fabrics				
	non-particulate lineations, rotated lithics and flow folds				
	lobate flow margins				
	widespread upper autobreccia				
	localised basal and/or internal autobreccia				
	angular or cusped shards preserved in ignimbrite				
	droplet shapes occasionally preserved				

viscosity, often controlled by melt composition, temperature and volatile content (Freundt 1998; Mahood 1984).

Welded ignimbrites can be described in terms of their 'grade' (Walker 1983) within a continuum (Table 2-1), from low-grade tuffs (e.g. the Campanian ignimbrite; Barberi *et al.* 1978), which are not welded, to intermediate-grade (e.g. the Bishop Tuff, California; Ragan & Sheridan 1972), which show 'classic' compaction-welding profiles with non-welded zones upper and lower zones and a eutaxitic central zone to high-grade (e.g. ignimbrite 'D', Gran Canaria; Kobberger & Schmincke 1999), which are predominantly welded throughout, even when thin and show a strong eutaxitic fabric with rheomorphic zones. These high-grade deposits are thought to form dominantly by particle agglutination, but may also be affected by load welding (Freundt 1999). Extremely high-grade tuffs, (e.g. ignimbrite 'TL', Gran Canaria, Sumner & Branney 2002; the Greys Landing ignimbrite, Idaho, Andrews *et al.* 2008) are intensely welded, and rheomorphic ignimbrites with lava-like zones in which the lithologies can be difficult to distinguish from silicic lavas.

Rheomorphism is the ductile deformation of the hot, welded pyroclastic deposit either during or shortly after deposition, with development of elongation lineations and folds. Kinematic and structural studies of rheomorphic ignimbrites have shown that, in extremely high-grade ignimbrites and some high-grade ignimbrites, rheomorphism begins through rapid agglutination and coalescence of hot particles during deposition ('primary' *sensu* Wolff & Wright 1981b), with shearing in a thin, sub-horizontal, ductile shear zone around the current-deposit interface, producing intense elongation lineations and folds (Andrews & Branney 2010; Branney *et al.* 2004; Branney & Kokelaar 1992).

The deformation may continue after deposition of the density current due to gravity spreading or slumping down slopes ('secondary' as envisaged by Wolff & Wright 1981b). Intense welding and rheomorphism is favoured by high temperatures (Andrews & Branney 2010; Freundt 1998; Russell *et al.* 2003) and an eruption style that minimizes cooling (Mahood & Hildreth 1986). A peralkaline composition (Mahood 1984) also favours rheomorphism, as does a high water or halogen content (Giordano *et al.* 2005). Rheomorphic folding typically includes open, curvilinear folds to tight isoclinal folds, including oblique folds and sheathfolds (Andrews & Branney 2010;

Branney *et al.* 2004). Other rheomorphic features include lineations parallel to shear direction, foliation and colour banding, stretched vesicles and fiamme, autobrecciation of upper surfaces, boudinage and tension gashes (Branney & Kokelaar 1992; Kobberger & Schmincke 1999; Pioli & Rosi 2005; Schmincke & Swanson 1967; Sumner & Branney 2002).

### ***Peralkaline composition***

Peralkaline magmatism (an excess of alkalis over alumina;  $\text{Na} + \text{K} > \text{Al}$ ) affects the physical characters of mildly silica-undersaturated to oversaturated pyroclastic deposits, their volcanic edifices and related calderas (Mahood 1984). Rheomorphic ignimbrites are particularly common in strongly peralkaline volcanic systems (where  $\text{Na} + \text{K} / \text{Al} > 1.1$ ; Mahood 1984) and occur in a variety of settings, but particularly in continental rift zones (e.g. the Fantale Tuff, African Rift, Gibson 1794, 1970; Pantelleria, Italy, Mahood 1984; Wright 1980; this study) and other continental extensional settings (e.g. McDermitt caldera complex, Nevada, Hargrove & Sheridan 1984; Wallace *et al.* 1980; the Gomez Tuff, Texas, Parker & White 2008). It also occurs in some oceanic islands (e.g. Morgan and Fataga Formations of Gran Canaria, Freundt & Schmincke 1992; Leat & Schmincke 1993; Sumner & Branney 2002). The following factors are thought to favour the welding of peralkaline pyroclastic particles at the instant of deposition (Mahood 1984; Stevenson & Wilson 1997) through their effect on viscosity.

1. *Melt composition.* Silica networks rely on equal proportions of alkalis and alumina to form silica chains ( $\text{Na} + \text{K} = \text{Al}$ ), meaning that peraluminous rhyolites ( $\text{Na} + \text{K} < \text{Al}$ ) or peralkaline rhyolites ( $\text{Na} + \text{K} > \text{Al}$ ) subsequently have lower viscosities than metaluminous rhyolites. It is thought that peralkaline rhyolites have viscosities similar to silicic andesites, despite having  $\text{SiO}_2$  contents of up to around 70% (Baker & Vaillancourt 1994; Mahood 1984).
2. *Water and halogen content.* High water contents have a disproportionate effect on lowering viscosities of peralkaline magmas compared to other rhyolitic systems (Dingwell *et al.* 1998), and peralkaline magmas have moderate to high water concentrations (Barclay *et al.* 1996; Lowenstern & Mahood 1991) and high halogen contents (Aines & Lowenstein 1990; Carroll 2005; Gioncada & Landi, 2010; Lowenstein 1994). Halogens, as silica network modifiers, also significantly reduce viscosity.

3. *Temperature.* Temperature estimates of 950 °C for the Green Tuff Formation (Wolff & Wright 1981a) and 750-900 °C for the Gomez Tuff (Parker & White 2008) are closer to temperatures expected for less viscous andesites than rhyolites. Eruption columns are inferred to be low, which minimizes cooling of pyroclastic particles, so that emplacement temperatures are thought to be well above the threshold for welding (Quane & Russell 2005).

The styles and features of rheomorphism seen in peralkaline systems are similar to those of other high-grade to extremely-high-grade ignimbrites, such as those of the Snake River, USA (Branney *et al.* 2008). Schmincke (1974) highlights some rheomorphic fabrics and structures, which include stretching of pumice blocks and lapilli, lineations and foliations, folds on the micro to metre scale, ramp structures, pull apart structures and tension gashes, gas blisters (Gibson 1970), upper and basal autobreccias and rotated clasts (Schmincke & Swanson 1967). Features more particular to peralkaline rheomorphism include welding throughout the deposit despite thin deposit thicknesses (typically < 30 m) including deposits of only a few cm and on steep slopes on Pantelleria (Korringa 1971), large gas cavities unrelated to individual pyroclastic particles, small glass shards or ‘globules’ showing spherical shapes, round bubbles in previously deformed pumice particles, crystallization that is commonly advanced, common mafic groundmass minerals, and pumice or glass shard structures that are often homogenized during welding compaction.

#### **2.2.4. Terminology**

Lithofacies in this chapter are defined using a non-genetic terminology, based upon internal sedimentary structures, grain size and lithology (adapted from Branney & Kokelaar 2002). A lithofacies is non-stratigraphic. Where possible, terminology with genetic implications is avoided. Lithofacies abbreviations used follow those of (Branney & Kokelaar 2002) and are explained in Table 2-2.

An ignimbrite is the deposit of a pumiceous pyroclastic density current rich in ash.

Valley-fill deposits here include deposits which have preferentially accumulated into palaeovalleys (elsewhere sometimes described as ‘valley ponded’ e.g. (Wilson & Walker 1982). The term is used to distinguish these deposits from thinner deposits on topographic highs. The term ‘vener ignimbrite’ is avoided due to its genetic inference (e.g. from the tail of a pyroclastic density current (Walker *et al.* 1981b).

**Table 2-2: Non-genetic lithofacies terms and abbreviations used throughout the text and figures.**

<b>Symbol</b>	<b>Lithofacies</b>
pL	pumice lapilli
LT	lapilli-tuff
T	tuff (ash)
m	massive
s	stratified
ds	diffuse-stratified
b	bedded
xs	cross-stratified
dxs	diffusely cross-stratified
//	parallel bedded
lenspL	lens of pumice lapilli
lenspC	lens of pumice cobbles
lBr	lithic breccia
lBrpods	pods of lithic breccia
e	eutaxitic
v	vitrophyre
rheo	rheomorphic
j	sheet-jointed

I use the term ‘caldera’ for a topographic depression caused by subsidence after magma withdrawal from a subvolcanic magma chamber. Caldera walls are the fault scarps related to this subsidence.

An eruption-unit is a formation inferred to record a single eruption. It may, for example, be bound by palaeosoils and/or sediments.

The term ‘flow-unit’ is interpretive and follows that defined by Branney & Kokelaar (2002), meaning the deposit of a discrete current. An ignimbrite sheet may be simple and comprise a single flow-unit, or it may be compound and comprised of several flow-units. An inferred flow-unit may be defined by ‘flow-unit boundaries’ which are horizons that record a cessation of current activity such as a pumice or ash fallout layer. Bedding, grainsize changes or scours within a deposit may or may not record cessation of flow: they may for example record unsteady deposition, or a period of non-deposition

or erosion through a progressively aggraded single flow-unit (Branney & Kokelaar 2002).

### **2.3. Lithofacies of the Green Tuff Formation**

The Green Tuff Formation (Fig. 2-1) is well exposed particularly in caldera scarps, on extra-caldera flanks and sea cliff sections. The lowermost, bedded facies (Sections 2.3.1 - 2.3.6) are confined geographically to the Kattibucale and Cinque Denti scarps (Fig. 2-4) and stratigraphically to the lower 2 metres of the Green Tuff Formation. They represent the first moments of the eruption (Chapter 4). The majority of the Formation, the high-grade massive lapilli-tuff facies and its associated facies (Sections 2.3.8-2.3.7) are defined at locations along the Monastero scarp (Fig. 2-5). Individual lithofacies are described and interpreted below.

UTM coordinates in the text refer to European Datum 1950 zone 32S or 33S as individually stated.

#### **2.3.1. Massive pumice-lapilli (mpL)**

*Description:* The massive pumice-lapilli facies comprises massive, framework-supported, well sorted angular, pantelleritic pumice-lapilli (1-2 cm) and subordinate lithic lapilli (0.5-1.5 cm; Fig. 2-6). The predominant lithic type is black scoria. Locally the facies exhibits parallel bedding.

*Occurrences and associations:* The facies is best exposed at the base of the Green Tuff Formation at the caldera rim at the Bagno dell Acqua scarp (Fig. 2-2) and at Cala dei Cinque Denti (Fig. 2-2), where it lies directly on the palaeosoil at the top of the c. 85 ka ignimbrite of Eruption-unit 3 (Chapter 6). No soil is developed in it. Where it is overlain by a welded deposit, pumice clasts in its upper part are slightly flattened and welded, but remain framework-supported. The facies thins in all directions away from the caldera wall and is absent at other, more distal locations (Fig. 2-7). At some locations where it is absent, an ash facies is present at the corresponding stratigraphic level at the base of the formation (Section 2.3.3).

*Interpretation:* The massive pumice-lapilli facies is interpreted to be a pumice-fall deposit on the basis of its very good sorting, angular pumice, and openwork clast-

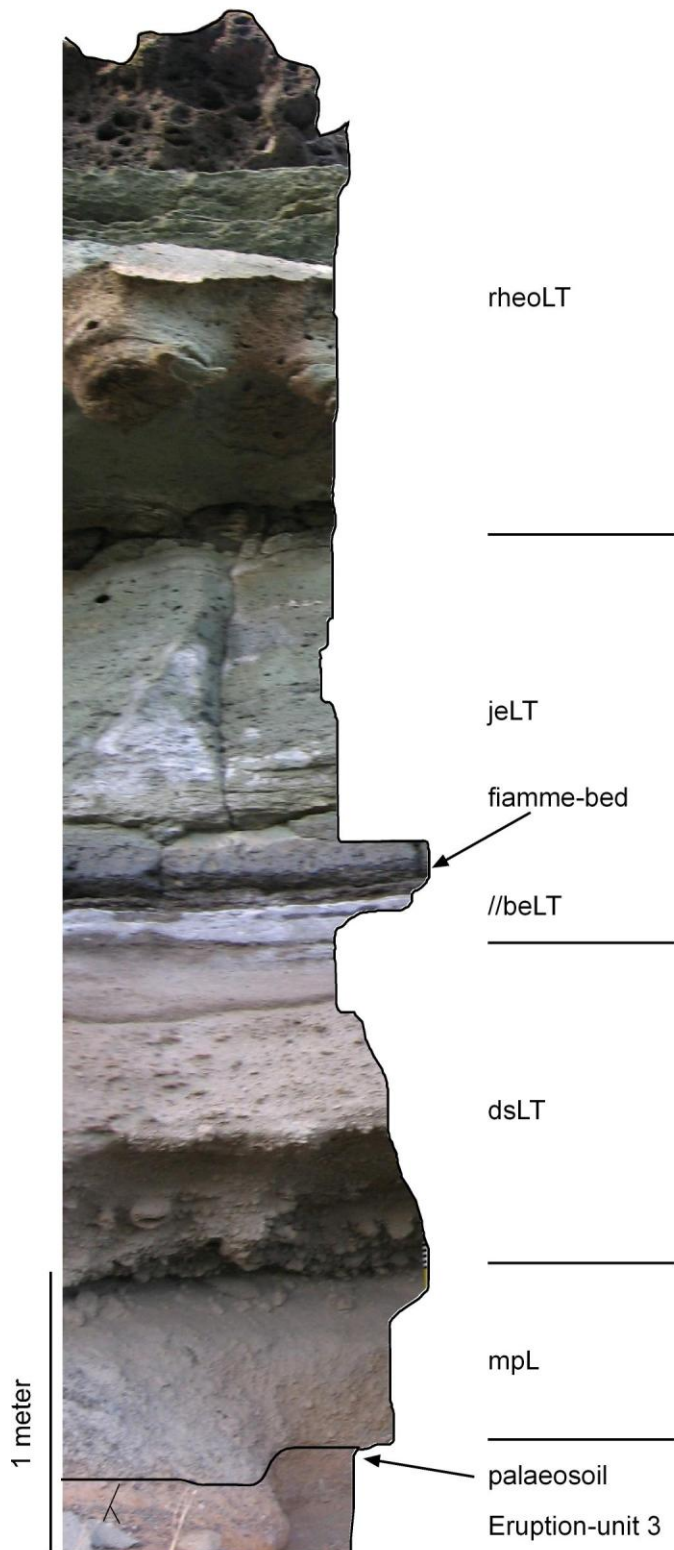


**Fig. 2-4:** Typical section along the Cinque Denti scarp (location 8; UTM 32s, 0767300, 4079212) where the lowermost, bedded Green Tuff Formation is defined.

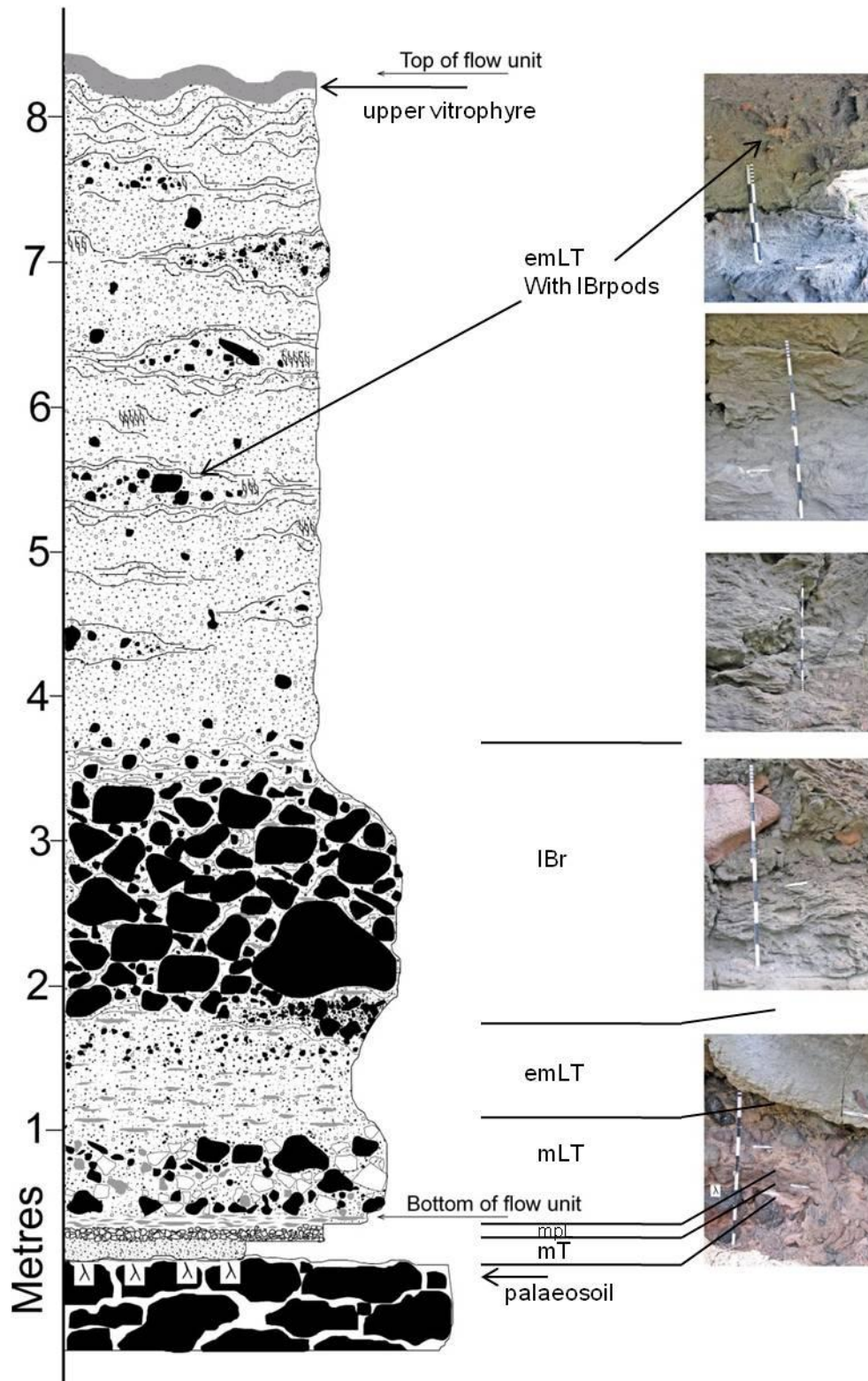
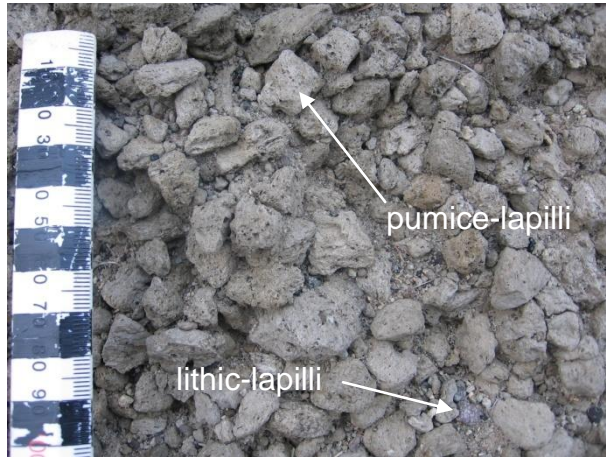


Fig. 2-5: Typical section along the Monastero scarp (location 44; UTM 32s, 0765634, 4074662) where the Green Tuff Formation is defined (new type locality).

supported texture. Exposures are limited to the north-east of the island (Fig. 2-7), and isopach mapping is not possible. However, the ubiquitous absence of the deposit at more distal exposures indicates a very limited dispersal, probably strombolian (at best sub-plinian) in terms of scale. At some locations it may have been eroded by successive pyroclastic density currents.



**Fig. 2-6: Massive pumice-lapilli facies near Cinque Denti (location 9; Fig. 2-2). Scale divisions in 1cm.**

### 2.3.2. Cross-stratified pumice-lapilli (xsPL)

*Description:* The cross-stratified pumice-lapilli facies (Fig. 2-8) comprises well sorted angular pumice lapilli and subordinate poly-lithic lapilli with local lenses of lithic-rich (Fig. 2-9A) and pumice-blocks (Fig. 2-9B). It is rather less well-sorted than the massive pumice-lapilli facies. Typically, maximum pumice and maximum lithic clast sizes are larger than seen in the massive pumice-lapilli facies (Fig. 2-10). The facies is clast-supported and the pumice and lithic lapilli are angular. Cross-stratification in the facies is at relatively high angle ( $\sim 20\text{-}30^\circ$ ), are not unidirectional (Fig. 2-8) and are transverse to the inferred current direction. Dune-form bedding, or other aggradational bedforms are not observed. At Bagno dell'Acqua, scour and fill structures are seen that are filled with very poorly sorted, lithic rich lenses (Fig. 2-8; Fig. 2-9A). These structures are relatively small ( $< 30$  cm deep and  $< 50$  cm wide), and occur at the base of the cross-stratified pumice-lapilli facies. The scours are cut into the massive pumice-lapilli facies.

*Occurrences and associations:* The cross-stratified pumice-lapilli facies is exposed at Bagno dell'Acqua (location 1; Fig. 2-2). It locally grades vertically from the massive pumice-lapilli facies (e.g. near Cala dei Cinque Denti, location 9; Fig. 2-2). At Bagno dell'Acqua it overlies the massive pumice-lapilli facies with an erosional contact (location 1; Fig. 2-2).

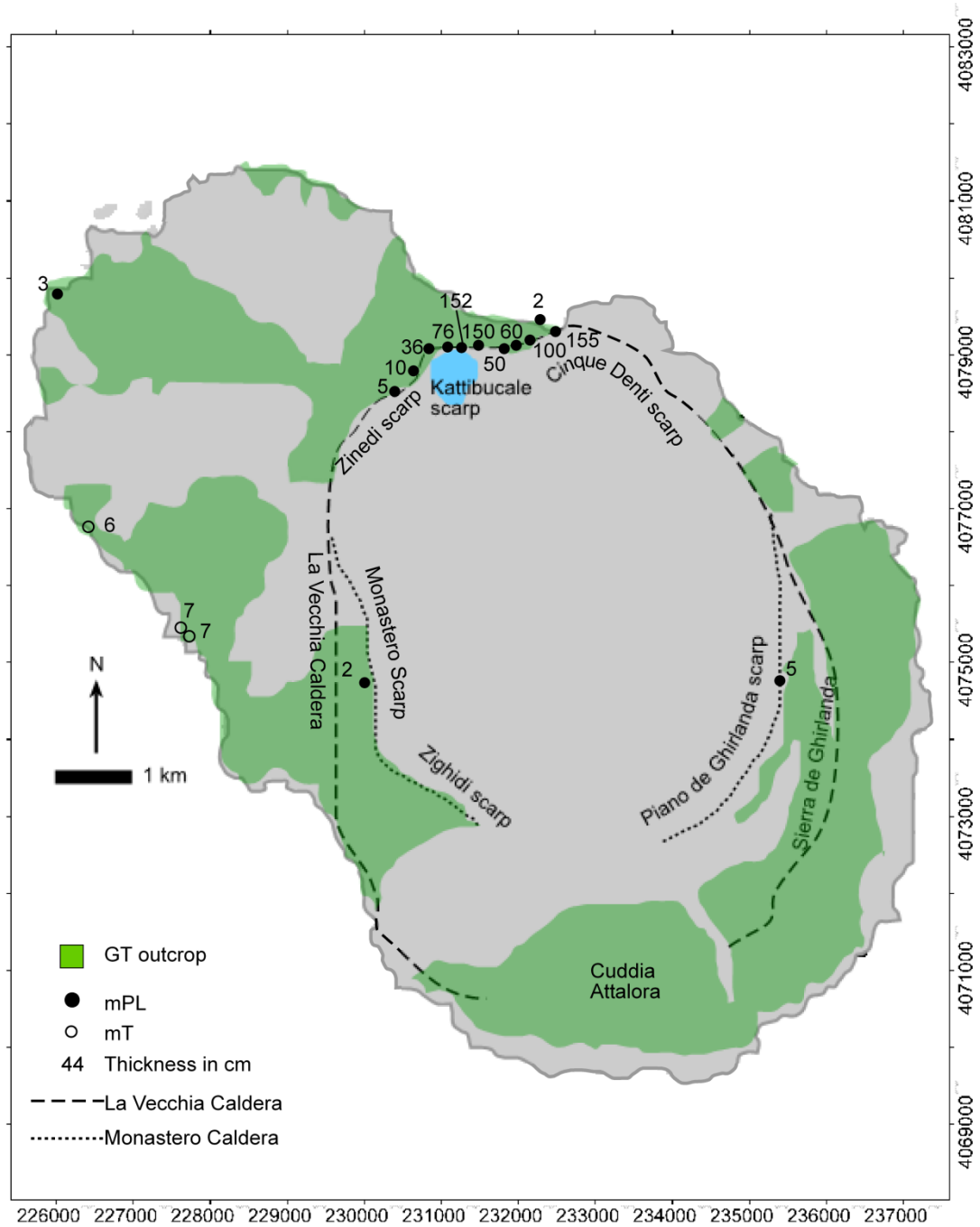


**Fig. 2-7:** Distribution map of the massive pumice-lapilli deposit (mPL) and crystal-rich and lithic-rich massive tuff (mT). The limited dispersal, and thin thickness of the mPL suggests that the eruption column was not high, or that preservation of this lithofacies was low. Grid numbers are for UTM zone 32N.

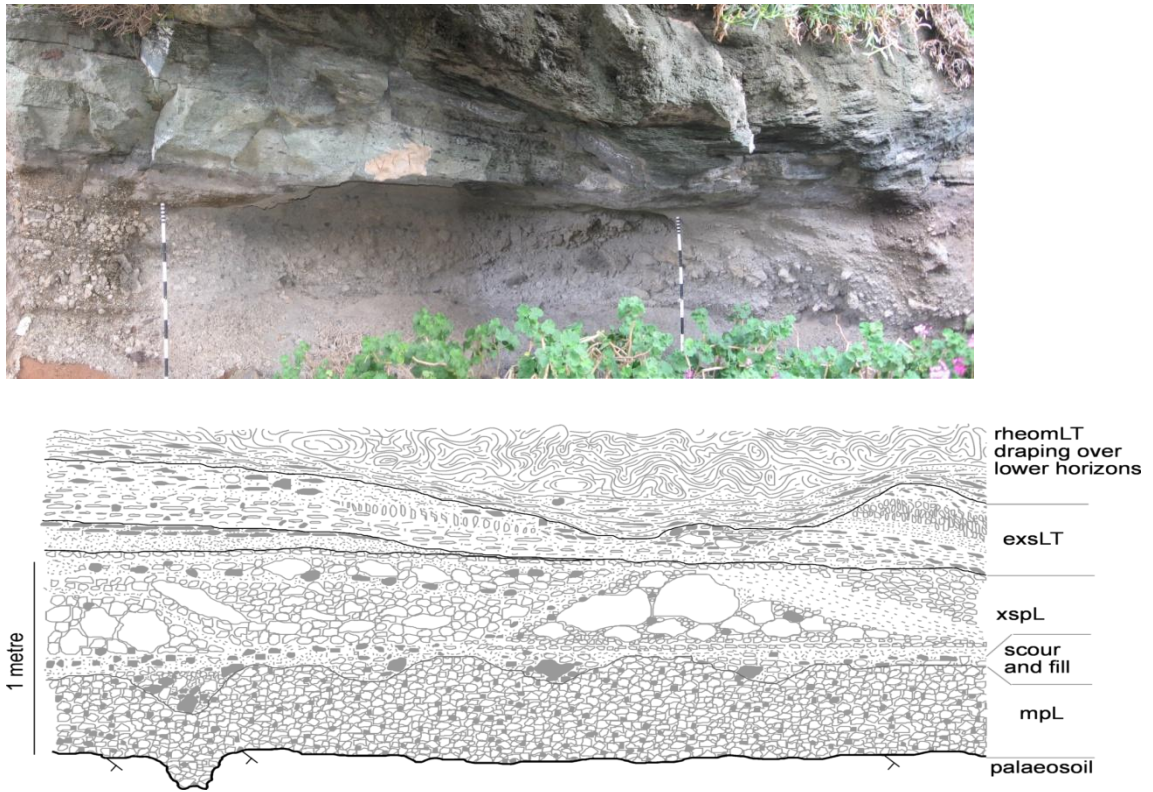


**Fig. 2-8:** Photo and sketch of the massive pumice-lapilli facies (mpL) and the cross-stratified pumice lapilli facies (xspL) with pumice blocks and lithic rich lenses at Bagno dell'Acqua (location 1; Fig. 2-2). Here, it is overlain by eutaxitic, cross-stratified lapilli-tuff (exsLT) which grades vertically into rheomorphic massive lapilli-tuff (rheomLT, 2 m thick, top not shown).

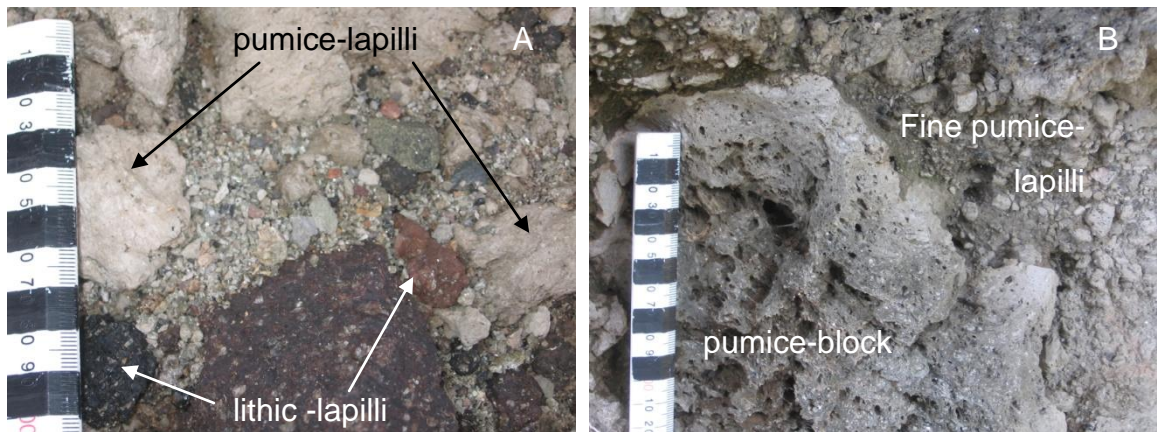


**Fig. 2-9:** The cross-stratified pumice-lapilli facies at Bagno dell'Acqua (location 1; Fig. 2-2). A: Poorly-sorted poly lithic-rich lens in scour and fill. B: Pumice-block in pumice-lapilli. Scale divisions in 1cm.

*Interpretation:* The cross-stratified pumice-lapilli facies has several characteristics of pumice-fall deposits such as clast support, angular pumice and lithic clasts, openwork texture, and it locally grades upwards from the underlying fall deposit. However several features are incompatible with a fallout origin, such as cross-bedding, erosional bases and scours, and the lack of aerodynamic equivalence between adjacent clasts (i.e. lithic-lapilli are not systematically smaller than the pumice-lapilli). This 'hybrid' facies is therefore inferred to represent fallout material that has been subjected to some type of lateral current.

Three possible emplacement mechanisms are considered: (1) aqueous reworking of proximal pumice fall material during the Green Tuff eruption; (2) transport of a pumice-fall by strong winds associated with coeval pyroclastic density currents (e.g. Wilson & Hildreth 1998); and (3) fallout into fully dilute pyroclastic density currents (e.g. Valentine & Giannetti 1995).

The restriction of the cross-stratified pumice-lapilli facies to the proximal caldera rim is an unlikely location for extensive syn-eruption alluvial or aqueous reworking, as there is no catchment or upslope source. The outcrop localities at Bagno dell'Acqua and Cala dei Cinque Denti are at the top of a caldera rim. The bedding of the underlying massive pumice-lapilli facies is horizontal indicating that the local topography at the time of the eruption was horizontal as it is at the present day. Thus, there is no upslope source for the reworked material, and furthermore, there are no outcrops of reworked material further down the slope, as expected if fluvial reworking was the dominant process. Therefore the cross bedding is attributed to pyroclastic processes.

In the Bishop Tuff, California, transport of the pumice-lapilli facies by wind currents associated with coeval pyroclastic density currents are recognised by low-angle cross-lamination without a uniform dip-direction and a wide range of pumice-rounding (Wilson & Hildreth 1998). The hybrid deposits have the same grain size and componentry as the associated normal fall deposits. Scour and fill structures are not observed. The stratigraphic position of the hybrid deposit is associated with deposits from pyroclastic density currents at other locations, indicating that currents activity was coeval with the fallout. However, in the Green Tuff Formation, the componentry of the underlying fall deposit and the hybrid deposit differ: the pumice-fall deposit contains smaller pumice clasts and much smaller lithic clasts (Fig. 2-10), dominated by black

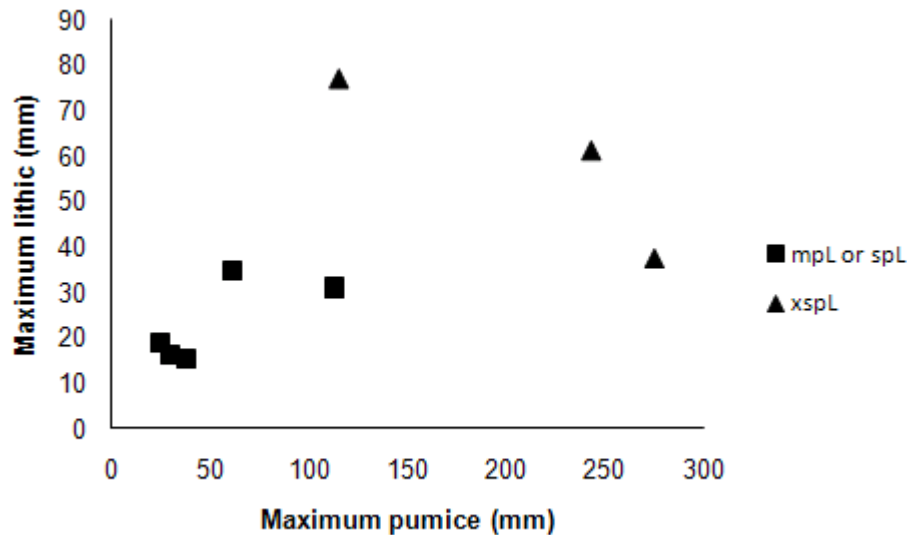


Fig. 2-10: Maximum pumice (mm) versus maximum lithic (mm) for the pumice deposits at four locations (1, 5, 9, 26b; see Table 2-33). mpL – massive pumice-lapilli, spL – stratified pumice-lapilli, xspL – cross-stratified pumice-lapilli.

Table 2-3: Location, UTM and maximum clast data for Fig. 2-10. For facies type code, see text. Maximum clast measurements are an average of 10 measurements, except for first mpL for loc. 9 lithics (only two present).

Location	UTM	Facies Type	Maximum pumice (mm)	Maximum lithic (mm)
9	32s, 0767520, 4079266	mpL	29.88	16.1
9	32s, 0767520, 4079266	mpL	24.78	18.76
9	32s, 0767520, 4079266	xspL	115.24	77.16
5	33s, 0232503, 4079244	mpL	112.79	31.15
1	32s, 0766375, 4079104	mpL	38.11	15.39
1	32s, 0766375, 4079104	spL	61.41	34.83
1	32s, 0766375, 4079104	xspL	243	61.2
26b	32s, 0766223, 4079739	xspL	275	37.23

scoria, whereas the cross-stratified deposit has a wider size range of clast compositions with larger maximum pumice and lithic clasts (Fig. 2-9; Fig. 2-10). Thus, an origin simply by clear-air reworking of the preserved pumice-fall deposit is unlikely. Other differences include higher angle of cross-stratification in the Green Tuff compared to the Bishop Tuff, the presence of scour and fill structures, not observed in the Bishop Tuff and a lack of coeval pyroclastic density current deposits.

The most likely scenario is that the eruption column waxed, providing larger pumice and lithic clasts. Very proximal fallout is sometimes less well sorted (Houghton *et al.* 2004) and as these clasts fall from the plume, fully dilute, turbulent currents passed by adding a vigorous lateral velocity component (e.g. Valentine & Giannetti 1995). These proximal turbulent currents did not travel far because the deposits are not longitudinally extensive and are absent at more distal locations. I propose that the cross-stratified pumice-lapilli facies is a hybrid deposit formed by the modification of very proximal fallout by short-lived ephemeral density currents on the proximal caldera rim. Similar hybrid fall/flow deposits are recorded in the Zaragoza ignimbrite at the Protreros caldera rim, Mexico (Branney & Willcox, pers. com) and in the caldera rim deposits of the Poris Formation, Tenerife (Smith, pers. com).

### 2.3.3. Massive ash (mT)

#### *Fines-rich mT*

*Description:* The massive ash (mT; Fig. 2-11), facies is a non-welded, fines-rich, juvenile ash layer. It is typically very thin <10 cm .

*Occurrences and associations:* The massive ash facies does not outcrop at many locations. It occurs within the basal part of the Green Tuff Formation in more distal places and at localities where the massive pumice lapilli deposit is absent. It is particularly well exposed along road-cut sections near Sataria (location 114; Fig. 2-2). At this location it overlies the coarser, crystal-rich massive tuff described below.

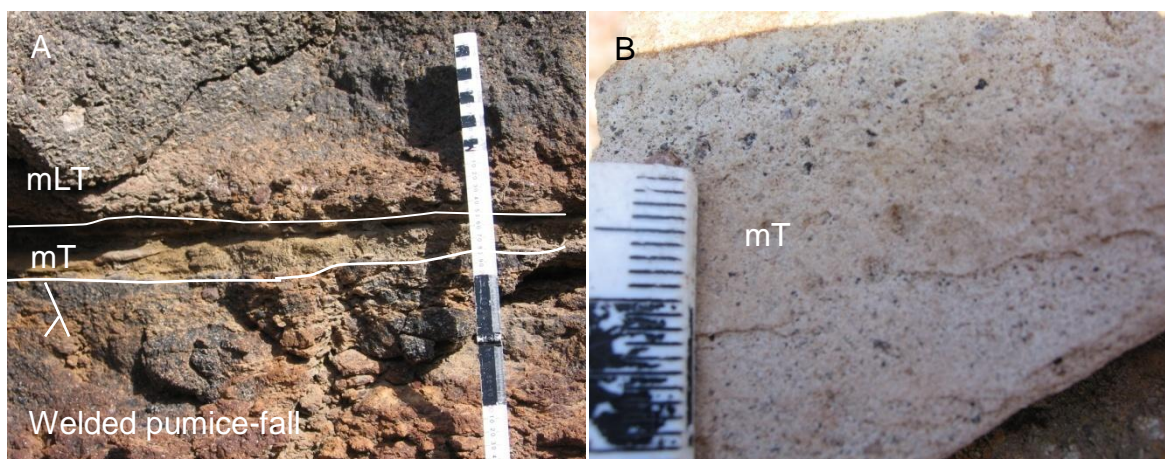


**Fig. 2-11A:** Thin tuff (mT) at the base of the Green Tuff ignimbrite (mLT; 1.5 m thick, top not shown) where it overlies an older welded pumice fall deposit near Sataria (location 114; Fig. 2-2 ). **B:** Close-up of the fines-rich tuff (mT) at Sataria. Small scale divisions in 1cm.

*Interpretation:* The massive ash facies is interpreted as an ash-fall deposit on the basis of exceptional good sorting, lack of sedimentary features suggesting lateral transport (e.g. imbrication, cross bedding, scours) and its occupation of the same stratigraphic position as the proximal pumice fall.

### ***Crystal-rich MT***

*Description:* The crystal-rich massive ash facies (Fig. 2-12) is a non-welded, crystal-rich coarse ash layer. It is typically very thin (< 5 cm) and is vertically graded to a fine ash.

*Occurrences and associations:* The crystal-rich massive ash facies only occurs near Sataria (location 114; Fig. 2-2) where it is preserved under the massive ash facies.

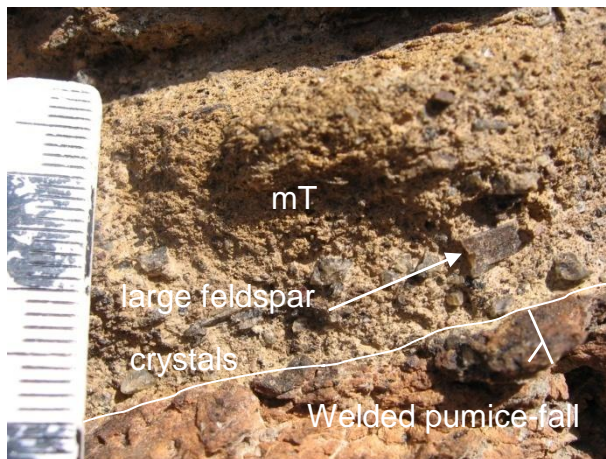


**Fig. 2-12: : Coarse, crystal rich tuff at the base of the Green Tuff ignimbrite (mLT, 1.5 m thick, top not shown) near Sataria (location 114; Fig. 2-2). Scale divisions in 1cm.**

*Interpretation:* The crystal-rich massive ash facies is interpreted as an ash-fall deposit on the basis of exceptional good sorting, lack of sedimentary features suggesting lateral transport (e.g. imbrication, cross bedding, scours) and its occupation of the same stratigraphic position as the proximal pumice fall. It is interpreted to represent a coarse facies of the massive ash facies described above. The limited occurrences of this facies mean that any interpretation on its origin is uncertain.

### ***Lithic-rich MT***

*Description:* The lithic-rich massive ash facies (Fig. 2-13) is a non-welded, well sorted, fines-poor, coarse ash layer which is rich in sand-sized lithic clasts (1-5 mm).

*Occurrences and associations:* The lithic-rich massive ash facies is observed at a handful of locations and is best exposed at the quarry near Pantelleria Town where it is the lateral equivalent of a fines-poor lithic-rich lens at the base of the massive lapilli-

tuff and at Monastero (location 86; Fig. 2-2). It occurs at the base of massive lapilli-tuff, described below.

*Interpretation:* The lithic-rich massive ash facies is here interpreted to be a fine-grained, fines-poor facies of the massive lapilli-tuff, which is a deposit from a pyroclastic density current. Fines-poor lithofacies at the base of ignimbrites are a common feature and have previously been termed a ‘ground layer’ (*sensu* Walker *et al.* 1981a). This term specifically related to deposits thought to have been sedimented from a fluidised ‘flow head’ where ingestion of cold air at the front of a pyroclastic density current results in expansion, turbulence and a loss of fines. However, other mechanisms for the emplacement of a fines-poor, coarse ash deposit include turbulent winnowing around the lower flow boundary, granular segregation, elutriation associated with vigorous sedimentation or by deposition from a current that contained little ash (Branney & Kokelaar 2002). The limited outcrop of this facies in the Green Tuff Formation does not permit a detailed interpretation on its origin.

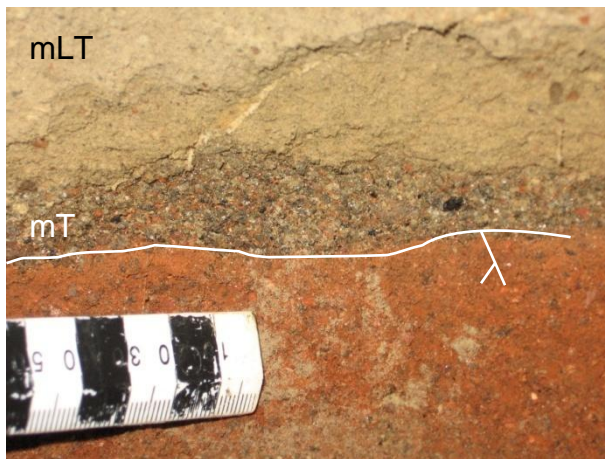


**Fig. 2-13: Lithic-rich tuff (mT) at the base of the massive lapilli-tuff (mLT; 5 m thick, top not shown) at Monastero Scarp (location 86; Fig. 2-2). Scale divisions in 1cm.**

#### **2.3.4. Massive lapilli-tuff (mLT and emLT)**

*Description:* The massive lapilli-tuff (mLT) facies is a poorly sorted, matrix-supported lapilli-tuff with abundant sub-rounded juvenile and few sub-rounded lithic clasts supported in a pistachio-green or beige ash matrix (Fig. 2-14). The juvenile component ranges from glassy, black fiamme to vesiculated clasts with scoriaceous textures. Lithic lapilli are typically < 10 cm and are red or grey. Fiamme and lithics are often

imbricated. The deposit is typically massive and in places is inverse graded (Fig. 2-14A). The massive lapilli-tuff is commonly welded (emLT; Fig. 2-14B), particularly in its upper parts, and only contains fiamme juveniles and not scoriaceous juveniles.

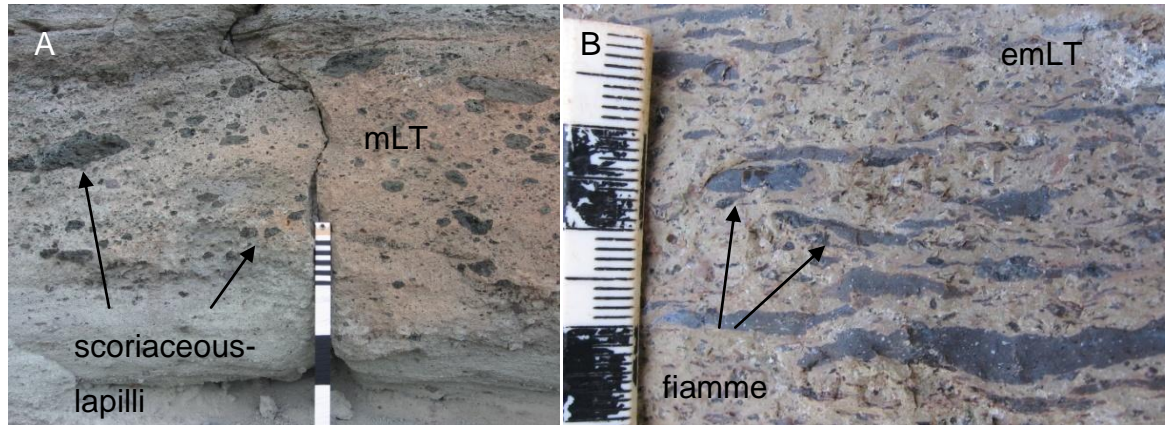


**Fig. 2-14A:** Massive lapilli-tuff (mLT) at Bagno dell' Acqua (location 1; Fig. 2-2) showing vesicular juvenile lapilli (scoriaceous texture) in a fine-grained, pistachio green, weakly welded tuff matrix. **B:** Eutaxitic massive lapilli-tuff (emLT) showing black, glassy fiamme in a fine-grained, welded tuff matrix. Small scale divisions in 1cm.

*Occurrences and associations:* The massive lapilli-tuff facies locally overlies the massive pumice-lapilli facies and cross-stratified pumice-lapilli facies and grades upwards into parallel-bedded eutaxitic lapilli-tuff (Section 2.3.6) which overlies it. It is the most abundant facies of the Green Tuff Formation, accounting for about 90 % of the deposit across the island. It can reach thicknesses of up to 20 m.

*Interpretation:* The massive lapilli-tuff deposit is interpreted to be the deposit from a pyroclastic density current on the basis of the very poor-sorting, local imbrication, juvenile component, and local gradations into diffuse cross-stratified lapilli-tuff (Section 2.3.5). The poor sorting and massive nature indicates rapid progressive aggradation from a high-concentration granular fluid-based pyroclastic density current in which turbulent winnowing and traction were suppressed by high particle concentrations (Branney & Kokelaar 2002; Girolami *et al.* 2010; Vrolijk & Southard 1997). The upwards increase in grain size through the deposit indicates a waxing capacity of the current. Adjacent fiamme and non-flattened scoriaceous lapilli suggest that at least some of the fiamme have not formed through flattening. Obsidian cobbles and obsidian fiamme may be rags of non-vesiculated magma as seen in other ignimbrites (e.g. Onano Formation, Vulcini; Palladino & Simeì 2002).

### 2.3.5. Diffuse stratified and cross-stratified lapilli-tuff (dsLT and dxsLT)

*Description:* The diffuse stratified and cross-stratified lapilli-tuff comprises sub-rounded juvenile and lithic clasts in a pistachio-green or beige ash matrix. The facies is poorly sorted, matrix-supported and can be either diffusely stratified (dsLT, Fig. 2-15A), or diffusely cross-stratified (dxsLT, Fig. 2-15B). This facies grades both vertically and laterally into massive lapilli-tuff (Fig. 2-15B). Juvenile clasts may be either black, glassy fiamme, or scoriaceous clasts. Lithic lapilli are small (< 10 cm), red or grey clasts.

*Occurrences and associations:* The diffuse stratified or cross-stratified lapilli tuff is a local facies to the massive lapilli-tuff, into which it grades from both vertically and laterally. It is best exposed along the Kattibucale Scarp.

*Interpretation:* The diffuse stratified and cross-stratified lapilli-tuff deposit is interpreted to be the deposit from a pyroclastic density current on the basis of the very poor-sorting, local imbrication, juvenile component, and diffuse cross-stratification. A lateral or vertical gradation from the massive lapilli-tuff to diffuse stratification and cross-stratification indicates current unsteadiness and periods of fully dilute turbulence with fluctuations in grain size (Branney & Kokelaar 2002).

### 2.3.6. Parallel-bedded eutaxitic lapilli-tuff (//beLT)

*Description:* The parallel-bedded eutaxitic lapilli-tuff facies (Fig. 2-16A) is lithic poor, typically very poorly sorted, matrix-supported lapilli-tuff rich in black fiamme, which are commonly imbricated in a pistachio-green matrix, Lithic clasts are rare. It is strongly welded (eLT, Fig. 2-1, Fig. 2-5) and is locally parallel-bedded (//beLT, Fig. 2-4, Fig. 2-16A) with a distinctive fiamme-bed that is better sorted than the other beds (Fig. 2-16B) and is almost clast supported by black, glassy fiamme which occasionally show an imbrication. This bed is sometimes so strongly welded in places to the extent of forming a vitrophyre (//bveLT, Fig. 2-4; Fig. 2-17). Locally, the fiamme-bed laterally grades into a weakly-welded (sintered), open-work lapilli-tuff with pumice clasts that show point-contact welding (Fig. 2-17).

Above the fiamme bed, the eutaxitic lapilli-tuff becomes sheet jointed (jeLT, Fig. 2-1). This slab-like appearance is due to very elongated vesicles. The fiamme in this horizon

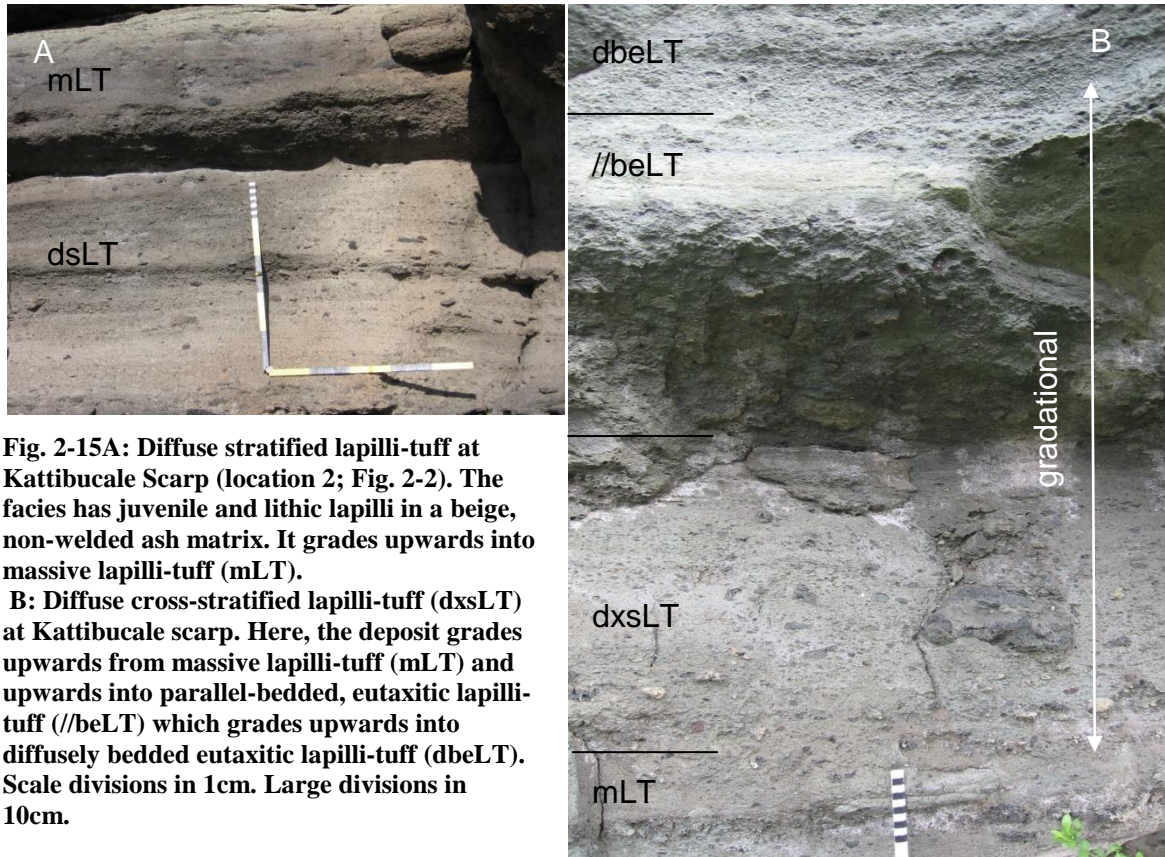


**Fig. 2-15A:** Diffuse stratified lapilli-tuff at Kattibucale Scarp (location 2; Fig. 2-2). The facies has juvenile and lithic lapilli in a beige, non-welded ash matrix. It grades upwards into massive lapilli-tuff (mLT).

**B:** Diffuse cross-stratified lapilli-tuff (dxsLT) at Kattibucale scarp. Here, the deposit grades upwards from massive lapilli-tuff (mLT) and upwards into parallel-bedded, eutaxitic lapilli-tuff (//beLT) which grades upwards into diffusely bedded eutaxitic lapilli-tuff (dbeLT). Scale divisions in 1cm. Large divisions in 10cm.

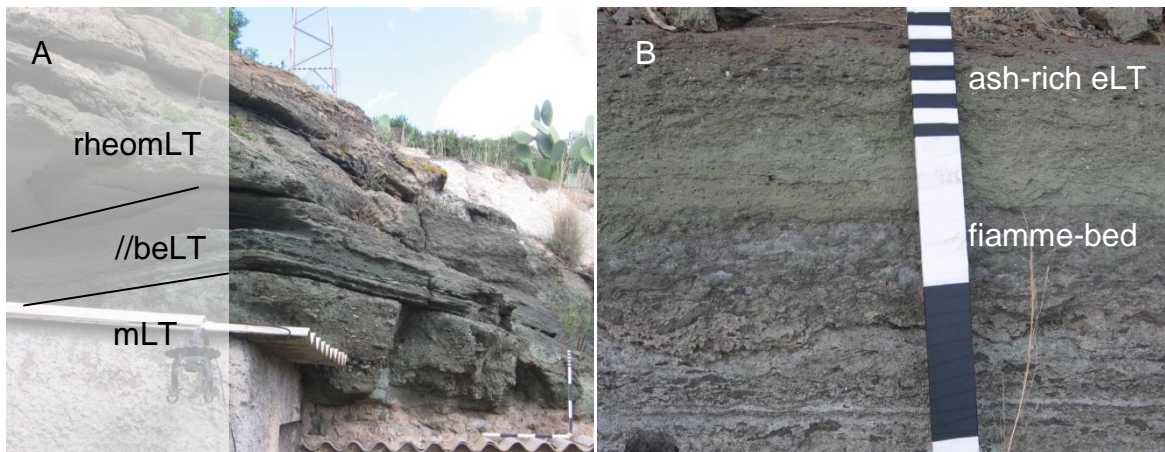


**Fig. 2-16A:** Distinctive parallel-bedded, eutaxitic lapilli-tuff (//beLT) facies at Bagno dell' Acqua (location 1; Fig. 2-2). Here, the contacts are quite sharp, elsewhere they are gradational. **B:** Varying grain size seen in parallel-bedded, eutaxitic lapilli-tuff (//beLT) from fiamme rich, to ash-rich eutaxitic lapilli-tuff. Large scale divisions in 10cm.

are also very elongate and some are vesicular with abundant round vesicles. The vesicles and fiamme are inclined relative to bedding at some locations.

*Interpretation:* The eutaxitic lapilli-tuff facies is interpreted to be a parallel-bedded ignimbrite due to the abundant juveniles (fiamme), ash-matrix and poor sorting. Imbricated clasts show that this unit was predominantly a deposit from a pyroclastic density current rather than a pyroclastic fall. The eutaxitic texture indicates that this unit is strongly welded, compared to the underlying lapilli-tuff. The parallel-bedding, which is only laterally continuous along the Cinque Denti scarp, may record current unsteadiness within the lower flow-boundary of a current, that was transitional between granular flow-dominated and fluid-escape dominated flow (Branney & Kokelaar 2002). The bedding is interpreted to represent abrupt changes in sedimentation during a single, sustained current, rather than emplacement by multiple currents. The parallel-beds are not laterally continuous, do not show inverse grading typical of flow-units and there is a lack of evidence for a pause in the current between beds such as co-ignimbrite ash fall or pumice fallout layers or reworked sediment. This does not favour an interpretation of multiple-flow units, however the possibility of pauses cannot be excluded.

It is possible that this horizon represents 'Member C', the "fall or surge" horizon of Orsi & Sheridan (1984) but it does not trace widely around the island, and is not interpreted here as a 'surge' due to the absence of tractional stratification, dune-form or cross-bedding, normally diagnostic of surge deposits (Cas & Wright 1987). The fiamme-bed could represent the "pumice fall bed" inferred to be part of 'Member C' (Orsi & Sheridan 1984). It is typically fiamme rich, is lenticular and is matrix-supported with a green tuff abundant between clasts. However, when this bed is intensely welded to a vitrophyre (Fig. 2-17) it is not possible to distinguish clasts from matrix. Near Cala dei Cinque Denti (location 9; Fig. 2-2), the fiamme bed is weakly welded, as the deposit appears openwork with sintering occurring between pumice lapilli (Fig. 2-16). However a pumice-rich, fines-depleted facies does not necessarily represent a pumice-fall origin and could be a welded pumice concentration such as common in ignimbrites elsewhere (e.g. Branney & Kokelaar 2002; Pittari *et al.* 2005) formed by segregation of pumice by a pyroclastic density current. This interpretation is consistent with an unsteady current with a transitional (granular to fluid-escape dominated) flow-boundary zone.

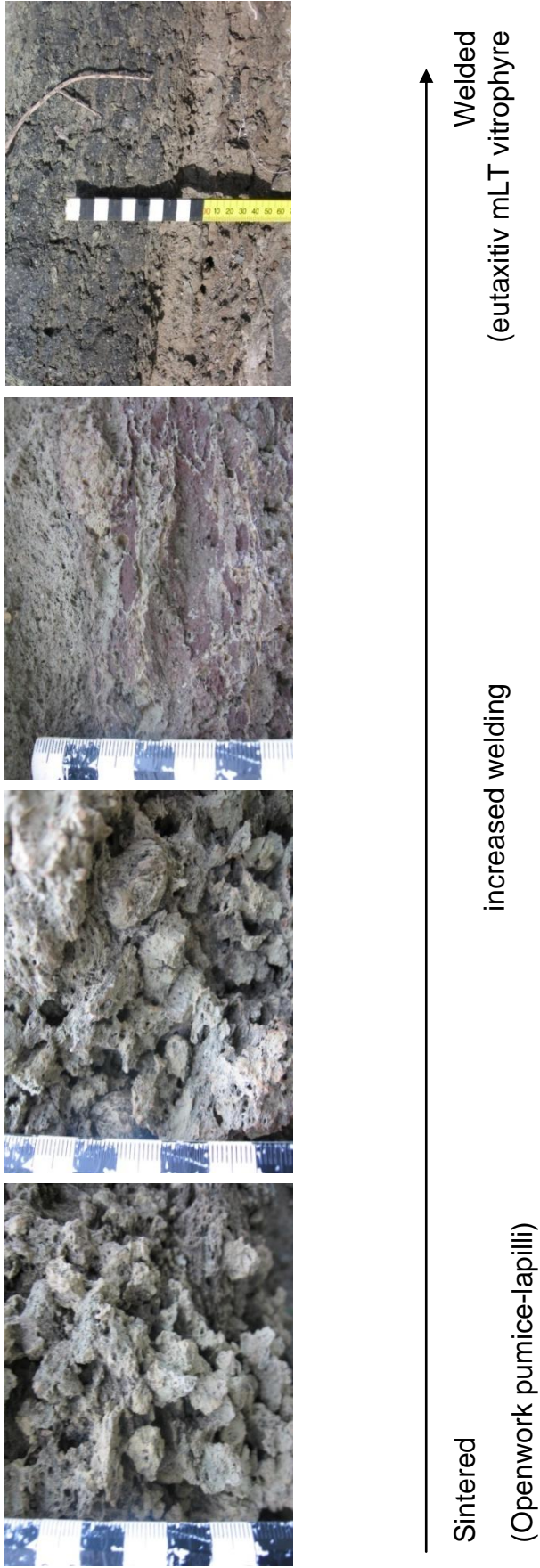


**Fig. 2-17: Rare, localised openwork pumice-lapilli facies in the Green Tuff ignimbrite that grades laterally into a welded fiamme-bed. Varying degrees of welding occurs laterally along 15 m section from sintered, point-contact welding to vitrophyric where fiamme and matrix are welded together into glass. Near Cinque Denti (location 9; Fig. 2-2). Scale divisions in 1cm.**

The presence of spherical vesicles in strongly flattened fiamme records late-stage exsolution and revesiculation. The elongate vesicles which grade into sheet-like joints represent vesiculation during rheomorphic flow (Andrews & Branney 2010; Pioli & Rosi 2005). The species of the gas responsible for the late-stage vesiculation is unknown. Pantellerites have the highest chlorine concentrations of any igneous rocks (Barclay *et al.* 1996; Lowenstein 1994) and chlorine or fluorine may have been involved (see Section 2.4.7).

### **2.3.7. Rheomorphic massive lapilli-tuff (rheomLT)**

*Description:* The rheomorphic massive lapilli-tuff is well foliated, lithoidal or vitrophyric eutaxitic lapilli-tuff with abundant crystal fragments, black, glassy fiamme and local lenses of lithic lapilli and blocks (Fig. 2-5). It is poorly-sorted and matrix-supported. In the north of the island, this horizon contains abundant grey lapilli which appear to be derived from an underlying ignimbrite. These lithic lapilli are grey, crystal-rich and have a tuff matrix. Welding and rheomorphism locally affect the entire deposit, except for the basal pumice fall if present, even when thin (Fig. 2-18A).

Degrees of rheomorphism change from eutaxitic with extremely stretched fiamme and vesicles to chaotically folded (Fig. 2-18B). A description of the particular rheomorphic features seen in the Green Tuff ignimbrite are given in Section 2.4. Foliation planes are often strongly lineated. Lineations radiate out from an inferred source location, except where the dip of local palaeoslopes are at a high angle to the inferred regional current direction. Here lineations often have a down-slope component. The rheomorphism does not obliterate primary structures in the massive lapilli-tuff. Even when it is folded, it is possible to see grain size changes, lithic rich-lenses and diffuse bedding.

*Occurrences and associations:* The rheomorphic massive lapilli-tuff facies is widespread and occurs island-wide (Fig. 2-1). It is found draped on slopes of up to 90° (Fig. 2-18C), including inward dipping slopes on the Zinedi, Kattibucale and Cinque Denti caldera scarps (Fig. 2-2).

The rheomorphic lapilli-tuff facies grades vertically from the eutaxitic massive lapilli-tuff facies or the rheomorphic lithic breccia (Section 2.3.8).

*Interpretation:* The rheomorphic massive lapilli-tuff facies is interpreted to be an ignimbrite on the basis of its poor-sorting, large thickness variation from <1 m on valley

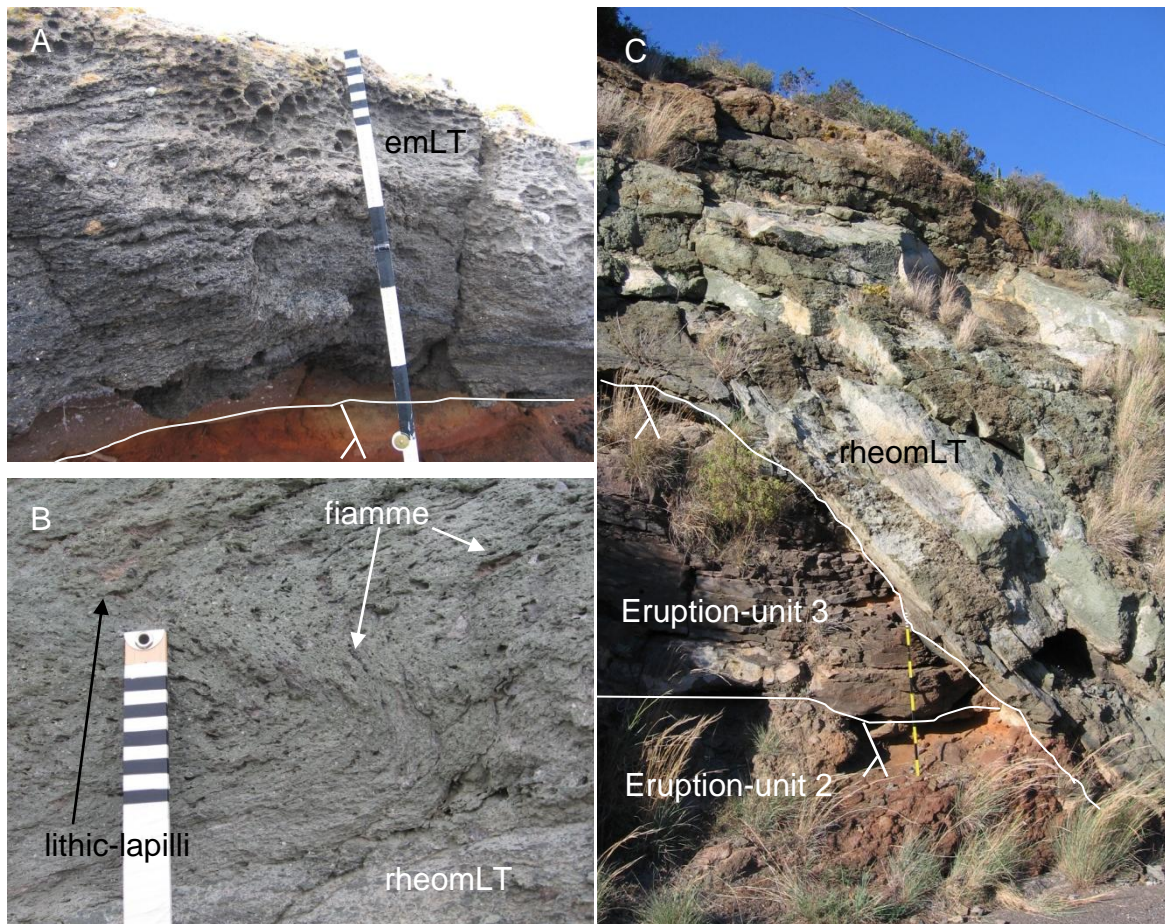


**Fig. 2-18A:** The Green Tuff ignimbrite is welded even when thin. This photo shows eutaxitic massive lapilli-tuff (emLT) which is less than 50 cm thick. **B:** Primary textures and fabrics are not obliterated in the Green Tuff ignimbrite even when it is rheomorphic. This photo shows an s-fold in rheomorphic massive lapilli-tuff (rheomLT). It is possible to see fiamme (which have a continuous size and shape through the fold), lithic lapilli supported in a green matrix. **C:** The Green Tuff ignimbrite drapes slopes. Here, the rheomorphic massive lapilli-tuff facies (rheomLT) has been deposited onto the Kattibucale scarp (location 15, Fig. 2-2). Angle of basal contact is typically  $45^\circ$  but can be up to  $80-90^\circ$ . The base of the rheomLT here is vitrophyric and drapes over successively older ignimbrites (Eruption-units 1-3 of Chapter 6; drape onto Eruption-unit 1 not shown). Small scale divisions in 1cm. Large scale divisions in 10cm.

sides to  $>20$  m in valleys, vertical and lateral coarse-tail grading, gradations into facies that record deposition from a current such as diffuse cross-stratified lapilli-tuff, imbrication of fiamme clasts which are supported in a fine-ash matrix. These features (Table 2-1) variation of the massive lapilli-tuff (and eutaxitic massive lapilli-tuff)

which is an ignimbrite deposited from a pyroclastic density current. The strain exerted upon the increasingly trachytic deposit increased upwards through the deposit thickness.

The welding profile of the Green Tuff ignimbrite is not typical of compaction welding. The ignimbrite is welded to the top of the unit (Fig. 2-1) and, even when thin ( $<50$  cm),

the unit can be completely welded. Welding by agglutination during deposition is the preferred explanation for the mode of emplacement (Branney & Kokelaar 1992; Freundt 1998, 1999).

The shear induced onto a progressively aggrading agglutinate deposit by an over-riding current would cause rheomorphism of that deposit. As the deposit aggrades, the shear-zone would migrate upwards (Andrews & Branney 2010) as recorded by pervasive shear fabrics through the deposit thickness such as micro-folds and imbrication. The rheomorphism in the Green Tuff ignimbrite rarely affects the entire deposit; rather it occurs on a small scale with deposit-scale folding occurring only very locally. This indicates that the large thickness variations observed (from 1 m to up to 20 m) are not reconcilable with rheomorphic flow alone. Furthermore, micro-scale rheomorphism is not sufficient to ‘stir up’ the chemical zonation of the deposit (Chapters 3 and 4).

### **2.3.8. Lithic breccia (lBr)**

*Description:* The lithic breccia facies is a polyolithic, matrix-supported, poorly sorted lithic breccia with clasts up to 60 cm in diameter (Fig. 2-19A). The tuff matrix is strongly welded and rheomorphic (Fig. 2-19A), and commonly the lithic breccia is clast-supported (Fig. 2-19B). Foliations are deformed around individual lithic clasts. The rheomorphic lithic breccia contains a variety of clasts: (1) juvenile (cognate) clasts such as obsidian; (2) accessory clasts such as coarse-grained, crystalline intrusive (Fig. 2-19C); and (3) accidental clasts of local lithologies. Many of these lithic clasts show curvilinear fragmentation inferred to record thermal spalling (Fig. 2-19D).

A predominantly monolithic, locally-derived lithic breccia commonly occurs at the base of the Green Tuff ignimbrite in palaeovalleys, where clasts are mostly accidental clasts from local lithologies (e.g. scoria from local scoria cone). This type of locally derived lithic breccia occurs island-wide and is considered a separate lithofacies to the one considered here.

*Occurrences and associations:* The polyolithic, lithic breccia facies is most abundant along the Monastero caldera scarp (location 44; Fig. 2-2;) where it is best exposed and up to 1 m thick (Fig. 2-5). It is common as lithic-rich lenses in exposures along the western coastline. It vertically grades from the eutaxitic massive lapilli-tuff or rheomorphic massive lapilli-tuff. Away from proximal locations, it commonly occurs as lithic rich lenses or pods.

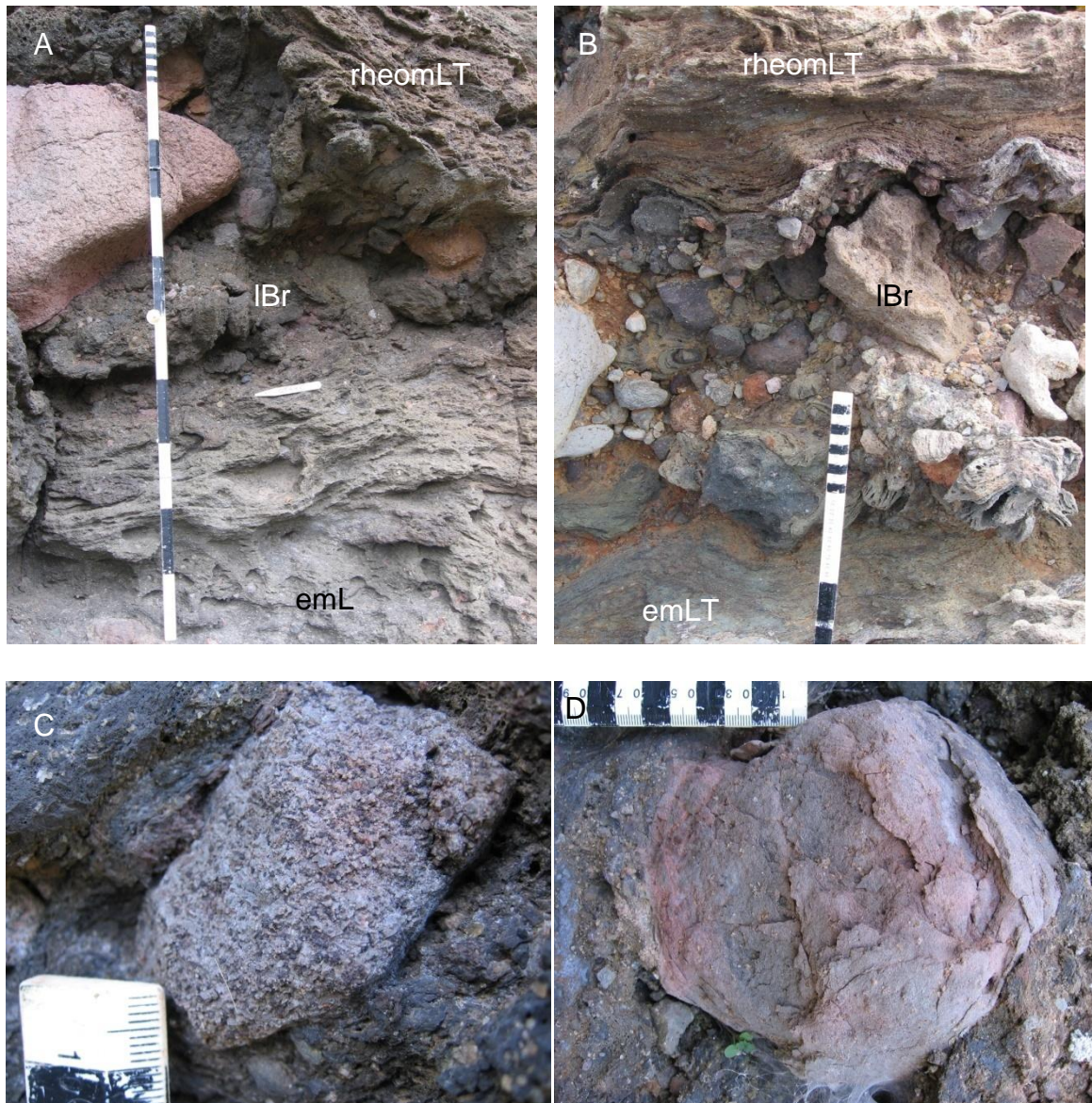


**Fig. 2-19A:** Lower 50 cm of the lithic breccia (IBr) at Monastero Scarp (location 44; Fig. 2-2) with blocks up to 60 cm in diameter, vertically grading from eutaxitic massive lapilli-tuff (emLT) and into rheomorphic massive lapilli-tuff (rheomLT). Here it is fines-rich and matrix-supported in places. **B:** Polyolithic lithic breccia lens (IBr) near Scauri (location 71; Fig. 2-2). The lens is contained in rheomorphic massive lapilli-tuff (rheomLT). Lithic breccia is clast supported. **C:** Coarse-grained, crystalline accessory clasts **D:** Curvilinear-fragmentation of fresh lithic inferred to record thermal spalling due to expansion and contraction. Small scale divisions in 1cm. Large scale divisions in 10cm.

*Interpretation:* The lithic breccia is interpreted to be a coarse facies of the rheomorphic massive lapilli-tuff, which bounds it, and grades into it. The baked and thermally-spalled clasts indicate that they were emplaced hot and imbrication of clasts indicates that they were emplaced by flow.

Lithic breccias are common in ignimbrites and may be derived from source (e.g. Druitt & Bacon 1986) or be entrained from substrate during pyroclastic density current transport (e.g. Buesch 1992).

Whilst many similarities of this facies are shared with classic ‘co-ignimbrite lag breccias’ this term is not applied here due to its specific genetic connotation. Deposition from rapid fall from an eruption column in a ‘proximal deflation zone’ (e.g. Walker 1985) is discounted due to imbrication which records a lateral velocity only possible by flow. The absence of impact structures and the persistence of the breccia to distal locations where it grades into and out of rheomorphic lapilli-tuff as lenses and pods further discounts emplacement as a lag-breccia.

The poly lithic nature of the breccia, and the presence of plutonic lithologies, suggests that these breccias are not merely the result of incorporation of local lithologies. Rather, the abundance of coarse-grained, altered and fresh crystalline clasts suggests that a component of the breccia was sourced from within the volcano, for example, from erosion or collapse of the eruption conduit walls. Breccia emplacement has often been related to the onset of caldera collapse (e.g. Druitt 1985) during an eruption. Caldera collapse would lead to increased discharge rate, and erosion of the collapsing roof materials and/or vent walls and this would introduce abundant lithic blocks into the current from a variety of depths and lithologies. It is likely therefore, that the rheomorphic lithic breccia in the Green Tuff ignimbrite records some degree of caldera collapse. However, distribution of the lithic breccia is limited to the west of the island and is only relatively thin (up to 1m). This may suggest that the caldera ‘collapse’ was only partial, i.e. reactivation along one or two fault scarps during this stage of the eruption rather than piston-style caldera collapse. This theme is revisited in Chapter 5

The local, monolithic breccias seen at the base of the Green Tuff ignimbrite are here interpreted to be a locally-derived breccia as their assemblage matches the local substrate.

#### **2.4. Welding and rheomorphism of the Green Tuff Formation**

This section is not intended as a detailed study of the rheomorphism of the Green Tuff Formation. Rather, it documents the variety of features in the Green Tuff ignimbrite and offers some simple interpretations. Further study of these features, and a structural study with detailed analysis of the temperature, viscosity and halogen content of the Green Tuff ignimbrite would prove to be an interesting and worthwhile future endeavour,

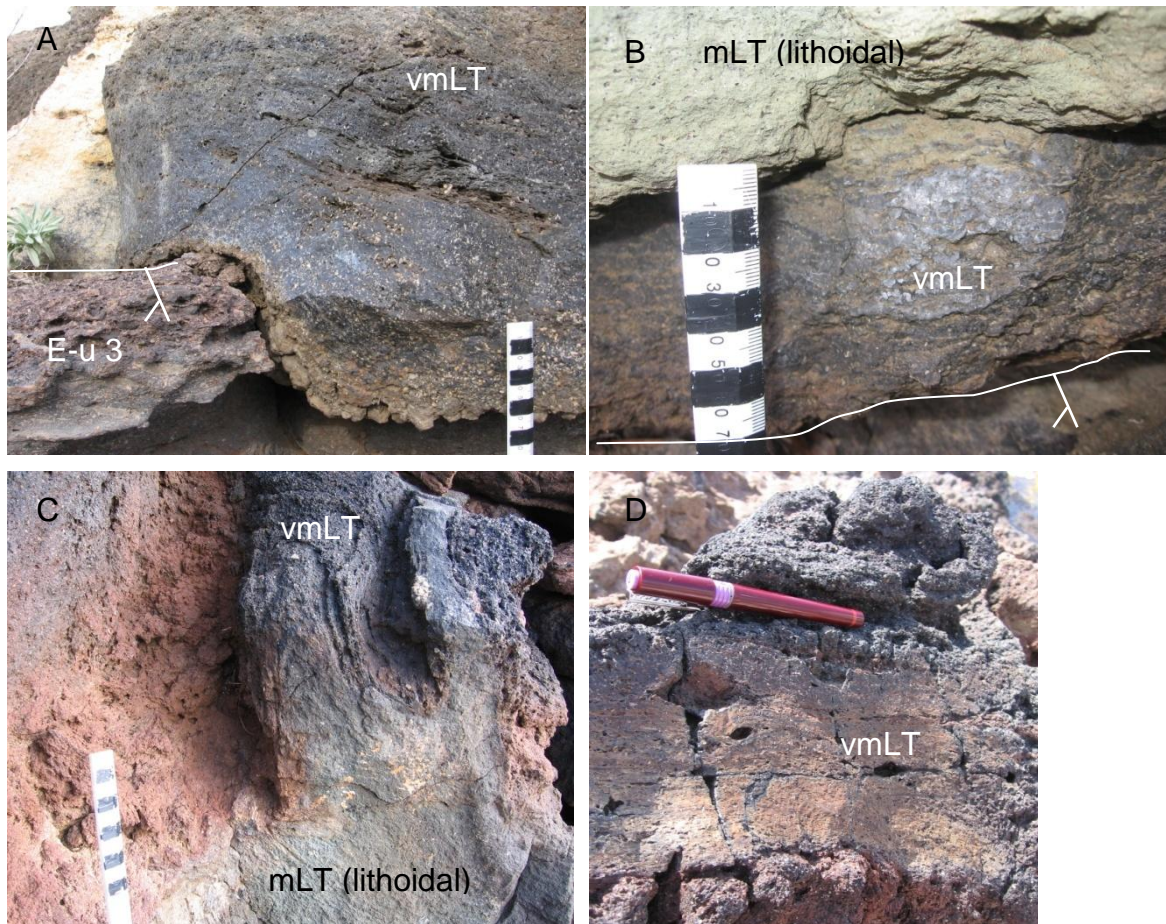


**Fig. 2-20.** Upper and lower vitrophyre of the Green Tuff ignimbrite. The upper vitrophyre is an important marker for the top of the unit. **A:** Basal vitrophyre (vmLT) in undulating contact with Eruption-unit 3 (E-u 3). **B:** Basal vitrophyre (vmLT) grading into pistachio green massive lapilli-tuff (mLT) **C:** Upper folded surface of Green Tuff ignimbrite. Note that the outer surface is vitrophyric (mLT) and the body of the ignimbrite is lithoidal (mLT). **D:** Upper vitrophyre. Scale divisions in 1cm.

particularly in light of recent advances in understanding rheomorphic ignimbrites (Andrews & Branney 2010; Andrews & Branney 2005; Pioli & Rosi 2005).

#### 2.4.1. Vitrophyres

In the absence of a pumice-lapilli deposit or ash-tuff, the base of the Green Tuff ignimbrite is commonly defined by a basal vitrophyre (Fig. 2-20A). Typically, this vitrophyre is black, fiamme-rich and remains glassy (Fig. 2-20B). An upper vitrophyre is also preserved at the top of the Green Tuff ignimbrite at some locations (Fig. 2-20D). It is typically folded and auto-brecciated and sometimes is dark red in colour (Fig. 2-20C).

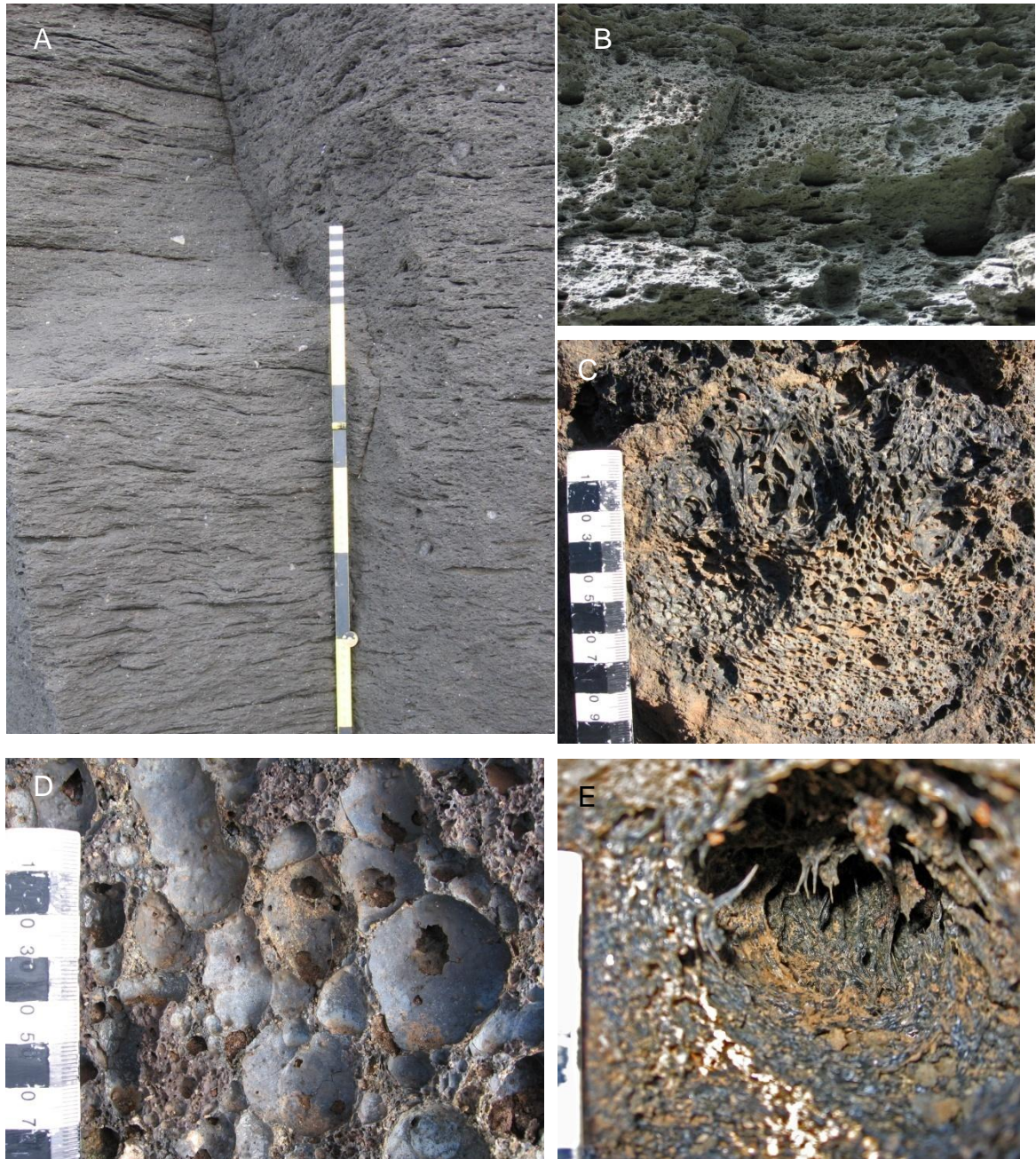


**Fig. 2-21. Vesiculation types seen in the Green Tuff ignimbrite. A: Stretched vesicles which formed and were deformed syn-depositionally. These can define a lineation and foliation. B: Frothy vesicular texture in the upper horizons. The round vesicles indicate that the vesiculation occurred after compression. C: Vesiculated obsidian fiamme. The round vesicles indicate that vesiculation occurred after compression.**

Significant post-rheomorphism vesiculation is observed in the trachytic end-member of the deposit, indicating late-stage exsolution of a gas species. The structures seen in the following photos also indicate a low-viscosity of the deposit as it vesiculated. D: Bubble walls preserved in vitrophyre E: Stringy glass in vesicle cavity.

Small scale divisions in 1cm. Large scale divisions in 10cm.

### ***Interpretation***

Vitrophyres occur when the hot pyroclastic particles have rapidly chilled against either the substrate at the first instant of deposition, or against the air after the pyroclastic density current had ceased.

#### **2.4.2. Fiamme and vesicles**

Fiamme are abundant in all the welded horizons. They are typically small (up to 5 cm in length), black or brown, and show characteristic flame edges (Fig. 2-14B). At some locations, the fiamme are stretched and can be traced for several meters. However, some fiamme can also have a ‘bomb’-like shape, be well rounded, flat and are made of fresh glass.

Vesicles are common in the welded horizons (Fig. 2-21A). They are typically a similar size to the fiamme (up to 10 cm) but can also be stretched to beyond several centimeters in length, whilst only a couple of mm high. The upper horizons of the ignimbrite can be very vesicular with an almost frothy appearance (Fig. 2-21B). At some locations it is possible to see very vesiculated regions of vitrophyre (Fig. 2-21C), remnants of bubbles (Fig. 2-21D), and occasionally cavities with ‘strings’ of glass (Fig. 2-21E).

Fiamme and vesicles can both contain abundant spherical vesicles despite large flattening ratios. They are also commonly imbricated (Fig. 2-22).

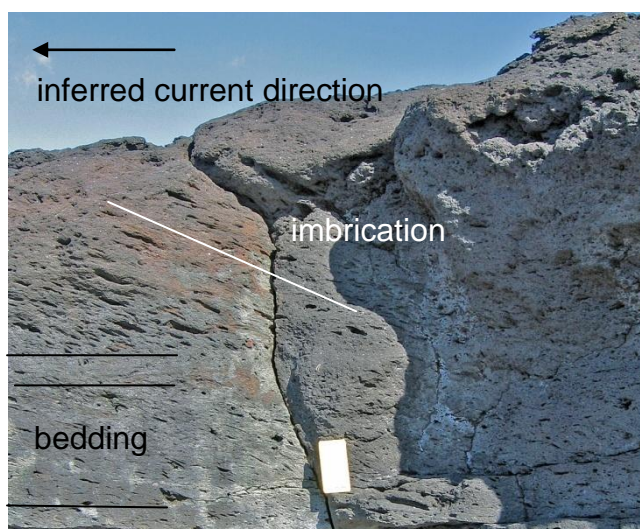


**Fig. 2-22: Inclined vesicles and fiamme in a tuff matrix. Inclined clasts are interpreted to be a form of imbrication. Inferred current direction is from right to left. Notebook for scale.**

### ***Interpretation***

Fiamme are a common feature of welded ignimbrites and are likely to be flattened lapilli due to either ‘load’ welding (Peterson 1979; Smith 1960) or due to a very low viscosity enabling clasts to flatten and agglutinate in the absence of a load strain (Branney & Kokelaar 1992; Capaccioni & Cuccoli 2005; Freundt 1998, 1999). The clasts could be pumice-lapilli in the case of the characteristic flame-textured fiamme, or blebs of hot magma or spatter in the case of the obsidian bombs. Load welding is discounted here due to persistent welding and eutaxitic texture in even the thinnest occurrences of the ignimbrite (~ 20 cm).

Abundant vesicles in the ignimbrite show that the deposit was gas-rich, and this is common for other rheomorphic ignimbrites (Andrews & Branney 2010; Schmincke & Swanson 1967). Spherical bubbles show that there was significant post-rheomorphism vesiculation. As previously discussed, the exact species of gas is unknown. The stringy glass seen inside vesicle cavities suggests that when re-vesiculation occurred, the deposit had a very low viscosity and behaved almost like a Newtonian fluid (Andrews, pers. com.).

The inclined fiamme and vesicles are here interpreted to be a form of imbrication, despite being matrix-supported. Imbrication is a common sedimentological feature and can be used to infer palaeo-current direction (Nichols 1999). The plunge and plunge direction indicate the direction from which the current flowed. Imbricated vesicles and fiamme in ignimbrites indicate a lateral velocity component and these have previously been used to determine flow direction (Andrews & Branney 2010; Pioli & Rosi 2005).

### **2.4.3. Lineations and foliation**

The Green Tuff ignimbrite has a well developed lineation and foliation fabric.

Lineations are linear features visible on planar surfaces such as bedding planes, foliation planes or sheet-joints. They are commonly stretched vesicles, but are sometimes defined by stretched fiamme or crystal alignment. Occasionally, the lineation fabric is so strong the lineations become ‘rodded’ (Fig. 2-23A).

The foliation fabric is pervasive in the rheomorphic lapilli-tuff (Fig. 2-23B). It is a planar feature, often parallel to bedding or the basal contact. It is unclear what defines the foliation, although it appears to be defined by alternating, extremely stretched (> 2 m) fiamme and vesicles.

### ***Interpretation***

A pervasive lineation and foliation fabric is a common feature of shear zones (Passchier & Trouw 2005) and is characteristic of high-grade welded ignimbrites (Andrews & Branney 2010; Pioli & Rosi 2005; Schmincke 1974; Schmincke & Swanson 1967). The lineation in the Green Tuff ignimbrite is predominantly a stretching lineation, defined by alignment of stretched vesicles. Lineations record the direction of shear, for example by the overriding density current. Intense shear could also have caused the foliation: a pervasive foliation fabric in the Greys Landing ignimbrite, Idaho, has been interpreted to be the result of a flat-lying zone of intense ductile shear (Andrews & Branney 2010). As the deposit aggraded through addition of hot, agglutinating particles, the zone of shear migrated upwards (Branney & Kokelaar 1992). Thus, the lineation and foliation at any height through the deposit records the shear acting upon the deposit at that moment in time. Therefore, it is possible to use the lineation direction to infer palaeocurrent direction (Andrews & Branney 2005; Sumner & Branney 2002). However, lineations cannot give a unique sense of shear.



**Fig. 2-23A:** Rodded lineations observed in the Green Tuff ignimbrite in rheomorphic massive lapilli-tuff (rheomLT) near the airport . Regional current direction is from right to left. **B:** Pervasive foliation observed in the Green Tuff ignimbrite. Exact cause of foliation is unknown, but may be due to alternating extremely stretched fiamme and vesicles. This photo is taken looking down onto eroded foliation planes. Scale divisions in 10cm. Small scale divisions in 1cm.



**Fig. 2-24** Rare, localised examples of extreme rheomorphism of the Green Tuff ignimbrite A: Large u-shape fold in upper surface, folding foliation B: 'Festoon-type' fold in upper vitrophyre C: Closed 'festoon-type' fold in upper vitrophyre D: Large, m-scale fold E: Sheathfold F: 'Blister' or vertical sheathfold-like structure. G: Chaotically folded domain. Large scale divisions in 10cm. Small scale divisions in 1cm.

#### **2.4.4. Folding**

Folding is abundant in the rheomorphic massive lapilli-tuff. Outcrop-scale (metre to several metre size) folds generally occur as isolated structures in the upper surface of the deposit as deformed, u-shaped structures (Fig. 2-24A-B). Fold axes are generally parallel to the lineation direction and occasionally, these u-shaped folds are seen to ‘close’ (Fig. 2-24C). Sheathfolds are also common (Fig. 2-24E) and occur parallel to lineation, or as vertical ‘blister’ structures (Fig. 2-24F). These folds can deform local, thin layers, or can affect almost the entire deposit thickness (Fig. 2-24D).

The foliation of the rheoLT is typically chaotically folded from the microscopic to the mesoscopic scale (Fig. 2-24G). Typically individual folds do not deform layers more than a few decimeters thick. Foliations above folded layers return to plane-parallel. They vary in form from symmetric to asymmetric, can be open or closed and can be rootless.

#### ***Interpretation***

As most fold axes trend parallel to lineation, it is likely that they were caused by the same shear, i.e. from the overriding pyroclastic density current. The return to parallel-foliation draping folds, is evidence for syn-depositional folding, occurring within an upwards migrating shear zone in an aggrading deposit. This is also known as ‘primary rheomorphism’.

Folding was progressive, and identifying stages of deformation is difficult. The folds must post-date the formation of the foliation as it is itself folded. In the chaotically folded domain, folds are refolded. The large folds at the free upper surface of the deposit often affect a greater thickness of the deposit, refolding the micro to mesoscopic folding. The fold axes for these folds do not systematically run-parallel to the lineation. Elsewhere, these have been termed ‘festoon-type’ folds, and may have formed similar to ropey structures at the surface of a pahoehoe lava flow where fold axial trends can rotate (Andrews & Branney 2010; Branney & Kokelaar 1992). Free-standing, upper-surface folds are commonly found in areas that have irregular topography, particularly where a palaeo-slope runs parallel to general current direction. These folds therefore, may represent shortening at the free upper surface caused by the effect of the slope.

### 2.4.5. Flow structures

A number of flow structures are observed in the Green Tuff ignimbrite. Here, each one is described and its use as a kinematic indicator assessed.

- As previously discussed, imbricated fiamme and vesicles are abundant in the Green Tuff ignimbrite, and are not restricted to a particular horizon (c.f. Schmincke & Swanson 1967). Rather, they occur throughout the deposit, even when thin.
- Rotated clasts are a common feature in the rheomorphic lapilli-tuff. They are easier to see when the ignimbrite is foliated. Rotational structures around lithic clasts of all sizes can be seen in outcrop from boulders to lapilli (Fig. 2-25). In

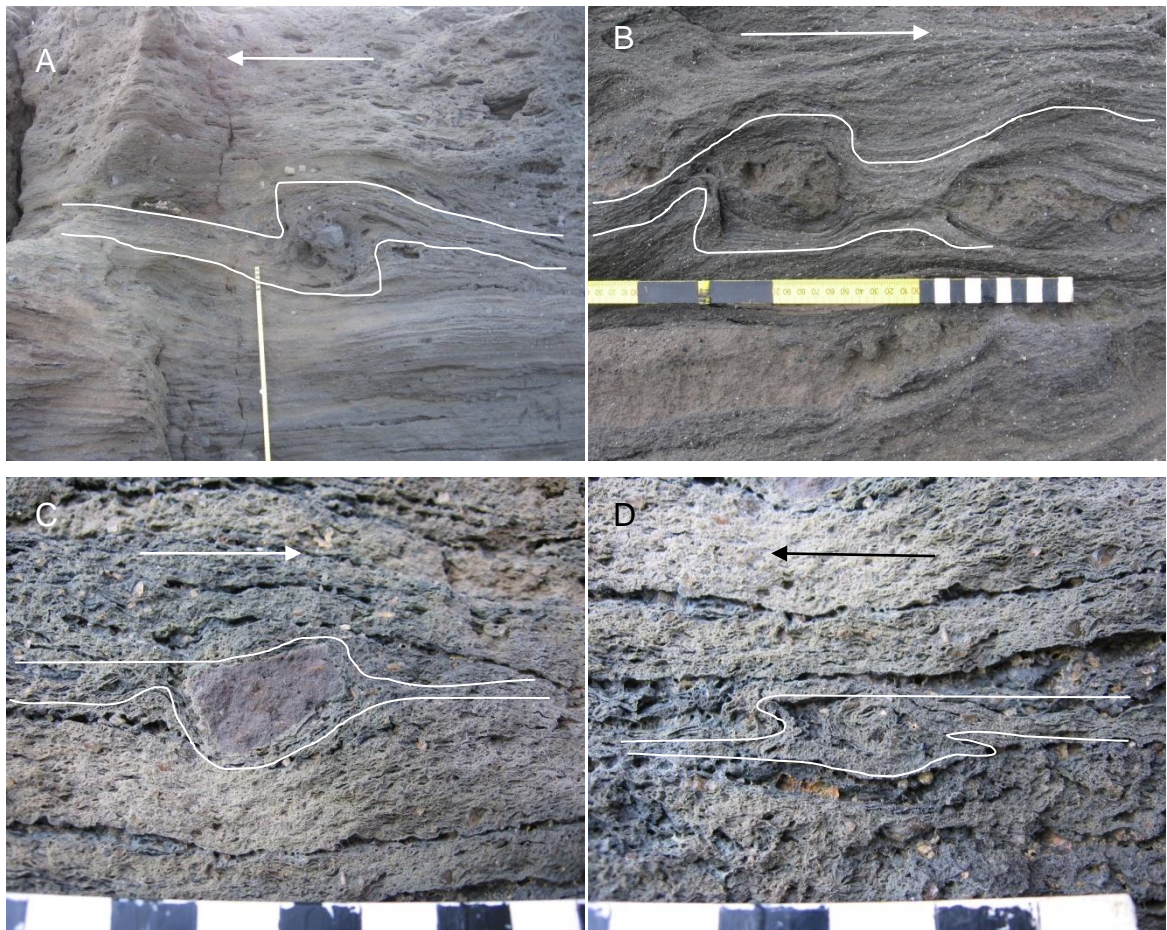


**Fig. 2-25: Kinematic indicators in the rheomorphic massive lapilli-tuff (rheomLT) facies of the Green Tuff ignimbrite.  $\delta$ -objects of different size and interpretation of palaeo-current direction from sense of shear (arrow direction). A: Top-left shear sense indicates palaeocurrent direction is from right to left. B: Bottom-left shear sense indicates palaeocurrent direction is from left to right. C: Bottom-left shear sense indicates palaeocurrent direction is from left to right. D: Top-left shear sense indicates palaeocurrent direction is from right to left. Note the 'quarter-folds' (Passchier & Trouw, 2005) around this object. Large scale divisions in 10cm. Small scale divisions in 1cm.**

thin section, rotational structures around crystals or mm-size lithics are also seen.

- At Cuddia di Scauri (location 60; Fig. 2-2), recumbent flames are seen at the base of vitric Green Tuff ignimbrite. Here, the ignimbrite was emplaced over an unconsolidated pumice lapilli deposit. The recumbent flames point in the direction of the lineation plunge direction (Fig. 2-26).
- Tension gashes and fractures are common on the upper surface of the Green Tuff ignimbrite. Tension gashes tend to be small scale (cm sized) and are not laterally extensive. The upper surface is commonly autobrecciated and fractured.

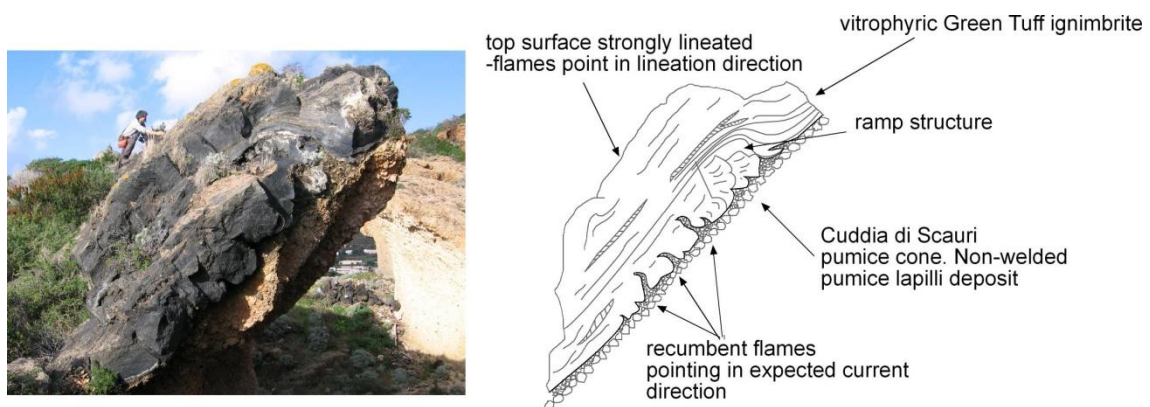


**Fig. 2-26: Recumbent flame structures in the base of the Green Tuff ignimbrite where it has flowed over a steep, unconsolidated surface near Scuari (location 60; Fig. 2-2). Mike Branney for scale.**

### ***Interpretation***

- A pervasively imbricated fabric throughout all levels of the deposit records the upward agglutination and shear of the deposit by a sustained, over-riding pyroclastic density current (Branney & Kokelaar 1992; Sumner & Branney 2002). Imbricated clasts are sourceward-dipping, and can be used as kinematic indicators in conjunction with lineations. They give a unidirectional sense of shear.
- Rotated clasts can also be used as kinematic indicators and have also been used to indicate rheomorphic sense of shear (Catalano 2007; Pioli & Rosi 2005; Schmincke & Swanson 1967). They can occur as either  $\delta$ -objects or  $\sigma$ -objects (Fig. 2-27; Passchier & Trouw 2005). Most common are  $\delta$ -objects, where quarter folds are often observed. These are effective kinematic indicators, but are often difficult to identify in the field. They should be best observed in thin

section, when a section is cut parallel to the lination direction. However, this technique has been less successful in this study, but some examples of where they have been observed in the Green Tuff ignimbrite include deposit drapes on very steep slopes (Fig. 2-28). The rotated clasts here give an uphill sense of shear, suggesting that the Green Tuff ignimbrite was able to flow uphill and that emplacement on these slopes was not merely the result of post-depositional rheomorphic slumping ('secondary rheomorphism' e.g. Wolff & Wright 1981b).

- Recumbent flames have not previously been used as a kinematic indicator, although experimental modeling suggests that they should form in natural

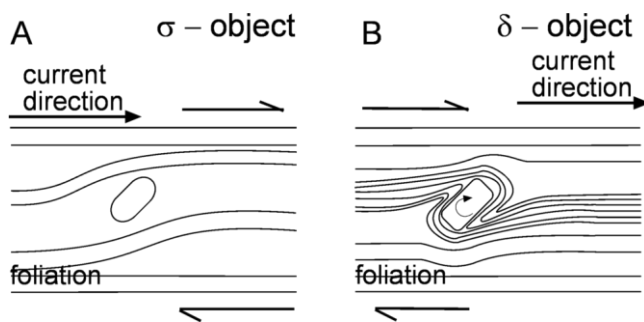


**Fig. 2-27: Schematic diagram showing A:  $\sigma$  and B:  $\delta$  objects (Passchier & Trouw, 2005). These rotated clasts should be seen in a surface parallel to lination to determine shear sense.**

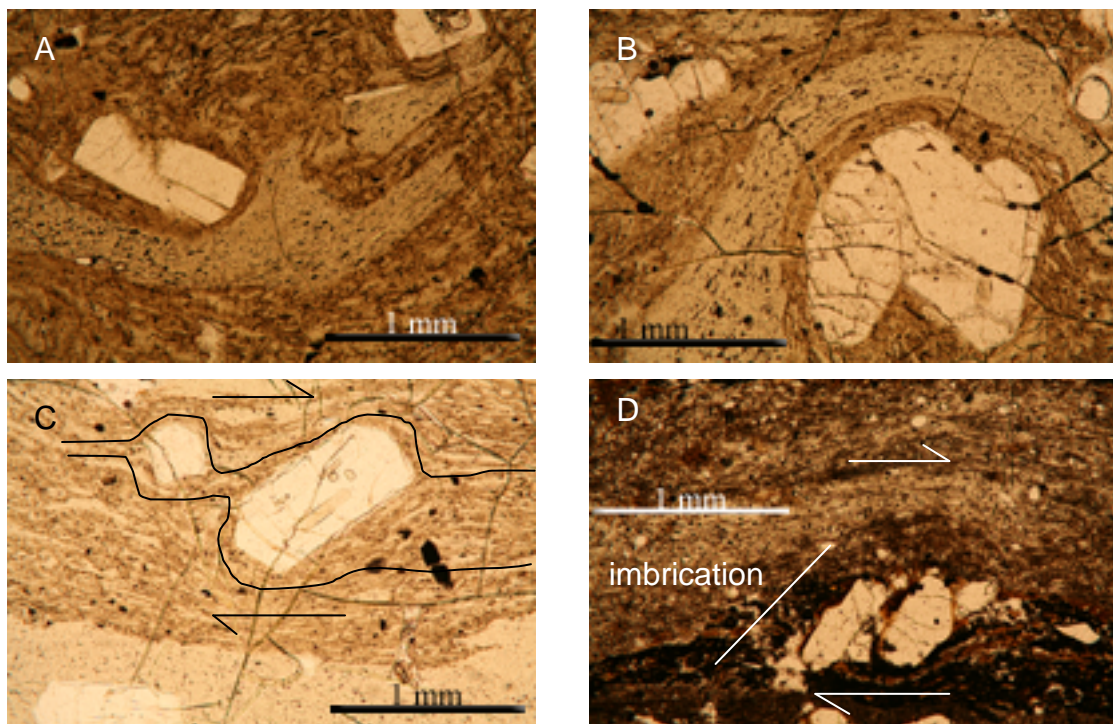


**Fig. 2-28 A-B: Collapsed pumices draping crystals, no sense of shear, in eutaxitic massive lapilli-tuff. C: Rotated crystal ( $\delta$ -object) indicates top-right shear in rheomorphic massive lapilli-tuff. D: Imbricated crystals. This section is taken from the Green Tuff ignimbrite drape at the base of the Zinedi scarp and indicates top-right shear which shows uphill flow.**

pyroclastic density currents but are not often observed (Rowley 2010). These folds are unique to one location in the Green Tuff ignimbrite, and may be the result of a combination of circumstances: (1) unconsolidated substrate; (2) very steep depositional slope; and (3) a vitrophyre which suggests that the deposit was quenching rapidly, ‘freezing in’ structures which may have otherwise been sheared out at other locations.

- Tension gashes and autobreccias occur when strain rates during emplacement locally cause cooler and more degassed deposit to fragment brittely, similar to the formation of autobreccias in lavas (Sumner & Branney 2002). This effect would have been increased at the upper surface of the deposit where the hot agglutinate chilled against the air. Upper autobreccias have been recorded in many rheomorphic ignimbrites (e.g. Andrews & Branney 2010; Branney & Kokelaar 1992; Henry & Wolff 1992; Sumner & Branney 2002) but do not provide a sense of shear direction. Tension gashes are a common kinematic indicator in metamorphic shear zones (Passchier & Trouw 2005), and have also been applied to rheomorphic ignimbrites (Schmincke & Swanson 1967). However, the type of shear they represent could be post-depositional slumping down topography as well as syn-depositional shear from an overriding current and they should only be used in conjunction with other observations (e.g. lineations, imbrication, rotated clasts).

#### **2.4.6. Post-depositional features**

Here, two examples of unique features are presented. They are each only observed at one location.

The first is a large listric fault (Fig. 2-29A) at Gadir (location 34; Fig. 2-2). The listric fault dips in a down-slope direction. Its appearance is similar to a crevasse in a glacier, which occur perpendicular to glacier flow and at the head of the glacier and are interpreted as extensional features. No other similar feature is known to have been observed at other rheomorphic ignimbrites. It is here interpreted to be an extensional fault which opened up due to shear from an underlying slope. The listric form to the fault suggests that the internal deposit was still hot and ductile whilst the upper surface was brittle.

The second feature is a number of vitrophyric droplets preserved within an upper autobreccia (Fig. 2-29B) at Porto di Scauri (location 63; Fig. 2-2). Viscous melt was able to ooze through the autobreccia and drip onto horizontal surfaces below the droplets. These droplets must have formed after deposition of the ignimbrite and Formation of the autobreccia. This suggests that there may have been melt lenses (such as fiamme) that were less viscous than the matrix of the tuff during cooling, or that they were able to retain heat for longer. They may be similar to the ‘ooze-outs’ documented in the Wineglass Welded Tuff, Crater Lake (Kamata *et al.* 1993). There, fiamme are observed to ooze down vertical tension fractures in the tuff. Viscous melt protruded up to 3 cm from the fiamme, leaving a cavity. ‘Squeeze-out’ features are also observed in the Wineglass Welded Tuff, which occurred when re-vesiculation forcibly squeezed fiamme to protrude from the welded tuff. Similar squeeze-out features have been observed in the Aso ignimbrites (Ono & Watanabe 1974; Watanabe *et al.* 1983).



**Fig. 2-29A:** Listric fault with an autobreccia infill on the upper surface of the Green Tuff ignimbrite. Meter rule for scale is orientated parallel to underlying slope. **B:** Vitrophyric droplets in the upper trachytic autobreccia of the Green Tuff ignimbrite at Porto di Scauri (Location 63, Fig. 2-2). This ooze-out feature indicates there were lenses of very low viscosity melt (such as fiamme) compared to the surrounding matrix during cooling. Scale divisions in 1cm.

### 2.4.7. Geochemical causes of welding in the Green Tuff Formation

Agglutination welding and syn-depositional welding is favoured by a number of factors in the Green Tuff ignimbrite. Whole rock samples were analysed by XRF, for details on analytical methods, see Chapter 3.

1. *Melt composition.* The Green Tuff ignimbrite is strongly peralkaline (Fig. 2-30A) with agpaitic index (A.I: molar  $(\text{Na}_2\text{O} + \text{K}_2\text{O})/\text{Al}_2\text{O}_3$ ) values generally over 1.1 (e.g. Mahood 1984). A large number of alkalis over alumina lowers viscosities.
2. *Water and halogen content.* The Green Tuff ignimbrite has very high chlorine concentrations between 1000-6000 ppm (Fig. 2-30). This range in values does not correlate to proximity to the sea, and these values are considered to be magmatic, although Cl may have been leached locally from the rock. Cl behaves similarly to F, thus when Cl is high it can be assumed that F is high. Cl and F are both effective viscosity-reducing agents. High water contents have been measured in melt inclusions (Lowenstern & Mahood 1991) and here are inferred from loss of ignition data (LOI). LOI data are typically inferred to represent total volatile content in the rock (Rollinson 1993) and values of 1-2% are typical for the Green Tuff ignimbrite, but can be as high as 4% (Fig. 2-30B)
3. *Temperature.* Temperature estimates of 950°C for the Green Tuff Formation (Wolff & Wright 1981a) are closer to temperatures expected for less viscous andesites than rhyolites. Eruption columns are inferred to be low which minimizes cooling of pyroclastic particles during fountaining (Mahood & Hildreth 1986).

Thus, the Green Tuff ignimbrite consisted of hot, sticky particles that agglutinated as an aggrading deposit from a pyroclastic density current. The low viscosities meant that the overriding current was able to cause shearing in the underlying deposit which formed a variety of complex rheomorphic features. Many of these features record a sense of shear direction and would be useful tools in analyzing current direction and behaviour. However, as the deposit slowly cooled, it may have been able to undergo further rheomorphism when deposited on steep slopes. This is recorded in tension gashes and the listric fault at the surface of the deposit which give a sense of down-slope shear.

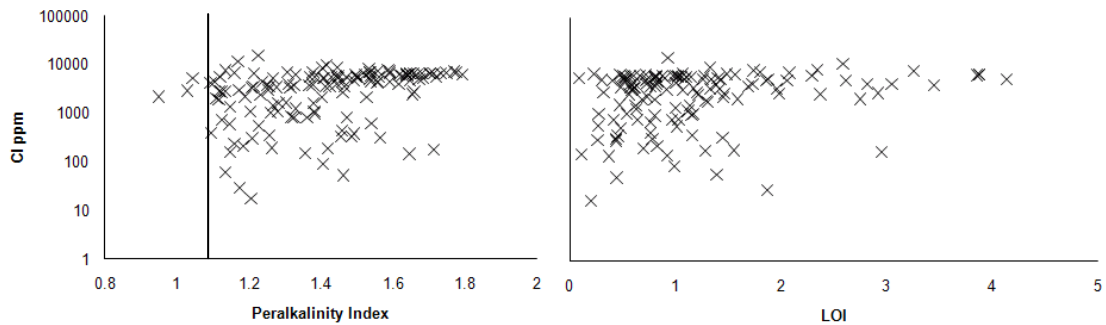


**Fig. 2-30: Peralkalinity index (molar  $[\text{Na}_{20}+\text{K}_{20}]/\text{Al}_{203}$ ) and LOI (loss of ignition) versus chlorine ppm. Line indicates ‘strongly peralkaline’ at  $>1.1$  (Mahood, 1984). Chlorine is exceptionally high regardless of peralkalinity or LOI. This suggests that chlorine would have been abundant in the deposit, even when peralkalinity was low, which may explain the very low-viscosity features seen in the mildly peralkaline trachyte. Samples analysed by bulk rock XRF.**

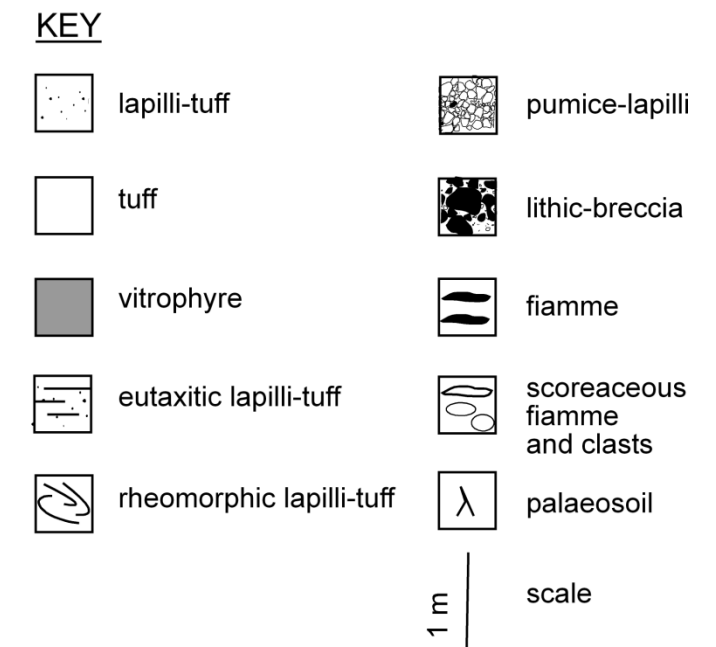
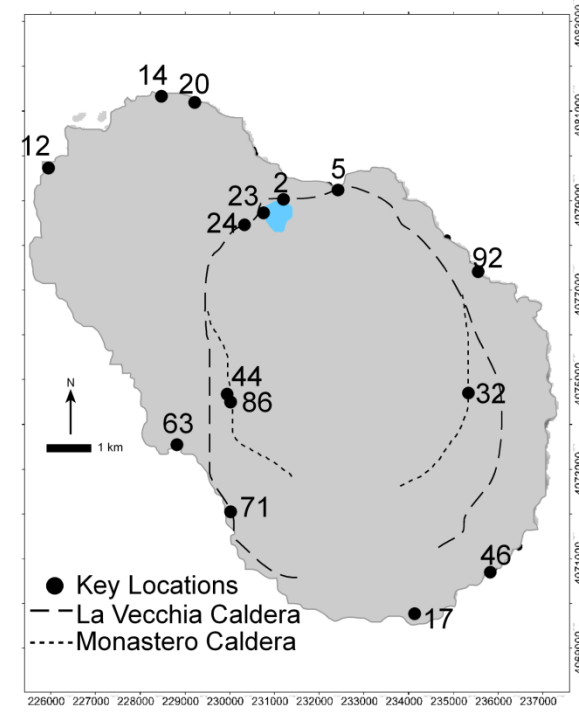
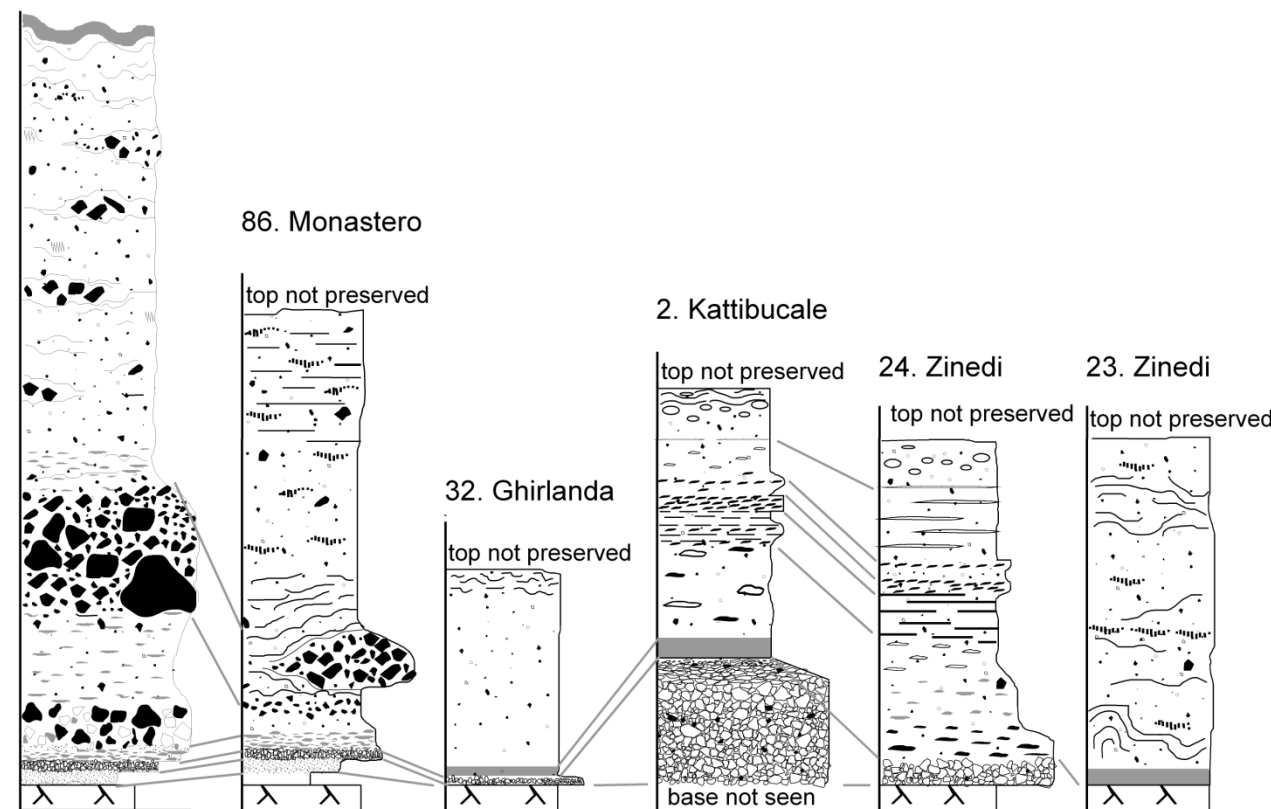
## 2.5. Lateral variation

The Green Tuff Formation is laterally variable (Fig. 2-31). Lithofacies are not spatially extensive and are here not used as a basis for a lithostratigraphy. The concept of the flow-boundary zone suggests that the characteristics of a deposit depend upon the conditions within that zone. For example, a turbulent current with a traction-dominated flow-boundary zone would deposit a cross-stratified horizon. Whereas, elsewhere, the current may have had turbulence suppressed through high particle concentration and deposit a massive horizon. As the current waxes and wanes, the deposit it leaves behind is variable. For example, Orsi & Sheridan (1984) correlate the rheomorphic horizon as a Member. During this study the rheomorphic horizon has been observed to grade into a non-welded facies laterally, or into eutaxitic lapilli-tuff. This is interpreted to be a lateral variation in entrainment of air by the pyroclastic current (which would cool pyroclasts), and variations in shear exerted onto the deposit. Each lithofacies is a product of the current at a particular point in space, at a particular point in time. Correlations of lithofacies are thus expected to be diachronous (explored further in Chapter 4 and 7).

## 2.6. Areal extent and aspect ratio

The Green Tuff ignimbrite was deposited across the entire island of Pantelleria, an area of  $100 \text{ km}^2$ . An 8 m-thick, poorly-sorted, coarse, lapilli-tuff deposit has been recorded in offshore boreholes and interpreted to represent the direct deposition from the Green

44. Monastero



17. Balata dei Turchi

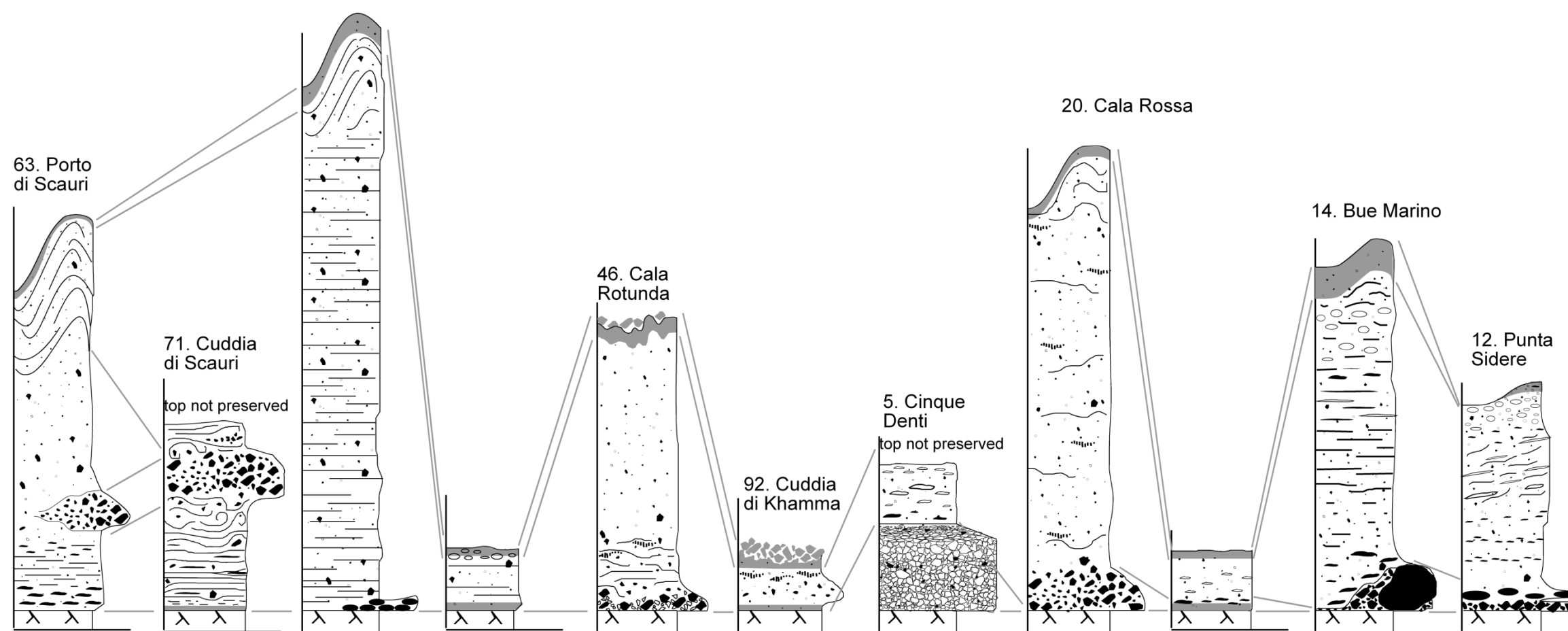
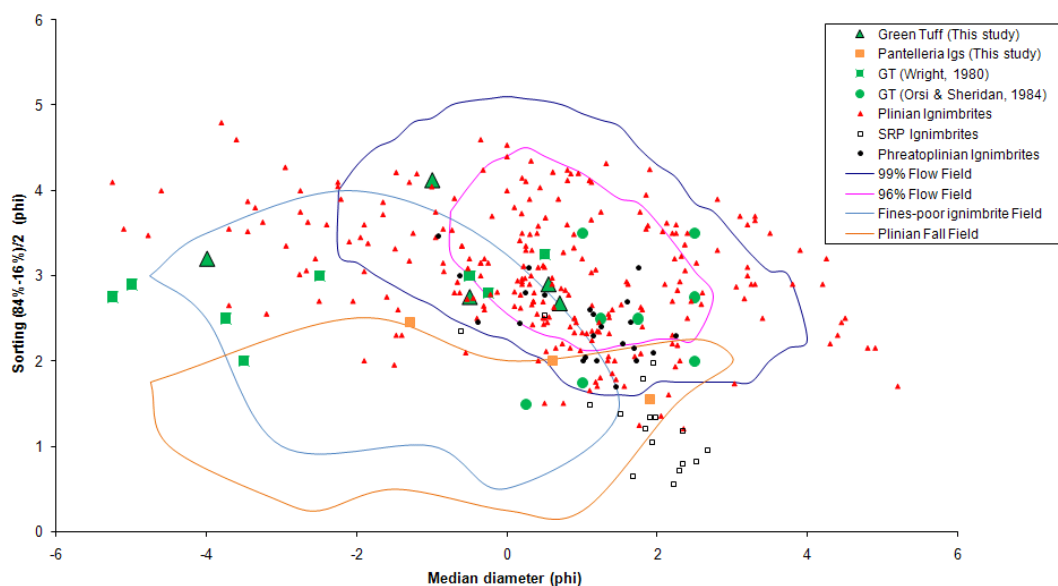


Fig. 2-31: Simplified graphic logs of key locations along the caldera rim (top) and coast (bottom) of the Green Tuff Formation.

Tuff pyroclastic density current under the sea (Anastasakis & Pe-Piper 2006), based on its poor-sorting, lack of carbonate content and massive nature. It is overlain by a 10 m thick turbidite which resulted from flow transformation of the pyroclastic density current into a hyperconcentrated turbidity current. Thus, the maximum run out distance recorded for the Green Tuff ignimbrite is up to 45 km from an inferred central vent. The ignimbrite ranges from less than 1 m to over 20 m thick, with an average thickness of 5 m. Aspect ratio (which is the ratio of the average thickness of the deposit to the horizontal extent) is estimated to be a minimum of 1:1200 (if only onshore deposits are considered) up to 1:9000, which is in the range for 'low-aspect ratio' ignimbrites.

## 2.7. Granulometry

Granulometry datasets for the Green Tuff ignimbrite are rare as the majority of the deposit is strongly welded. Five samples of nonwelded Green Tuff ignimbrite were sampled for granulometry (3 from location 86, 1 from location 52, and 1 from location 1). The data for these five locations are plotted with data previously published for the Green Tuff Formation (Orsi & Sheridan 1984; Wright 1980) and three samples from



**Fig. 2-32: Granulometry of massive lapilli-tuff facies (triangles) for the Green Tuff ignimbrite compared to published data. Size parameter plot of median diameter ( $\Phi$ ) vs. sorting ( $\sigma$ ) (parameters from Inman, 1952). Fields after Walker, 1971. Plinian and Snake River Plain (SRP) type volcanism data courtesy of B. Ellis (pers. comm.). Many of the samples fall within the 99% Walker flow field, indicating emplacement by pyroclastic density current. Samples that fall to the left of this field are fines-depleted. Samples from Wright (1980), may have been collected from the basal pumice-lapilli deposit and not from the lapilli-tuff deposit.**

nonwelded locations of older ignimbrites (Fig. 2-32). The Green Tuff ignimbrite samples generally fall into the ‘flow field’ (Walker 1971) and do not stand out as being particularly unusual (Fig. 2-32). Of this study, one data point is clearly outside of this field and in the ‘fines-poor ignimbrite’ field and this is a sample of unwelded lithic breccia, which also appears fines-poor in outcrop. Several data points from Wright (1980) fall outside of the ‘flow field’ and are more typical of fall deposits. However, as Wright (1980) considered the entire Green Tuff Formation a fall deposit, it is uncertain whether these samples were taken from what is now interpreted to be the ignimbrite or from the pumice fall at the base of the Formation as sample locations are not given.

## 2.8. Phenocrysts

The phenocryst population is dominated by anorthoclase feldspar. Other minerals include aenigmatite, olivine and clinopyroxene (see Chapter 3 for further details).

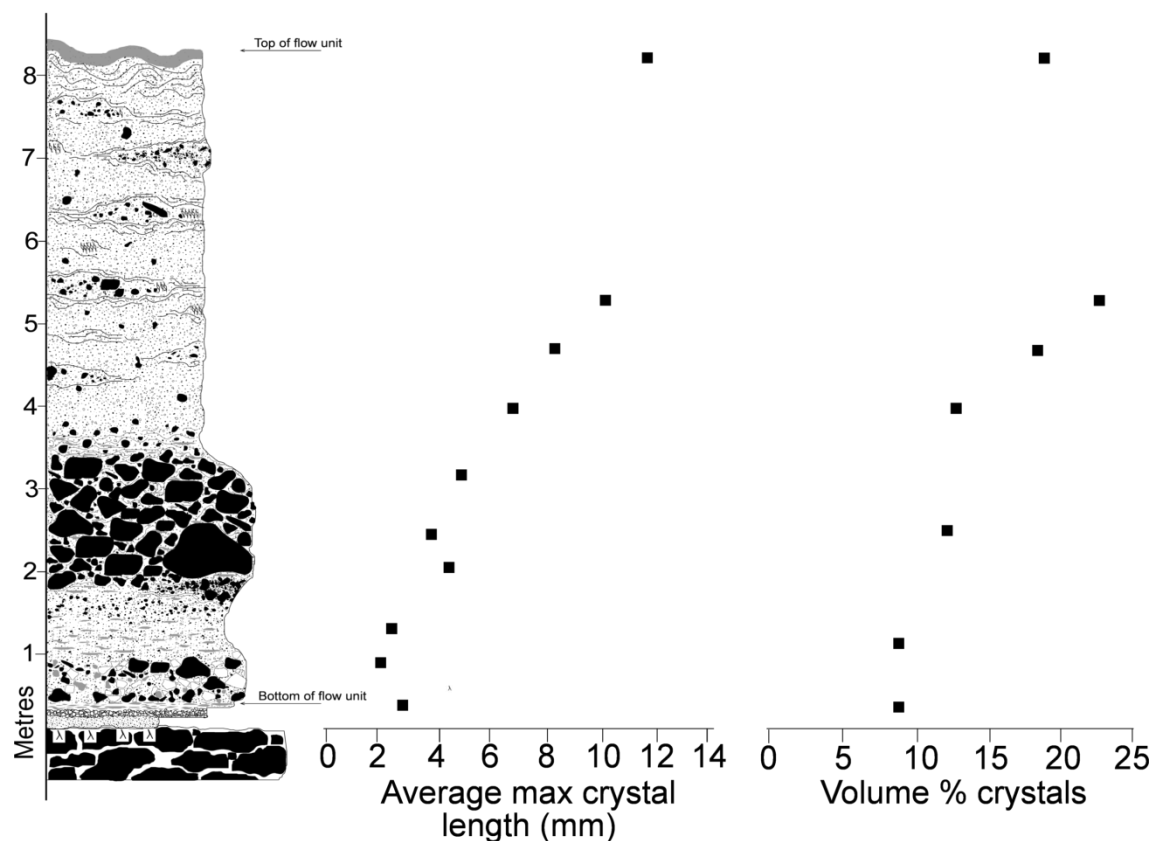


Fig. 2-33: Size and volume percent of feldspar crystals vs. height at Monastero Scarp (location 44; Fig. 2-2). Variation in size and volume % is gradational (note gap between 5.5 m and 8 m due to inaccessible cliff) and increases with height.

The size and volume percentage of the anorthoclase crystals varies widely in the Green Tuff Formation. One of the type sections used to define the lithofacies (location 44) has been chosen as a representative type section for the range in anorthoclase population, as it shows a significant change in feldspar size and volume percent. Maximum crystal size was measured in the field using digital calipers which are accurate to 0.01 mm; values are averages of the 10 largest crystals. Thin sections from this location were studied and the percentage of crystals in each section was analysed using Image J, an image processing freeware (Rasband, W.S., ImageJ, U. S. National Institutes of Health, Bethesda, Maryland, USA, <http://rsb.info.nih.gov/ij/>, 1997-2009). Vesicularity of the samples was also analysed using Image J and used to normalize the crystal percentage data.

Feldspars are c. 2 mm at the base of the unit and represent less than 10% of the whole rock (Fig. 2-33). The size and percentage increases linearly with height through the section. At the top of the unit, feldspar crystals are c. 12 mm (up to a maximum of 16 mm) and represent up to 25% of the whole rock (Fig. 2-33).

### ***Interpretation***

A variation in crystal size and abundance across several localities had previously been noted (Mahood & Hildreth 1986) and the variation interpreted to relate to a magma composition variation from pantellerite to trachyte. Study of a single location (location 44) shows that the variation is systematic with height through the deposit (Fig. 2-33). The crystal size and volume percent increases linearly with height through the deposit and therefore with time during the emplacement of the ignimbrite. The upward increase in crystal size and abundance and how it relates to a trend in magma composition is further considered in Chapter 3.

## **2.9. Discussion**

Detailed logging and lateral tracing of the Green Tuff Formation has enabled new interpretations of the emplacement style of the unit.

### **2.9.1. Overview of the Green Tuff Formation**

The base of the Green Tuff Formation typically sits upon a soil which has developed in the top of Eruption-unit 3 (this study, Chapter 6). The Green Tuff Formation comprises a proximal pumice-lapilli deposit and a hybrid, pyroclastic current-modified pumice-

lapilli deposit. Distally, this horizon is replaced by a thin ash-tuff. The majority of the Green Tuff ignimbrite comprises a massive (commonly eutaxitic) lapilli-tuff. The lowermost parts of the Green Tuff ignimbrite, at localities along the Kattibucale and Cinque Denti scarps, comprise bedded eutaxitic lapilli-tuff and sheet-jointed tuff. This upwardly grades into massive lapilli-tuff or eutaxitic massive lapilli-tuff. This locally rheomorphic facies is present across the entire island, contains lithic breccia lenses and pods, and can grade from any of the underlying units, depending upon location. The top of the Green Tuff Formation is defined by an upper vitrophyre, which is commonly folded and autobrecciated when preserved. A soil does not typically develop in the top of the Green Tuff Formation, except where younger pumice has been deposited on top of the unit, particularly within its folds.

### ***Flow versus fall emplacement***

The debate over a flow-versus-fall origin for the welded tuffs of Pantelleria has centred on the Green Tuff Formation. This study concurs with the most recent work on the Green Tuff Formation, and interprets most of the deposit as a welded ignimbrite, except for a local, unwelded pumice fall deposit at the base of the Formation. Evidence for this includes:

#### *This study*

1. Imbricate structures are pervasive through the deposit indicating a sub-horizontal transport component.
2. Some lower facies clearly cross-stratified, indicating a turbulent dilute density current.
3. The deposit thins over topographic highs and thickens into palaeovalleys.
4. Granulometry analyses of nonwelded samples fall in the 'flow field' of (Walker 1971), which is typical for ignimbrite deposits.
5. The internal architecture of the deposit suggests a diachronous emplacement, unrelated to pervasive wind direction, which is not consistent with a fall origin (this study, Chapter 4).

#### *Previous studies*

1. Thinning of the deposit on leeward sides of topographic obstacles (Mahood & Hildreth 1986).

2. Lack of systematic variation of lithics, contrary to what would be expected for a fall deposit. This has resulted from a reinterpretation of published isopleths maps (Fig 11 in Wright, 1980,) which are poorly constrained (Mahood & Hildreth 1986).
3. Other demonstrable fall deposits on the island are not pervasively welded, either vertically or laterally (Mahood & Hildreth 1986). The density profile for the Green Tuff Formation is ambiguous and is not definitive for fall (Orsi & Sheridan 1984).
4. Transport and inclusion of locally derived clasts from cinder cones (Orsi & Sheridan 1984).

### ***One flow-unit versus multiple-flow units***

A flow-unit is the deposit from a single pyroclastic flow. An ignimbrite may comprise of a single flow-unit, or several (a compound ignimbrite).

Initially, flow units were interpreted from a layering scheme of a ‘typical ignimbrite’ (Sparks *et al.* 1973). The base of the flow-unit was defined by ‘Layer-1’, a fine grained layer thought to represent a ‘surge’ from the head of a pyroclastic density current. Layer-2 was the main body of the pyroclastic density current, deposited *en masse* and Layer-3 was the deposit from a co-ignimbrite ash cloud. However, recent work has shown that ignimbrites are deposited progressively as an aggrading deposit (Branney & Kokelaar 2002; Branney & Kokelaar 1992; Girolami *et al.* 2010) and that ‘massive’ thick ignimbrite is formed in the same way as thin, stratified ignimbrite. Thus, a single current can deposit a range of lithofacies with differences in sorting, grain size and grading (McCaffrey *et al.* 2003). It follows then, that grain size variations and the presence of a fine grained basal layer can no longer be interpreted to delineate flow units.

A flow-unit can only be identified through identification of a layer that represents a break in pyroclastic density current activity. This could include a pumice fall layer, a co-ignimbrite ash layer, the accumulation of sediments and most definitively a palaeosoil, although this latter feature would also represent a significant time gap in between periods of deposition. In a welded ignimbrite, these primary features may be more difficult to recognize. However, a period of non-deposition would result in

significant cooling of the upper surface of the welded deposit. This would be identified in the deposit as a zone of competency or an internal, well developed vitrophyre which may have been subsequently boudinaged or fractured through extension if rheomorphosed by post-depositional creep or shear from a later current.

No such features have been identified in the Green Tuff Formation. Whilst the possibility of separate flow units cannot be completely excluded, their existence is unlikely. First, all features such as a co-ignimbrite ash or internal vitrophyre, would have to have been eroded completely, everywhere. Secondly, the linear grading seen in the feldspar population (and in the geochemistry, see Chapter 3) would have to have been emplaced by a series of very thin flow units, each with a slightly increased feldspar population, otherwise sharp 'steps' in the compositional grading would have been observed. The changes in feldspar population do not correlate with bedding breaks or grain size changes. It is more likely that the Green Tuff ignimbrite represents a single flow unit, deposited from a single, sustained pyroclastic density current that was tapping increasingly crystal-rich magmas through the eruption.

### **2.9.2. The eruption history of the Green Tuff Formation**

After emplacement of the ignimbrite in Eruption-unit 3 at approximately  $87.9 \pm 1$  ka (Chapter 6; La Felice *et al.* 2009), Pantelleria volcano had a period of effusive volcanism lasting from ~80 to 50 ka (Mahood & Hildreth 1986).

1. The eruption of the Green Tuff Formation (ca. 50 ka) began with a strombolian (at most, sub-plinian) eruption column. This emplaced a local pumice-lapilli deposit and more distally, an ash deposit.
2. As the eruption waxed, introducing larger pumice and lithic clasts into the plume, the column was no longer able to remain fully buoyant. Turbulent near-vent currents or eddies deposited hybrid fall and current deposits along caldera scarps.
3. The eruption style rapidly evolved into low-fountaining, producing a quasi-steady, sustained pyroclastic density current. This current was initially a high-concentration, granular fluid-based current, but experienced periods of turbulence.
4. As the eruption sourced hotter particles, the current unsteadiness remained and the flow boundary zone was transitional between granular flow-dominated and

fluid-escape dominated flow regimes. The hot, sticky particles welded instantly upon deposition.

5. As the eruption further waxed, the current exerted intense shear on the aggrading agglutinate, deforming the deposit. As the deposit continued to aggrade, the zone of shear migrated upwards.
6. Progressive evacuation of the magma chamber brought up magma that was more crystal rich, possibly from deeper depths within the chamber.
7. The onset of the climactic phase is marked by a lithic breccia deposited in the west of the island. The eruption caused fragmentation or erosion of the conduit walls or the roof of the magma chamber. Partial caldera-collapse may have occurred at this stage.
8. The pyroclastic density current continued, becoming more widespread, depositing upon the entire island. The current travelled up to 45 km along the sea bed, initiating volcanoclastic turbidites which travelled even further (Anastasakis & Pe-Piper 2006). Shear intensity increased, causing dramatic rheomorphism of the aggrading Green Tuff deposit.
9. The eruption ended with the pyroclastic density current, which covered the entire island in a hot, glassy deposit sterilizing over 100 km<sup>2</sup> of land and an unknown area of the sea floor.
10. The uppermost horizon of the deposit, folded dramatically by the final phase of the current, chilled against the air and autobrecciated.
11. As the deposit cooled, further rheomorphism occurred as the deposit crept down slopes and pockets of hot melt oozed before chilling rapidly.
12. After the Green Tuff eruption, effusive activity resumed immediately, with the eruption of the Mount Gibebe trachyte lava shield (Mahood & Hildreth 1986). The top of the Green Tuff ignimbrite is commonly eroded when not covered by younger deposits. It is also often stripped for use as a building material. There is no evidence of a well-developed soil.

## 2.10. Conclusions

This study has revealed that:

- The Green Tuff Formation comprises of a single ignimbrite flow-unit, emplaced by a sustained, quasi-steady pyroclastic density current, on to a plinian fall deposited at the start of the eruption.
- The eruption style was a large, catastrophic, low aspect-ratio ignimbrite forming eruption, and not of a Montserrat-style eruption of a series of small, discrete pyroclastic density currents.
- Rheomorphism primarily happened syn-depositionally. The rheomorphism has not altered primary sedimentary fabrics and structures.
- The deposit welded instantly upon deposition, including on slopes up to 90°.
- Kinematic indicators represent syn-depositional shear from an overriding current. They can be used to infer current direction.
- Caldera-collapse was likely to be small, and may not be responsible for the large scarps seen in the centre of the island (explored further in Chapter 5).
- The deposit is zoned from a crystal poor magma at its base to a crystal rich magma at its top with height through the deposit. Although inferred previously (Mahood & Hildreth 1986), the dramatic change from <10%, c. 2 mm anorthoclases, to >25% c. 12-16 mm anorthoclases was not observed at a single location to vary systematically with height. This is defined at Monastero scarp (location 44), which is now defined as the type locality for the Green Tuff ignimbrite and is discussed in more detail in Chapter 3. The type locality for the lower horizons of the Green Tuff Formation, including the pumice fall and hybrid deposits, is at Bagno dell' Acqua (location 1). Chemical zonation within this deposit is explored further in Chapter 3.

# 3. The chemical stratigraphy of the Green Tuff Formation: evidence for progressive tapping of a single, zoned magma chamber

---

## 3.1. Abstract

Geochemical analyses of glass, phenocryst and whole rock samples through a single type section of the Green Tuff Formation are presented here. The deposit is broadly zoned from pantellerite at its base to less evolved trachyte at its top. It shows weak chemical variation in the major elements but strong variations in the trace and rare earth elements. Feldspar populations are relatively homogeneous and do not show zoning within individual crystals; however, resorption textures indicate that the trachytic end member inherited some crystals from the more evolved melts. Clinopyroxenes are present throughout the section and show minor trends in Fs/En ratios. Aenigmatite is common in the basal, pantelleritic units but missing at the top, trachytic units where olivine occurs. The linear zoning in the Green Tuff is here interpreted to represent the inverse picture of a zoned magma chamber. Chemical variation was likely due to fractional crystallization of a basaltic parent. As the magma chamber was progressively tapped during the eruption, the aggrading ignimbrite records changes in the chemical composition at source, suggesting that chemical variations within the ignimbrite can be used as a chemical stratigraphy, or ‘proxy’ for time slices through the eruption.

## 3.2. Introduction

The type section of the Green Tuff ignimbrite at Monastero Scarp (location 44) has been defined by its wide range of lithofacies, including the distinctive lithic breccia, but also due to its vertical zonation of phenocrysts (Chapter 2). The feldspar phenocrysts range from c. 2 mm at its base to c. 12 mm at its top, with a coinciding volume percent increase of less than 10% to greater than 25%.

Previous workers reported a wide range of geochemical compositions for the Green Tuff Formation (Civetta *et al.* 1988; Mahood 1984), and (Mahood & Hildreth 1986) stated that the whole rock geochemical variation coincided with a variation in phenocryst size and volume percentage. Therefore, detailed analysis of the type section presents an opportunity to investigate the chemical variation of the Green Tuff Formation.

### **3.2.1. Aims and objectives**

The aim of this study is to characterize the chemical stratigraphy of the Green Tuff Formation, through the following objectives:

- to identify the nature and extent of chemical zoning of major, trace and rare earth elements in both the whole-rock and groundmass glasses.
- to identify any changes in phenocryst phases through the deposit and whether there is any chemical variation in single minerals through the deposit
- to use chemical zonation in the Green Tuff Formation as a guide to understanding the nature of the pre-eruptive magma chamber.

### **3.2.2. Methods**

Closely-spaced sampling vertically through the type section was carried out after detailed logging, photographing and lithofacies interpretation (Chapter 2). Multiple samples were taken from single horizons within the ignimbrite when more than one component was identified (e.g. pumice and obsidian blocks). Twenty samples were taken for bulk rock analysis and 11 of these were sub-sampled in order to make 100 µm polished sections for spot analyses of glass and phenocrysts.

#### **Laser ablation- inductively coupled plasma mass spectrometry (LA-ICP-MS)**

Laser ablation analysis was performed on polished 100 µm sections. Prior to analysis, the major element concentrations of the individual mineral grains and glassy areas were determined by electron microprobe in order to help calibrate the LA-ICP-MS data.

Back-scattered images were also obtained in order to help locate the laser spots as close as possible to the probe points. LA-ICP-MS work was carried out at the Open University on an Agilent 7500A quadrupole ICP-MS, coupled with a New Wave UP213 Nd:Yag deep UV (213 nm) laser system. Instrumental operating conditions are summarised in Table 3-1.

Samples were ablated in a pure He atmosphere, and the analyte was carried in He and then mixed with Argon via a “Y” connector before entering the plasma. The use of He gives a 2 – 3-fold increase in sensitivity, and significantly reduces background intensity. Data were acquired across the mass range from  $^7\text{Li}$  to  $^{238}\text{U}$ . The total time for each analysis was 220 s. During the first 100 s, the gas blank is measured, during which the laser beam is blocked by a shutter. This shutter is then removed and the sample is ablated for a further 60 s. The transient signals from the analyte are acquired for a final 60 s. A 150 s wash-out period was carried out between analyses. Data reduction was carried out using GLITTER software (van Achterbergh *et al.* 2001).

A glass standard (NIST 612) was used as external calibration. The standard was analysed twice at the start of each run, and then after every 8 or 9 spot samples. The standard was also analysed twice at the end of each run. Detection limits are usually between 1 and 10 ppb range.

**Table 3-1: LA-ICP-MS operating conditions**

<b>Conditions Used</b>	
<b>Scan Parameters</b>	
Detection modes	Dual (analogue and pulse detector are cross-calibrated prior to each session)
Dwell time	10 – 100 ms
Integration time	10 ms
<b>Laser</b>	
Laser	UP-213 (New Wave Research)
Type	Nd:YAG frequency quintupled
Wavelength	213 nm
Repetition rate	10 Hz
<b>Spots</b>	
Ablation duration	60 s
Spot Size	80 $\mu\text{m}$
Energy	0.8 mJ

### **Electron microprobe (EMPA)**

Electron microprobe analysis was performed on carbon-coated, polished thin sections. Prior to analysis, photomicrographs of thin sections and target areas were obtained to locate the probe beam. Analyses were carried out at the University of Leicester with a JEOL JXA-8600S electron microprobe, with various operating conditions depending on

the target material, summarised in Table 3-2. Count times of 20 s were used for measurement of characteristic peak intensities, with 10 s at each of the background positions selected on either side of the peak. Quantitative background corrected results were standardised against a combination of synthetic materials and well-characterised natural minerals and corrected for matrix effects using a ZAF correction procedure. Minimum detection limits, calculated as 3 standard deviations above background, under the analytical conditions used, range from typically 0.02 wt% for Na<sub>2</sub>O to 0.05 wt% for FeO and NiO.

Previous experiments (Ellis, 2009) have shown that using standard operating conditions of 30 nA probe current and a beam diameter of 10 µm resulted in excess volatilisation of sodium from the sample and corresponding increases in the proportions of other elements such as silica. To mitigate this problem glass analyses used a beam diameter of 30 µm.

**Table 3-2: Electron microprobe operating conditions**

	<b>Conditions Used</b>	
	<b><i>Glass</i></b>	<b><i>Phenocryst</i></b>
Beam Diameter	30 µm	10 µm
Probe current	10 nA	10 nA
Accelerating voltage	15 keV	15 keV

### **Scanning electron microscope**

Back-scattered electron images were obtained to aid in analytical work using the Hitachi S3600-N SEM in the Department of Geology, University of Leicester, using 15kV accelerating voltage.

### **X-ray fluorescence spectrometry**

Bulk rock samples of welded ignimbrite and unwelded pumice-fall deposits were prepared for X-ray fluorescence spectrometry at the University of Leicester. Samples were split by hand and where necessary, weathered crusts removed with a rock saw. Samples were crushed to a 2-3 mm gravel using a flypress, removing lithic fragments to ensure the sample represented only juvenile material. The remaining material was then ground to a fine powder in a Retsch planetary mill for 20 minutes, at 250 revolutions per minute using agate pots and grinding balls. Powdered samples were then split into

two parts to make fusion beads and powder pellets for major oxide and trace element analyses respectively.

### ***Fusion beads***

To determine major oxide abundances, powdered samples are first dried over night in an oven at 110°C. Loss of ignitions (LOI) are calculated by igniting the samples at high temperatures and calculating the weight lost. The peralkaline nature of these rocks causes samples to fuse at the temperatures normally used at the University of Leicester for LOI determination (950°C). Therefore, a two-stage LOI method was developed to deal with this.

First, disposable LECO crucibles are used instead of the standard ceramic crucibles to minimize costs if samples accidentally fused to the crucible. The weight of the crucible and the weight of the crucible plus sample before and after ignition are recorded in order to determine the weight loss. The ignitions are performed in a muffle furnace at 750°C for 1.5 hours. After ignition, the samples are allowed to cool to room temperature in a dessicator before reweighing. After reweighing, a portion of the ignited powder is then transferred to a clean 10 ml glass vial with plastic snap tops for storage in a dessicator prior to fusion bead preparation. The remaining sample is then returned to the furnace at 950°C for 1 hour, cooled to room temperature and reweighed to account for any further weight loss. The percentage weight loss (LOI) can then be determined.

From the sample kept aside after ignition at 750°C, 0.6 g of powder is mixed with 3g of metaborate flux (plus a previously determined weight loss of dried flux). Both powders are accurately weighed into a 95% Pt/5% Au crucible. These are then thoroughly mixed together, melted over a Spartan burner, and cast into a disc using a Pt/Au casting dish.

### ***Powder pellets***

To determine the trace element abundances of geological materials by XRF, powdered samples are mixed with a binding agent and then compressed in a mould to form a pellet. Currently, the typical method of powder pellet preparation at the University of Leicester involves a liquid binder. Rock samples are first crushed in a fly press to chip sized fragments (2-3 mm) and then milled to produce a fine powder. A Retsch Planetary Mill with agate pots and balls is used to reduce approximately 60g of material to a uniform powder, 10 g of which is then weighed into a disposable beaker with a variable amount (dependent upon rock type) of an aqueous based solution (7% Polyvinyl

alcohol, Moviol 8-88 type solution in a 1:5 mixed CH<sub>3</sub>OH/H<sub>2</sub>O solvent). This mixture is then placed in a die and subjected to 10 tonnes per square inch to produce a smooth pellet. The pellets are then left to dry. Pellets produced using the liquid-binding method described above, formed a white crust on the surface of the pellet or crumbled completely. It is thought that this was caused by the remobilization of Cl by the aqueous binding agent to form a salt crust. The heavy nature of chlorine dampened the signal of other elements when these pellets were analysed and incorrect analyses were obtained. In order to avoid this issue, a new method of preparation was developed using a wax-based binding agent.

The wax-based binding technique uses 6 g of fine rock powder which is carefully weighed into a disposable plastic beaker. To this, 1.5 g of a paraffin binder (Hoechst Wax C/SPEX CertiPrep 3646) is added. Three disposable glass beads are added to the mixture and then mixed for 3 minutes using a mechanical shaker which ensures a homogenous mix of rock material and binding agent. The mixture is then placed in a 32 mm diameter die and pressed to 10 tonnes per square inch as above. The resulting powder pellet does not need to be left to dry like standard liquid-binded pellets and there is no remobilisation of Cl in the sample to form a crust. The use of disposable beakers and glass beads ensures that there is no cross-contamination of samples.

### ***Analytical technique***

XRF analyses were carried out at the University of Leicester using a PANalytical Axios Advanced X-Ray Fluorescence spectrometer. The machine runs a 4Kw Rhodium (Rh) anode end window super sharp ceramic technology X-Ray tube. Operating conditions are optimised for sensitivity and resolution.

### **Oxygen isotopes**

Oxygen isotopes were analysed at the University of Oregon stable isotope laboratory by B. Ellis with the assistance of I. Bindeman. Samples were first crushed, wet sieved and handpicked by myself at the University of Leicester under a binocular microscope for 1.5 to 2 mg of sample (approximately 3-4 plagioclase crystals) prepared for each analysis. Feldspars were chosen as the mineral to analyse in the absence of quartz throughout the deposit. Samples were analysed using CO<sub>2</sub>-laser fluorination and a 35-W laser in the presence of purified BrF<sub>5</sub> reagent to liberate oxygen. The gases generated were purified through cryogenic traps and a small mercury diffusion pump to

remove traces of fluorine gas. Oxygen was converted to CO<sub>2</sub> gas by a small platinum-graphite converter, the yield measured, and then the CO<sub>2</sub> gas was analyzed on a MAT 253 mass spectrometer. Standards were analyzed together with the unknowns during each analytical session with the San Carlos olivine ( $\delta^{18}\text{O} = 5.35\text{‰}$ ) and Gore Mountain garnet ( $\delta^{18}\text{O} = 5.75\text{‰}$ ) used as standards. Day-to-day  $\delta^{18}\text{O}$  variability on standards ranged from +0.1‰ to -0.3‰, and these values were added or subtracted to the unknowns to correct for day-to-day variability. Values are reported on a standard mean ocean water (SMOW) scale.

### 3.3. Results: chemical stratigraphy of the Green Tuff type section

Each lithofacies through the type section was sampled for geochemical analysis. Whole rock samples were analyzed by XRF for major oxides and trace elements. Polished, 100  $\mu\text{m}$  sections were made of 11 samples for analysis by EMPA and LA-ICP-MS. Geochemical data are here presented in Table 3-3 to Table 3-9 and are plotted against height to determine vertical chemical zonation through the deposit.

#### 3.3.1. Trends in major elements

Analyses for the type section show a range of whole-rock chemistries from peralkaline rhyolites (pantellerite) to trachyte (Fig. 3-1) and also show some variation with height. This is best represented by TiO<sub>2</sub> and Al<sub>2</sub>O<sub>3</sub> (Fig. 3-2) and less so by SiO<sub>2</sub>. An increase in TiO<sub>2</sub> and Al<sub>2</sub>O<sub>3</sub> combined with a decrease in SiO<sub>2</sub> are all consistent with the deposit becoming less evolved with height. This is mirrored by a decrease in peralkalinity index with height (Fig. 3-3). Spot analyses from EMPA match the same trends as the whole rock XRF, though show a greater range of values. This is likely to be due to three issues. Firstly, there could be natural heterogeneity on the small scale. This could be particularly relevant for the trace element results where analyses close to phenocrysts show greater variability than analyses taken in the middle of large areas of glass, potentially due to element diffusion. Secondly, the samples from the type section were not ideal for glass analysis due to matrix commonly having a lithoidal texture. Whilst glassy areas were chosen for study, some data points will have included microcrysts. With this in mind, the XRF data give a more robust, integrated, indication of the geochemical nature of the deposit. Finally, and most importantly, the whole rock XRF data are an average composition for both the glass and phenocrysts. This effect is most noticeable in the trace elements.

Table 3-3: XRF whole rock data for Green Tuff Formation type section.

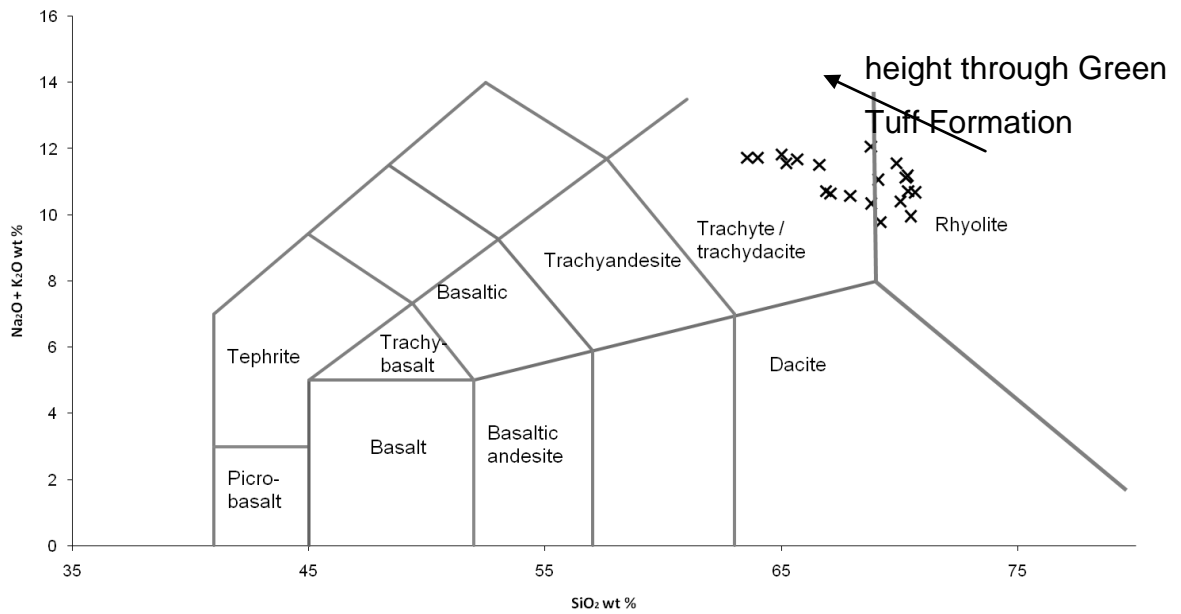
Sample Height (cm)	GT44B	GT44DI	GT44D	GT44Dii	GT44E	GT44Ei	GT44Ev	GT44Eiii	GT44Eiv	GT44Evi	GT44Eiv	GT44F	GT44F	GT44G	GT44H	GT44I
	25	75	85	110	125	215	215	250	295	325	365	400	465	520	815	
SiO <sub>2</sub>	69.4	63.6	69.5	69.5	65.3	66.3	68.1	67.5	66.7	66.1	65.8	64.7	64.1	63.5	62.7	
TiO <sub>2</sub>	0.5	0.5	0.5	0.5	0.7	0.6	0.6	0.6	0.6	0.7	0.6	0.7	0.7	0.8	0.8	
Al <sub>2</sub> O <sub>3</sub>	8.4	8.1	9.0	9.2	13.5	10.1	10.8	11.5	12.3	12.3	12.2	14.1	13.6	15.3	15.7	
Fe <sub>2</sub> O <sub>3</sub>	8.6	8.3	8.4	8.6	6.8	8.2	8.1	8.0	7.9	7.7	7.5	6.7	6.9	6.3	6.3	
MnO	0.3	0.3	0.3	0.3	0.3	0.3	0.3	0.3	0.3	0.3	0.3	0.3	0.3	0.2	0.2	
MgO	0.1	0.2	0.1	0.3	0.2	0.4	0.3	0.2	0.2	0.3	0.2	0.2	0.3	0.2	0.2	
CaO	0.4	0.4	0.4	0.4	0.9	0.6	0.5	0.7	0.7	0.8	0.8	0.9	1.0	1.1	1.1	
Na <sub>2</sub> O	6.3	5.5	6.0	5.4	6.8	5.3	5.8	6.0	6.0	6.2	6.7	6.7	6.9	7.1	7.1	
K <sub>2</sub> O	4.2	4.0	4.5	4.4	4.8	4.1	4.4	4.5	4.6	4.4	4.7	4.8	4.8	4.6	4.4	
P <sub>2</sub> O <sub>5</sub>	0.0	0.0	0.0	0.0	0.1	0.1	0.1	0.1	0.1	0.1	0.1	0.1	0.1	0.2	0.2	
SO <sub>3</sub>	0.0	0.0	0.0	0.0	0.1	0.0	0.0	0.0	0.0	0.1	0.0	0.0	0.0	0.0	0.1	
LOI	0.2	1.1	0.6	1.0	0.2	0.5	0.5	0.3	0.2	0.8	1.0	0.1	0.9	0.2	0.5	
Total	98.4	91.8	99.5	99.6	99.8	96.2	99.5	99.7	99.6	99.6	99.8	99.3	99.5	99.5	99.3	
Ba	38.6	73.0	60.0	66.3	568.6	237.0	159.0	136.4	174.7	178.8	164.9	650.9	572.7	1891.2	2267.8	
Ce	392.3	337.9	410.1	380.4	157.1	288.5	280.4	257.7	226.6	206.2	233.9	131.3	159.5	103.1	91.4	
Cl	7016.5	5983.3	—	4587.4	—	1610.3	6100.8	1048.5	17.4	6487.4	—	156.4	—	—	—	
Co	5.1	4.6	10.3	4.2	8.0	4.6	6.7	4.2	3.9	2.9	8.4	2.3	6.3	7.1	7.0	
Cr	21.1	13.5	—	—	—	3.8	2.0	—	3.6	—	3.0	—	—	0.9	—	
Cs	5.7	5.5	12.1	5.7	0.3	2.9	3.4	2.9	2.9	1.7	4.9	0.5	—	—	—	
Cu	0.9	2.4	1.5	0.5	—	0.4	—	-0.8	—	—	—	—	—	—	—	
Ga	32.8	36.0	36.0	34.9	35.2	34.4	37.0	38.1	36.7	36.8	36.5	35.2	35.0	32.2	30.6	
La	219.8	194.7	235.6	205.9	87.9	163.8	150.1	136.4	126.2	114.1	132.8	73.1	106.4	75.9	56.3	
Mo	21.2	13.1	10.6	6.0	4.4	7.4	6.6	5.3	5.2	6.5	4.4	3.4	3.2	2.2	1.4	
Nb	390.5	376.1	353.7	360.7	139.7	288.8	285.0	244.9	214.3	196.9	194.2	119.9	130.5	78.0	66.5	
Nd	168.1	148.4	162.7	163.3	73.0	125.3	117.4	113.4	104.6	96.3	99.7	65.2	81.9	58.4	45.1	
Ni	4.2	4.0	1.6	1.9	—	2.8	1.8	1.1	1.8	1.0	—	0.6	—	—	—	
Pb	14.5	13.6	15.6	14.2	7.8	11.8	8.5	8.2	6.1	5.9	7.7	3.9	6.0	3.4	3.9	
Rb	197.0	189.5	176.7	180.6	80.2	148.2	145.8	126.7	111.1	91.5	100.8	65.2	66.8	48.2	39.3	
Sc	0.3	0.1	2.6	0.6	6.7	0.4	1.5	0.2	2.7	2.4	5.7	4.9	8.3	10.1	12.7	
Sr	4.2	10.9	8.0	10.8	17.0	22.1	13.8	12.0	14.2	14.8	13.8	18.9	20.9	54.3	64.0	
Th	35.1	34.1	34.4	32.6	11.0	25.5	24.1	19.2	16.5	13.9	16.3	7.6	9.6	4.9	4.9	
U	10.3	9.8	9.8	8.2	4.4	8.3	5.7	4.2	2.6	2.8	3.3	2.3	2.9	1.5	1.9	
V	0.4	0.7	3.3	—	4.4	—	1.9	1.7	2.3	1.1	3.1	—	4.5	7.3	9.4	
Y	182.7	178.3	170.7	164.0	67.4	147.1	122.8	100.6	92.4	94.1	88.4	65.5	75.5	51.1	31.1	
Zn	429.4	409.7	389.3	399.3	179.0	331.1	323.6	294.6	288.9	218.4	209.6	134.5	166.6	136.8	100.2	
Zr	2060.8	1985.3	1871.2	1912.7	1594.1	1483.2	1456.8	1185.4	1012.1	904.1	905.7	486.6	550.8	317.8	291.0	

Table 3-4: EMPA glass data averages for Green Tuff Formation type section.

Sample Height (cm)	GT44A	GT44B	GTCia	GTCib	GTCii	GT44D	GT44E	GT44F	GT44G	GT44H	GT44I
	0	15	45	45	45	85	215	365	465	520	815
SiO <sub>2</sub>	66.6	69.0	66.9	68.4	68.8	70.0	66.9	62.1	62.5	62.8	63.8
TiO <sub>2</sub>	0.4	0.3	0.3	0.4	0.6	0.4	0.7	1.1	1.0	0.7	0.7
Al <sub>2</sub> O <sub>3</sub>	7.1	7.3	7.0	7.2	8.6	7.3	11.5	10.8	12.8	15.1	15.1
Cr <sub>2</sub> O <sub>3</sub>	0.0	0.0	0.0	0.0	0.0	0.0	0.0	0.0	0.0	0.0	0.0
FeO	6.9	7.6	7.4	7.6	7.6	7.8	7.1	10.0	8.5	4.7	4.6
MnO	0.3	0.3	0.3	0.3	0.3	0.3	0.3	0.5	0.4	0.2	0.1
MgO	0.1	0.0	0.1	0.1	0.1	0.1	0.2	0.4	0.5	0.2	0.2
CaO	0.3	0.3	0.3	0.3	0.5	0.3	0.7	1.4	1.2	0.7	0.8
Na <sub>2</sub> O	5.7	5.6	5.5	5.2	5.6	5.3	5.7	5.6	6.0	6.9	6.6
K <sub>2</sub> O	4.2	4.3	4.4	4.3	4.8	4.8	4.9	4.5	4.8	4.9	5.0
NiO	0.0	0.0	0.0	0.0	0.0	0.0	0.0	0.0	0.0	0.0	0.0
Total	91.6	94.9	92.3	93.9	96.8	96.4	97.8	96.4	97.8	96.3	96.9
n =	3	21	9.00	25	40	18	13	12	12	7	18

Table 3-5: LA-ICP MS glass data averages for Green Tuff Formation type section

<i>Sample</i>	GT44B	GT44CiB	GT44Cii	GT44D	GT44E	GT44F	GT44G	GT44H	GT44I
<i>Rel Height</i>	15	45	45	85	215	365	465	520	815
Li7	35.7	43.2	10.7	24.2	24.0	30.9	24.6	12.6	3.4
Be9	13.7	14.2	13.3	13.7	10.2	6.1	9.6	1.9	2.2
Mg24	1990.1	1654.1	1305.2	1057.3	1818.7	4341.8	4862.2	3446.8	4387.3
Mg26	2041.8	1793.9	1254.1	1114.4	2043.3	4531.9	5106.0	3203.3	4512.1
Si29	322482.8	323066.0	320186.5	325395.0	323203.1	270998.0	291897.2	290155.2	298263.7
Ca43	5214.7	3262.7	3948.9	2945.4	4830.5	9143.3	11523.1	9592.6	11335.7
Ca44	5173.4	3197.9	3888.5	2906.3	4375.7	9195.8	11279.5	9347.3	11253.7
Sc45	4.6	4.5	7.5	4.7	8.5	8.3	12.2	10.6	13.8
Ti47	2649.8	2558.6	3893.6	2861.6	4655.0	3702.3	4485.8	5602.5	5738.7
V51	0.4	0.3	0.2	0.3	0.4	0.5	1.0	1.0	1.4
Cr53	0.8	0.5	0.1	0.5	0.3	0.5	1.3	0.5	0.5
Mn55	2140.1	2190.9	2236.6	2325.1	2410.0	2218.3	2407.1	1342.0	1434.1
Fe57	58567.1	55098.1	47822.1	63981.7	56755.8	67003.0	54791.8	38861.7	48097.8
Co59	0.3	0.2	0.3	0.3	0.5	0.4	0.5	0.4	0.6
Ni60	0.8	0.3	0.0	0.3	0.2	1.7	1.3	0.6	0.4
Cu63	14.3	3.2	1.5	6.0	2.6	3.6	18.9	3.6	2.8
Zn66	483.8	527.5	473.1	526.9	240.9	264.8	281.6	181.4	134.8
Ga71	27.1	28.4	28.0	29.4	28.9	28.5	28.3	22.4	25.9
Ge72	3.1	3.2	3.1	3.5	3.3	2.9	2.6	1.7	1.9
As75	10.0	10.4	8.2	9.4	2.6	1.7	1.8	1.4	1.4
Rb85	186.4	190.5	169.0	174.3	84.4	104.9	86.1	42.2	47.2
Sr88	5.4	3.8	2.9	4.6	5.5	11.7	20.6	34.8	22.5
Y89	207.6	227.7	194.1	206.6	126.6	177.9	91.6	32.5	27.7
Zr90	2465.3	2340.0	2314.9	2361.8	1846.3	1458.7	883.9	255.3	362.8
Nb93	490.3	482.9	449.4	499.3	407.5	329.2	213.3	95.4	106.8
Mo95	22.5	22.9	20.3	16.6	6.5	4.4	4.6	2.0	1.8
Cd111	0.6	0.6	0.5	0.5	0.1	0.2	0.2	0.2	0.1
In115	0.3	0.4	0.3	0.4	0.3	0.3	0.4	0.2	0.1
Sn118	15.5	14.6	13.6	17.9	12.1	17.2	12.2	6.7	5.3
Sb121	0.8	0.8	0.6	0.7	0.3	0.3	0.8	0.1	0.2
Cs133	2.3	2.4	2.0	2.0	0.5	0.2	0.1	0.1	0.2
Ba137	54.6	51.1	64.5	54.2	93.9	72.0	503.1	1236.2	860.7
La139	253.5	253.1	235.7	261.6	281.7	277.5	115.3	41.7	46.6
Ce140	459.2	462.5	409.9	474.8	507.6	439.9	185.8	77.1	71.9
Pr141	51.5	52.6	48.5	54.9	56.2	56.2	25.1	10.0	10.8
Nd146	187.4	190.1	176.8	195.0	197.1	209.8	99.6	40.4	41.9
Sm147	38.1	38.3	35.6	39.3	37.2	40.9	20.6	8.5	8.6
Eu153	5.5	5.7	5.2	5.7	5.7	6.7	4.7	3.5	2.8
Gd157	36.5	36.3	34.4	36.9	29.9	37.7	19.6	8.4	7.6
Tb159	5.9	5.9	5.6	6.0	4.3	6.0	2.9	1.2	1.1
Dy163	38.3	39.4	35.7	38.4	25.9	35.5	18.3	7.7	6.4
Ho165	7.7	8.0	7.2	7.7	4.9	7.3	3.6	1.5	1.2
Er166	22.4	23.5	21.0	22.2	14.1	19.4	10.7	4.1	3.2
Tm169	3.3	3.4	3.2	3.3	2.1	2.8	1.5	0.6	0.4
Yb172	21.2	22.4	20.5	21.3	14.4	17.7	10.2	3.7	3.0
Lu175	3.1	3.2	2.9	3.1	2.2	2.6	1.5	0.5	0.5
Hf178	54.8	54.3	52.8	53.9	42.8	35.3	20.4	7.7	8.5
Ta181	29.1	29.3	28.0	29.0	24.8	19.5	12.2	6.7	6.1
W182	5.5	5.8	5.0	5.5	2.4	1.3	2.2	0.9	0.8
Ti205	0.2	0.1	0.2	0.1	0.0	0.1	0.0	0.0	0.0
Pb208	15.9	15.4	11.2	13.0	3.8	6.8	7.1	2.8	3.2
Bi209	0.1	0.1	0.0	0.0	0.0	0.0	0.1	—	0.0
Th232	42.9	43.7	41.1	41.0	35.8	32.5	19.8	4.7	6.1
U238	10.2	11.6	9.2	11.2	5.1	4.2	3.4	0.8	1.3
n=	13	5	5	9	3	2	5	3	5



**Fig. 3-1:** Total alkalis ( $\text{Na}_2\text{O} + \text{K}_2\text{O}$  wt %) versus silica ( $\text{SiO}_2$ ) (TAS) plotted for whole rock XRF data through the type section. Samples from the bottom of the Green Tuff Formation plot in the rhyolite field whereas samples from the top of the ignimbrite plot in the trachyte field.

### 3.3.2. Trends in trace elements and rare earth elements

The trace elements show a stronger variation with height than the major element oxides. In particular, incompatible elements such as Nb, Rb, and Zr show gradual depletions with respect to height through the deposit (Fig. 3-4). Compatible elements, particularly those which are related to the fractionation of feldspar such as Ba and Sr, show enrichment with height through the deposit in the whole-rock analyses but less so in the glass analysis. This is an effect of the XRF data averaging the glass and phenocryst compositions. The upper horizons of the ignimbrite have a feldspar volume of >25 % compared to <10 % at the base of the deposit. Therefore, there is a stronger input of Ba and Sr-rich feldspars at the top of the deposit. The glass data show less enrichment with height. These trends are all consistent with the major element trends, and support an interpretation that the deposit becomes less evolved from its base to its top. The rare earth elements all show gradual, linear depletion with height (Fig. 3-5).

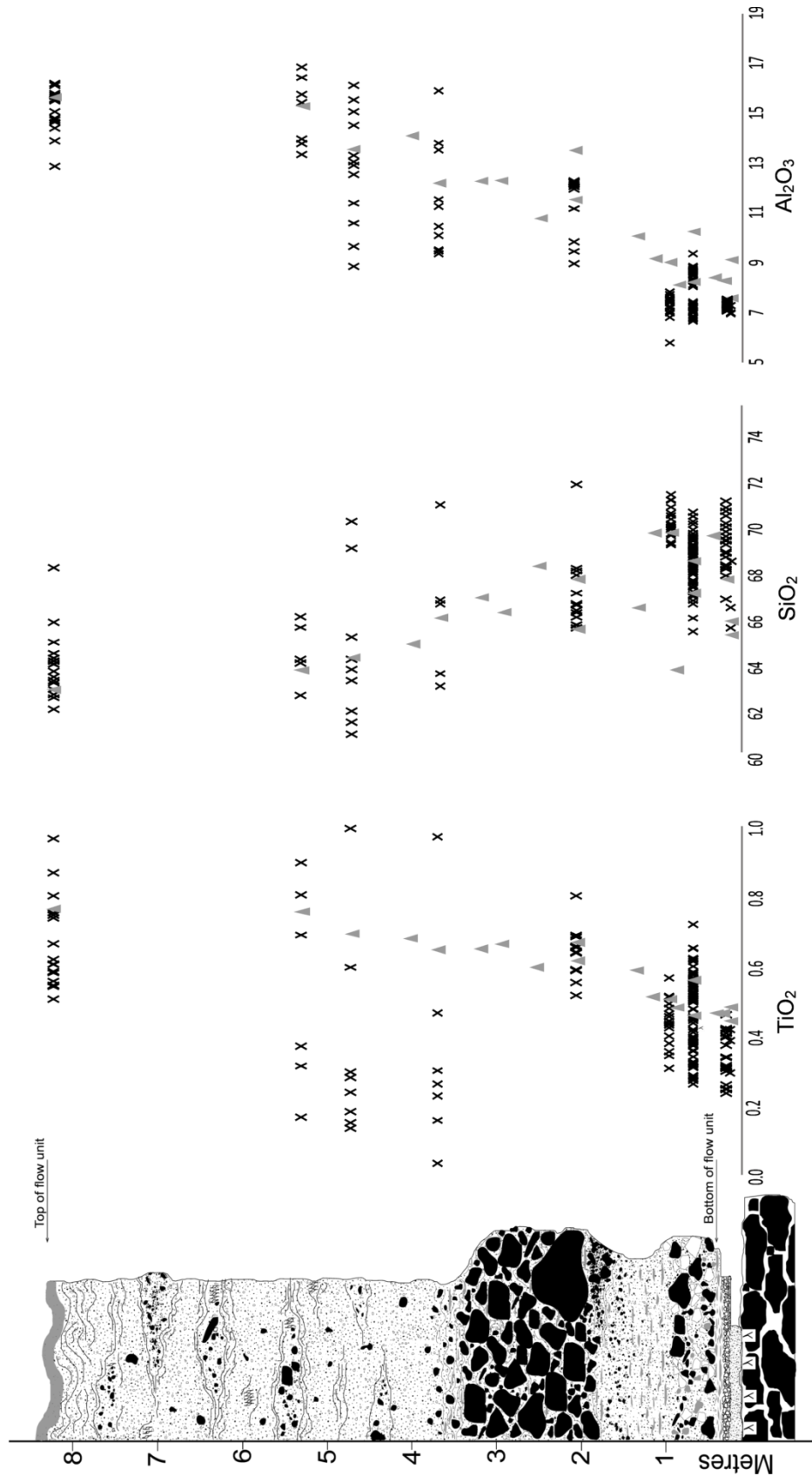
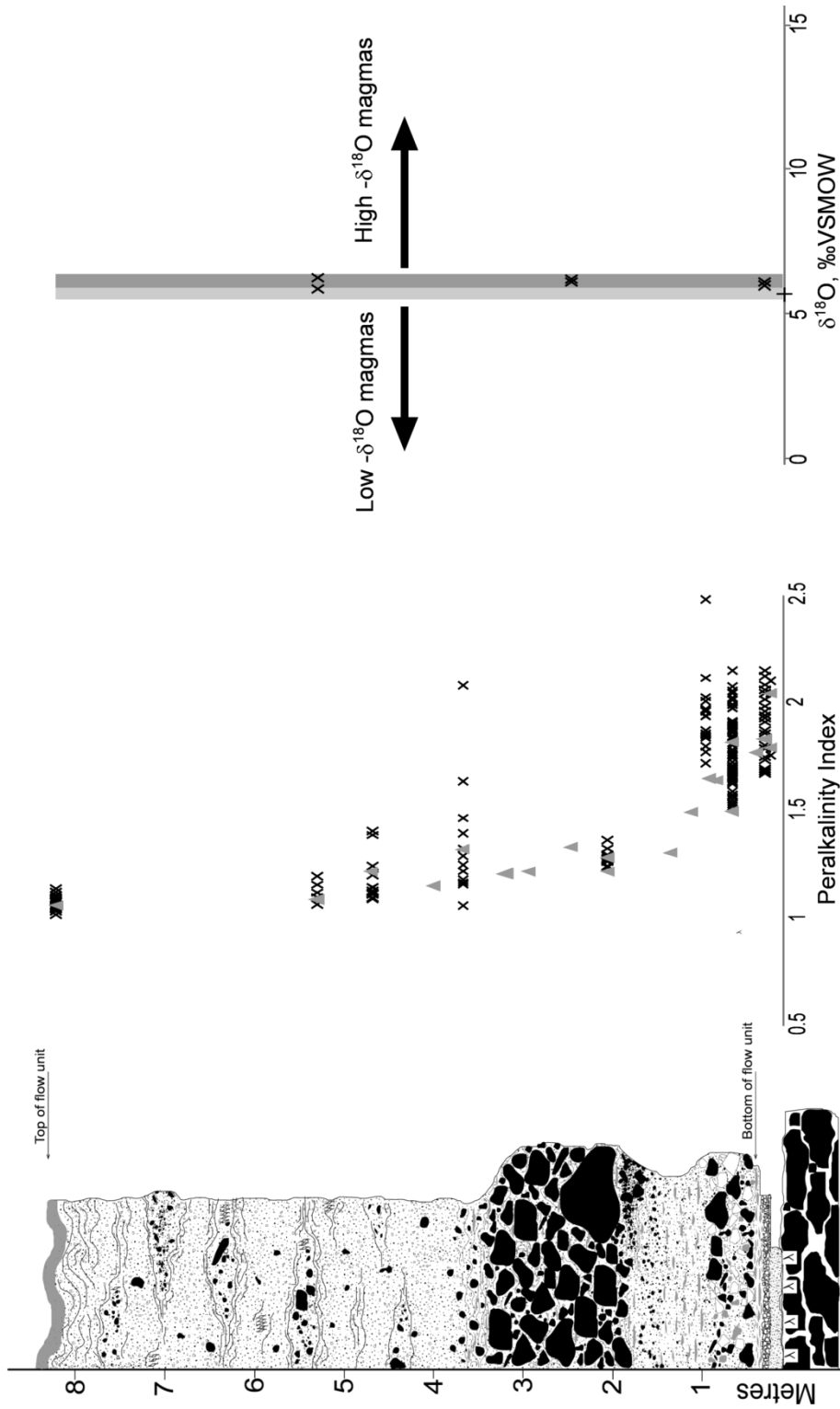


Fig. 3-2: Selected major elements in weight %, determined by whole rock XRF (triangles) and single spot EMPA of glass (crosses), shown against height through the type section. Note the increasing trends for  $TiO_2$  and  $Al_2O_3$  which is accompanied by a decreasing trend in  $SiO_2$ .



**Fig. 3-3: A) Peralkalinity (Molar  $[\text{Na}_2\text{O} + \text{K}_2\text{O}]/\text{Al}_2\text{O}_3$ ) plotted against height for whole rock (triangles) and glass spot analyses (crosses). As the deposit becomes less evolved, it also becomes less peralkaline. Peralkaline rocks have a peralkalinity value greater than 1 and strongly peralkaline rocks have a value greater than 1.1 (Mahood, 1984). B) Oxygen isotope variations for feldspar crystals plotted against the type section. The grey bands represent ‘normal-  $\delta^{18}\text{O}$ ’ magmas.**

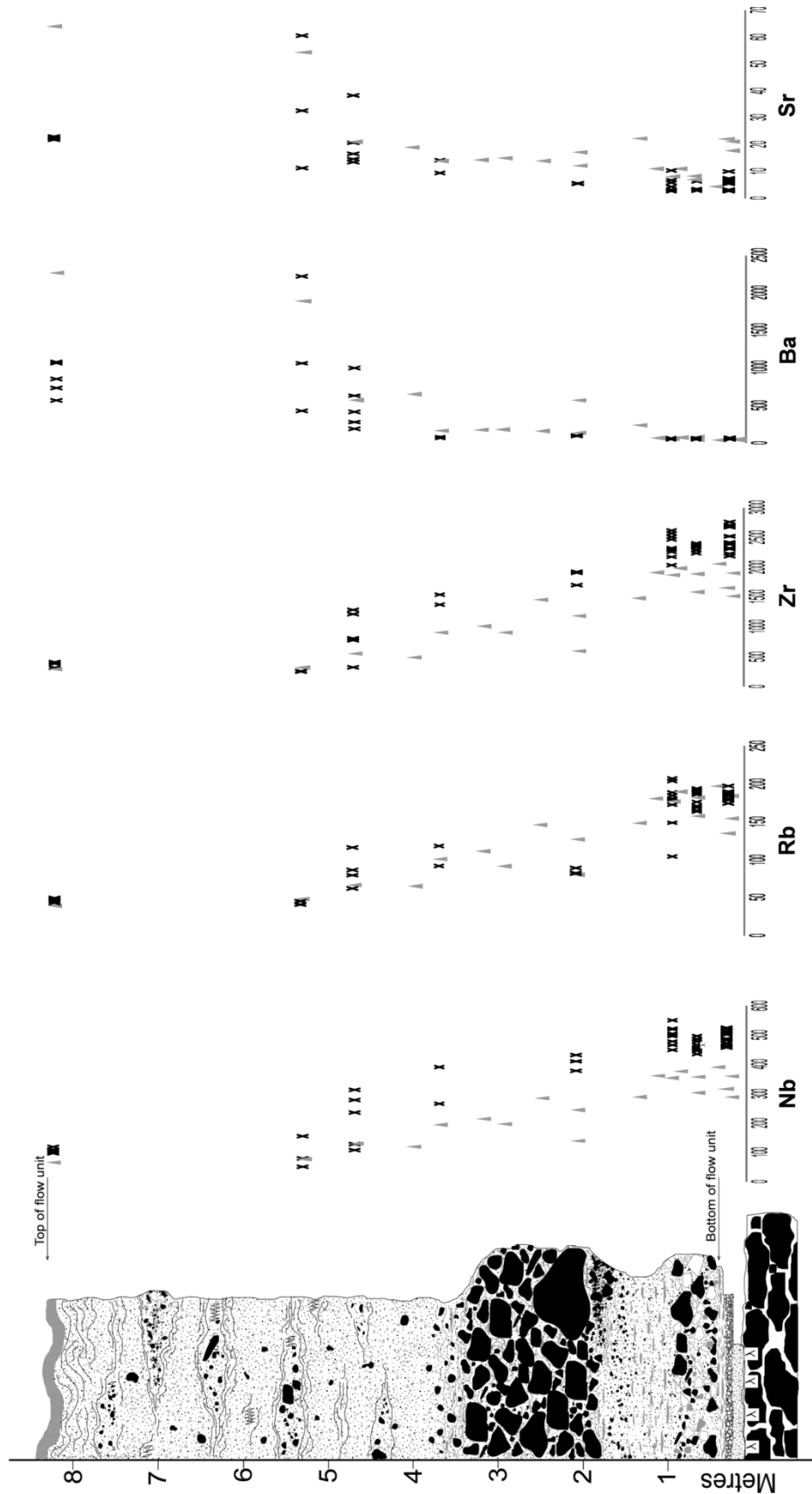


Fig. 3-4: Selected trace elements in ppm, determined by XRF for whole rock analysis (triangles) and LA-ICP MS for spot glass analysis (crosses). Note the decreasing trends for the incompatible elements (Nb, Rb, Zr) but the increasing trend for feldspar-compatible elements (Ba, Sr).

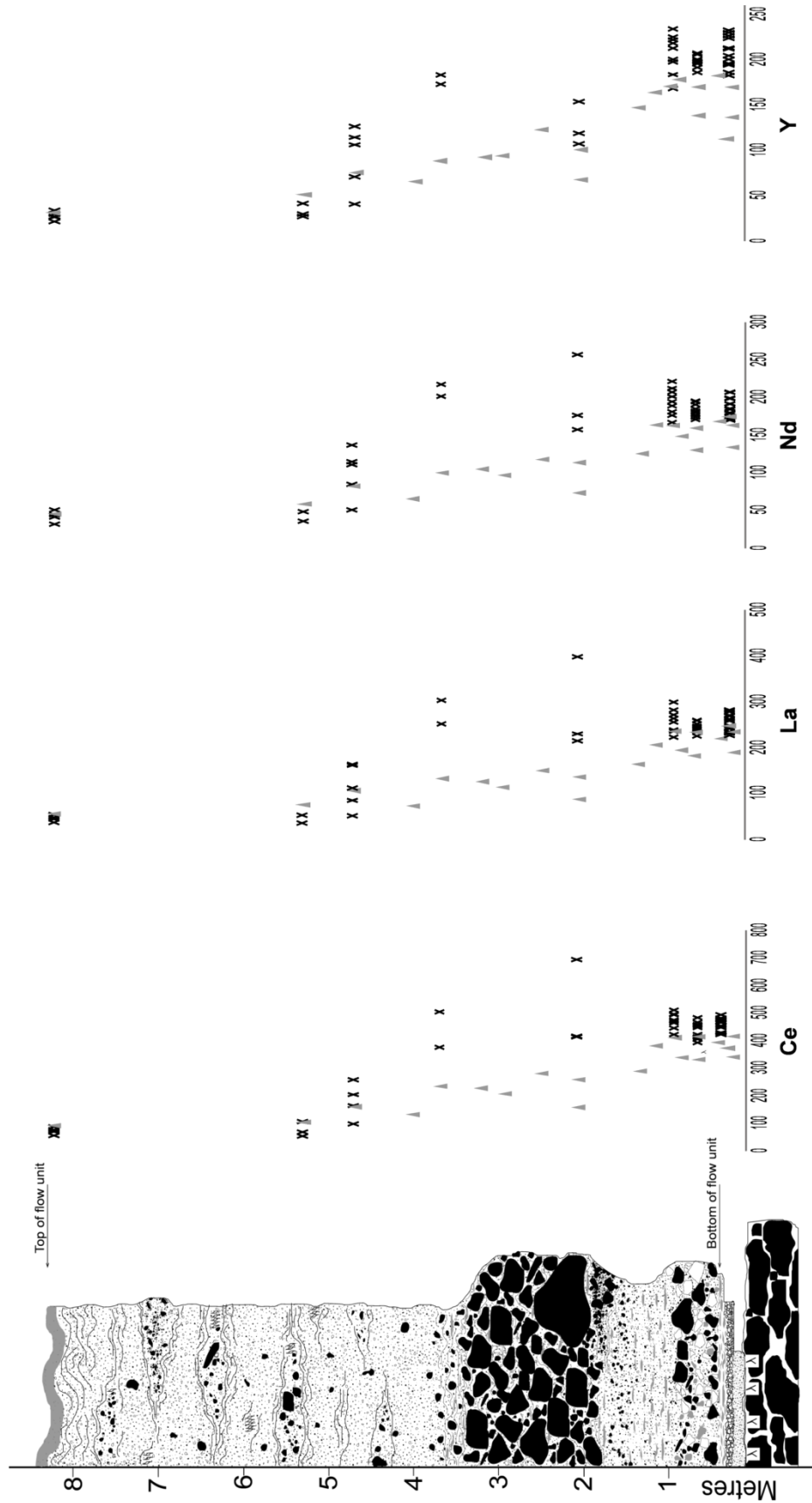
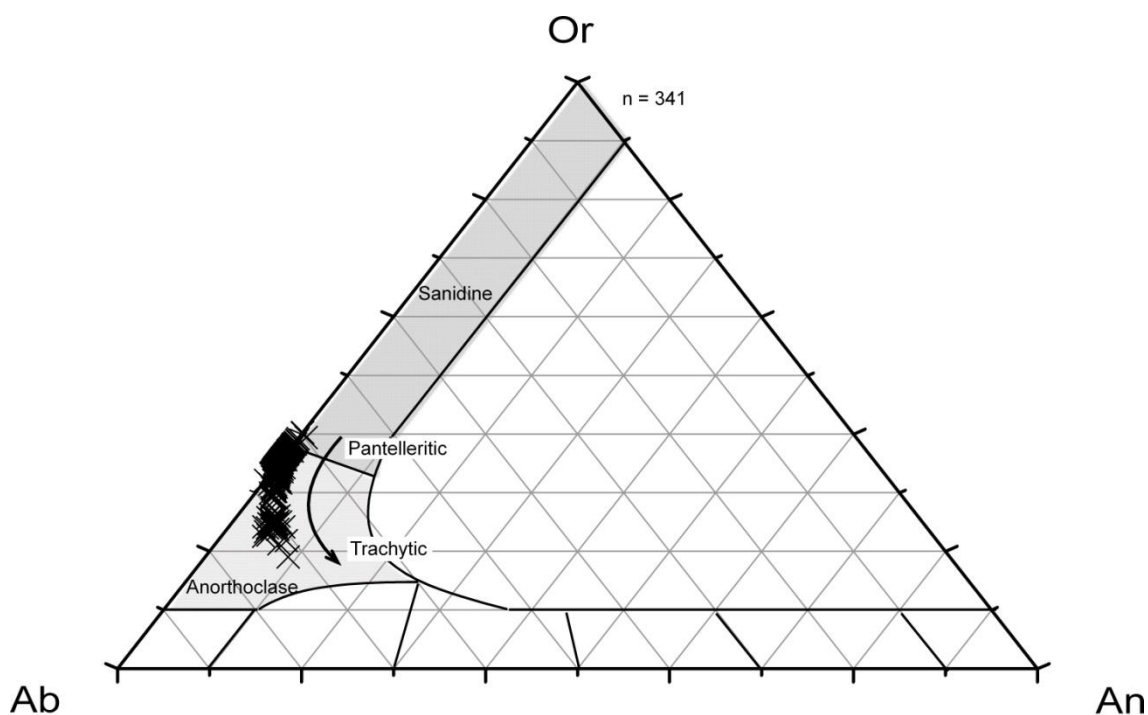


Fig. 3-5: Selected rare earth elements in ppm (chosen due to their ability to be analysed both by XRF and LA-ICP MS) analysed by XRF for whole rock (triangles) and LA ICP-MS for glass spot analyses (crosses).

### 3.3.3. Trends in Phenocrysts

Feldspars are the dominant phase throughout the deposit. Rare sanidines are found in the most evolved units, but the predominant feldspar type is anorthoclase (Fig. 3-6). There is a trend from more potassic anorthoclase ( $Ab_{63}Or_{37}$ ) to more sodic and calcic anorthoclase ( $Ab_{70}Or_{25}An_5$ ) with height through the type section. There is little to no zoning within individual crystals. The trend away from high potassic anorthoclase is mirrored by a trend from low Ba, high Rb feldspars in the pantelleritic end member to high Sr, high Ba feldspars in the trachytic end member (Fig. 3-7). This is a typical fractional crystallization trend, where basalt and trachyte-derived feldspars take up all the Ba and Sr from the melt, leaving an evolved melt, from which Rb-rich feldspars crystallize. However, low-Ba feldspars are also found in the trachytic groundmass, and typically show resorption textures. This indicates that these crystals have not grown *in situ* in the trachyte glass but are inherited from a low-Ba melt, such as the pantellerite.



**Fig. 3-6: Ternary plot for feldspars showing trend from Or-rich anorthoclases and rare sanidines in the pantelleritic base of the type section through to more Ab and An rich anorthoclases in the trachytic top of the type section. From EMPA analysis.**

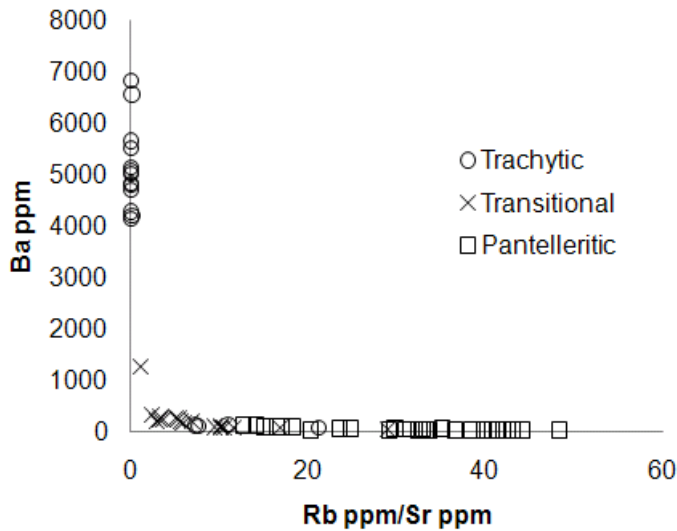


**Fig. 3-7:** Trace element concentrations in feldspars showing typical fractional crystallisation trend from high Ba-feldspars in the more mafic end member to low Ba, low Sr, high Rb-feldspars in the more evolved, pantelleritic end member. From LA ICP MS analysis.

The dominant mafic phase in the pantelleritic base of the type section is aenigmatite. It does not occur in the transitional composition or in the trachytic top of the section.

Clinopyroxenes occur throughout the type section and are Na-rich augites. There is a small trend from ferrositic-augite ( $\text{Wo}_{42}\text{En}_{11}\text{Fs}_{47}$ ) in the pantelleritic end member at the base of the type section to enstatitic-augite ( $\text{Wo}_{44}\text{En}_{27}\text{Fs}_{29}$ ) in the trachytic end member at the top of the type section. There is little to no zoning seen in individual minerals.

Olivines occur in the transitional zone and trachytic end member of the type section.

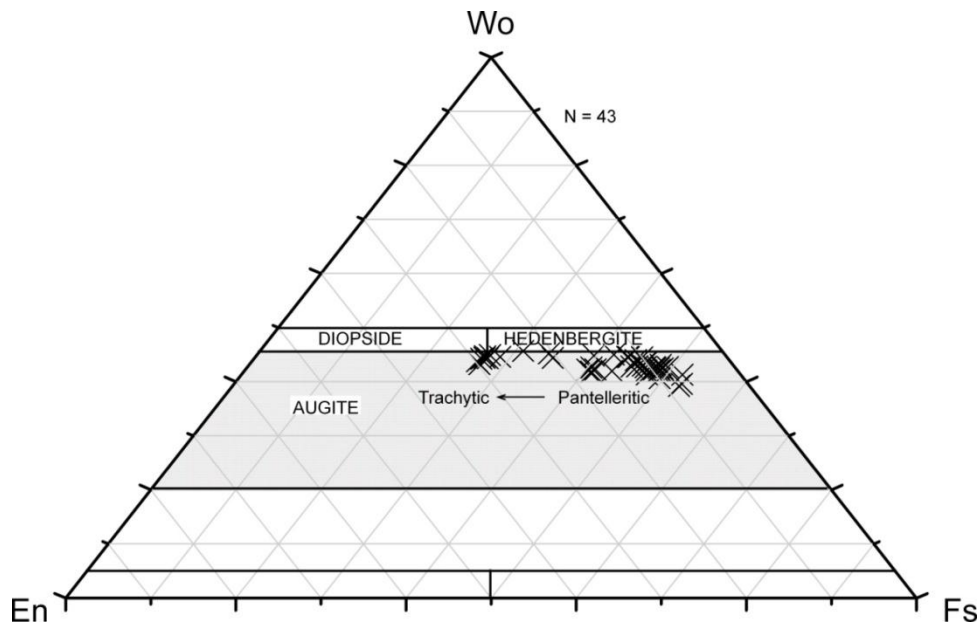


**Fig. 3-8:** Classification plot of the 'quadrilateral' pyroxenes based on end member compositions of Ca (Wo:  $\text{Ca}_2\text{Si}_2\text{O}_6$ ), Mg (En:  $\text{Mg}_2\text{Si}_2\text{O}_6$ ) and Fe (Fs:  $\text{Fe}_2\text{Si}_2\text{O}_6$ ). There is a trend from a more Fs rich composition in the pantelleritic end member to a more En rich composition in the trachytic end member.

**Table 3-6: Representative EMPA and LA-ICP MS feldspar analyses for the Green Tuff Formation.**

SAMPLE	GT44B	GT44Cib	GTCii	GT44D	GT44E	GT44F	GT44G	GT44H	GT44I
<b>Wt %</b>									
SiO <sub>2</sub>	66.7	65.6	67.5	65.7	65.7	65.9	65.9	64.3	64.4
TiO <sub>2</sub>	0.0	0.0	0.0	0.0	0.0	0.0	0.0	0.1	0.0
Al <sub>2</sub> O <sub>3</sub>	18.3	17.6	18.8	17.5	18.2	17.9	17.8	19.3	19.4
Cr <sub>2</sub> O <sub>3</sub>	0.0	0.0	0.0	0.0	0.0	0.0	0.0	0.0	0.0
FeO	0.9	0.8	0.7	1.1	0.4	0.7	0.7	0.3	0.3
MnO	0.0	0.0	0.0	0.0	0.0	0.0	0.0	0.0	0.0
MgO	0.0	0.0	0.0	0.0	0.0	0.0	0.0	0.0	0.0
CaO	0.0	0.0	0.0	0.0	0.1	0.1	0.0	0.9	0.7
Na <sub>2</sub> O	7.1	7.2	7.4	7.5	7.7	7.5	7.3	8.2	7.9
K <sub>2</sub> O	6.2	6.3	6.0	6.1	5.9	6.0	6.3	4.3	4.5
NiO	0.0	0.0	0.0	0.0	0.0	0.0	0.0	0.0	0.0
Total	99.2	97.5	100.4	97.9	98.2	98.2	98.0	97.4	97.2
<b>Formula (8 Oxygens)</b>									
Si	3.0	3.0	3.0	3.0	3.0	3.0	3.0	2.9	2.9
Ti	0.0	0.0	0.0	0.0	0.0	0.0	0.0	0.0	0.0
Al	1.0	1.0	1.0	0.9	1.0	1.0	1.0	1.0	1.0
Cr	0.0	0.0	0.0	0.0	0.0	0.0	0.0	0.0	0.0
Fe <sub>2</sub>	0.0	0.0	0.0	0.0	0.0	0.0	0.0	0.0	0.0
Mn	0.0	0.0	0.0	0.0	0.0	0.0	0.0	0.0	0.0
Mg	0.0	0.0	0.0	0.0	0.0	0.0	0.0	0.0	0.0
Ca	0.0	0.0	0.0	0.0	0.0	0.0	0.0	0.0	0.0
Na	0.6	0.6	0.6	0.7	0.7	0.7	0.7	0.7	0.7
K	0.4	0.4	0.3	0.4	0.3	0.4	0.4	0.3	0.3
Ni	0.0	0.0	0.0	0.0	0.0	0.0	0.0	0.0	0.0
Total	6.2	6.3	6.2	6.3	6.3	6.3	6.3	6.3	6.3
<b>Mol %</b>									
An	0.0	0.0	0.2	0.0	0.7	0.4	0.1	4.3	3.6
Or	36.6	36.6	34.7	35.0	33.4	34.5	35.9	24.6	26.2
Ab	63.4	63.4	65.1	65.0	65.9	65.0	64.0	71.1	70.2
<b>ppm</b>									
Li7	0.3	0.1	0.1	1.6	0.0	<0.1	0.0	<0.1	0.4
Be9	1.2	1.6	0.7	2.1	0.2	0.7	0.6	<0.1	0.1
Mg24	19.2	19.2	28.7	208.0	14.6	16.6	13.7	37.8	36.1
Mg26	20.1	20.6	23.1	229.7	20.4	18.1	16.6	37.8	38.0
Si29	311641.8	306687.0	315381.3	307201.2	307294.6	308042.5	307949.1	300376.5	300890.7
Ca43	384.5	324.4	490.4	783.6	1240.8	759.8	424.5	5812.1	5433.3
Ca44	263.9	189.5	342.2	738.0	1175.5	628.1	288.2	5495.2	5287.3
Sc45	1.0	0.8	1.1	1.2	0.7	0.8	0.9	0.5	0.9
Ti47	93.3	65.4	119.4	471.1	218.1	108.0	103.4	409.9	434.3
V51	0.0	0.0	0.0	0.0	<0.1	<0.1	<0.1	0.1	0.0
Cr53	0.1	0.3	0.1	0.2	<0.1	<0.2	<0.2	0.3	<0.1
Mn55	3.9	4.2	2.8	285.0	2.0	4.4	2.9	5.1	4.2
Fe57	7925.0	6941.9	4365.4	13673.9	2770.7	5727.2	4582.3	1887.3	1947.6
Co59	0.0	0.0	0.0	0.0	0.0	<0.1	<0.1	<0.1	<0.1
Ni60	0.2	0.1	0.2	0.4	0.1	0.1	0.1	0.1	0.2
Cu63	1.3	1.1	1.2	9.1	1.2	1.0	1.0	1.4	1.4
Zn66	10.6	10.9	6.1	68.8	2.2	6.7	4.9	2.3	2.4
Ga71	44.3	43.3	36.1	39.2	27.9	38.7	34.4	21.2	20.6
Ge72	1.4	1.3	1.4	1.5	1.3	1.4	1.4	1.0	1.0
As75	0.1	0.2	0.1	0.6	<0.1	<0.1	<0.1	<0.2	<0.1
Rb85	48.1	47.7	42.0	60.7	26.5	26.5	44.9	8.4	7.8
Sr88	1.1	1.2	3.0	1.8	10.6	2.6	2.1	113.5	70.7
Y89	0.0	0.0	0.0	13.5	<0.1	<0.1	<0.1	0.1	0.1
Zr90	0.1	0.1	0.0	243.9	0.0	0.0	0.0	0.5	0.2
Nb93	0.0	0.0	0.0	58.3	0.0	0.0	<0.1	0.0	0.1
Mo95	0.0	0.0	0.0	0.7	<0.1	<0.1	<0.1	<0.1	<0.1
Cd111	0.0	0.1	0.1	0.1	<0.1	<0.1	<0.1	0.2	0.0
In115	0.0	0.0	0.0	0.1	0.0	0.0	0.0	0.0	0.0
Sn118	1.4	2.8	2.5	3.8	2.6	2.7	1.9	3.5	2.3
Sb121	0.0	0.0	0.0	0.1	<0.1	<0.1	<0.1	<0.1	<0.1
Cs133	0.0	0.0	0.0	0.1	0.0	<0.1	0.0	<0.1	<0.1
Ba137	43.3	46.2	126.8	51.6	331.9	88.9	82.2	5018.4	6583.2
La139	0.0	0.1	0.1	16.2	0.4	0.1	0.0	1.0	0.8
Ce140	0.1	0.1	0.1	38.2	0.4	0.1	0.1	1.1	1.0
Pr141	0.0	0.0	0.0	3.6	0.0	<0.1	<0.1	0.1	0.1
Nd146	0.0	0.1	0.0	12.8	0.0	0.0	<0.1	0.2	0.2
Sm147	0.0	0.0	0.0	2.4	<0.1	<0.1	<0.1	0.1	0.0
Eu153	0.1	0.1	0.3	0.5	1.2	0.3	0.2	4.9	4.3
Gd157	0.0	0.0	0.0	2.2	<0.1	<0.1	<0.1	<0.1	<0.1
Tb159	0.0	0.0	0.0	0.4	<0.1	<0.1	<0.1	<0.1	<0.1
Dy163	0.0	0.0	0.0	2.6	<0.1	<0.1	<0.1	<0.1	0.0
Ho165	0.0	0.0	0.0	0.6	<0.1	<0.1	<0.1	<0.1	0.0
Er166	0.0	0.0	0.0	1.6	<0.1	<0.1	<0.1	0.0	<0.1
Tm169	0.0	0.0	0.0	0.3	0.0	<0.1	<0.1	0.0	<0.1
Yb172	0.0	0.0	0.0	1.8	<0.1	<0.1	<0.1	<0.1	<0.1
Lu175	0.0	0.0	0.0	0.3	<0.1	<0.1	<0.1	<0.1	<0.1
Hf178	0.0	0.0	0.0	5.3	0.0	<0.1	<0.1	0.0	0.0
Ta181	0.0	0.0	0.0	3.4	0.0	0.0	0.0	0.0	0.0
W182	0.0	0.0	0.0	0.4	<0.1	<0.1	<0.1	<0.1	<0.1
Tl205	0.0	0.0	0.0	0.0	0.0	0.0	0.0	<0.0152	0.0
Pb208	0.1	0.1	0.2	2.8	0.5	0.2	0.2	0.3	0.3
Bi209	0.0	0.0	0.0	0.0	<0.1	<0.1	<0.1	<0.1	<0.1
Th232	0.0	0.0	0.0	3.0	<0.1	<0.1	<0.1	<0.1	<0.1
U238	0.0	0.0	0.0	0.9	0.0	<0.1	<0.1	<0.1	<0.1
Rb/Sr	42.0	39.8	14.2	33.3	2.5	10.2	21.3	0.1	0.1

**Table 3-7: Representative EMPA analyses of Olivines for the Green Tuff Formation type section.**

<b>SAMPLE</b>	<b>GT44E</b>	<b>GT44E</b>	<b>GT44G</b>	<b>GT44H</b>	<b>GT44H</b>	<b>GT44H</b>	<b>GT44H</b>	<b>GT44H</b>	<b>GT44I</b>
<b>wt%</b>	Core	Rim	Core	Core	Core	Rim	Core	Rim	Core
SiO <sub>2</sub>	30.4	30.9	29.1	31.3	31.3	30.9	31.8	31.9	30.5
TiO <sub>2</sub>	0.0	0.0	5.1	0.0	0.0	0.0	0.0	0.0	0.1
Al <sub>2</sub> O <sub>3</sub>	0.0	0.0	0.0	0.0	0.0	0.0	0.0	0.0	0.2
Cr <sub>2</sub> O <sub>3</sub>	0.0	0.0	0.0	0.0	0.0	0.0	0.0	0.0	0.0
FeO	58.1	58.1	55.9	52.9	50.0	53.2	50.3	51.0	46.6
MnO	3.9	3.9	2.6	3.4	2.9	3.2	3.0	3.0	2.6
MgO	4.8	5.2	1.8	8.6	10.8	7.8	10.8	9.6	8.3
CaO	0.5	0.5	0.1	0.5	0.6	0.5	0.5	0.5	0.5
Na <sub>2</sub> O	0.0	0.0	0.0	0.0	0.0	0.0	0.0	0.0	0.0
K <sub>2</sub> O	0.0	0.0	0.0	0.0	0.0	0.0	0.0	0.0	0.0
NiO	0.0	0.0	0.0	0.0	0.0	0.0	0.0	0.0	0.0
Total	97.8	98.7	94.6	96.7	95.6	95.5	96.4	96.1	88.8
<b>Formula</b>									
Si	1.0	1.0	1.0	1.0	1.0	1.0	1.0	1.0	1.1
Ti	0.0	0.0	0.1	0.0	0.0	0.0	0.0	0.0	0.0
Al	0.0	0.0	0.0	0.0	0.0	0.0	0.0	0.0	0.0
Cr	0.0	0.0	0.0	0.0	0.0	0.0	0.0	0.0	0.0
Fe	1.6	1.6	1.6	1.4	1.4	1.5	1.3	1.4	1.3
Mn	0.1	0.1	0.1	0.1	0.1	0.1	0.1	0.1	0.1
Mg	0.2	0.3	0.1	0.4	0.5	0.4	0.5	0.5	0.4
Ca	0.0	0.0	0.0	0.0	0.0	0.0	0.0	0.0	0.0
Na	0.0	0.0	0.0	0.0	0.0	0.0	0.0	0.0	0.0
K	0.0	0.0	0.0	0.0	0.0	0.0	0.0	0.0	0.0
Ni	0.0	0.0	0.0	0.0	0.0	0.0	0.0	0.0	0.0
<b>Mol (%)</b>									
Fo (Mg)	12.1	13.1	5.2	21.3	26.6	19.7	26.6	24.0	23.1
Fa (Fe)	82.3	81.4	90.5	73.8	69.2	75.8	69.2	71.7	72.8
Te (Mn)	5.5	5.5	4.3	4.8	4.1	4.5	4.2	4.3	4.1

**Table 3-8: Representative EMPA analyses of Clinopyroxenes for the Green Tuff Formation type section.**

<b>SAMPLE</b>	<b>GT44B</b>	<b>GTCia</b>	<b>GT44Cib</b>	<b>GT44Cii</b>	<b>GT44D</b>	<b>GT44E</b>	<b>GT44F</b>	<b>GT44G</b>	<b>GT44H</b>	<b>GT44H</b>	<b>GT44I</b>
<b>wt%</b>											
SiO <sub>2</sub>	47.4	49.0	48.2	48.4	48.7	48.2	48.9	49.6	50.2	49.9	50.1
TiO <sub>2</sub>	0.4	0.3	0.3	0.3	0.4	0.4	0.4	0.4	0.6	0.6	0.6
Al <sub>2</sub> O <sub>3</sub>	0.1	0.1	0.1	0.1	0.1	0.2	0.1	0.3	0.6	0.6	0.5
Cr <sub>2</sub> O <sub>3</sub>	0.0	0.0	0.0	0.0	0.0	0.0	0.0	0.0	0.0	0.0	0.0
FeO	23.0	27.1	24.8	21.7	26.0	24.4	25.5	20.2	15.9	16.0	15.9
MnO	1.5	1.5	1.5	1.6	1.4	1.4	1.4	1.3	1.1	1.2	1.1
MgO	3.2	2.2	3.2	5.2	2.9	3.3	2.5	6.6	9.5	9.2	9.0
CaO	16.8	15.9	17.2	17.4	18.0	18.6	17.7	19.9	20.5	20.1	20.4
Na <sub>2</sub> O	1.9	2.7	1.9	1.5	1.4	1.3	1.8	0.6	0.5	0.5	0.6
K <sub>2</sub> O	0.0	0.0	0.0	0.0	0.0	0.0	0.0	0.0	0.0	0.0	0.0
NiO	0.0	0.0	0.0	0.0	0.0	0.0	0.0	0.0	0.0	0.0	0.0
Total	94.3	99.0	97.1	96.1	98.9	97.7	98.3	99.0	98.8	98.1	98.2
<b>Formula</b>											
Si (T)	2.0	2.0	2.0	2.0	2.0	2.0	2.0	2.0	2.0	2.0	2.0
Ti (M1)	0.0	0.0	0.0	0.0	0.0	0.0	0.0	0.0	0.0	0.0	0.0
Al (T)	0.0	0.0	0.0	0.0	0.0	0.0	0.0	0.0	0.0	0.0	0.0
Fe (M1 or M2)	0.8	0.9	0.9	0.8	0.9	0.8	0.9	0.7	0.5	0.5	0.5
Mn (M2)	0.1	0.1	0.1	0.1	0.0	0.0	0.0	0.0	0.0	0.0	0.0
Mg (M1 or M2)	0.2	0.1	0.2	0.3	0.2	0.2	0.2	0.4	0.6	0.5	0.5
Ca (M2)	0.8	0.7	0.8	0.8	0.8	0.8	0.8	0.9	0.9	0.9	0.9
Na (M2)	0.2	0.2	0.2	0.1	0.1	0.1	0.1	0.0	0.0	0.0	0.0
Sum (T)	2.0	2.0	2.0	2.0	2.0	2.0	2.0	2.0	2.0	2.0	2.0
Sum (M1+M2)	2.0	2.1	2.0	2.0	2.0	2.0	2.0	2.0	2.0	2.0	2.0
<b>Mol %</b>											
Wo	42.8	39.6	42.0	41.8	42.5	44.0	43.1	44.4	44.4	44.4	44.9
En	11.4	7.8	10.7	17.3	9.4	11.0	8.5	20.5	28.6	28.2	27.6
Fs	45.8	52.6	47.2	40.9	48.0	45.0	48.4	35.1	27.0	27.4	27.4

**Table 3-9: Representative EMPA analyses of Aenigmatite and Iron-Titanium oxides for the Green Tuff Formation type section.**

SAMPLE wt %	GT44A		GT44B		GTCia		GT44Cib		GT44Cii		GT44D		GT44F		GT44I		GT44I	
	Aenigmatite	Ilmenite	Magnetite	Magnetite	Ilmenite	Magnetite	Ilmenite											
SiO <sub>2</sub>	39.9	39.7	40.9	39.8	0.0	40.4	41.2	0.0	40.4	41.2	0.0	0.0	0.0	0.0	0.1	0.1	0.0	0.1
TiO <sub>2</sub>	8.8	9.0	9.0	9.3	49.3	9.1	9.1	9.1	9.1	9.1	50.4	25.3	30.2	46.8	0.1	0.1	0.0	0.1
Al <sub>2</sub> O <sub>3</sub>	0.5	0.7	0.6	0.5	0.0	0.7	0.8	0.0	0.7	0.8	0.0	0.5	0.5	0.3	0.0	0.0	0.0	0.0
Cr <sub>2</sub> O <sub>3</sub>	0.0	0.0	0.0	0.0	0.0	0.0	0.0	0.0	0.0	0.0	0.0	0.0	0.0	0.0	0.0	0.0	0.0	0.0
FeO	34.9	35.8	38.7	36.5	44.0	38.3	36.7	44.0	38.3	36.7	43.8	65.8	59.2	46.2	0.0	0.0	0.0	0.0
MnO	1.1	1.1	1.1	1.2	2.1	1.2	1.2	2.1	1.2	1.2	2.4	1.7	2.2	1.8	0.0	0.0	0.0	0.0
MgO	1.1	1.2	1.2	1.1	0.4	1.1	1.1	0.4	1.1	1.1	0.0	0.2	0.8	0.9	0.0	0.0	0.0	0.0
CaO	0.5	0.7	0.5	0.5	0.0	0.6	0.6	0.0	0.6	0.6	0.0	0.0	0.0	0.0	0.0	0.0	0.0	0.0
Na <sub>2</sub> O	7.2	7.2	7.6	7.3	0.0	7.4	7.5	0.0	7.4	7.5	0.0	0.0	0.0	0.1	0.0	0.0	0.0	0.0
K <sub>2</sub> O	0.0	0.0	0.0	0.0	0.0	0.0	0.0	0.0	0.0	0.0	0.0	0.0	0.0	0.0	0.0	0.0	0.0	0.0
NiO	0.0	0.0	0.0	0.0	0.0	0.0	0.0	0.0	0.0	0.0	0.0	0.0	0.0	0.0	0.0	0.0	0.0	0.0
Total	94.1	95.6	99.7	96.3	95.9	98.8	98.2	95.9	98.8	98.2	96.6	93.5	93.0	96.2	96.2	96.2	93.0	96.2

There is a trend from fayalite olivine in the transitional zone ( $\text{Fo}_{12}\text{Fa}_{82}\text{Te}_6$ ) to more magnesium-rich olivines in the trachyte ( $\text{Fo}_{23}\text{Fa}_{73}\text{Te}_4$ ) top of the section.

### 3.3.4. Oxygen isotope results

Feldspar separates of three samples, which represent the range of chemical variation, were analysed for oxygen isotopes to test for isotopic variation with height. In the Green Tuff Formation oxygen isotope ratios show a limited range of values from  $\delta^{18}\text{O} = 5.9\text{‰}$  to  $6.3\text{‰}$ . Results show that there is no variation with height (Fig. 3-3).

The pale grey band on Fig. 3-3, between 5.5 and 5.9 per mil, represents 'normal- $\delta^{18}\text{O}$  magmas' for ultramafic and basaltic rocks that constitute predominantly mantle compositions (Bindeman 2008). The dark grey band at 5.8 to 6.5 per mil indicates the values expected for andesites and rhyolites: the products of mantle melting and closed system differentiation (Bindeman 2008). The 'normal'  $\delta^{18}\text{O}$  range of  $5.9\text{‰}$  to  $6.3\text{‰}$  for the Green Tuff Formation is consistent with fractional crystallization of a basaltic magma and provides no evidence for either an input from continental crust or assimilation of hydrothermally altered rocks.

## 3.4. Discussion

Geochemically zoned ignimbrites are not an uncommon phenomenon. Hildreth (1981) states that he "knows of no pyroclastic eruption greater than  $1\text{ km}^3$  that is not compositionally heterogeneous, and many that are an order of magnitude smaller exhibit marked zonation". Eruptive sequences often show a progression from most-evolved to least-evolved up section, such as that seen in the Green Tuff Formation. It follows, therefore, that these zoned eruptions are not tapping into a chemically homogeneous magma reservoir (Bachmann & Bergantz 2008).

### 3.4.1. Chemically zoned ignimbrites

Zoned ignimbrites have been classified in the literature by the type of geochemical gradient seen in the deposit, as summarized in Table 3-10 (adapted from Bachmann & Bergantz 2008). Low sampling density, incomplete or complex deposit patterns and partial mixing during magma ascent have often hindered studies of chemical zonation in ignimbrites. This in turn limits precise reconstruction of magma chambers from which ignimbrites have erupted. However, due to the rapid withdrawal and quenching of magma during these explosive volcanic eruptions of large volume ( $>1\text{ km}^3$ ) ignimbrites

Table 3-10: Classification scheme for zoned ignimbrites, Bachmann &amp; Bergantz (2008) pp. 652.

	<b>Abruptly zoned units</b>	<b>Linearly zoned units</b>	<b>Homogenous units</b>
Examples	Normally zoned: Purico ignimbrite, Crater Lake ignimbrite, Katmai 1912, Los Humeros, Timber Mountain/Oasis Valley caldera complex. Reversely zoned: Whakamaru Ignimbrite, Bonanza Tuff	Bishop Tuff, Bandelier Tuff, Huckleberry Ridge Tuff, La Primavera Tuff, Taylor Creek Rhyolite, Loma Seca Tuff, Laacher See Ignimbrite, Campanian Ignimbrite, Aso Ignimbrite	Fish Canyon Tuff, Lund Tuff, Cerro Galan ignimbrite, Atana ignimbrite, Oranui ignimbrite
Gradients in:			
Major elements	Abrupt gaps (up to 20 wt% SiO <sub>2</sub> )	Generally limited (few wt% at most)	Not measurable
Trace elements	Significant	Significant	Not measurable
Isotopic ratios	Limited or absent in some cases, and important in others	Significant, and often correlated with Differentiation Index	Some heterogeneities at the whole-rock scale
Crystallinity	Abrupt change (few percent to >30%). More mafic end member generally more crystal-rich	Significant increase from early-erupted to late-erupted (~1 to >20 vol %)	Not measurable
Temperature	Up to 100°C in cases but absent in others	Reported (up to 100°C)	Not measurable
Gas content	Top richer in volatiles	Top richer in volatiles	Not measurable

(or ash flow tuffs in the older literature), these deposits can provide a snapshot of the state of the magma chamber before eruption. Therefore, vertical zoning in ignimbrites can be considered to be an inverse image of at least part of a compositionally zoned, shallow reservoir.

### Zoning in peralkaline ignimbrites

Peralkaline ignimbrites appear to be commonly zoned (Ignimbrite A, Gran Canaria, (Troll & Schmincke 2002); Ignimbrite E, Gran Canaria, (Leat & Schmincke 1993); Menengai, Kenya, (Leat *et al.* 1984; Macdonald *et al.* 1994)). The Menengai ignimbrites have been studied in detail, similarly to this study of the Green Tuff Formation (Leat *et al.* 1984; Macdonald *et al.* 1994). Assuming that the gradients in the ignimbrite are inverted gradients in the magma chamber, the Menengai ignimbrite records roofward enrichment of Fe and Mn, but depletion in Al, Mg, Ca, K, Ti and P, although all ratios are small for the major elements. Except for Ba, Sc, Co, Sr, and Eu,

all the trace elements and rare earth elements show roofward enrichment. A very strong enrichment factor for Cs is regarded with caution as it is likely the result of analytical error due to low concentration values. As with the Green Tuff Formation, Zr has a high enrichment factor of 5, as compared with 7 in the Green Tuff Formation. McDonald et al., (1994) conclude that this gradient can be derived from fractional crystallization of a basaltic parent magma, and that a roofward enrichment of Ni and depletion of K argues against a strong input of either mixing with a new basalt source or partial melting of a more mafic source. In particular, the feldspars show a resorbed crystal structure, chemical zonation and a lack of systematic relationship indicating that they were not in chemical equilibrium with host melt. This further supports a model of fractional crystallization within a single magma chamber as the cause of the chemical gradient preserved in the Menangai ignimbrite.

### **3.4.2. Withdrawal mechanisms for zoned magma chambers**

The question arises how a zoned magma chamber can be tapped in such a way to be able to reproduce its gradient inversely in an ignimbrite. The homogenization of different zones from a magma chamber during eruption is dependent upon the flow behaviour within the conduit (Blake 1981). If the flow is turbulent, homogenization is encouraged and is not likely to produce a linearly graded ignimbrite, although laminar flow in the conduit will suppress mechanical homogenization. Therefore it is possible to relate chemical horizons within a magma chamber to associated chemical horizons within a deposit. Using the derived equation  $V = (2\pi/9)R^3$  (Blake 1981) which relates erupted volume (V) to the maximum depth tapped (R) it could even possible to calculate the depths of certain chemical 'zones' in the magma chamber based upon the volume of the related 'zone' in the deposit. However, reconstructions of the composition-depth relationship in the pre-eruptive magma chamber in this way are generally hindered by incomplete field data.

### **Implications for magma chamber dynamics**

The Green Tuff Formation shows a linear compositional zoning from pantellerite at its base, to trachyte at its top. Similar to other linearly zoned units the gradient is best seen in the variation in trace elements, and an increase in crystallinity, but major element variation is generally limited. Typically, linearly zoned ignimbrites also show a significant variation in isotopic ratios, temperature and gas content (Bachmann & Bergantz 2008), but these data are not available for the Green Tuff Formation.

If we compare data points from the type section to samples collected elsewhere around the island (Chapter 4), the type section samples mimic the full range of compositions found in the Green Tuff Formation as a whole. Variation diagrams with SiO<sub>2</sub> on the abscissa (Fig. 3-9) show trends typical for fractional crystallization dominated by crystallization of anorthoclase and clinopyroxene (White *et al.* 2009), the dominant phases in the Green Tuff.

An enrichment plot (Fig. 3-10) of matrix glass shows strong enrichment in incompatible elements such as Rb, Zr, Ce and Th, but also Mo which behaves incompatibly in peralkaline melts (Lowenstern 1993). These incompatible elements will have been enriched in the melt relative to compatible elements that were locked into different phases during fractional crystallization. Enrichment of the incompatible elements, particularly Zr, can therefore be used as a proxy for evolution and a key element in defining the chemical zonation of the deposit.

The REE plots for glass data of the Green Tuff show a change from pantellerite to trachyte (Fig. 3-11). The pantelleritic end member is characterized by a moderate LREE enrichment (Ce/Yb = 6.02) and a strong negative Eu anomaly. The trachytic end member also has a moderate LREE enrichment (Ce/Yb = 6.5), but has a much less pronounced negative Eu anomaly. The flat Eu anomaly and the low concentrations of incompatible trace elements and Ba (~ 250 – 1000 ppm) in the glass, but high concentrations of Ba (~ 1900 – 2200 ppm) in the whole rock analysis, are interpreted to be the result of accumulation of alkali feldspars in the trachyte end member. For other trachyte lavas that show these characteristics, White *et al.* (2009) have suggested that this may represent up to 40% accumulation of feldspar crystals. This is also compatible with the large 20% volume increase of feldspar phenocrysts seen through the section. A net downward movement of feldspar through a compositionally zoned magma chamber as an accumulation mechanism is a commonly observed phenomenon (Edgar *et al.* 2002; Storey *et al.* 1989).

There is no evidence that the chemical variation is due to the tapping of distinct magma chambers, such as envisaged for some volcanoes which show distinct geochemical groups (e.g. Campi Flegrei, Pabst *et al.* 2008). The constant phenocryst chemistry, the crystal fractionation trends in variation diagrams and enrichment in incompatible trace and REE elements all favour a single, closed system fractionating magma chamber.

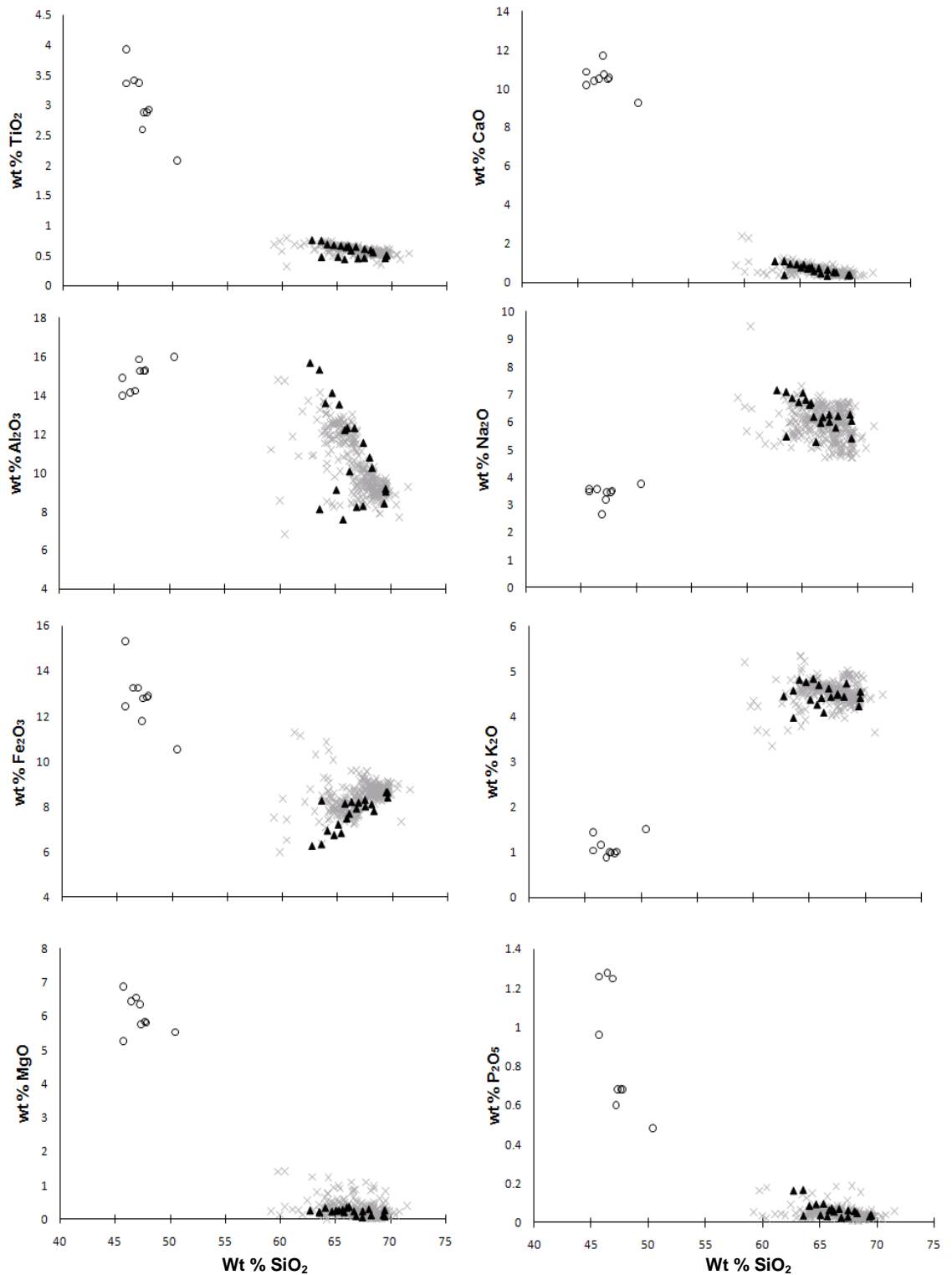


**Fig. 3-9:** Major element variation (Harker) diagrams for whole rock data for the type section (triangles), as compared to data for Green Tuff Formation elsewhere around the island,  $n=310$  (crosses). Trends are typical for fractional crystallisation of a basaltic parent magma. Note the presence of the 'Daly Gap', common for suites from Pantelleria. Also shown are data for pantescan basalts (circles) from Civetta, 1998.

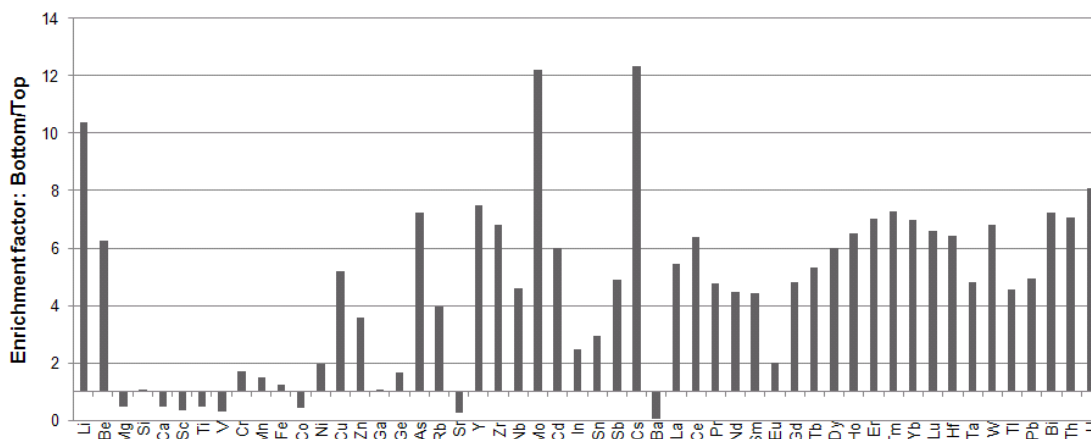


**Fig. 3-10: Enrichment factors for 51 elements in the Green Tuff type section. Enrichment factor is calculated by dividing the average composition of the earliest ejecta (bottom of section) by the average composition of the latest ejecta (top). Elements are arranged by atomic number. These enrichment factors will be a minimum estimate of the zonation present in the magma chamber as the eruption will have tapped an unknown proportion of the magma chamber.**

Other workers have also invoked a single magma chamber that has produced evolved pantellerites through fractional crystallization, although there has been some debate over the involvement of partial melting of alkali gabbro (Chapter 1). On the basis of major and trace element modelling and thermodynamic models (Civetta *et al.* 1998; White *et al.* 2009), the composition of the metaluminous trachyte can be produced from 70-75% low-pressure fractional crystallisation of a hydrous basalt magma. Similarly, the peralkaline trachytes and pantellerites can be explained by 20 to 80% fractional crystallisation of an assemblage dominated by alkali feldspar from the metaluminous trachyte magma (White *et al.* 2009). The most evolved lavas and tuffs can be explained by 95% fractional crystallisation of transitional basalt (White *et al.* 2009). It is possible that the magma chamber is a two-layer system consisting of a lower, trachytic layer and an upper pantelleritic layer. This is suggested in a slight composition jump in the Ba composition of the feldspars (Fig. 3-7). Mixing of these two-layers could give rise to the transitional zone. However, this compositional gap is not seen in the Rb or Sr values. Furthermore, whilst feldspars that show resorption textures are found in the trachytic end-member which indicates these were formed in a different (more evolved) melt, feldspars with this texture are not seen in the transitional or pantelleritic zones. This suggests that the resorbed feldspars in the trachytic zone were inherited through crystal settling from the more evolved magma at the top of the magma chamber. Magma mixing would cause feldspars that had crystallised in the less evolved trachytic layer to

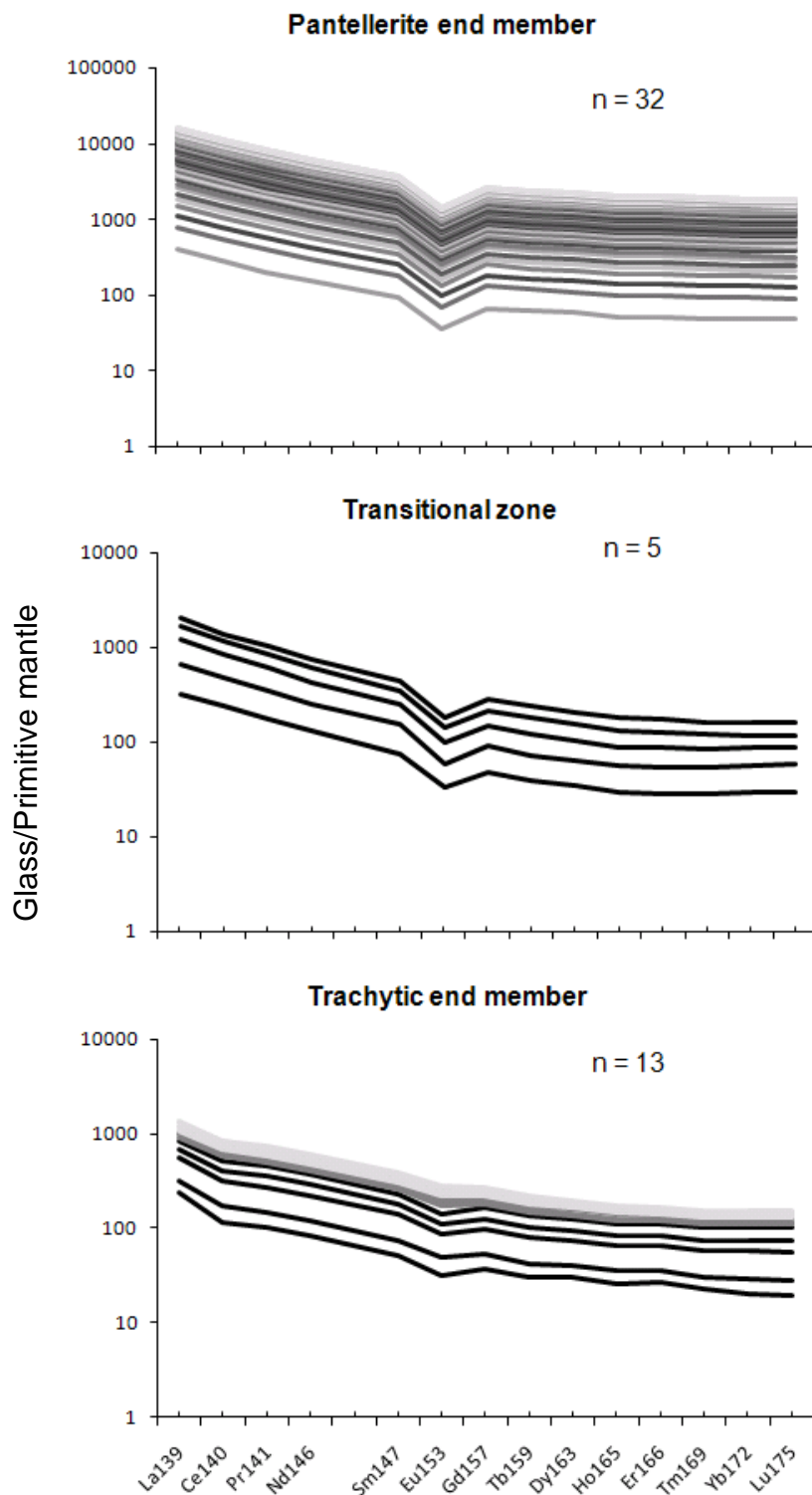


Fig. 3-11: Rare earth element (REE) plots normalised to primitive mantle (Sun & McDonough, 1989) for glass in the Green Tuff type section (analysed by LA-ICP MS). In the bottom plot, the pale greys indicate more trachytic samples. Note the decreasing Eu anomaly. In the most trachytic samples, a small positive Eu anomaly can be seen.

be in the transitional zone and this is not seen. This is supported by a lack of mixed mafic minerals and evidence for magma mixing in hand specimen.

A fractionating, shallow magma chamber (3-4 km depth) as suggested by geochemical and petrological studies (Civetta *et al.* 1998) is confirmed by geophysical profiles (Civile *et al.* 2008). Similarly, ground deformation surveys also suggest a spherical point source at 4 km depth (Mattia *et al.* 2007).

### **3.4.3. A zoned magma chamber**

Before the Green Tuff eruption, a single zoned magma chamber is envisaged (Fig. 3-12A). The variation in composition is likely due to fractional crystallization of a mafic source, creating a cumulate base, a trachytic, crystal rich zone and then a pantelleritic, crystal poor zone. It is likely that a resulting thermal gradient would have caused sluggish convection, causing linear grading rather than abrupt zones (Bachmann & Bergantz 2008). Each zone would crystallize mineral phases, with the pantelleritic zone contributing a significant feldspar population to the more mafic compositions through crystal settling. Upon eruption, the less dense, volatile-rich pantelleritic zone would be the first to erupt (Fig. 3-12B). As the eruption continued, magma at the top of the chamber would have been progressively tapped and deeper, more mafic magmas erupted (Fig. 3-12C). Following on from Blake (1981), as the magma chamber was progressively tapped during the eruption, the aggrading ignimbrite recorded changes in the chemical signature at source, suggesting that chemical variations within the ignimbrite can be used as a chemical stratigraphy, or proxy, for time.

## **3.5. Conclusions**

- The Green Tuff type section represents a range of chemistries from pantellerite at the base to trachyte at the top.
- The Green Tuff is a deposit from a single eruption that has tapped a single, compositionally zoned magma chamber
- Pantellerite and trachyte are the products of extreme crystal fractionation of a parental basalt.
- The magma chamber likely showed roofward enrichment in incompatible trace elements and rare earth elements, and a depletion in Ba, Sr, TiO<sub>2</sub>, Al<sub>2</sub>O<sub>3</sub>, P<sub>2</sub>O<sub>5</sub>

- The progressively aggraded ignimbrite records the chemical variations at source caused by the progressive tapping of a zoned magma chamber. It follows that the chemical variation in the ignimbrite can be regarded as a chemical ‘stratigraphy’ which can be used as a proxy for time. Identifying the chemical characteristics of a section of the ignimbrite anywhere across the island will enable placement of that location into the type section chemical stratigraphy and therefore its ‘time position’ with regards to ignimbrite emplacement in general.

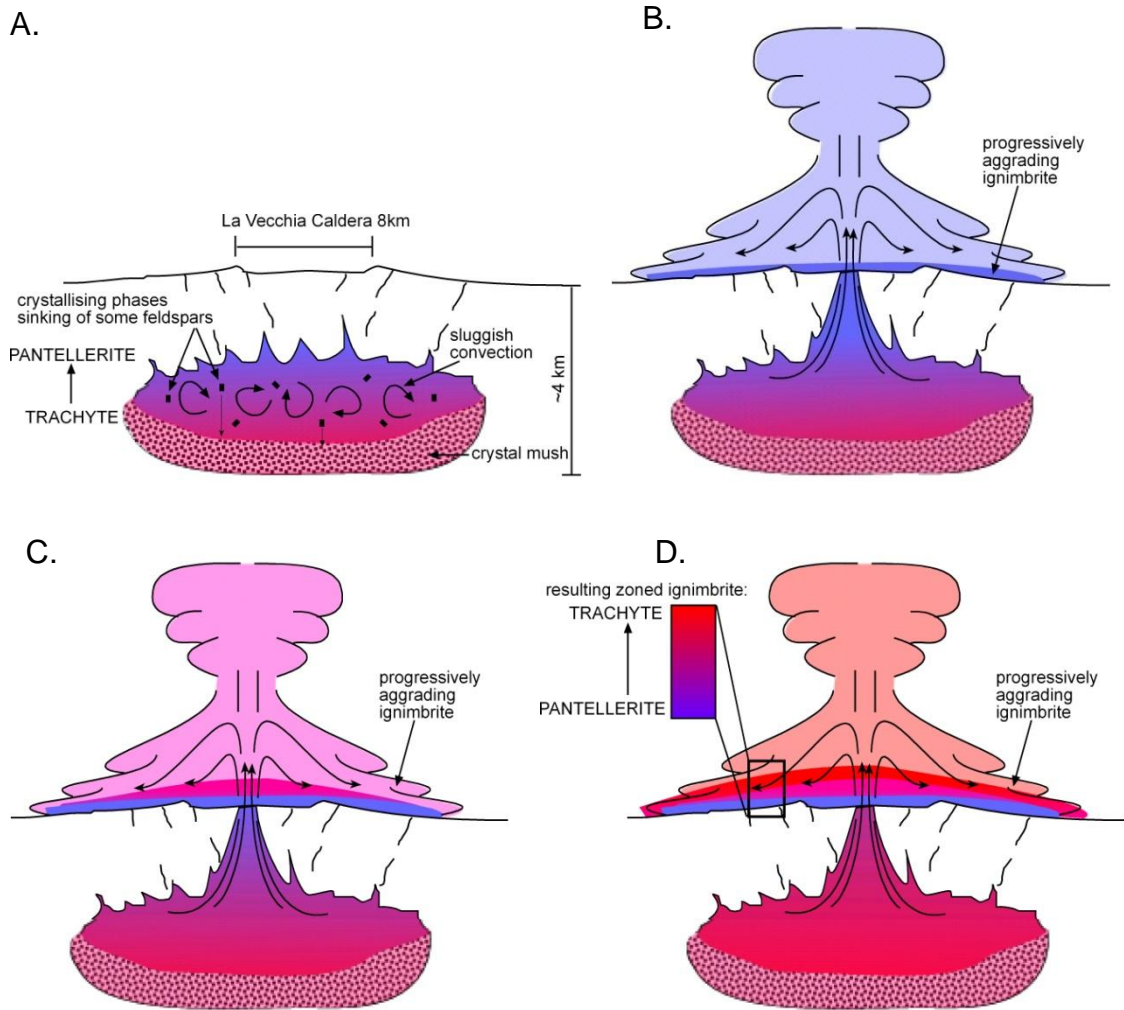


**Fig. 3-12: A: Pre-Green Tuff eruption magma chamber (not to scale). Fractional crystallisation and sluggish convection has resulted in a zoned magma chamber. B: First stage of the eruption taps the pantelleritic top portion of the magma chamber. The first deposit from the pumice fall and pyroclastic density current is pantelleritic in composition. C: The next phase of the eruption taps through the transitional zone. D: The final phase of the eruption taps into the crystal rich, trachytic zone in the magma chamber. The resulting ignimbrite has an internal chemical stratigraphy which is the inverse image of the magma chamber.**

# 4. How pyroclastic density currents evolve with time and space I: Diachronous emplacement of a thin, circular ignimbrite sheet

---

## 4.1. Abstract

Here, particularly hazardous, radial, high-velocity pyroclastic density currents from caldera-forming eruptions are studied. The inference of simultaneous, radial flow (Walker *et al.* 1980; Wilson 1985) for thin, circular (low aspect-ratio) ignimbrite sheets is tested by mapping out the internal chemical-architecture of a zoned pyroclastic density current deposit on the island of Pantelleria, Italy. This pristine, welded ignimbrite is gradually zoned from pantellerite to trachyte and the chemical variations allow us to divide the brief duration of the sustained current into successive time-slices. The vertical and lateral compositional variations have been mapped internally within the deposit and have enabled reconstruction of how the current shifted as it waxed then waned, and as it encountered and then overtopped topographic barriers. Results have shown: (1) the current did not flow radially for its entire duration; (2) the leading edge of the current progressively advanced during the waxing stage of the current and then retreated as the current waned; (3) the current shifted laterally with time, resulting in a broadly circular sheet; and (4) the current was not able to overtop topographic barriers at all stages during the eruption. Thus, not all low aspect-ratio ignimbrites are emplaced radially with full run-out achieved instantly. This has implications for estimates of volume, mass flux and run-out distances and therefore impacts on the models that rely on these parameters to simulate pyroclastic density currents. The chemical stratigraphy cuts through previous lithofacies correlations, demonstrating that lithostratigraphy cannot be used to unravel the temporal evolution of the current.

## 4.2. Introduction

Owing to their rapid emplacement, pyroclastic density currents are the most dangerous volcanic phenomenon faced by communities living near an active volcano and account for 26.8% of deaths caused by volcanic eruptions (Tanguy *et al.* 1998) and countless evacuations. To help mitigate the hazard, understanding the behaviour of pyroclastic density currents must be improved, in particular concerning how they react to topography and how they are emplaced through time and space.

### 4.2.1. Radial, low-aspect ratio pyroclastic density currents

Ignimbrites are the deposits of pyroclastic density currents, and can be described in terms of their aspect ratio (Walker *et al.* 1980), the ratio of the deposit thickness (averaged across its area) to the characteristic length of the deposit, as measured by the diameter of a circle with the same area as the deposit. High-aspect ratio ignimbrites (HARI:  $< 1:500$ ) have been interpreted to result from low-velocity pyroclastic currents which are confined to valleys, whereas low-aspect-ratio ignimbrites (LARI:  $> 1:500$ ) have been interpreted to record very high-velocity currents, which are thought to rapidly surmount high (several hundred meters) topographic barriers, even at significant distances from source and result in a near-circular, thin deposit sheet. The 30 km<sup>3</sup> Taupo Ignimbrite, New Zealand is a typical low-aspect-ratio ignimbrite, and extends to 80 km or more in all radial directions from the source, including over mountains  $\leq 50$  km from source and 1400 m higher than the vent, forming an axisymmetrical circular sheet. This deposit has been inferred to have been emplaced radially, simultaneously, by a current with an exceptional velocity of 200 ms<sup>-1</sup> (Wilson 1985). Most other low-aspect-ratio ignimbrites also have a radial distribution (e.g. the Mazama, Bandelier and Carpenter Ridge ignimbrites; Bacon 1983; Self *et al.* 1986; Steven & Lipman 1976). Interpretations of the behaviour of the currents that formed them have been made by a variety of field studies, modelling techniques, and through comparisons with high-aspect-ratio ignimbrites. However, the currents that produce low-aspect-ratio ignimbrites have not been witnessed, and the emplacement model of a radially spreading current remains to be tested. This chapter attempts to understand their radial distribution, whereas Chapter 5 considers how these currents interact with topography in more detail.

Experimental studies have concentrated on laboratory experiments on flows generated by pyroclastic fountaining, the principle mechanism for current generation. Pyroclastic fountaining (sometimes referred to as column collapse) occurs when an eruption column fails to achieve buoyancy (Sparks *et al.* 1997). Typical experiments use jets of saline water (Turner 1966), or water with a suspension of fine particles (Carey *et al.* 1988) into fresh water. A fountain is created, often forming a gravity current that spreads radially simultaneously in all directions from the source. This has led to the assumption that circular ignimbrite sheets are produced from a density current that spreads radially, simultaneously in all directions from the vent, particularly when palaeoflow indicators all point outwardly from the vent (Campanian ignimbrite, Fisher *et al.* 1993; Taupo ignimbrite, and others, Ui *et al.* 1989; Wilson *et al.* 1995; SEU of Sovanna Formation, Palladino & Taddeucci 1998; Pinatubo ignimbrite, Hoblitt *et al.* 1996), in contrast to a directed pyroclastic current from a lateral blast such as Mt. St. Helens, 1980. However, asymmetrical collapses have occurred in experiments (Carey *et al.* 1988; Woods & Caulfield 1992), with currents spreading across one sector (Carey *et al.* 1988). Thus, non-directed explosions can produce directed currents. If the current direction changed with time it would be possible to build up a broadly circular ignimbrite sheet. The assumption that a circular sheet results from a radially expanding current is one that needs to be tested.

Understanding how an ignimbrite sheet is emplaced requires assessment of its internal architecture so that how the ignimbrite was formed through time and space can be reconstructed (Branney & Kokelaar 2002). The lithofacies of an ignimbrite, as discussed in Chapter 2, reflects processes and conditions primarily in the flow-boundary zone. The lithofacies and thus the conditions at the base of the current may be localised, change rapidly, and be diachronous. Therefore, lithofacies traced through an ignimbrite sheet do not represent a time-stratigraphy. Reconstruction requires time-markers that must be independent of depositional environments, current direction and fluctuation in mass flux of the current.

#### **4.2.2. Entrachrons and their use in reconstructing ignimbrite emplacement**

A conceptual line or surface that joins the first appearance of pyroclasts in the deposit is a form of time-marker through the deposit and has been termed ‘entrainment isochrons’

or ‘entrachrons’ (Branney & Kokelaar 2002). An entrachron may be represented by the first appearance of a distinct composition of pumice, crystal or lithic clast. For example, the concept was used to infer deposition of the Acatlan Ignimbrite in Mexico, by progressive aggradation over irregular topography, using the changing composition of pumices from rhyolite to dacite (Branney & Kokelaar 1997) and to correlate condensed thin sequences with thick, massive sequences in the Zaragoza Ignimbrite, Mexico (Carrasco-Nunez & Branney 2005). Brown (2001) used the first and last appearance of accretionary lapilli to unravel ignimbrite architecture in the Poris Formation, Tenerife as the deposit thinned over topography and thickened in palaeovalleys. These detailed studies of single flow-units trace the internal architecture along transverse sections and have not attempted to unravel the entire ignimbrite sheet. This has been done using lithofacies-based deposit architecture for compound sheets where the ignimbrite consists of numerous flow-units (e.g. Bishop Tuff, Wilson & Hildreth 2003; Roccamonfina, De Rita *et al.* 1998). Fierstein & Wilson (2005) used a chemical-based deposit architecture based on changing pumice compositions to unravel the assemblage of the large compound Valley of Ten Thousand Smokes ignimbrite sheet which consists of several distinct flows. These cases either only study a transverse section of an ignimbrite (Acatlan, Zaragoza, Poris ignimbrites), or are a study of a compound ignimbrite (Valley of Ten Thousand Smokes, Bishop Tuff and Roccamonfina ignimbrites).

A thin, circular low aspect-ratio ignimbrite which consists of only one flow-unit has not been studied in this way. A chemically zoned ignimbrite that shows gradational zoning over a wide range of geochemical variation, such as the Green Tuff ignimbrite, could be divided into a large number of time zones based on the concept of chemical entrachrons and used to test the inference of radial flow.

### 4.2.3. Aims and hypothesis

The aim of this study is to use the chemical zoning as a chemical stratigraphy to test the following hypothesis:

- low aspect-ratio ignimbrites with a circular distribution were emplaced from currents that flowed radially, simultaneously in all directions from source.

Entrachrons, or time zones, could be mapped out through the ignimbrite sheet to understand its internal architecture. A 3-D analysis of this internal architecture could

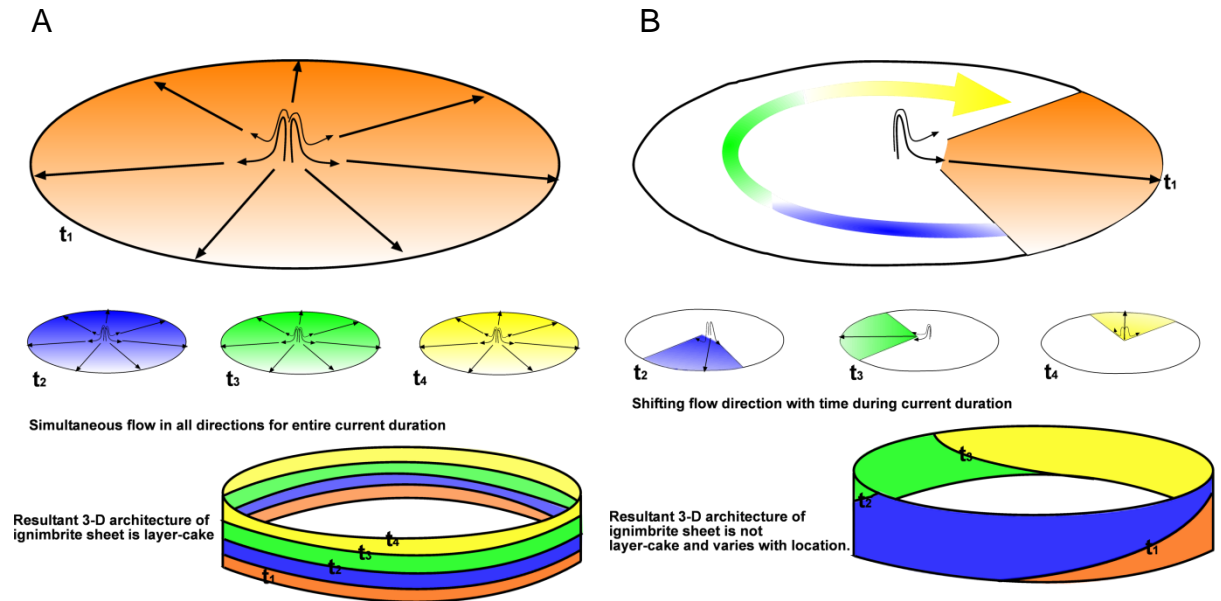


**Fig. 4-1A:** A sustained radial density current flows simultaneously from a vent. Deposits on a circumference around the vent will show a 'layer-cake' stratigraphy with each time-step during the current represented at all locations. **B:** a sustained density current flows from a vent but shifts flow direction with time. Deposits on a circumference around the vent will vary, representing a change in current direction or behaviour with time.

reveal whether the sheet was emplaced radially and simultaneously (Fig. 4-1A), or whether the current flowed sector by sector, building up a circular distribution with time through the eruption (Fig. 4-1B).

#### 4.2.4. Methods

The Green Tuff ignimbrite (50 ka, a.r. >1000), Pantelleria, has been chosen as a case study as it is excellently exposed both longitudinally from source but also laterally around the vent. Unfortunately, as with all ignimbrites, the outcrop is not 100% as the current flowed into the surrounding sea. However, it is still the best example for this type of investigation for a number of reasons. The deposit consists of a basal sub-plinian pumice- and ash-fall and an overlying ignimbrite, which is a single flow unit. The ignimbrite is not compound and represents a fluctuating quasi-steady current (Chapter 2). The deposit is almost entirely welded and the lack of a complex welding profile or internal vitrophyres supports the lithofacies interpretation that the ignimbrite is a single flow unit. The viscous nature of the pyroclasts and their agglutination style of deposition mean that deposits were left on the entire landscape, including slopes up to 90°, which means that it is unlikely that the current was able to bypass without leaving

behind evidence of its passing. Most importantly, The Green Tuff ignimbrite shows linear or gradational zoning.

Detailed geochemical study of a type section (Chapter 3) has revealed that this complex zoning can best be represented by whole rock zirconium values (Fig. 4-2). A wide range of elements show a linear trend through the deposit such as yttrium and neodymium (Chapter 3), but Zr shows the widest range spanning over 1400 ppm and is resistant to post-depositional weathering. Therefore, Zr values are used as a proxy for all the variations seen in the phenocrysts and the major, trace and rare earth elements. The decrease in Zr from over 2000 ppm at the base of the deposit to less than 800 ppm at the top tracks an evolutionary trend from pantellerite to trachyte and is thought to be the result of the eruption changing composition with time as it progressively tapped a single, zoned magma chamber (Chapter 3). This Zr trend has been used to define a chemical stratigraphy for the Green Tuff ignimbrite, where deposits of high Zr ppm were erupted at the start of the eruption and then decreasing values of Zr were progressively erupted with time through the eruption.

### **Data collection**

Over 115 locations of the Green Tuff ignimbrite were logged and studied in detail in the field. Of these, over 80 field locations across the island of Pantelleria were sampled for geochemical analysis. Closely-spaced sampling vertically through the deposit at locations with clearly defined upper and lower contacts (marked by palaeosoils and vitrophyres) yielded over 400 samples for analysis. In some locations, samples were taken from incomplete Green Tuff sections where no complete sections were available. Samples were prepared and analysed for Zr ppm by XRF, as described in Chapter 3.

### **Data analysis**

Concentrations of Zr ppm for over 400 samples from 80 locations were entered into a database with the x,y coordinates of their location. These data were imported into ArcMap 9.2 (ESRI inc.) as a shapefile feature class with point geometry (Fig. 4-3A) to allow the data to be studied spatially. Each point in the database has a geographical coordinate, a location name tag and a Zr ppm value. Using the built in 'select by attributes' tool, it is possible to query the database to show the spatial distribution of a particular Zr ppm value (Fig. 4-3B).

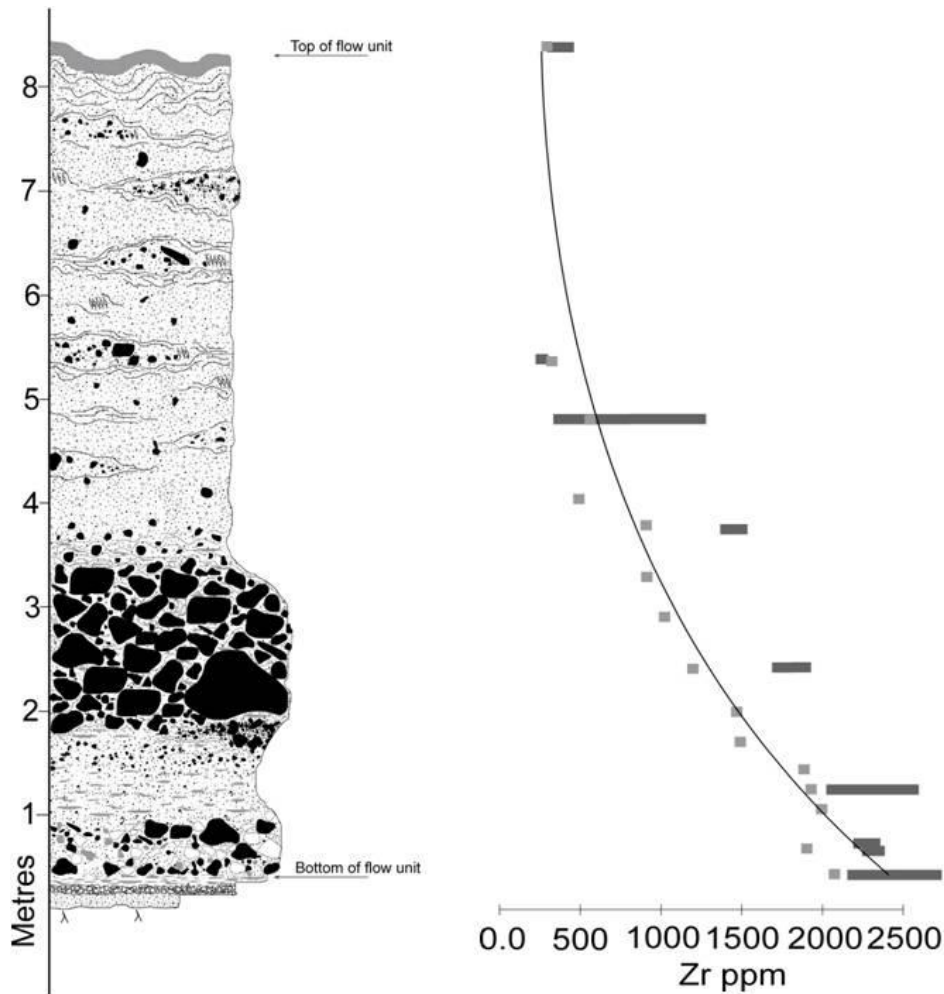


**Fig. 4-2:** Graphic log of the Green Tuff ignimbrite type section showing the linear grading of Zr values through the deposit. Pale grey squares show values from XRF whole rock analyses and dark grey shaded area shows range of values obtained for LA ICP MS spot analyses of matrix. Polynomial trend-line used. Note large gap due to cliff. This part of the unit has been sampled extensively elsewhere.

The Zr shapefile layer is overlain onto topographic data for the island. A 30 m resolution digital elevation model (DEM; Acquisition Date: 2002/08/15 Path: 190 Row: 34) was acquired from the ASTER datasets (<https://lpdaac.usgs.gov/>) for Pantelleria. A hillshade image is derived from this data to visually represent the topography using the ‘Hillshade tool’ in the Spatial Analyst toolbar. Study of the distribution of Zr values over the hillshade image allows the distribution of the deposit over topography to be analysed.

The validity of the stratigraphic model is confirmed by systematic upwards decreases in Zr values at all vertical sections through the Green Tuff ignimbrite.

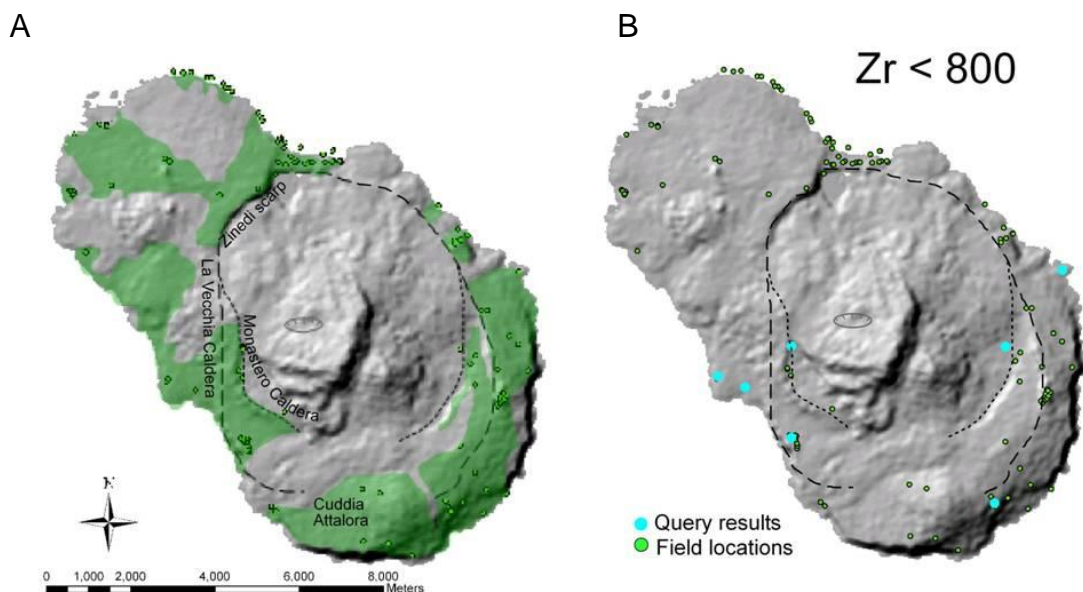


**Fig. 4-3A:** Hillshade raster derived from 30 m Aster DEM (Azimuth 315°) representing topography of Pantelleria with field locations marked as green circles. Assumed location of vent, caldera walls and Cuddia Attalora shield marked. Green Tuff Formation marked in green. **B:** results from ArcGIS database query ‘Zr < 800’.

### 4.3. Results and interpretation

Final results are shown in Figure 4-4. For simplicity the gradational variations of Zr ppm through the Green Tuff ignimbrite were divided into eight different zones to enable clear analysis of the distribution of Zr values through the deposit: the pantelleritic end member (>2000 ppm), the trachytic end member (<800 ppm) and intervals of 200 ppm through the gradational member. Each zone was queried in the ArcGIS database and isometric areas derived, i.e. areas were drawn around locations with the same Zr zone in the same way an isopach or isopleth map is made. These isometric areas are each interpreted to represent the ‘footprint’ of the depositing pyroclastic density current at an individual moment of time during the current’s evolution. The boundaries of the zones are intergradational and are equivalent to chemically defined entrachrons. Therefore, studying these footprints successively from high Zr to low Zr enables us to track how the current changed with time and how it behaved up and around topography.

Analysis of the density current footprint maps reveal that the sheet-like, low aspect-ratio Green Tuff ignimbrite was not emplaced simultaneously or entirely radially: rather, it flowed into certain sectors before others (Fig. 4-4). Figure 4-3A shows the outcrop of the Green Tuff (green shading). The Green Tuff is thought to occur in all parts of the island but has been covered by younger deposits (left blank).

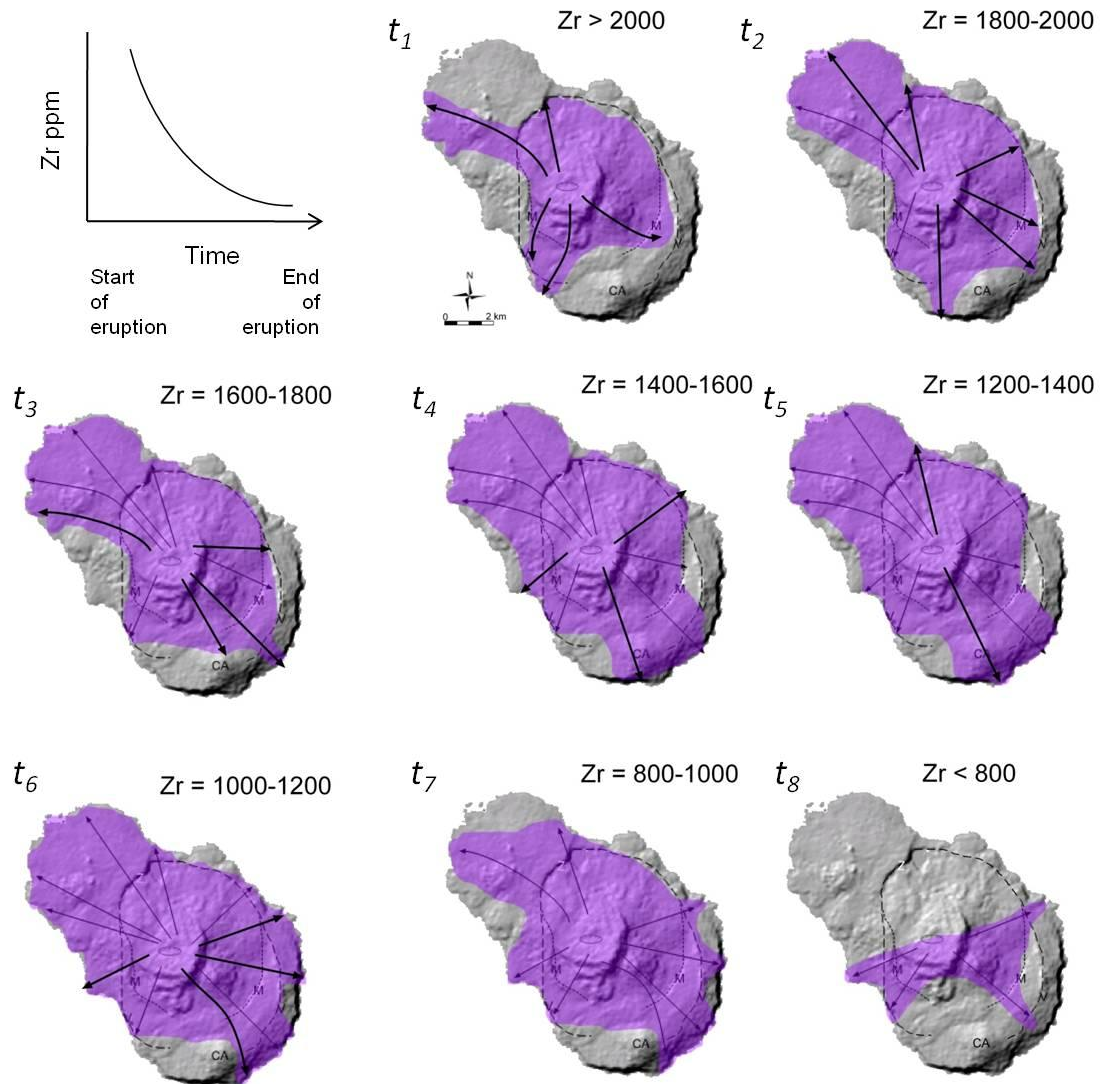


**Fig. 4-4:** Footprints of the density current at different time-slices through the evolution of the current from start ( $t_1$ ) to finish ( $t_8$ ) based upon Zr ppm. Arrows indicate inferred current direction from central vent. The inundation area increases as the current waxes to a climactic phase ( $t_{4-5}$ ) and then decreases as the current wanes. For example, in phase  $t_7$ , the footprint area has decreased although the eruption is still continuing showing that the area that is being deposited on land is decreasing as the current is waning. M - Monastero caldera wall, V - La Vecchia caldera wall, Z - Zinedi scarp, CA - Cuddia Attalora shield. Heavy arrows indicate a change in current from previous time-slice (pale arrow).

#### 4.3.1. The current reconstructed through time ( $t$ )

An initial phase of sub-plinian fallout was followed by pyroclastic fountaining. The first phase of the current ( $t_1$  of Fig. 4-4) was restricted to the north and east by the old Zinedi scarp and Monastero caldera wall (Fig. 4-3) but in the south it overtopped the

Monastero caldera wall but not the La Vecchia caldera wall (Fig. 4-3) outboard of this, except for a narrow breach west of the Cuddia Attalora shield (Fig. 4-3). To the northwest, the current flowed unfettered across the low lying topography into the sea.

During the next phase ( $t_2$  of Fig. 4-4) the current spread further northwards across the low lying area to the NNE, inundating the location of the modern town of Pantelleria, and it overtopped the Zinedi scarp to the north of Bagno dell'Acqua lake. The footprint of the current also expanded eastwards overtopping more of the Monastero caldera wall. To the east of the Cuddia Attalora shield, a narrow breach of the La Vecchia caldera wall allowed the leading edge of the current to extend towards the sea. The breach of the La Vecchia caldera wall to the west of the Cuddia Attalora shield increased and the current reached the sea.

As the current continued to wax ( $t_3$  of Fig. 4-4), its leading edge started to advance up the Cuddia Attalora shield, but at this time still fails to overtop the summit. However, to the east of this the current reached the sea. There is further inundation of the Monastero caldera wall in the eastern sector; however the current was still constrained by the La Vecchia caldera wall outboard of this. The current's footprint had increased in the northern sector as the leading edge of the current advanced NW.

In the next phase ( $t_4$  of Fig. 4-4) the current continued to grow as it overtopped significant topographic barriers including wide sections of the La Vecchia caldera walls in the NE and WSW and notably, had inundated the summit region of the Cuddia Attalora shield. The northern sector of the island continued to be fully inundated.

As the climactic phase of the eruption continued ( $t_5$  of Fig. 4-4), the current further inundated Cuddia Attalora and reached the sea beyond the shield. The large Zinedi scarp to the north of Bagno dell'Acqua also became completely inundated. However, flow remained restricted to the east and west until the next phase.

The next phase of the current inundated the entire island and reached the sea in all directions ( $t_6$  of Fig. 4-4). The La Vecchia caldera walls were overtopped both to the east and west. However, there are signs that the sustained current was starting to wane as its extent had retreated from the summit of the Cuddia Attalora shield, but rather was deflected around its eastern flanks.

In time-slice  $t_7$  (Fig. 4-4) the current was waning as its footprint has decreased significantly. The area over which it was depositing had reduced in size and in several sectors run-out distance of the current has decreased, particularly in the northern sector.

In the final phases of the current ( $t_8$  of Fig. 4-4), the current no longer travels to the north of the island and once again becomes restricted by the topographic barriers to the south. The current is mainly directed to the west and east.

#### **4.4. Discussion**

Chemical mapping of the internal architecture of the Green Tuff ignimbrite sheet has shown that it was not deposited from a radially expanding density current (Fig. 4-1A) and did not flow immediately to its full extent, neither was it produced by lateral shingling (Fig. 4-1B). Rather, the leading edge advanced at different rates in different sectors. Moreover, the footprint of the current laterally shifted with time. This ultimately produced a broadly circular deposit.

##### **4.4.1. Assumptions and potential problems**

###### **Bypassing**

Pyroclastic density currents do not always deposit along their entire reach. Some will involve broad bypass zones in which the current passes over land without leaving any deposit (Brown & Branney 2004). Therefore, we must consider how well the deposit footprint represents the full extent of the current. Whilst we cannot completely discount bypassing in the Green Tuff, we do not think it was significant for the following three reasons: (1) Bypass zones often occur on steep slopes where the current is accumulative or uniform; (2) Nowhere on Pantelleria are zones discovered distally where proximal equivalents are absent, such as is common where bypassing has been documented (Tenerife, Brown & Branney 2004); (3) The peralkaline nature of the Green Tuff Ignimbrite means that the hot pyroclasts were very 'sticky' (Chapter 2) and adhere to all slopes up to 90° (Korringa 1971). In this case the welding is thought to have been near-instantaneous agglutination rather than post-depositional load welding (Branney *et al.* 2004; Korringa 1971; Mahood 1984). It is therefore unlikely, in this case that the current was able to bypass without leaving a deposit. However, this would need to be considered if this method was to be applied to other ignimbrites. If the current had been able to bypass without depositing, it is likely that the footprint areas will be extended.

**Flow units**

The diachronous emplacement of the ignimbrite sheet may be the result of stacking of multiple flow units (e.g. Bishop Tuff and Valley of Ten Thousand Smokes ignimbrites, Fierstein & Wilson 2005; Wilson & Hildreth 1997) rather than the shifting flow path of a single, sustained but evolving current.

The Valley of Ten Thousand Smokes ignimbrite has been divided into nine ‘eruption-packages’ using the chemical zoning seen in the deposit (Fierstein & Wilson 2005). These compositionally distinct, sequentially emplaced packages each have distinctive proportions of rhyolite, dacite and andesite pumices as determined by pumice counts in the field and have been mapped in the field and flow paths and current behaviour inferred (Fig. 5 in Fierstein & Wilson 2005) in a similar way to the research here presented on the Green Tuff ignimbrite. These packages have been interpreted to record distinct and separate flows (Fierstein & Wilson 2005), defined by one or more out of seven key features: (1) sharp colour changes corresponding to an abrupt compositional change; (2) persistent finer-grained basal parts of inferred flow-units or inverse grading above a sharp contact (‘Layer 2a’ of (Sparks *et al.* 1973); (3) erosional channels cut by a current that then fills it; (4) lobate accumulations of one package; (5) intercalated fall deposit layers; (6) compaction swales; and (7) slumping and remobilization of one package subsequently buried by a later package. Flow-unit boundaries are not necessarily required for most of these features, except item (5) (Branney & Kokelaar 2002).

In the Green Tuff ignimbrite, in contrast to the Valley of Ten Thousand Smokes ignimbrite, the compositional change is mostly gradational throughout the deposit and sharp compositional variations rare (Chapter 3). Also, there is no evidence of significant time-breaks such as intercalated ash or pumice fall layers, compaction, or erosion surfaces (the latter can also occur during sustained currents). Similarly, in a strongly welded deposit such as the Green Tuff ignimbrite, even a short time break would allow some cooling and degassing resulting in a zone of vitrophyre or at least a zone of greater competence, which would be apparent by the rheomorphic deformation structures. Upper and lower vitrophyres are seen throughout the Green Tuff where the ignimbrite cooled either against the underlying deposits or the atmosphere. However, no internal vitrophyres and no internal zones of high competence are seen suggesting that

significant time breaks were largely absent. Certainly there could not have been sufficient multiple flow-units to take account of the gradational zoning.

Therefore, without evidence for time-breaks in the deposition of the Green Tuff ignimbrite, there is no reason to invoke multiple flow-units emplaced by multiple density currents. The most reasonable assumption is that it was emplaced by a quasi-steady, single, pyroclastic density current.

### **Multiple magma chambers**

This study shows that the composition of the Green Tuff eruption changed gradually with time from pantellerite to trachyte (Chapter 3). The cause of this variation does not affect our emplacement interpretation. However, the gradation is best reconciled with progressive, deeper tapping of a single, zoned magma chamber, rather than a more complex amount of magma chamber bodies for which we have no evidence.

Without further evidence such as isotopic or geochemical data to suggest multiple magma chambers, there is no requirement to invoke such a system over a single magma chamber.

### **Single vs multiple vents**

This study assumes a single, central vent. It is possible that there were multiple vents that erupted the Green Tuff ignimbrite. Vents erupting at different locations may have tapped different depths of the zoned magma chamber. This would have resulted in a sectoral pattern to the chemistry stratigraphy of the ignimbrite. Whilst the chemical-architecture of the Green Tuff Formation is sectoral, it also shows a consistent stratigraphy from more evolved compositions at the base to less evolved compositions at the top. There is no evidence for reverse zonation or overlapping of zones from currents being sourced at separate vents. Furthermore, each zone is found at some location in all directions. Thus, whilst it is possible that there were multiple vents during the eruption, there is no direct evidence for this.

### **Limitation of the dataset**

There are sites across the island where the Green Tuff ignimbrite down to its base is not exposed. This has meant that there are areas on the island that lack a data point for some zones. We appreciate that should more data points have been available in these areas the complexity of the footprint may have been more and the extent of the footprint for some

time-slices may have been greater. However, it is unlikely that the overall conclusion of a complex flow path of a waxing and waning current and diachronous emplacement of the sheet would change. Artefacts in the footprint maps due to areas without data points, or sections that were not exposed to the base, are discussed further in Appendix I.

#### **4.4.2. Diachronous emplacement of the ignimbrite sheet**

The entrachron stratigraphy demonstrates that even though the deposit is thin and broadly circular, the current was not 'virtually instantaneous', i.e. it did not immediately flow out to the distal limit of the ignimbrite sheet in all directions. Rather, the leading edge slowly advanced with time, progressively inundating the island as the current gradually waxed, and then later it progressively retreated source-ward while the current slowly waned (Fig. 4-5A & B). This demonstrates that the model for rapid radial flow, depicted in Fig. 4-1A, as originally conceived for the Taupo ignimbrite (Wilson 1985, 1997), in which the initial current velocity was very high (driven by kinetic energy due to column collapse from >50 km (Wilson & Walker 1985)) so that the current rapidly surmounted topographic hills to its distal limit, is not a tenable model for the Green Tuff ignimbrite. Rather the run-out distance was probably a function of mass flux (Branney & Kokelaar 2002; Bursik & Woods 1996), and as the mass flux slowly changed, so did the run-out distance.

#### **4.4.3. Radial flow during times of peak flow**

True radial flow was achieved (barring the effect of topographic obstacles) only during times of peak flow ( $t_{4.6}$ ). In this period, the ignimbrite underwent true progressive aggradation to form a layer-cake architecture (Fig. 4-5A).

#### **4.4.4. Lateral shingling**

The circular ignimbrite was not assembled with a shingled architecture as depicted in Fig. 4-1B, and did not arise as a result of sectoral flow whose orientation shifted clockwise (or anti-clockwise) with time. However, shingling is observed in a couple of locations (Fig. 4-5C) where the current shifted laterally with time. During periods of initial waxing and post-climactic waning shifting flow was most pronounced and the resultant internal architecture of the flow-unit is not 'layer-cake'.

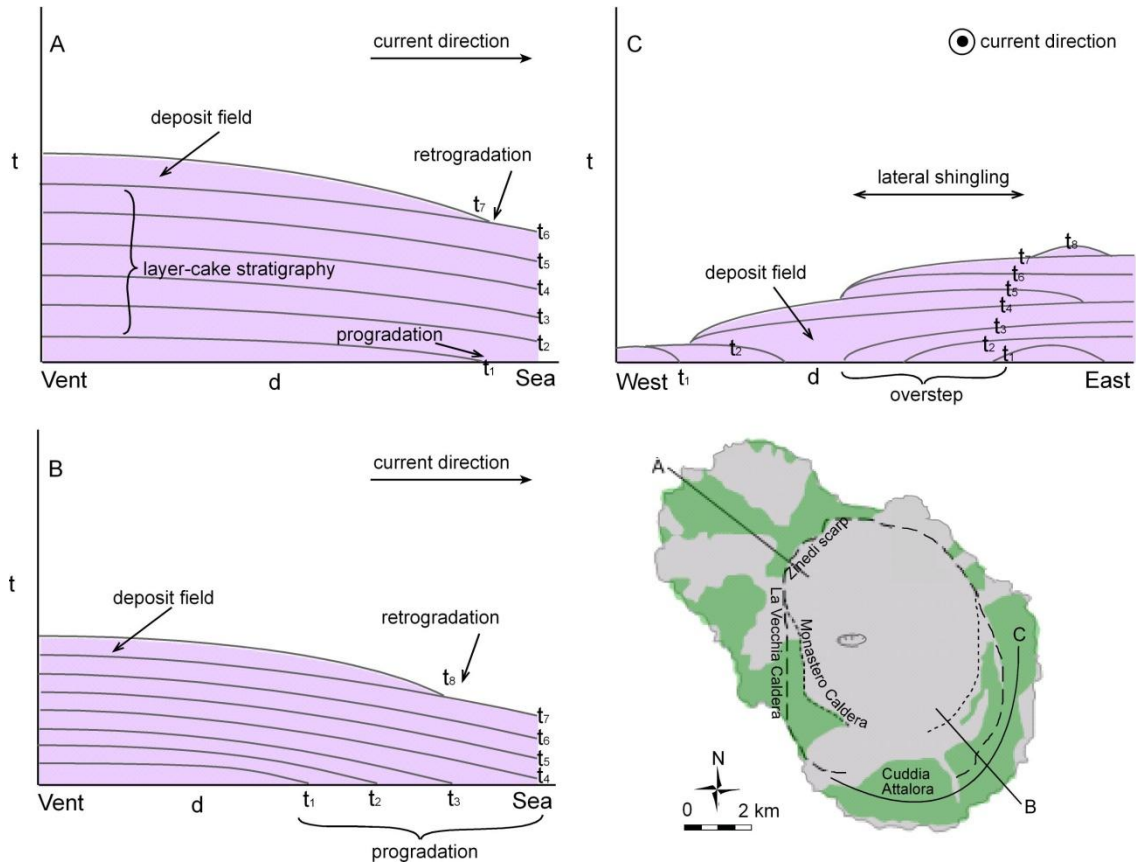


**Fig. 4-5: Schematic cross-sections through the deposit field showing entrachron architecture at three locations. Cross sections are not to scale. A: layer-cake stratigraphy seen in the north of the island, particularly during the climactic phase of the current. Some progradation is seen at the start of the current ( $t_{1-2}$ ) and some retrogradation seen at the end of the current ( $t_{6-7}$ ). The final stage of the current did not reach here ( $t_8$ ). B: Significant progradation is seen in the south as the current waxed through its initial stages ( $t_{1-4}$ ). During the climactic phase of the current, layer-cake stratigraphy is seen when the current is truly radial. During the final phase of the current the leading edge retrogrades ( $t_8$ ). C: Lateral shingling is seen in the south of the island. During the first phase of the current the leading edge of the current is limited to narrow fingers ( $t_{1-2}$ ). As the current waxed, the current shifted laterally to over step its own deposit from east to west ( $t_{2-4}$ ). As the current waned, the current again shifted eastward ( $t_{5-7}$ ) until only a narrow finger of the current remained ( $t_8$ ).**

#### 4.4.5. Implications for mass flux

The Green Tuff density current progressively aggraded with time as the leading edge of the flow advanced into different sectors and to varying run-out distances. The current was only truly radial during its climactic phase. During its waning phase, run-out distance again decreased and the current was restricted to certain sectors. It is important to consider this if an attempt were to be made to model how the current achieved a particular run-out distance.

Typically, models produced to simulate pyroclastic density currents use parameters such as flow run-out, mass flux, deposit volume and thickness derived from field observations of deposits (Bursik & Woods 1996; Kover 1995; Malin & Sheridan 1982; Sheridan & Malin 1983; Valentine & Wohletz 1989a, b; Wadge *et al.* 1998). However, for the Green Tuff ignimbrite, these parameters change significantly during the duration of the current. Firstly, the run-out distance increased then decreased with time. This would invalidate any application of the energy line concept (H/L after Sheridan 1979) when total run-out distance is considered for an entire ignimbrite sheet.

Secondly, estimated volumes for the different time-slices of the Green Tuff current have been calculated using the footprint area and an average thickness of 5 m (it has been arbitrarily assumed that each zone represents an equal 1/8th of the average thickness). The volume of the ignimbrite erupted in successive time slices gradually increased then decreased towards the end of the eruption (Fig. 4-6). The volumes for the time slices where the current entered the sea are a minimum estimate, any extra volume would be recorded offshore (dashed line on Fig. 4-6). The radial time-slices only account for less than 50% of the total volume of the ignimbrite. Thus, if the curve is interpreted as a proxy for mass flux, it is clear that the assumption that the entire current was emplaced radially, immediately, would greatly over estimate the actual mass fluxes involved.

When modelling how a current achieved a particular run-out distance, for example, the mass flux calculated for the entire ignimbrite sheet is irrelevant (e.g. when applying energy line concepts after Hayashi & Self 1992; Sheridan 1979; Walker *et al.* 1995). Rather, the mass flux of only that part of the ignimbrite sheet that corresponds with the particular time-slice that achieved the maximum run-out should be considered. Parts of the ignimbrite below and above this time-slice can have played no part in the current reaching the distal limits of the deposit sheet - this applies whatever modelling approach is used (e.g. Bursik & Woods 1996; Dade & Huppert 1996; Kover 1995).

#### **4.4.6. Lithofacies correlations as time-markers**

The entrachron architecture cross-cuts the lithostratigraphy based on correlation of lithofacies around the sheet (Orsi & Sheridan 1984) and demonstrates that lithofacies are diachronous and cannot be taken to represent a temporal history of flow events (Fig. 4-7). Many ignimbrite sheets do not show compositional zoning; in these cases it may

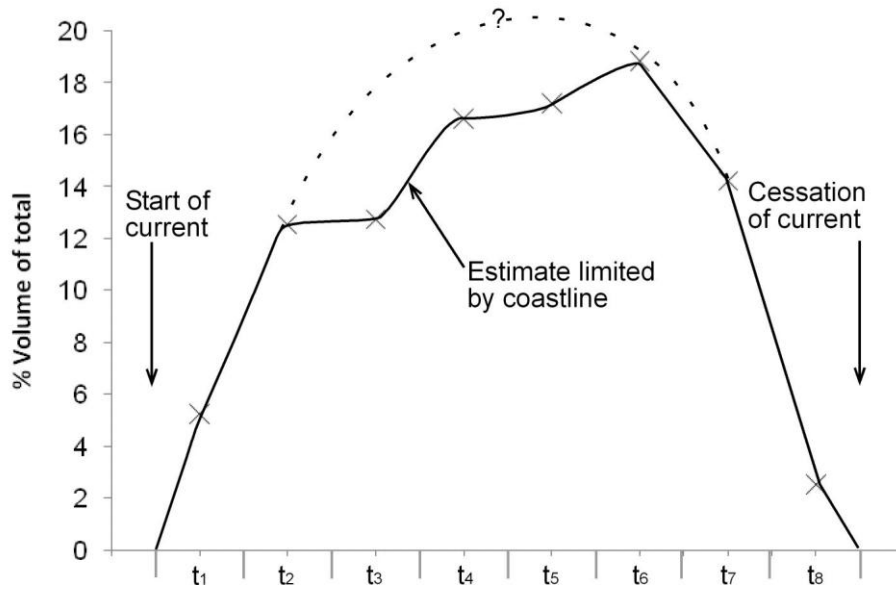


**Fig. 4-6:** Volume of the ignimbrite per time slice, represented as a % of the total volume. The dashed line represents uncertainty where total volume would only be recorded offshore.

be difficult to reconstruct the history of changing flow dynamics successfully as lithostratigraphy cannot be used. However, intercalations of several widespread fallout layers within the sheet would help.

Furthermore, if deposits are used to constrain models it is imperative that internal architectures of individual flow-units are documented. This is likely to be possible only for some natural examples. More fieldwork on targeted zoned ignimbrites is urgently required if we are to understand the possible range of flow behaviours from large explosive eruptions.

#### 4.4.7. Possible causes of asymmetric flow

Caldera subsidence has been shown to greatly affect ignimbrite emplacement. Asymmetric caldera collapse may cause directed currents (e.g. Kaingaroa ignimbrite, Beresford & Cole 2000), incremental down sag of a piecemeal caldera can affect the location of ignimbrite epicenters (e.g. Glencoe Volcano, Moore & Kokelaar 1998) and caldera rims can block or partially block currents causing ponding within existing calderas (Valentine *et al.* 1992). These effects are clearly seen in the Green Tuff ignimbrite, where the footprint of the current appears to be constrained by various caldera scarps at various stages of the eruption. The importance of topography on the distribution of the Green Tuff ignimbrite is discussed later (Chapter 5).

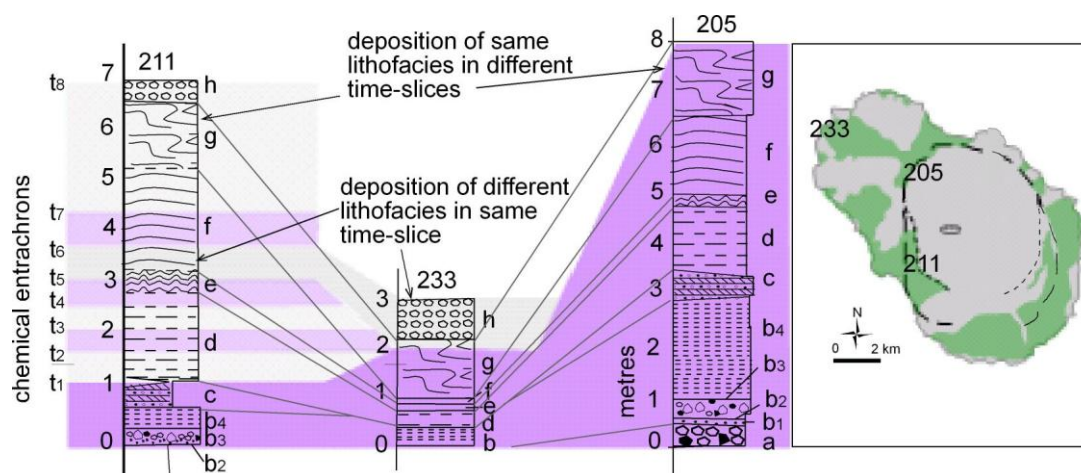


**Fig. 4-7:** Selected sections from Orsi & Sheridan (1981) and their lithostratigraphic correlations, with location map. Over-printed is the chemical stratigraphy from this study. The lithofacies are diachronous and thus cannot be used as time-markers.

Directed currents may also be generated at source from asymmetric collapse of vertical (Carey *et al.* 1988; Woods & Caulfield 1992) or directed pyroclastic fountains (Lagmay *et al.* 1999). The Green Tuff pyroclastic density current appears to have been significantly sectoral only during the waxing or waning stages of the current when fingers of current extended in certain directions. As the current waxed to its climax, the current became more fully radial, except where affected by topographic barriers. Similar behaviours have also been recognized elsewhere. A volcanic succession at Stromboli, Italy which has been interpreted to record two stages of an eruption with a first stage of low temperature, pulsatory low density pyroclastic currents that changed direction dependent upon topography, and a second climactic stage in which the current radially expanded pyroclastic current which was able to travel uphill (Giordano *et al.* 2008). However, this example is of discrete, multiple currents and an example of this behaviour for a single current does not currently exist.

Recent larger scale experiments simulated an eruption column of a fountaining pyroclastic jet and the generation of pyroclastic density currents (Dellino *et al.* 2007; Sulpizio *et al.* 2008). Preliminary results have shown that a long conduit will result initially in finger currents of material which are rapidly followed by a radially spreading current. This experiment is thought to represent a pressure-adjusted pyroclastic jet. Other simulations use a short conduit as a proxy for an over-pressurised jet from a transient explosion, in which the ejecting material was not able to equalize with the

atmospheric pressure. In this case, the collapsing column produced finger currents which covered different areas of the surrounding floor at different times. The resulting deposit is thin, widely and evenly distributed, and could be an analogue for the finger-like current footprint seen in the Green Tuff ignimbrite and the first example could be an analogue for the change from directed fingers of currents to radial flow.

Not all low aspect-ratio ignimbrites have a strictly radial deposit distribution (Arico Ignimbrite, Brown *et al.* 2003). Often, it is assumed that a non-circular deposit area was initially circular, but that the deposit is not preserved as the expectation is that low aspect-ratio ignimbrites should be radial. Apart from their deposit area, there is no other evidence to suggest that these ignimbrites had an emplacement mechanism which is different to true radial ignimbrites. It is possible that, if the eruption continued and dynamics such as those discussed above (changing column collapse direction, change in vent dynamics etc) changed, the current could have shifted, completing its almost-radial distribution.

It follows that it is not necessary to invoke special circumstances for circular, low aspect-ratio ignimbrites. A potential reinterpretation of circular ignimbrite sheets as the result of sector by sector accumulation of a progressively aggrading, sustained turbulent current would involve longer current durations and lower mass flux. This fundamentally different view of the emplacement of low aspect-ratio ignimbrites would have significant implications on the hazard that they pose. It is important therefore, that the term low aspect-ratio ignimbrite is considered a term which describes the physical characteristics of a deposit, and does not have inherent connotations regarding current behaviour and emplacement mechanisms (Branney & Kokelaar 2002; Dade & Huppert 1996). Inferences of current behaviour and mechanisms of emplacement should draw more on internal architectures of the ignimbrite sheet which can be used to decipher changing flow directions and conditions. Changing lithofacies and deposit characteristics can be used to infer current parameters at the flow-boundary zone but can only be thoroughly understood in a time framework, such as that provided by the internal ignimbrite architecture.

## **4.5. Conclusions**

This study has revealed that the hypothesis that radially distributed ignimbrites are emplaced by density currents that flow radially, simultaneously from source is false.

- The Green Tuff ignimbrite sheet was emplaced diachronously.
- The Green Tuff pyroclastic density current advanced progressively over Pantelleria island as it waxed, then the leading edge retreated as the current waned.
- The leading edge of the current shifted laterally as well as transversely from vent.
- The density current was not able to overtop topography at all stages during the eruption. The largest barriers were only inundated during the most climactic phase of the eruption.
- Flow paths of pyroclastic density currents are complex and topography controls their distribution.
- Detailed studies of the internal architecture of single ignimbrites can provide important information on the dynamics of eruptions and how these complex, incredibly hazardous currents behave. We have shown that by understanding the nature of chemical zoning within ignimbrites and the distribution of chemical zones within an individual ignimbrite sheet, it is possible to unravel its cryptic internal architecture. Careful analysis of this cryptic internal architecture allows for interpretative reconstruction of how the current evolved with time and space and how the ignimbrite flow-unit was progressively aggraded diachronously through time and how it was emplaced.
- The term ‘low-aspect ratio ignimbrite’ is a term to describe the physical characteristics of an ignimbrite sheet. It should not have genetic connotations. Details of current behaviour and emplacement mechanisms of individual low aspect-ratio ignimbrites should be considered case by case, using deposit and lithofacies characteristics which should be interpreted on a time-framework provided by an internal architecture of an ignimbrite sheet, such as chemical zoning.

# 5. How sustained pyroclastic density currents evolve with time and space

## II: behavior at topographic barriers

---

### 5.1. Abstract

Chemical variations (pantellerite at the base to trachyte at the top) in the Green Tuff ignimbrite, Pantelleria, allow reconstruction of the flow history of the pyroclastic density current that deposited it by dividing the brief duration of the sustained current into successive time-slices ( $t_1$ - $t_8$ ). The vertical and lateral compositional variations mapped internally within the deposit have enabled reconstruction of how the geographic footprint of the current shifted as the current waxed and then waned (Chapter 4). This chapter considers how the current behaved as it encountered and then overtopped a variety of local topographic barriers, including scoria cones of different sizes, transverse topographic ridges and palaeovalleys. Results show that the radial density current did not overtop all topographic barriers as it initially encountered them. Rather, it first was unable to over top the barrier but then progressively inundated each barrier until, presumably, the current had waxed sufficiently to be able to pass over. The current was reflected at some barriers, and was deflected around the lower flanks of others. Even small barriers affected current behaviour during its initial waxing phase. There is no distinct caldera collapse signature related to the Green Tuff ignimbrite. Either caldera collapse was minimal or, the caldera may have formed progressively during the eruption.

### 5.2. Introduction

Pyroclastic density currents are the greatest hazard to many communities near volcanoes. Improved understanding of the behaviour of density currents would allow for better hazard and risk assessments. Traditionally, hazard maps have been based on mapping of volcanic deposits and more recently using numerical modelling and computer simulations that rely on topographic data to produce hazard maps and delineate safe zones (Sheridan *et al.* 2005).

In hazard assessments topographic barriers have been used to predict lee-side ‘safe zones’ such as at Guagua Pichincha, Ecuador, where the city of Quito is thought to be protected by the older volcanic edifice of Rucu Pichincha which is known to have stopped pyroclastic density currents reaching the city (Barberi *et al.* 1992). Similar conclusions were drawn at Campi Flegri where historic pyroclastic density currents have been confined by a caldera rim and therefore thought to not pose a risk to the large population further around the volcano (Lirer *et al.* 2001).

However, how density currents interact with topography is not yet fully understood, particularly with regard to sustained currents, and energetic currents that are not confined to within valleys (e.g. those that deposit low aspect-ratio ignimbrites). Pyroclastic density currents are known to have overwhelmed topographic barriers far from source (Aramaki & Ui 1966; Ferriz & Mahood 1984; Fisher *et al.* 1993; Miller & Smith 1977; Wilson 1985). Similarly, turbidity currents are commonly sustained and are known to scale large barriers (Muck & Underwood 1990). However, because turbidites are generally not zoned, it is not possible to reconstruct how the flow behaviour evolved with space and time. Study of chemically zoned ignimbrites may provide valuable insights to the behaviour of different types of geophysical density currents, such as: (1) changes in flow behaviour as the current waxes or wanes (Chapter 4); (2) changes in flow behaviour as a result of modification of substrate topography as the current erodes and/or deposits; and (3) how topography may affect deposition from a current so that field evidence can be properly examined.

### **5.2.1. Previous work on density currents and topography**

Ignimbrite sheets that have been emplaced over irregular topography commonly show spatial variations, e.g. valley-pond facies and their temporally equivalent veneer deposits (e.g. Taupo, Wilson 1985; Laacher See, Schumacher & Schmincke 1990; Abrigo ignimbrite, Pittari *et al.* 2006). Breaks in slope may be associated with a change in clast size (Giordano 1998) or lithofacies (Fisher 1990; Sulpizio *et al.* 2008a). Similar features occur in turbidites where changes in deposit thickness over topographic irregularities are interpreted to result from depletion of the current on encroaching a barrier (Alexander & Morris 1994; Kubo 2004). Topographic barriers are also able to deflect or reflect currents (Edwards *et al.* 1994; Kneller *et al.* 1991; Pickering *et al.* 1992).

Deposits of such currents also have been found to exist on the summit of topographic highs beyond mountain ranges. Upslope flow has been recorded in the deposits of numerous turbidity currents (e.g. Dolan *et al.* 1989; Muck & Underwood 1990) and pyroclastic density currents are thought to have crossed high topographic barriers long distances from source, as seen on a relatively small scale (e.g. the currents from Mt. St. Helens scaled barriers of 500 m, Druitt 1992; Hoblitt *et al.* 1981; 500 m at Fisher caldera, Miller & Smith 1977; 600 m at Ito, Japan, Yokoyama 1974) and a large scale (e.g. 800 m at Ata caldera, Aramaki & Ui 1966; 1000 m by the Campanian ignimbrite, Italy, Barberi *et al.* 1978; Fisher *et al.* 1993; and 1500 m at Taupo, Wilson 1985).

Two contrasting alternative models have been proposed to explain the ability of density currents to scale topographic barriers. The first is that of a thin, highly concentrated, short-duration current such as was envisaged for the emplacement of the Taupo ignimbrite (by Wilson 1985; Wilson & Walker 1982). In this scenario, the current originates from the collapse of a very high ( $> 50$  km) ultraplinian eruption column. The collapsing column rapidly condensed to form a thin, very high concentration granular flow, the high momentum of which derived from the descent from 55 km. The current travelled at speeds in excess of  $150 \text{ ms}^{-1}$ . The current duration was very short and it reached its maximum run out distance near instantaneously. The main transport of material is by concentrated flow. These thin flows are able to surmount topographic barriers due to their high momentum.

The alternative model is of a dilute current in which particles are transported by fluid suspension (Baer *et al.* 1997; Bursik & Woods 1996; Dade & Huppert 1996; Fisher *et al.* 1993; Valentine 1987). Suspension currents may be short or long duration (sustained). Small clasts held in turbulent suspension drop out of the current as it decelerates, therefore the particle concentration falls with time, and the run out distance of the current is controlled by the mass flux (Bursik & Woods 1996). High mass-flux discharge results in long transport distances. These expanded suspension currents are able to surmount topographic barriers due to their thickness: they are often considered to be thicker than the barriers they meet (Gardner *et al.* 2007).

More recently, modellers have incorporated both end-members into the models of pyroclastic density currents (Doyle *et al.* 2010). This work builds on the idea that currents are density stratified (Valentine 1987), with more dilute upper levels and

denser lower levels (Branney & Kokelaar 2002; Legros & Kelfoun 2000). The lower levels of a density stratified current may be blocked by a topographic barrier and upper levels pass over: this has been termed detachment or flow stripping (Piper & Normark 1983) and has been inferred from studies of both small-scale currents such as at May 1980 Mt. St. Helens, USA; Merapi volcano, Indonesia; Colli Albani volcano, Italy; and Soufriere Hills volcano, Montserrat (Bourdier & Abdurachman 2001; Calder *et al.* 1999; Fisher 1990; Giordano *et al.* 2002 respectively) and large, caldera-forming eruptions such as at Okmok volcano and Fisher Caldera, Alaska (Burgisser 2005; Gardner *et al.* 2007 respectively).

Each of these models has attempted to explain the variety of topography-controlled behaviours seen in field-based studies. The numerical models of dilute currents predict deflection, reflection and changes in deposit thickness (Bursik & Woods 2000; Woods *et al.* 1998) and can match deposit morphology and run-out distances (Dade & Huppert 1996). However, they cannot account for the range in lithofacies variations (Wilson 1997). The numerical models and the simple laboratory experiments often used to validate them only partially resemble the complexities in natural cases. Most striking is the use of limited particle sizes (e.g. 10 – 100  $\mu\text{m}$ ) and low particle concentrations (Sulpizio *et al.* 2008b). Whilst modelling of density stratified flows is a step towards a more complex model (Doyle *et al.* 2010) this is a relatively new advance with little validation. Although harder to model, it has been proposed that transfer of mass between upper or lower components may be significant, and that it is unrealistic to model density stratified currents as two independent flows (Branney & Kokelaar 2002). Clearly, there is a case for further detailed field studies of density currents over topography (Druitt 1998; Sulpizio *et al.* 2008b) to provide the ‘ground-truth’ data that must underpin any physical model.

### **5.2.2. Aims**

The aim of this study is to use the field relations of the internal chemical stratigraphy of the Green Tuff ignimbrite over topographic barriers to investigate:

- how do sustained geophysical density currents interact with different shapes of topography?

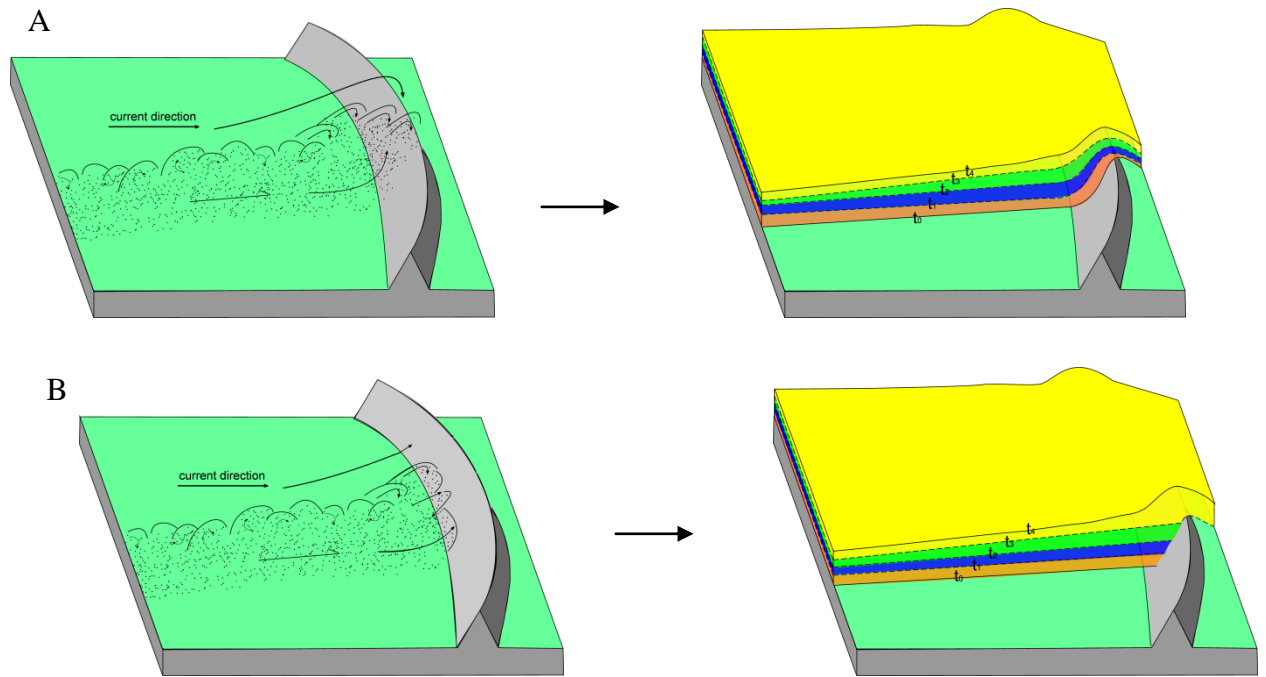


**Fig. 5-1** How density current behaviour at a transverse barrier might be recorded by internal entrachron stratigraphies. **A:** current overtops barrier at all times, resulting in a layer-cake stratigraphy that drapes the barrier. **B:** Current is initially blocked, reflected or deflected by the barrier. The deposit will build up before the current is able to overtop the barrier resulting in an onlap style stratigraphy to the deposit.

Experiments indicate a variety of ways in which density-stratified pyroclastic density currents can interact with topography (Bursik & Woods 2000; Gladstone *et al.* 2004; Kubo 2004; Rivas *et al.* 2005; Woods *et al.* 1998). They can overtop topographic barriers (Fig. 5-1A) or partially overtop them by flow-stripping. Does the initial momentum of the current carry the leading edge over topographic barriers on initial encroachment, or does the mass flux have to increase above a certain threshold before the current is able to overtop the hill (Fig. 5-1B)? Alternatively, the topography may have to be modified by deposit aggrading to the stoss side of the topographic barrier before a sustained density current can surmount the barrier (Valentine *et al.* 1992).

### 5.2.3. Methods

The Green Tuff ignimbrite, Pantelleria, drapes a variety of topographic features, including caldera scarps, old scoria cones, vents on caldera scarps and it fills palaeovalleys which are excellently exposed along the coast. This study takes advantage of the coexistence of three features: (1) present day topography is closely similar to that at the time of Green Tuff emplacement; (2) the Green Tuff ignimbrite is very well

exposed and its relation with topographic features is clear; and (3) the internal chemical zones of the ignimbrite means that response to topography can be reconstructed for the different stages of the currents history. A variety of different case studies have been investigated (Fig. 5-2): conical barriers of three different sizes (Cala del'Alca scoria cone, Cuddia di Khamma and Cuddia di Scauri), ridges perpendicular to the currents direction (Piano and Serra di Ghirlanda) and two palaeovalleys parallel to palaeocurrent direction (Cala Rossa and Balata dei Turchi).

### **Data collection**

Each case-study was mapped in the field onto an enlarged 1:25,000 topographic map (Istituto Geografico Militare, Edizione 2, 1972) using a handheld Garmin GPS and a Silva compass clinometer. The dip and strike of the contact of the Green Tuff with the substrate indicates the pre-Green Tuff ignimbrite slope. Bedding of the Green Tuff ignimbrite was measured where seen, or where it was not seen the dip and strike of foliation was taken where it had not been modified by rheomorphic folds. The plunge and plunge direction of imbricated fiamme and clasts relative to bedding give an indication of the direction of depositing parts of the current. For example, an imbrication of 10°E with respect to bedding indicates an inferred current direction of east to west (Branney & Kokelaar 1992; Schmincke & Swanson 1967). However, accurate imbrication measurements require good 3D exposure. In the absence of this they provide only apparent current directions. Imbricated clasts are mapped as arrows pointing in the inferred current direction. The plunge and plunge direction of lineations on bedding or welding-foliation planes give an indication of shear direction at the base of the current at that moment in the final stages of agglutination (Branney *et al.* 2004). Shear may be the result of the overriding current, or due to gravity acting on the hot agglutinate on a local topographic slope. Lineations are not unidirectional indicators. A lineation that is plunging 10°E may indicate a current direction to the west or to the east. Other studies have taken advantage of directional fabrics to attempt to understand the emplacement of density currents across topography (Capaccioni *et al.* 2001; Fisher *et al.* 1993; Suzuki & Ui 1982, 1983; Ui *et al.* 1989). In the present study, directional (kinematic) data are recorded in conjunction with a chemical-entrachron stratigraphy so that uniquely the inferred emplacement of the density current has temporal control.

The Green Tuff ignimbrite was logged and sampled across each topographic barrier. Sampled vertical sections were selected where the base of the ignimbrite unit was

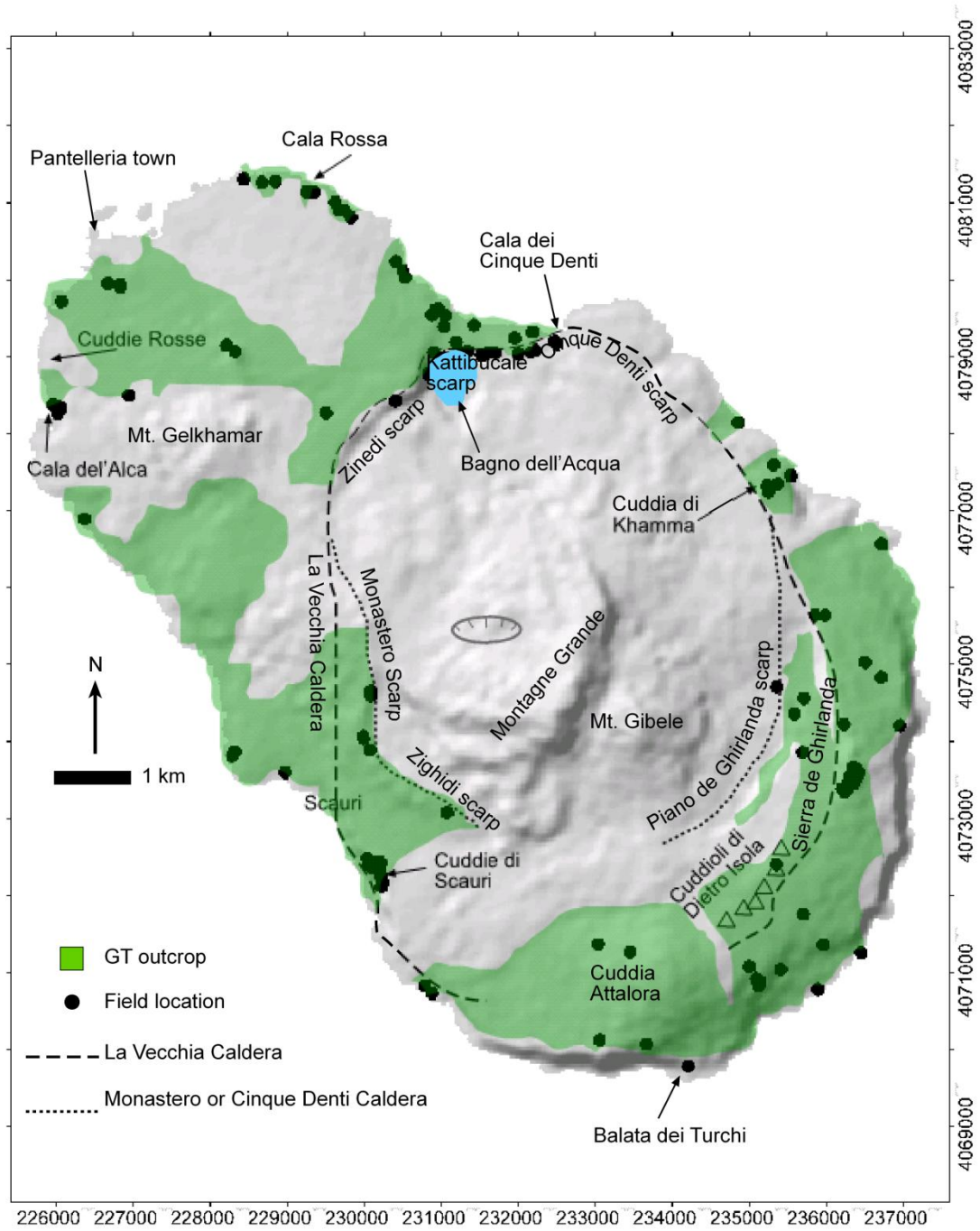


**Fig. 5-2: Location map of important location discussed in this chapter, including topographic barriers and caldera scarp. Grid numbers are for UTM Zone 32N**

exposed to ensure that the very first part of the current was recorded. Care was taken to sample the very top of the ignimbrite, but some erosion of uppermost parts is common. In sites that do not preserve the upper vitrophyre, it is not certain that the top of the unit is present.

### **Data analysis**

Samples were analysed by XRF for whole rock major and trace elements as described in Chapter 3. The Zr ppm values were entered into an ArcGIS database so that they could be analysed spatially over and around each barrier, as described in Chapter 4. However, the database is not able to resolve vertical sections: therefore, cross sections were constructed through the barriers to help resolve the relations of the chemical-entrachron stratigraphy with topography.

## **5.3. Results and interpretations**

A sketch map is produced for each topographic barrier, with locations of sections sampled for geochemistry marked on an aerial photo of the same area. The results are presented as either a cross section through the deposit or as chemical footprints across the barrier as appropriate.

### **5.3.1. Interaction with cones**

#### **Scoria cone at Cala del'alca**

A small (c.15 m high) scoria cone is draped entirely by the Green Tuff ignimbrite on the northwest coast of Pantelleria (Fig. 5-2). To the east of it, the Green Tuff is covered by Mt. Gelkhammar lava flows which bank against the flanks of the scoria cone. To the north, the Green Tuff ignimbrite is covered by basaltic lavas from another nearby scoria cone, Cuddie Rosse.

The inferred current direction, from a source vent near the centre of the island, is from the southeast. This is consistent with SE-NW trending rheomorphic lineations in the Green Tuff ignimbrite (Fig. 5-3). However, on the scoria cone flanks, current indicators appear to be strongly affected by the slope: both lineations and imbricated clasts show down slope flow (Fig. 5-3).

The entrachron stratigraphy in the Green Tuff ignimbrite changes across the cone. In particular, the base of the ignimbrite is demonstrably diachronous (Fig. 5-4B). The

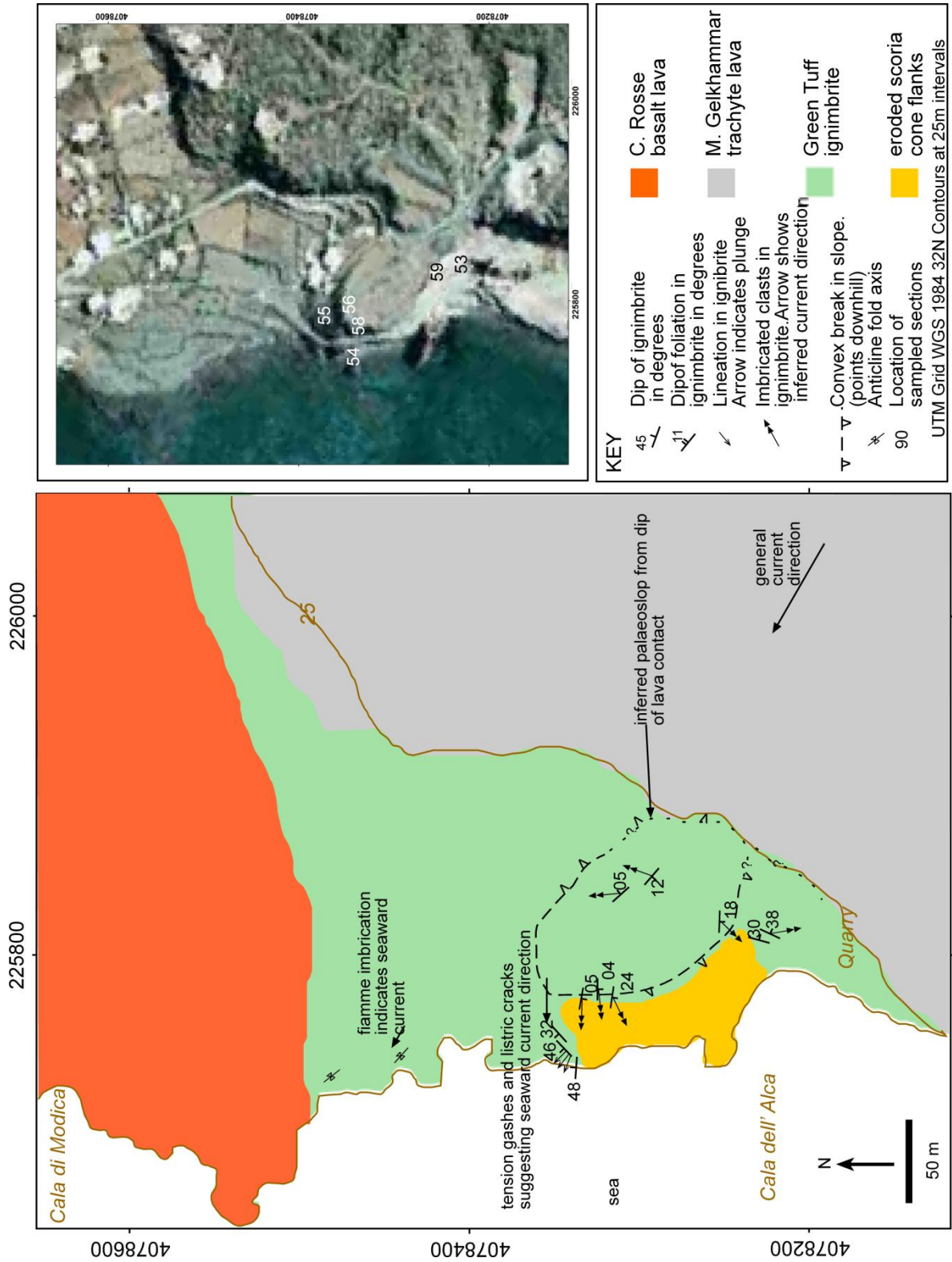
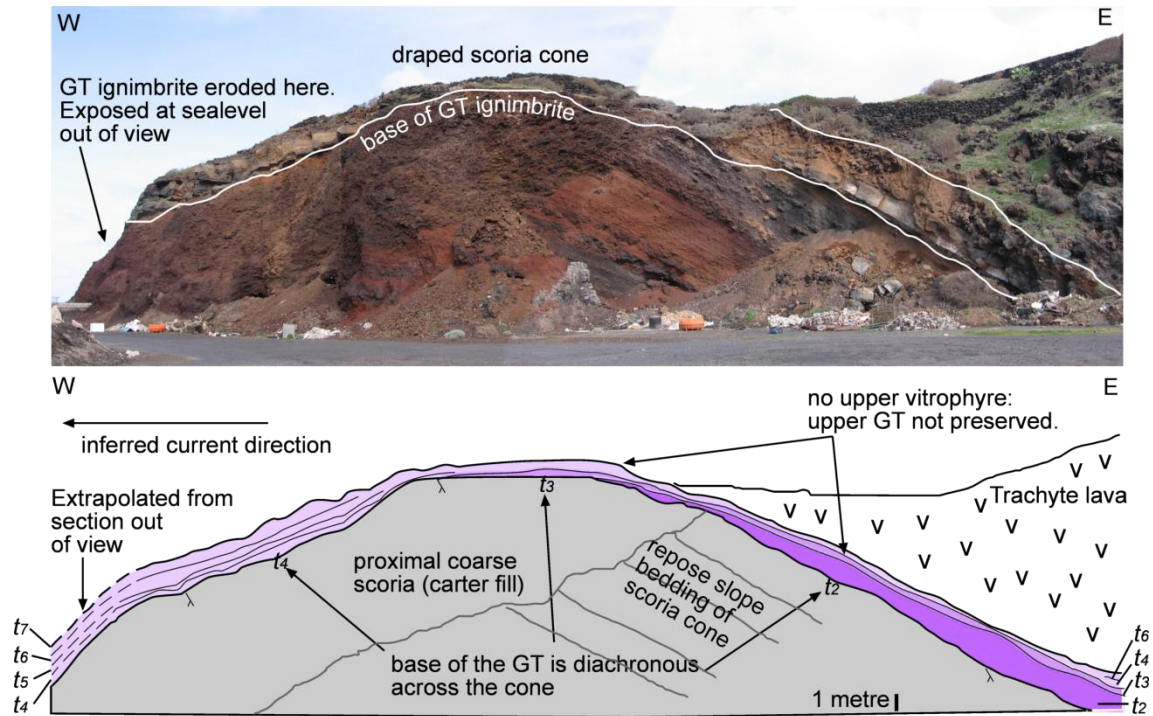


Fig. 5-3: Sketch map of Cala dell'Alca, NW Pantelleria. Location of individual sections sampled for geochemical study shown on aerial photo.



**Fig. 5-4 A:** Photograph (viewed towards the N) of an exposed cross section through the scoria cone at Cala del'Alca. Note metre ruler for scale. The Green Tuff ignimbrite drapes the cone on its western and eastern flanks, and has been buried by Mt. Gelkhammar trachyte lavas on the east (right). The ignimbrite thickens westward. The Green Tuff drape of the western flank is not seen in this view but is exposed nearby to sea-level. **B:** Schematic cross-section through the Green Tuff ignimbrite over the scoria cone showing its diachronous base, marked by zone  $t_2$  being overlapped by zone  $t_3$  which is overlapped by zone  $t_4$ .

first zone ( $t_1$  of Chapter 4) of the ignimbrite is absent in this part of the island. The next zone of the current ( $t_2$ ) only drapes the eastern flank of the cone and zone  $t_3$  is only recorded on the eastern side of the summit. Zone  $t_4$  is present across the entire zone including the lee side of the cone. All subsequent chemical entrachrons ( $t_{5-7}$ ) are present on the lee side of the barrier. The western draping section (location 54 on inset in Fig. 5-3) has an upper vitrophyre, suggesting that the ignimbrite is complete here. The final zone ( $t_8$ ) is absent.

### **Interpretation**

The first phase of the current ( $t_1$ ) did not reach this part of the island. The leading edge of the current advanced with time, reaching the cone by  $t_2$ , but was unable to surmount it. The next phase of the current,  $t_3$ , was able to inundate the cone further but it is not until time-slice  $t_4$  that the current is able to pass over the barrier completely. The current continues to flow over the barrier, but the leading edge retreats during  $t_7$  and the final phase of the current  $t_8$  did not reach here.

The maximum velocity ( $U$ ) of the current that was blocked by a topographic obstacle of a certain height ( $H$ ) can be roughly estimated by converting the kinetic energy into potential energy using Equation (1) (Legros & Kelfoun, 2000),

$$U = \sqrt{2gH}, \quad (1)$$

which for  $H=15$  m gives a maximum velocity  $\sim 17$  m s<sup>-1</sup>. However, this velocity calculation is valid as long as the flow depth is small compared to the obstacle height. Other factors not considered by this equation are mass flux and momentum. Therefore, whilst it is likely that the current during time-slice  $t_2$  was thin and of low-velocity, this value should be regarded with caution.

### **Cuddie di Khamma**

In the east of the island, along an inferred caldera scarp (La Vecchia scarp of Mahood & Hildreth, 1986), the Cuddia di Khamma lava shield volcano (208 m a.s.l., differential height c. 30 m) is draped by the Green Tuff ignimbrite (Fig. 5-2). In the heart of the village of Khamma, buildings on the Green Tuff and a mausoleum on the summit of the volcano restricts exposure. However, sections to the base of the unit occur on both stoss and lee sides of the volcano.

The inferred general current direction from a source in the centre of Pantelleria is to the northeast, consistent with lineations on the stoss flank of Cuddia di Khamma, which trend SW-NE (Fig. 5-5). At one location (location 93 on inset Fig. 5-5), imbricated fiamme indicate transport to the northeast. This trend continues on the lee flanks of the barrier, and these imbrications and lineations do not appear to have been affected by the palaeotopography.

At Cuddie di Khamma, the base of the Green Tuff ignimbrite is diachronous (Fig. 5-6). Basal sections are exposed on both the stoss and lee flanks of the volcano (locations 90, 91 and 93 in inset, Fig. 5-5). The first zone ( $t_1$ ) of the ignimbrite is absent in this part of the island. Zones  $t_2$ ,  $t_4$  and  $t_5$  are only recorded on the stoss flanks of Cuddie di Khamma. Zone  $t_3$  is absent. Zone  $t_6$  is recorded across the summit of Cuddie di Khamma and on the lee flank. An upper vitrophyre is preserved on the lee flank and this is also zone  $t_6$ .

### ***Interpretation***

The first phase of the current recorded here is time-slice  $t_2$  which is only recorded on the western flank which suggests that the current was not able to over top the barrier at the time (Fig. 5-6B). The initial phase ( $t_1$ ) of the current did not reach Cuddie di Khamma. During phase  $t_3$  the current also apparently did not reach the site, although it is possible that it only left a thin (cm) deposit which was not sampled. The current then started to inundate further up the hill, and inundated the southern flank ( $t_4$ ). However the current did not overtop the barrier ( $t_{4.5}$ ). The current eventually inundated the entire barrier during time-slice  $t_6$  (Fig. 5-6). This was the only phase of the current which was able to pass over this cone and presumably represents peak flow conditions at this site. The final phases of the flow ( $t_{7.8}$ ) are not recorded at Cuddie di Khamma and the upper vitrophyre records zone  $t_6$ . However, there is no upper vitrophyres on the stoss side of the barrier, and here the top is inferred to have been eroded. This explains why the full entrachron stratigraphy seen across the hill is missing at individual locations.

The maximum velocity ( $U$ ) of the current that was blocked by a topographic obstacle of a certain height ( $H$ ) can be roughly estimated by converting the kinetic energy into potential energy using Equation (1) (Legros & Kelfoun, 2000),

$$U = \sqrt{2gH}, \quad (1)$$

which for  $H= 30$  m gives a maximum velocity  $\sim 25 \text{ m s}^{-1}$ . However, this velocity calculation is valid as long as the flow depth is small compared to the obstacle height. Other factors not considered by this equation are mass flux and momentum. Therefore, whilst it is likely that the current during time-slice  $t_2$  was thin and of low-velocity, this value should be regarded with caution. It should also be noted that time-slice  $t_2$  is recorded near the top of the obstacle, but not on the summit or on the lee side. It is possible therefore that rather than a thin, concentrated current, it was a thicker, dilute current that lofted at this barrier at this time.

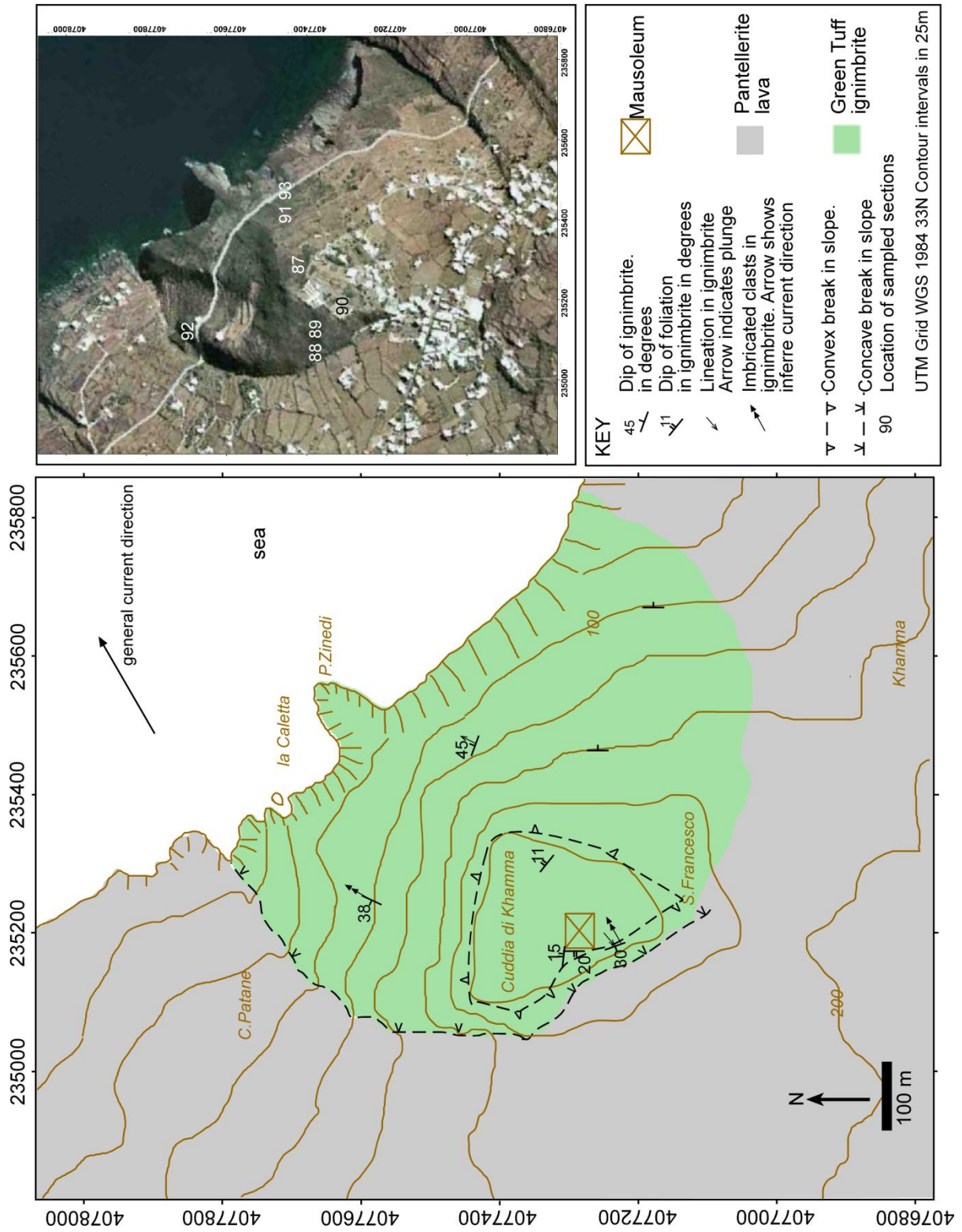
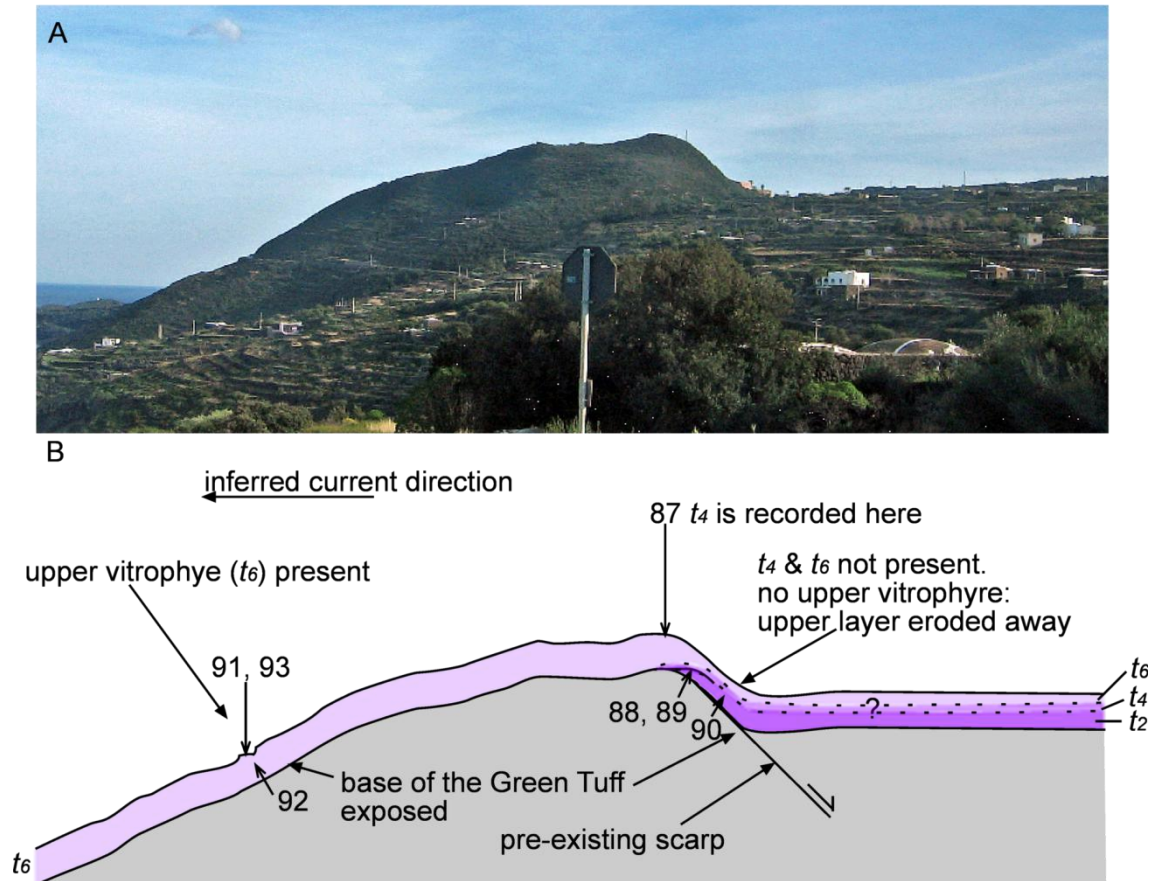


Fig. 5-5: Sketch map of Cuddia di Khamma, NE Pantelleria. Location of individual sections sampled for geochemical study shown on aerial photo.



**Fig. 5-6 A:** Photograph of Cuddia di Khamma looking southwards. Green Tuff ignimbrite general current direction is from right to left. The steep western side of the cone has been inferred to be a caldera scarp of the La Vecchia caldera (Mahood & Hildreth, 1986). **B:** Schematic cross section through the Green Tuff ignimbrite over Cuddia di Khamma showing its diachronous base at topographic scarp (thickness not to scale).

### Cuddia di Scauri

An eroded pumice cone, Cuddia di Scauri, rises above the surrounding topography to 192 m a.s.l. (differential height c. 30 m) along the La Vecchia caldera scarp near Scauri (Fig. 5-2). The Green Tuff ignimbrite drapes this cone, but is mostly thin (<1 m), and the base is always exposed and dips from 20° to 80° (Fig. 5-7).

The inferred general current direction of the Green Tuff pyroclastic density current is to the southwest, however, palaeocurrent indicators show a range of orientations (Fig. 5-7): on the south flanks of the cone, along an old caldera scarp, lineations indicate transport perpendicular to the scarp. Rotated clasts indicate upslope, seaward current

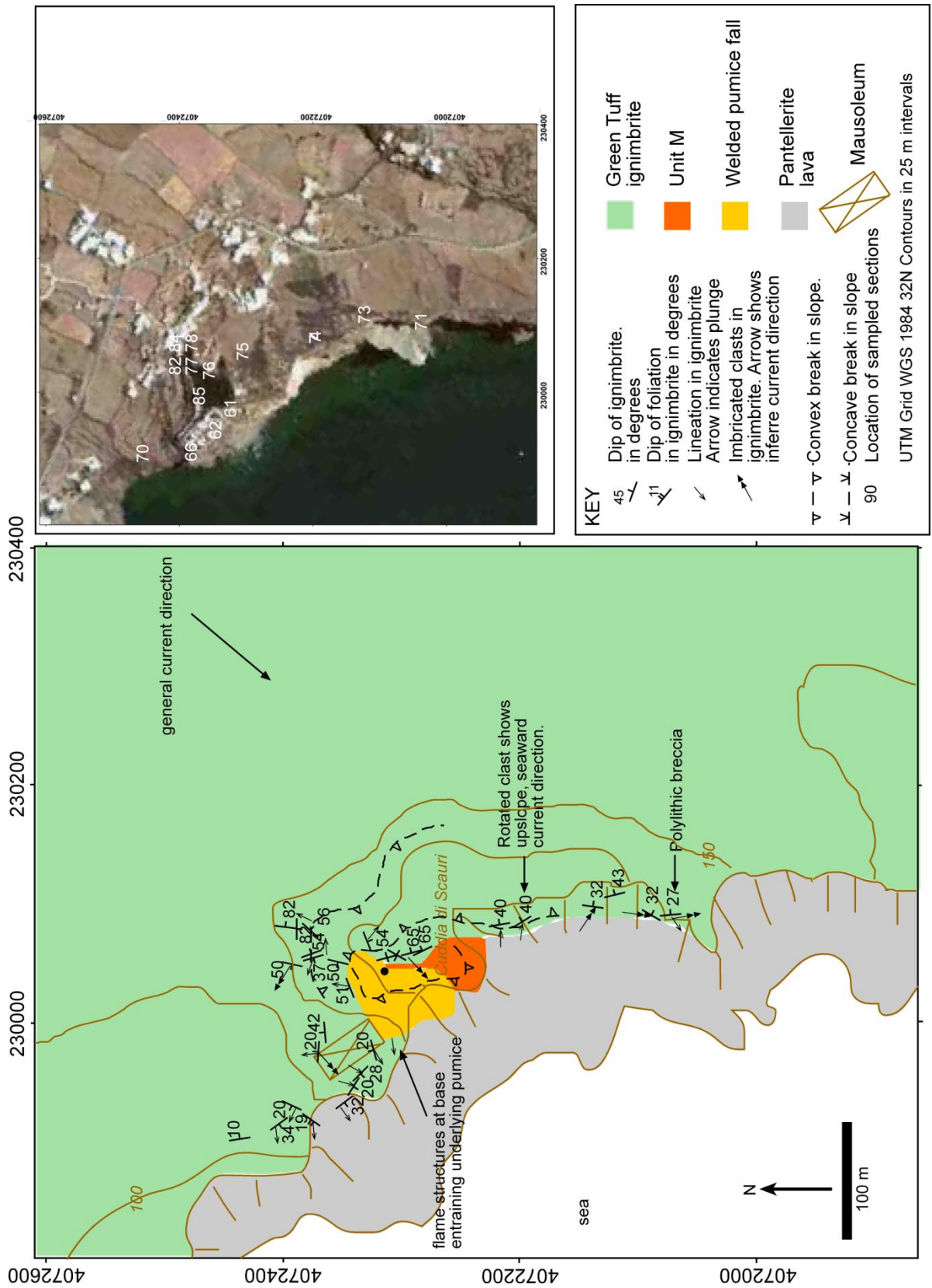
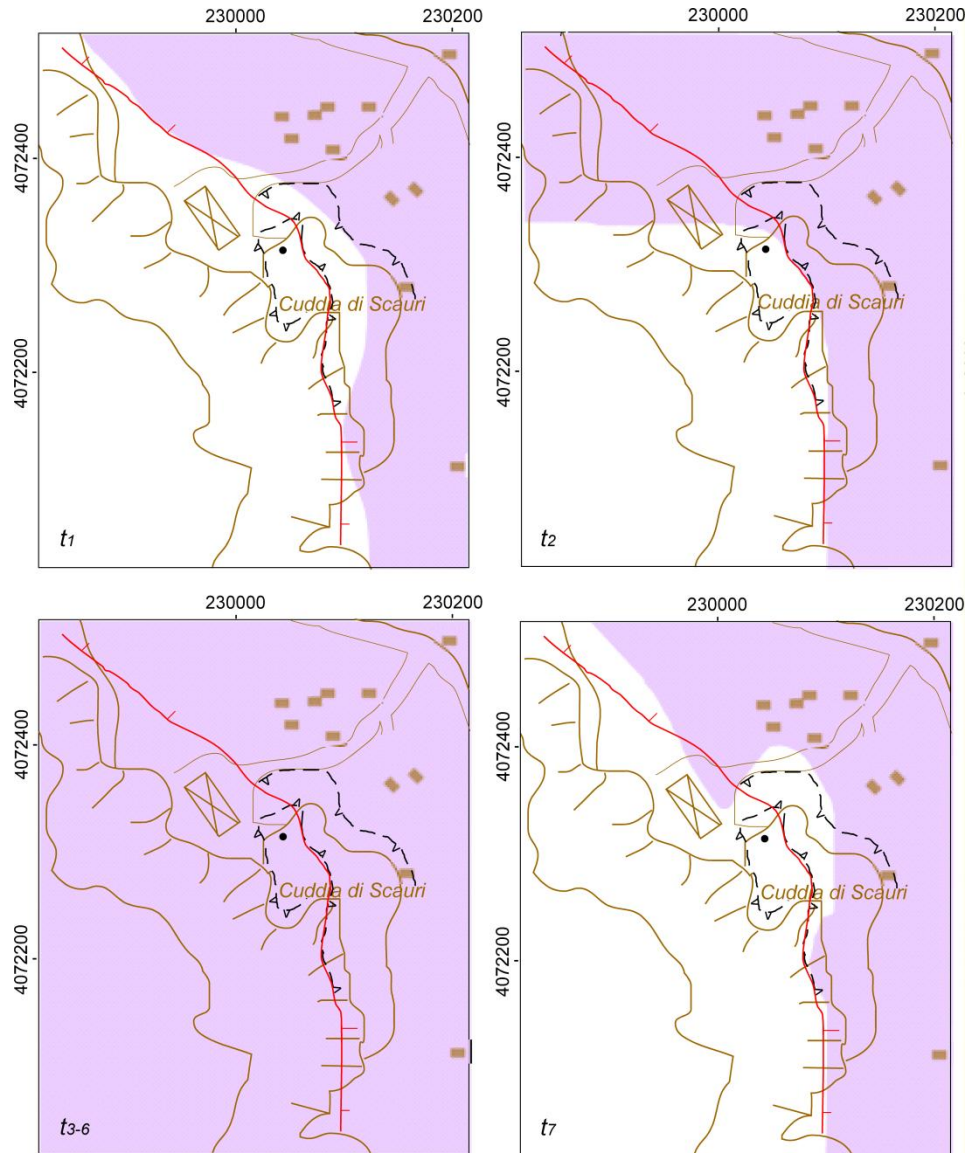


Fig. 5-7: Sketch map of Cuddia di Scauri, SW Pantelleria. Location of individual sections sampled for geochemical study shown on aerial photo.



**Fig. 5-8 :** Footprints of the density current at different time-slices through the evolution of the current from start ( $t_1$ ) to finish ( $t_7$ ) based upon Zr ppm. The final phase of the current ( $t_8$ ) is not recorded here.

direction. Further south, imbricated clasts indicate palaeocurrent direction to the south, down the flanks of the pumice cone (Fig. 5-7). At the summit of the pumice cone, imbricated fiamme indicate a palaeocurrent direction to the southwest but lineations on lee flanks of the cone show transport to the west or northwest. On stoss flanks of the cone, lineations trends vary from southeast to northeast.

Excellent exposure of the Green Tuff ignimbrite over the Cuddia di Scauri barrier, has enabled more sections, with exposed bases, to be sampled for geochemical analysis (inset Fig. 5-7) than at the examples considered above. This has enabled a more detailed

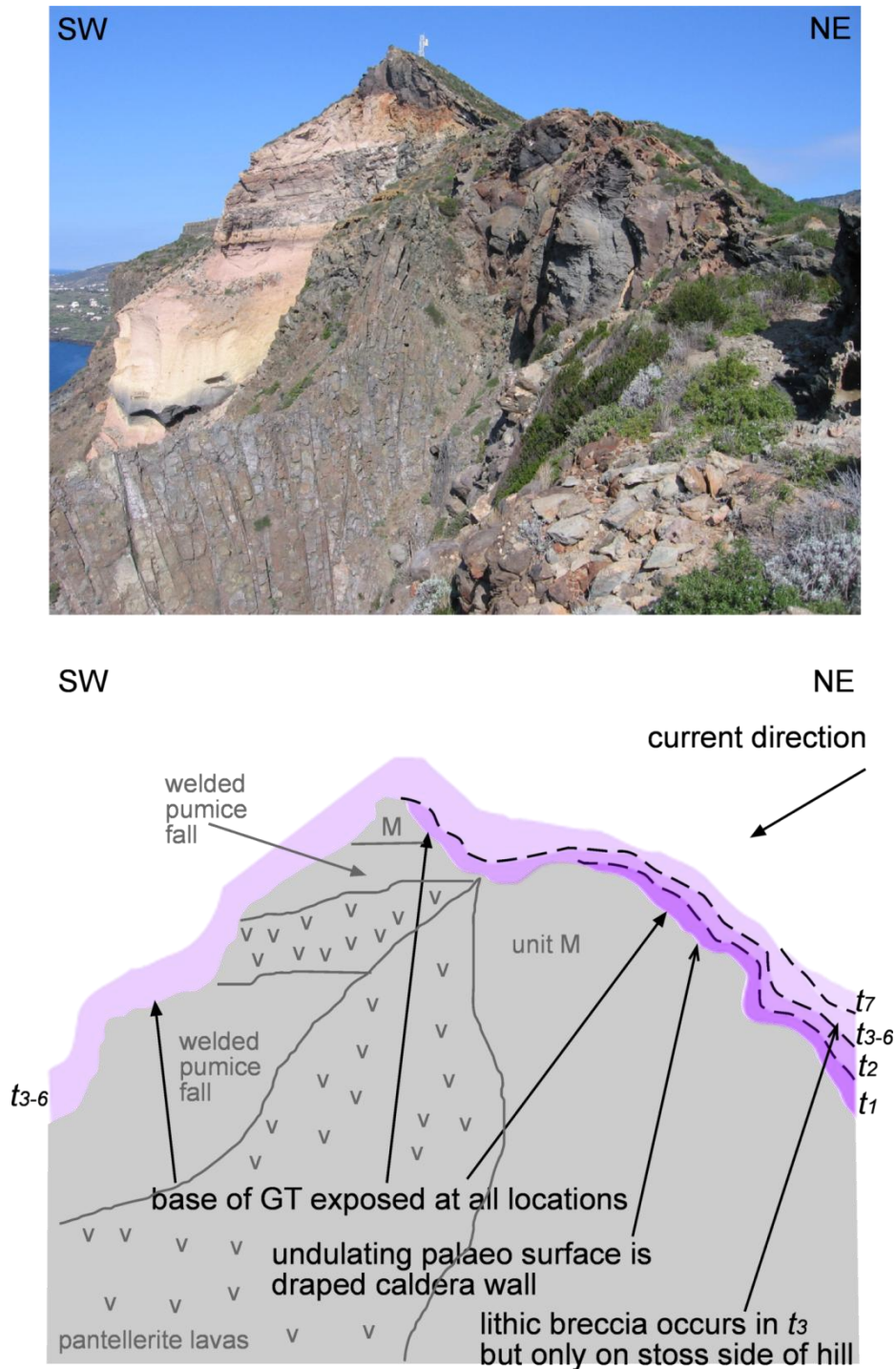


**Fig. 5-9A: Photograph of Cuddia di Scauri looking northwards along the La Vecchia caldera scarp. The general current direction is from right to left. The steep eastern side of the cone has been inferred to be part of the caldera scarp of the La Vecchia caldera dated by 'Unit M', c. 175 ka which is cut by the scarp, and 'Unit F', c. 106 ka which drapes the caldera scarp (Mahood & Hildreth, 1986) . The Green Tuff ignimbrite drapes this older unit which drapes the scarp. This older unit is not present behind the cone suggesting that the current which deposited it was not able to scale the barrier. Here, the Green Tuff ignimbrite lies directly on the pumice cone which forms the conical hill. B: Schematic cross section of the Green Tuff over Cuddia di Khamma showing its diachronous base.**

study of how the behaviour of the current at the barrier changed during the history of the sustained current. Fig. 5-8 shows four time slices through the eruption, or footprints such as in Chapter 4, but in greater detail. The first zone of the ignimbrite ( $t_1$ ) is only recorded on the stoss side of Cuddia di Scauri. The footprint of the ignimbrite increases through zone  $t_2$  on the northern flanks of the cone. The following four zones ( $t_{3-6}$ ) of the ignimbrite are recorded across the entire area (Fig. 5-8). The final zone recorded at Cuddia di Scauri is  $t_7$  and this is restricted to the stoss and northern flanks of the cone.

The draped steep caldera scarp and flanks of the cone are apparent on the cross section (Fig. 5-9), and photograph, which was taken along the caldera scarp looking northwards: note that the current is thought to have come from the northeast. In the schematic cross-section of the Green Tuff ignimbrite (Fig. 5-9) successive divisions in the chemical-entrachron stratigraphy overlap underlying zones, showing that the base of the unit is diachronous across the topographic barrier.

### ***Interpretation***

The lineations and kinematic indicators at the summit of Cuddie di Scauri indicate that the direction of the current that overtopped the barrier was not strongly affected by the palaeoslope. However, on the north and south flanks and on the stoss side of the topographic barrier, rotated lineation directions indicate that the palaeoslope was affecting the shear on the deposit at these locations. To the north of the cone, at its base, lineations and imbricated fiamme suggest a north westerly current direction which swings round to a more westerly direction further away from the cone. This may indicate that the current was being deflected here around the northern flanks of the cone.

The very first phase of the current reached this area ( $t_1$ , top left Fig. 5-8) but was only able to inundate the flatter areas around the cone. It also appears to be constrained by the caldera scarp which runs parallel to the coastline (scarp marked in red, Fig. 5-8). During  $t_2$  (top right Fig. 5-8) the current began to advance up the lower northern flanks of the cone. During this time lower parts of the current (at least) appear to have been deflected around the northern flanks of the cone. The current then surmounted the entire cone and continued this inundation during  $t_{3-6}$  (bottom right Fig. 5-8). During this time the lineation and imbricated fiamme data on the southern flanks indicate flow to the south. This suggests that the basal parts of the current during deposition are affected by the palaeotopography. However, at the very top of the cone the predominant flow

direction remained towards the SE, straight across the cone, with no deflection from the regional current direction. During  $t_7$ , the final (waning) stages of the current (bottom right, Fig. 5-8), the current reverted to once again not making it over the summit of the cone but rather flowed around its northern flanks and was constrained once again by the caldera scarp.

The phase of the current which overtops the barrier is associated with a lithic breccia which occurs on the south side of the barrier, but is absent on the lee side. This suggests that this phase ( $t_3-t_6$ ) of the current was peak flow and may represent a climactic phase of the eruption.

### 5.3.2. Interaction with transverse ridges

#### Piano & Serra di Ghirlanda

Two sub-parallel, circumferential ridges around the south of the island (Fig. 5-10) comprise the inboard ridge, Piano Ghirlanda, thought to be part of the Cinque Denti caldera (Mahood & Hildreth 1986) and the outermost Serra Di Ghirlanda ridge, which rises almost 100 m above the plain between it and Piano Ghirlanda to 386 m a.s.l and is thought to be the rim of an older caldera, La Vecchia caldera (Mahood & Hildreth 1986). The Green Tuff ignimbrite is cut by the inner Piano Ghirlanda scarp which indicates that some movement along this fault occurred during or after the eruption of the Green Tuff. A line of cones, named the Cuddiolo di Dietro Isola (Fig. 5-10), continues the trend of the outermost ridge where its topographic trace becomes buried underneath the Cuddia Attalora shield volcano which post-dates this scarp (Fig. 5-10).

Unfortunately, agricultural terraces, access problems and lack of exposed sections to the base of the Green Tuff ignimbrite have hindered mapping in this area. The Green Tuff drapes the Serra Ghirlanda scarp and the plains to the stoss and lee side of it. The top of the Green Tuff ignimbrite is constantly underfoot, but basal exposures are limited to a handful as are good exposures of lineations and foliations. Good sections through the Green Tuff ignimbrite occur along the coast (e.g. locations 17, 43, 46 and 47, Fig. 5-10) exposing both the lower contact and upper vitrophyres.

On Serra Ghirlanda, most lineations trend perpendicular to the ridge axis. At the southern end of the ridge, some trend SSE which is down slope in this area, suggesting the influence of the underlying topography (Fig. 5-10).

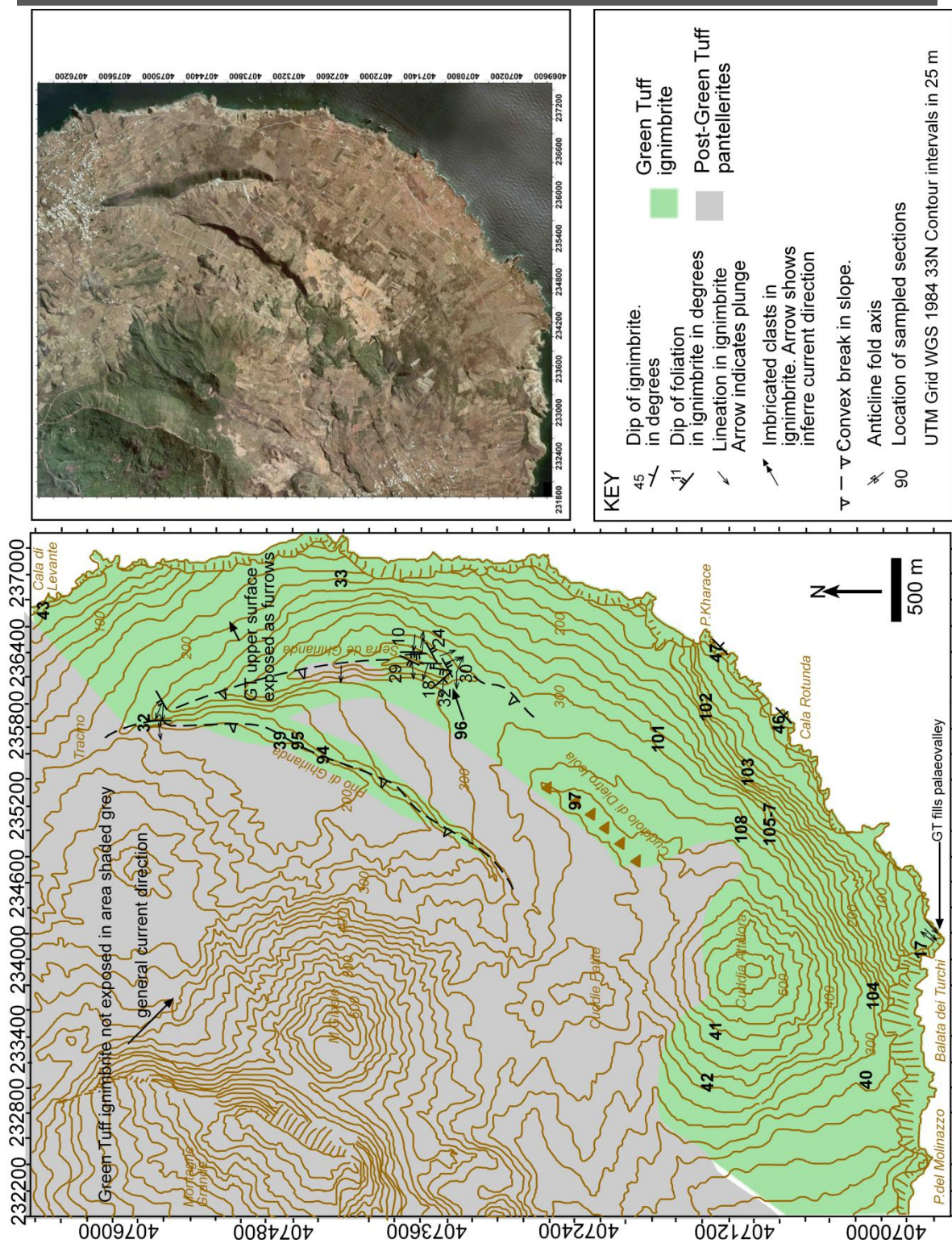


**Fig. 5-10:** Sketch map of the south of the island from the village of Tracino to the Cuddia Attalora shield. Location of individual sections sampled for geochemical study shown. The inner caldera scarp is Piano Ghirlanda and the outer scarp is Serra di Ghirlanda, seen clearly on the aerial photo.

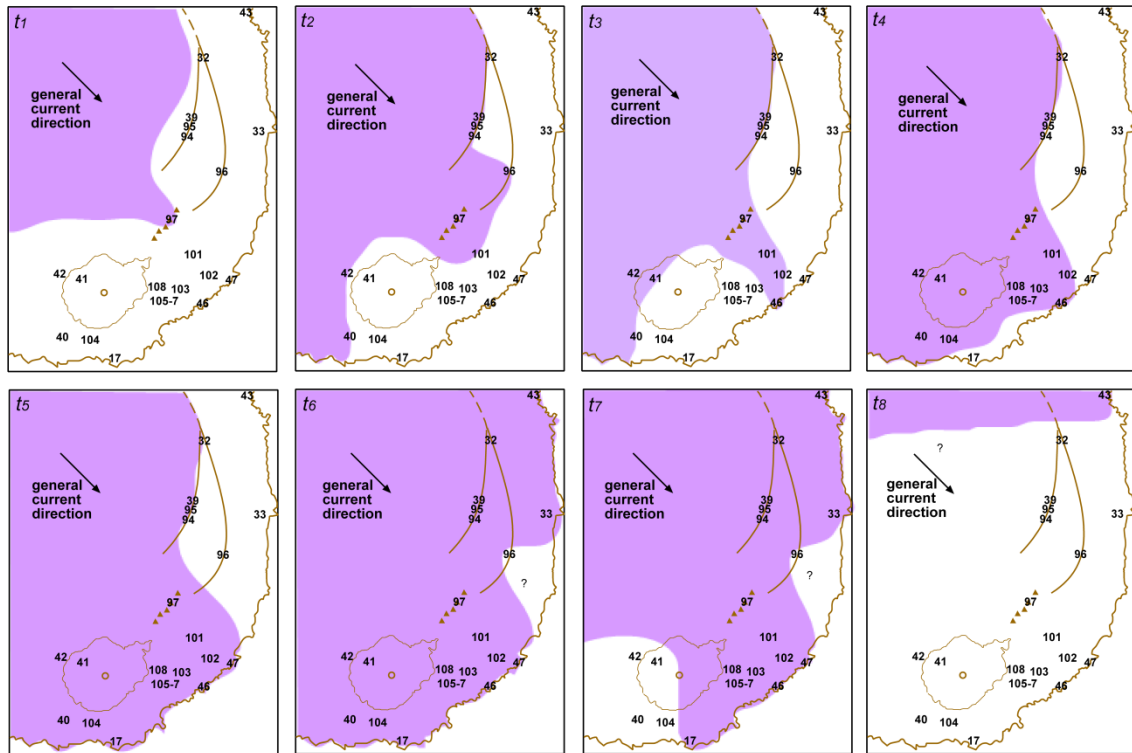


**Fig. 5-11: Footprints of the density current at different time-slices through the evolution of the current from start ( $t_1$ ) to finish ( $t_8$ ) based upon Zr ppm. The two caldera scarps, Cuddia Attalora shield volcano, the line of small cones and the locations sampled for geochemical analysis are marked.**

In Chapter 4, it was noted that advance and retreat of the currents leading edge was strongly affected by the topography in this area. Progradation and retrogradation was pronounced here, combined with lateral shingling. Unfortunately, mapping of the lineations and foliations in this area has not been able to enhance the interpretations which are solely based on the chemical stratigraphy. Geographic footprints are constructed for current inundation of the south of Pantelleria (Fig. 5-11). The first zones of the ignimbrite ( $t_{1-2}$ ) are recorded on the stoss sides of Piano Ghirlanda, Cuddiolo di Dietro Isola and Cuddia Attalora (Fig. 5-11). The next three zones ( $t_{3-5}$ ) show increasingly large footprints. Zone  $t_6$  is the only zone to be recorded over the entire area (Fig. 5-11). The following zone ( $t_7$ ) is recorded across the two scarps and along large sections of the coast, however, it is absent from the western flank of the Cuddia Attalora shield volcano (Fig. 5-11). The final chemical zone ( $t_8$ ) is only recorded in a narrow area at Cala Levante (location 43), and is absent from the scarps and Cuddia Attalora.

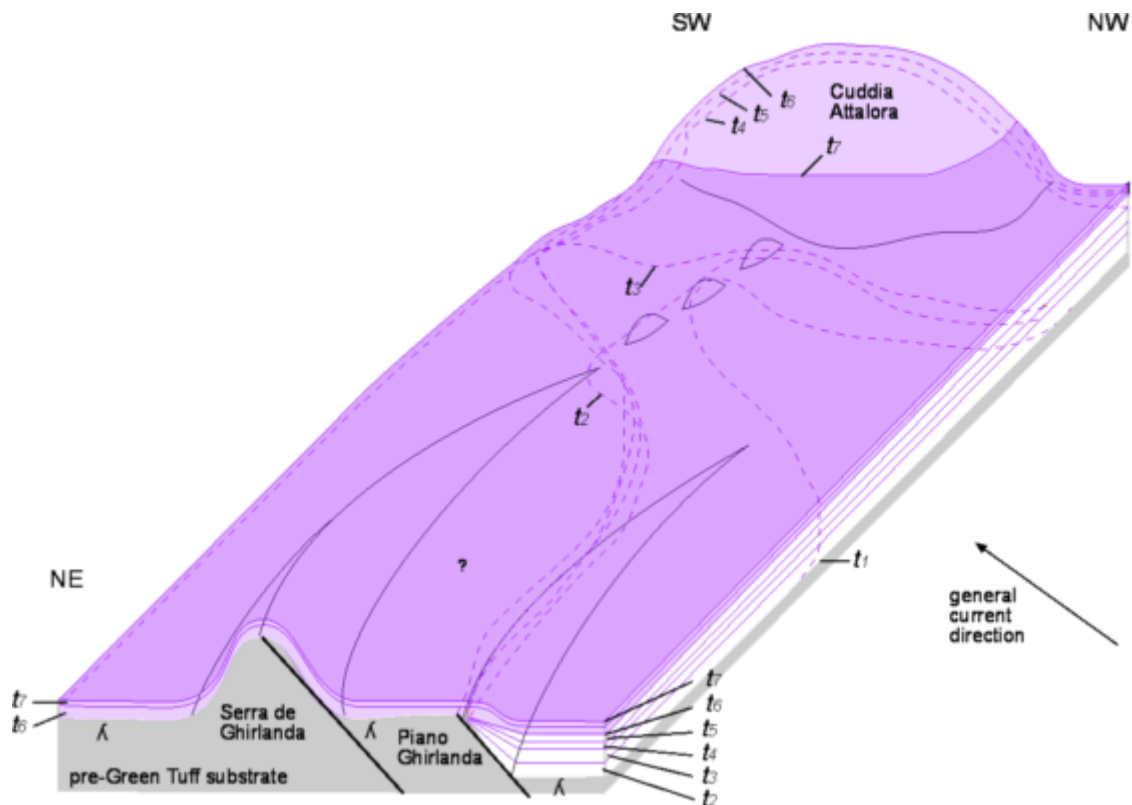


**Fig. 5-12: Schematic block diagram showing change of entrachron stratigraphy over the topographic barriers. Dashed lines indicate limits of buried entrachrons.**

### ***Interpretation***

At the very start of the current ( $t_1$ ) the leading edge was finger like and restricted to a topographic low between the two caldera scarps and Cuddia Attalora shield (Fig. 5-11). Shortly afterwards ( $t_2$ ), this finger broadened and the leading edge of the current encroached on the Piano Ghirlanda scarp (Fig. 5-11). As the current waxed further, its leading edge advanced over the low-lying plain where a narrow finger of current reached the sea. The current also began advance over across the Cuddia Attalora shield volcano (Fig. 5-11). This continued and Cuddia Attalora became entirely inundated, and the leading edge of the current advanced down its lee side towards the sea ( $t_4$ ). The current continued to extend further and entered the sea in all areas south and west of the Serra Ghirlanda scarp (Fig. 5-11), but did not overtop this significant barrier ( $t_5$ ). During the next, climactic phase ( $t_6$ ) the current inundates the entire landscape, overtopping all topographic barriers including Serra Ghirlanda and entering the sea all along this coastline (Fig. 5-11; note no data points exist for area with question marks). The current

then started to wane, and no longer inundated the entire Cuddia Attalora shield volcano (Fig. 5-11), rather it was deflected around its eastern flanks ( $t_7$ ). In its final phase ( $t_8$ ) the current had retreated as a narrow eastward-trending finger (Fig. 5-11).

The current distribution was strongly controlled by topography in this southern half of the island. It was initially blocked by the caldera scarp until the climactic phases of the current ( $t_{6-7}$ ; Fig. 5-12). The current flowed unfettered through a low-lying plain between these scarps, and the Cuddia Attalora shield volcano for most of its duration (Fig. 5-12), with its leading edge advancing towards the sea as the current waxed ( $t_{1-5}$ ), then retreating as the current waned ( $t_{7-8}$ ). The leading edge of the current also progressively inundated Cuddia Attalora after initially being deflected around its flanks and as the current waned again, its leading edge retreated and was deflected around the shield volcano's lower flanks ( $t_7$ ; Fig. 5-12). A gap in the dataset between the two caldera scarps is the result of the Green Tuff ignimbrite not being exposed to its base. It is possible that the current was able to encroach the base of the Serra Ghirlanda scarp, but not over top it prior to  $t_6$  (question mark, Fig. 5-12).

### 5.3.3. Interaction with palaeovalleys

The Green Tuff ignimbrite partially filled palaeovalleys and topographic highs. Where it is thick within a valley, it is here termed 'valley fill'. Where the ignimbrite is thin over an adjacent topographic high, it is here termed a veneer deposit. However, in this work these terms are used as intergradational descriptive terms without any genetic connotations (c.f. Wilson & Walker 1982)

#### Cala Rossa

The coast provides excellent cross-section exposure through palaeovalleys that were partly filled by the Green Tuff ignimbrite. Vertical cliffs make most inaccessible. At Cala Rossa (Fig. 5-2, UTM 32s 0764785, 4081013) a small palaeovalley is exposed (Fig. 5-13). Samples were analysed from the vitrophyric base and top of the draping veneer where the ignimbrite is 1 m thick, and also at the vitrophyric base and top of the valley fill section where the ignimbrite is 6 m thick. A middle sample was obtained above the vitrophyre, 1.1 m above the base of the unit. A vertical cliff prohibited further sample collection.

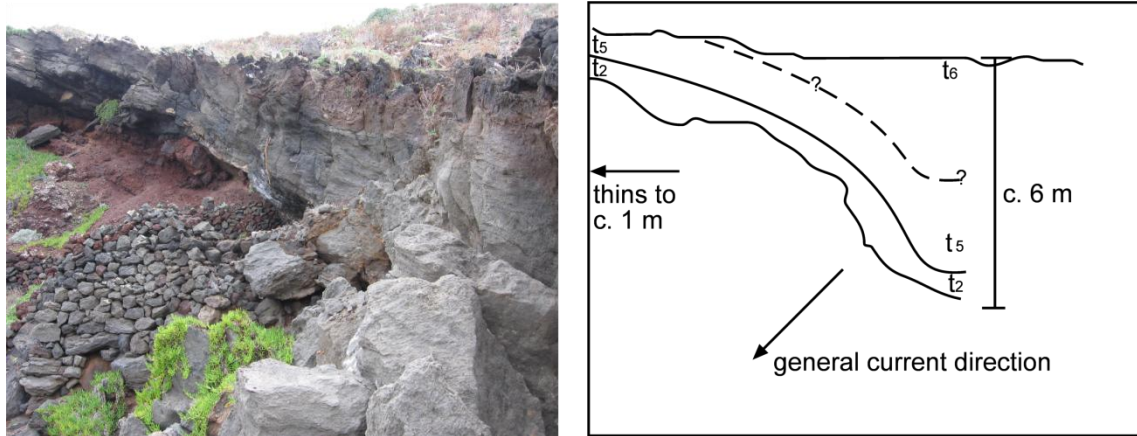


**Fig. 5-13 A:** Photograph of Cala Rossa (UTM 32s, 0764785, 4081013). Note how the Green Tuff is thick in the valley bottom to the right and thins over a small topographic high to the left. **B:** Schematic cross-section of the unit showing entrachron stratigraphy.

The 1 m thick veneer deposit records two chemical-entrachon zones ( $t_2$  and  $t_5$ ) and the 6 m thick valley fill deposit records three ( $t_2$ ,  $t_5$ ,  $t_6$ ). The thickness of zone  $t_2$  is roughly the same across the palaeovalley (Fig. 5-13).

### ***Interpretation***

At this site, the veneer deposit does not represent a stratigraphically condensed sequence equivalent to the entire valley fill. Rather, it was deposited at the same time as at least the lowest metre of the ponded ignimbrite. However, the valley fill continued to aggrade after deposition had ceased on the valley sides. One possibility is that during  $t_6$ , the current in this area was valley confined. Alternatively it was more widespread but overpassed the valley slopes and only deposited in the valley axis.

### **Balata dei Turchi**

A well exposed palaeovalley at Balata dei Turchi (Fig. 5-2, UTM 33s 0234198, 4069857) in the south of the island is partly filled by the Green Tuff ignimbrite. The Green Tuff Formation is up to 15 m in the valley fill and thins to less than a metre on the valley side. Here, both the valley fill and the veneer were emplaced during the same time-slice. This indicates that the current was not valley confined. Moreover, it deposited on interfluvial areas simultaneously with deposition in the valley axis, but the rate of deposition on interfluvial areas was lower.

## 5.4. Discussion

### 5.4.1. Progressive inundation of topographic barriers

A range of topographic barriers have been studied from small, conical barriers to large ridges. At each location, the entrachron stratigraphy shows overlap which indicates that the base of the Green Tuff is diachronous across the barrier. Without analyzing the entrachron stratigraphy, this diachronicity would not be apparent in the field. Schematic cross sections show that the current progressively advanced over each barrier. The initial phases of the current ( $t_{1-2}$ ) are not recorded on the lee sides of the barriers suggesting that the current did not overtop the barriers at this stage. As the current waxed ( $t_3$ ), it was able to rise up the stoss slope (e.g. at Cala del'Alca and Serra Ghirlanda) and overtopped Cuddia di Scauri. During the climactic phases of the current ( $t_{4-6}$ ), the current passed over all the barriers. In the final phases of the current ( $t_{7-8}$ ) the leading edge of the current retreated and no longer overtopped the barriers.

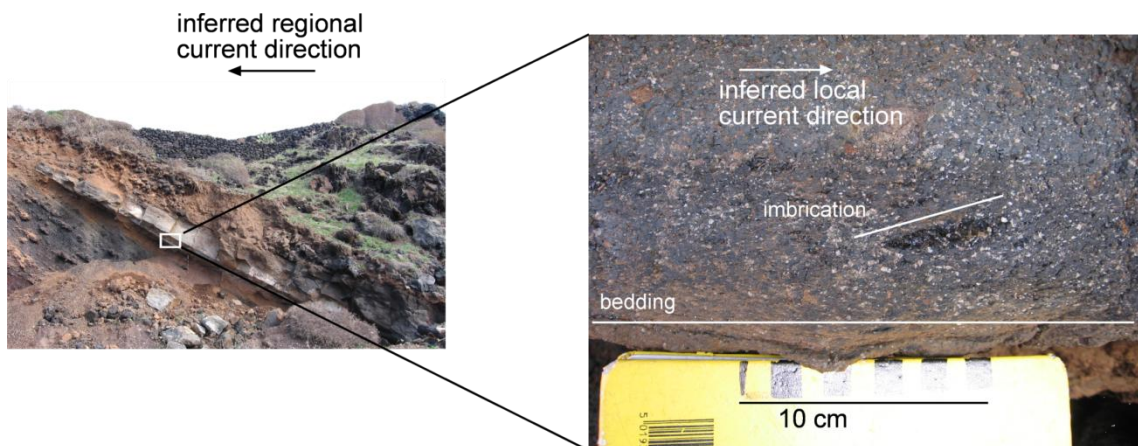


**Fig. 5-14: Imbricated fiamme at Cala dell'Alca which indicate that at the base of the current (at least), flow direction was in the opposite direction to regional current direction.**

### 5.4.2. Blocking, deflection and reflection of the current

The current was blocked in its initial phases by all the topographic barriers studied. At some locations (e.g. Cuddia di Scauri, Cuddia Attalora) the chemical-entrachrons wrap around the lower flanks of the cones. This suggests that the current was deflected around these lower flanks and this is supported by the directional indicators. At Cuddia di Scauri, for example, lineations and imbricated fiamme on the flanks of the cone are

perpendicular to the general current direction. They indicate that the lower parts of the current (at least), locally flowed down slope at right angles to the general transport direction. At Cala Dell'Alca, the imbricated fiamme and lineations on the up-current slope show that at the flow-boundary layer, the depositing current was actually travelling back in the direction of the general current direction (Fig. 5-14). This suggests that the current here was reflected by the cone in its initial stages. An alternative interpretation is that this kinematic indicator records post-depositional, downslope modification (Wolff & Wright 1981). However, the lack of rheomorphic folding or extensional features at this location does not support this.

### **5.4.3. Implications for mass flux**

In Chapter 4 the changing area of the chemical footprints with time was interpreted to record that the sustained density current gradually waxed to a climax and then gradually waned again. It is likely that this waxing and waning was linked to an increase in mass flux as run-out distances achieved by density currents are strongly controlled by the mass flux of discharge (Bursik & Woods 1996). Here, it is shown that topographic barriers were not overtopped in the initial waxing stages of the current. It was only during the peak flow conditions that the current was able to surmount even the smallest topographic barriers. During the waning stages, the current was once again restricted by topography. This suggests that aggradation of deposit in topographic lows was not a significant factor in the current managing to progressively surmount topographic barriers. Rather, it suggests that the main control on the ability of density currents to scale topographic barriers is the mass flux of the current as predicted by analogue and numerical modelling of fully dilute, turbulent currents where the minimum ridge height that affected the flow increased with mass eruption rate (Woods *et al.* 1998). In longer duration currents, however, deposit aggradation may be more significant and play a greater role in modifying the topographic contrasts (e.g. Acatlan ignimbrite, Branney & Kokelaar 1997).

The ability of currents to scale topographic barriers has been related to flow thickness by model results of uniform, turbulent turbidity currents (Muck & Underwood 1990). Thick currents can scale barriers where thin currents would be blocked or deflected. For example, the Fisher Tuff which is found down-current of significant barriers has been interpreted as the result from an incredibly thick (800-1100 m) fully dilute current with a dense undercurrent; the dilute current passed over the barriers and the dense portion

was blocked (Gardner *et al.* 2007). In contrast, the Green Tuff density current showed the same behaviour at both small (c. 15 m barriers) and large (> 100 m) barriers. During early phases of the current it was blocked by these barriers, but was subsequently able to surmount them. This would suggest that the early stage of the current had to be less than 15 m thick, but rapidly increased in thickness to an excess of 100 m. It is possible that the ability of this current to scale topographic barriers is controlled by the flow thickness, if such thickening of the current was possible. However, this cannot be resolved from field studies and further modelling would be required.

It is possible that the aggradation of a deposit in front of a barrier modified the topography such that later phases of the flow were able to surmount the barrier (Valentine *et al.* 1992). However, many of the barriers do not show significantly thick deposits (up to 5 m thick) on their up-current side so this effect is considered to be negligible.

#### **5.4.4. Formation of a caldera during the Green Tuff eruption**

In large explosive eruptions, caldera collapse is often associated with peaks in mass flux or discharge rate. Previous authors have suggested that the Green Tuff eruption was associated with a caldera forming event (Civetta *et al.* 1988; Cornette *et al.* 1983; Mahood & Hildreth 1986; Orsi *et al.* 1991). Could the increase in eruption vigour suggested by increased run-out distances and progressive inundation of topographic barriers relate to a caldera forming phase of the eruption?

#### **Relationship of the Green Tuff ignimbrite with proposed caldera walls**

Most authors have inferred that the Green Tuff eruption involved caldera collapse but the details of such inferred caldera formation have been debated. Two alternative subsidence structures are proposed (Fig. 5-15); the Cinque Denti caldera (Mahood & Hildreth 1986), and the Monastero caldera (Civetta *et al.* 1988; Orsi *et al.* 1991).

Authors concur that the Monastero fault and the Piano Ghirlanda fault formed during the Green Tuff eruption, as on both of these scarps the Green Tuff ignimbrite is cut by the fault scarp. This indicates fault movement after emplacement of the Green Tuff formation. However, the north and eastern rims of possible calderas are unclear, and are further considered here. On the Khattibucale scarp (inset; Fig. 5-16; Fig. 5-17; Fig. 5-18), the Zinedi scarp (inset; Fig. 5-16; Fig. 5-20; Fig. 5-21) and the Cinque Denti

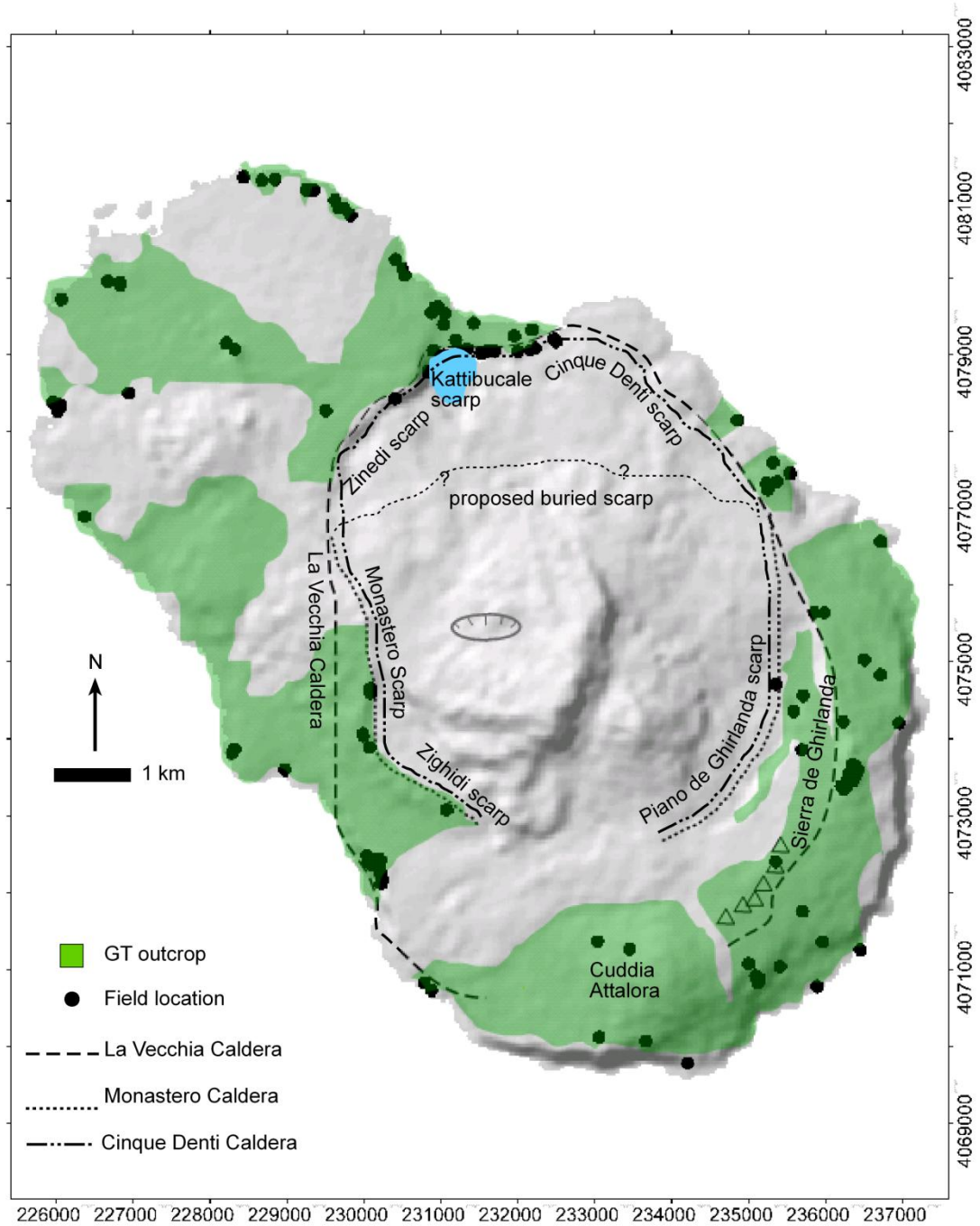


**Fig. 5-15:** Map showing location of proposed calderas from previous studies. La Vecchia caldera, age 106-175 ka (Mahood & Hildreth, 1986) is undisputed. Two different calderas are proposed for the c. 45 ka Green Tuff ignimbrite eruption: The Monastero caldera (Civetta *et al.* 1998; Orsi *et al.* 1991) which has buried, unidentified northern scarps and the Cinque Denti caldera (Mahood & Hildreth, 1986) which shares its northern scarps with the La Vecchia caldera. Local scarp names discussed in text also shown.

scarp (inset; Fig. 5-16; Fig. 5-19), lowermost parts of the Green Tuff ignimbrite appear to have been cut by the faults, but its upper parts (which outside the scarp conformably lie on the lower parts) drape the truncated horizons and dip into the caldera (Fig. 5-18; Fig. 5-21). Mahood and Hildreth (1986) have interpreted this relationship to indicate that these scarps formed during the eruption of the Green Tuff. It is assumed (as no other supporting evidence is given) that mantling of the scarp is used by the other authors (Civetta *et al.* 1988; Cornette *et al.* 1983; Orsi *et al.* 1991) to indicate that these three northern and eastern scarps pre-date the Green Tuff. An alternative scarp relating to the Green Tuff eruption is suggested to lie inside this older structure, now covered by younger lavas (Civetta *et al.* 1988; Cornette *et al.* 1983; Orsi *et al.* 1991).

New mapping at these scarps (Fig. 5-16) has revealed that the Green Tuff mantles the entire exposed scarps around Bagno dell'Acqua down to the present day exposure on the Zinedi scarp (Fig. 5-20) the Kattibucale and Cinque Denti scarps (Fig. 5-17). A roadcut exposes the Green Tuff ignimbrite in cross-section at the apex of the Kattibucale topographic rim (location 1; Fig. 5-16 and Fig. 5-17). A complicated relationship between the Green Tuff and the Kattibucale scarp exists (Fig. 5-18). The lower, unwelded horizons at location 1 appear to lie conformably with the underlying rim top. They have not been deposited on the scarp. Two metres above the base, bedding becomes dune-like and the ignimbrite becomes more welded. Above this, the rheomorphic horizon appears to cut through underlying horizons to lie unconformably over them directly on the scarp, progressively over-stepping older units (not shown). The sedimentary structures, such as imbricated fiamme, show northerly palaeocurrent direction (away from the caldera) but the rheomorphic folding shows minor movement southwards, into the caldera (Fig. 5-18).

Two scenarios are plausible to explain this exposure. The first is that the caldera scarp did not exist until the stratigraphic horizon with the dune bedding was deposited and certainly not until the draping part of the ignimbrite was deposited (chemical-entrachron zone  $t_2$ ). The second scenario is that the scarp existed prior to the Green Tuff eruption, and the non-welded lowermost units of the Green Tuff ignimbrite either bypassed the c. 60° slope, were stripped off by succeeding parts of the current, or were reworked down the slope. The densely welded units are the first to be deposited on the scarp because this was the first time that arriving pyroclasts were 'sticky' enough to agglutinate

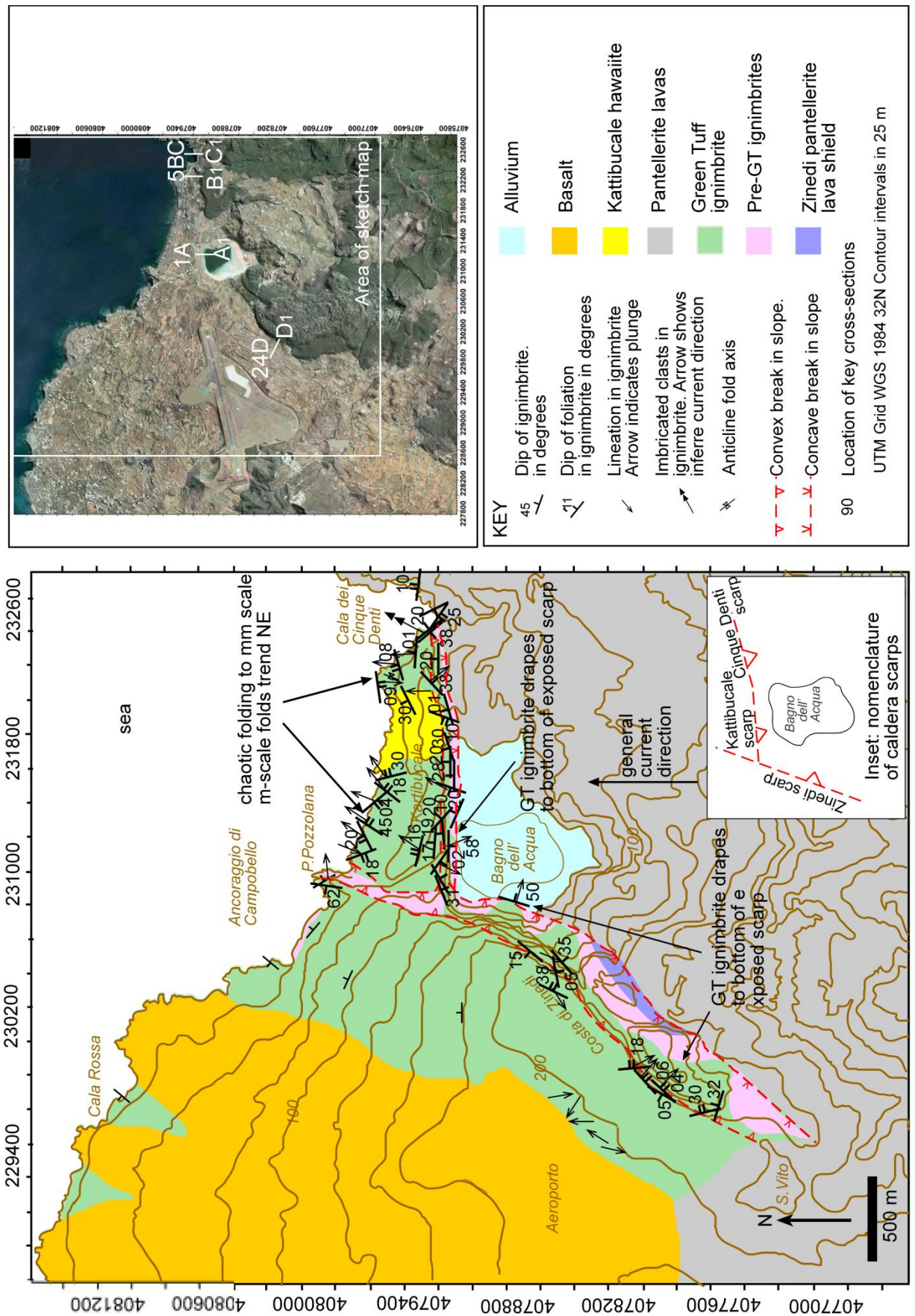
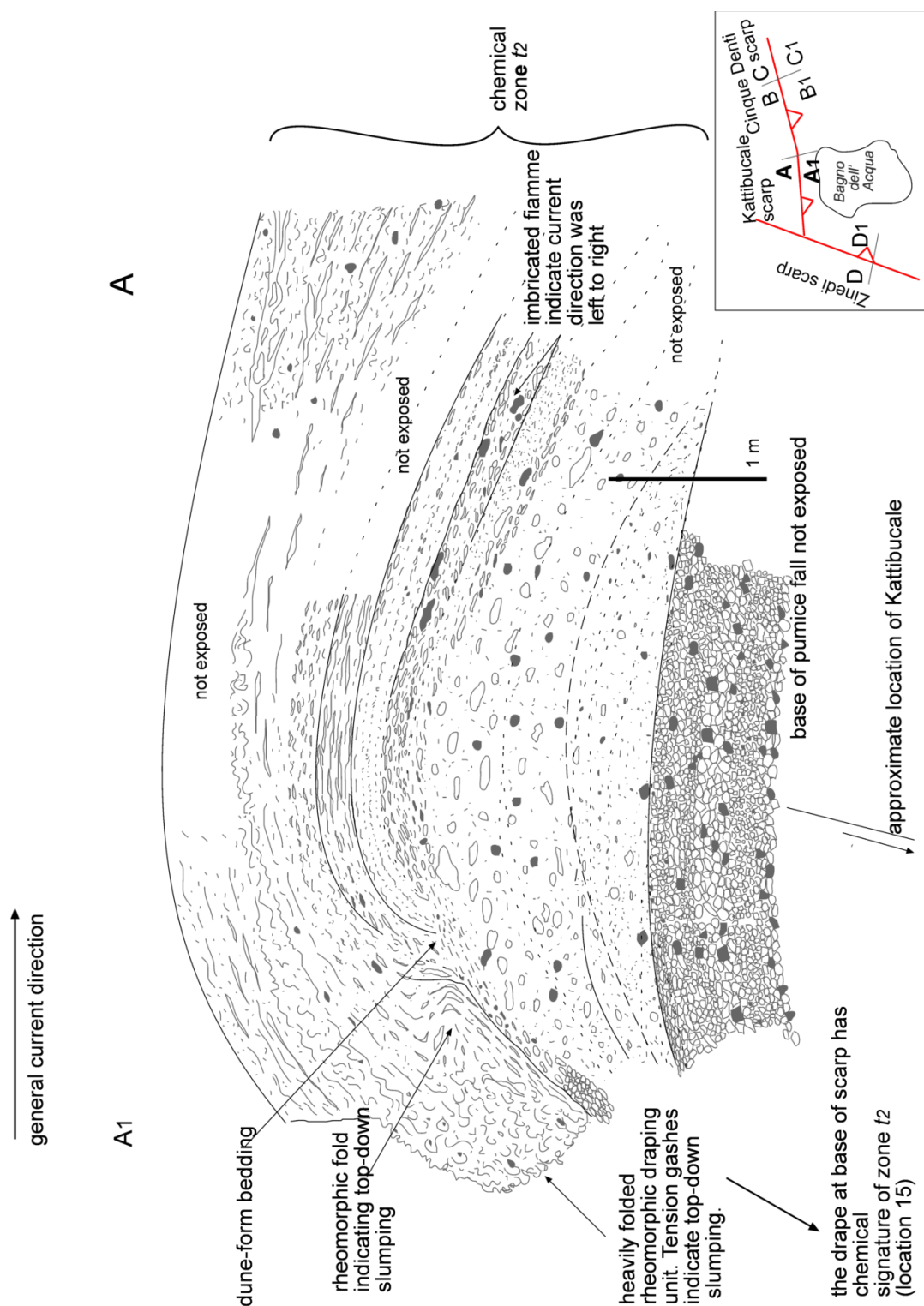


Fig. 5-16: Sketch map of the north of the island around Bagno Dell'Acqua. Inset details scarp nomenclature. Aerial photo shows location of cross-sections at locations 1, 5 and 24 along the Kattibucale, Cinque Denti and Zinedi scarps respectively.



**Fig. 5-17: View of the Kattibucale scarp and Cinque Denti scarp looking north. The Green Tuff ignimbrite outcrops along the top of these scarps and to the base at some locations. Location of cross-section sketches (Fig. 5-18 and Fig. 5-19) indicated. Green Tuff density current flowed into page.**



**Fig. 5-18:** Field sketch of longitudinal cross-section through the Green Tuff ignimbrite (top not shown) at the summit of Katibucale scarp (location 1 on Fig. 5-16 and Fig. 5-17; UTM 32s, 0766375, 4079104). Imbricated fiamme indicate paleocurrent direction was left to right, northwards, away from the caldera. The scarp is transverse to this. Basal, non-welded parts of the ignimbrite shows diffuse bedding and overlies the basal pumice fall deposit. Outboard of the scarp (right; A), the lower part of the Green Tuff ignimbrite is bedded parallel to the underlying slope. At approximately 2 m above the base, the rheomorphic facies drapes the stoss (left) side of the caldera scarp. This horizon traces to the base of the scarp, 15 m below at this location (A1) and up to 50 m at others, and is chemical zone  $t_2$ . Rheomorphic folding at the top break of slope suggests minor rheomorphic downslope slumping. This indicates that up to 50 m of the scarp was extant at the time of early ( $t_2$ ) stages of the Green Tuff ignimbrite.

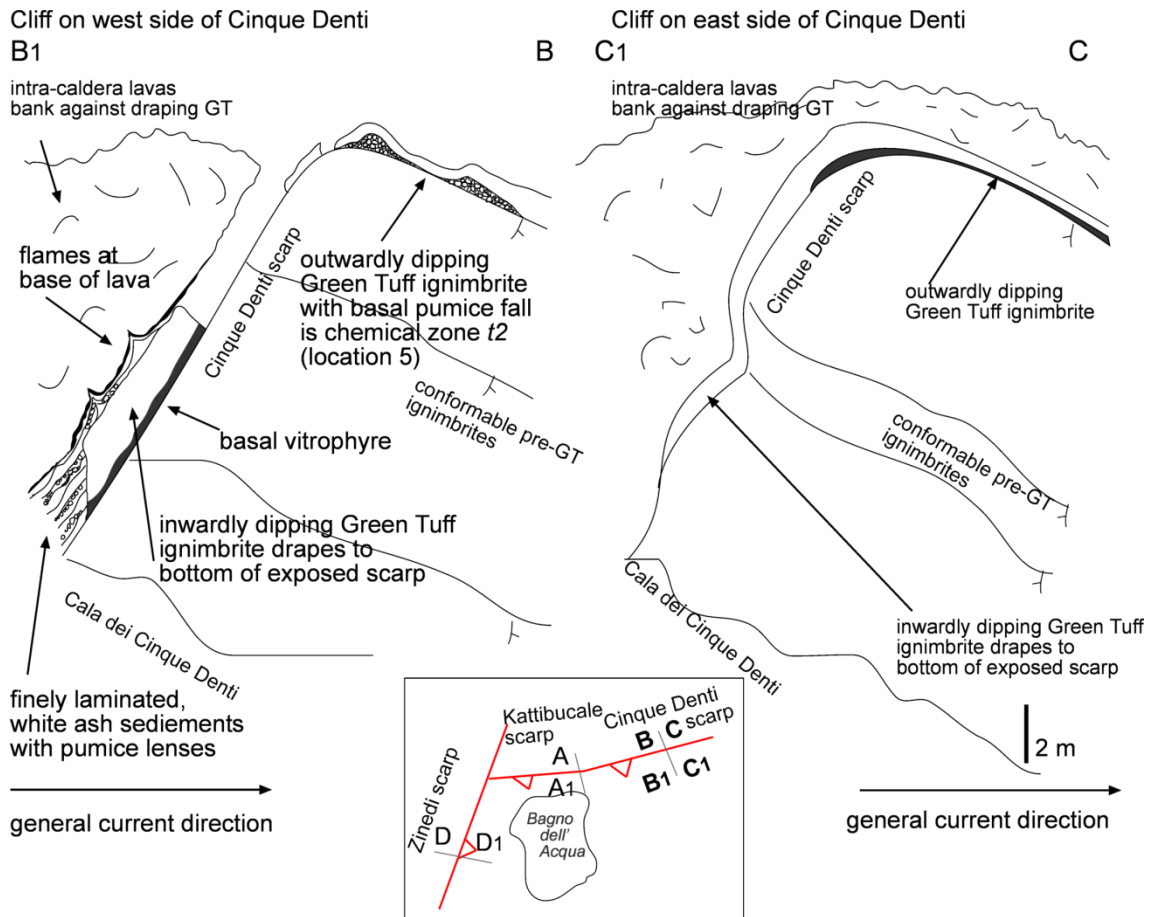


**Fig. 5-19:** Sketch of the Cinque Denti scarp viewed west (sketch of east side of Cala Cinque Denti has been reflected) at location 5 (Fig. 5-16 and Fig. 5-17; UTM 33s, 0232503, 4079244). At this location the sea has eroded through the caldera rim, exposing post-Green Tuff Formation intra-caldera lavas which preserve the palaeoslope (dipping to the left). The Green Tuff ignimbrite drapes both flanks of the caldera scarp to sea level (lee side) and c. 20 m to the base of the exposed scarp (stoss side) showing that at least 20 m of the caldera scarp was extant at the time of the Green Tuff ignimbrite.

against the slope. At location 15 (Fig. 5-16 and Fig. 5-17), the draping unit which drapes to the base of the exposed scarp (c. 20 m) belongs to time-slice  $t_2$  which suggests that if the caldera collapse occurred during the eruption of the Green Tuff, it must have occurred within the first two phases of the eruption.

Draping relationships are also seen on the Cinque Denti scarp (Fig. 5-19) and on the Zinedi scarp (Fig. 5-20). At Cinque Denti, the entire Green Tuff ignimbrite traces to the base of the exposed scarp (c. 20 m). The Green Tuff ignimbrite here is of zone  $t_2$ . On the Zinedi scarp, the lower horizons ( $t_2$ ) of the Green Tuff ignimbrite and its basal pumice fall are flat-lying, conformable with the unit below (Fig. 5-21). The upper, rheomorphic horizon ( $t_2$ ) drapes over these lower units to lie on progressively older ignimbrites (Fig. 5-21) and is found at the base of this c.200 m scarp at location 23 (Fig. 5-20). Both location 23 and 24 have the chemical signature of time-slice  $t_2$ . Again, this

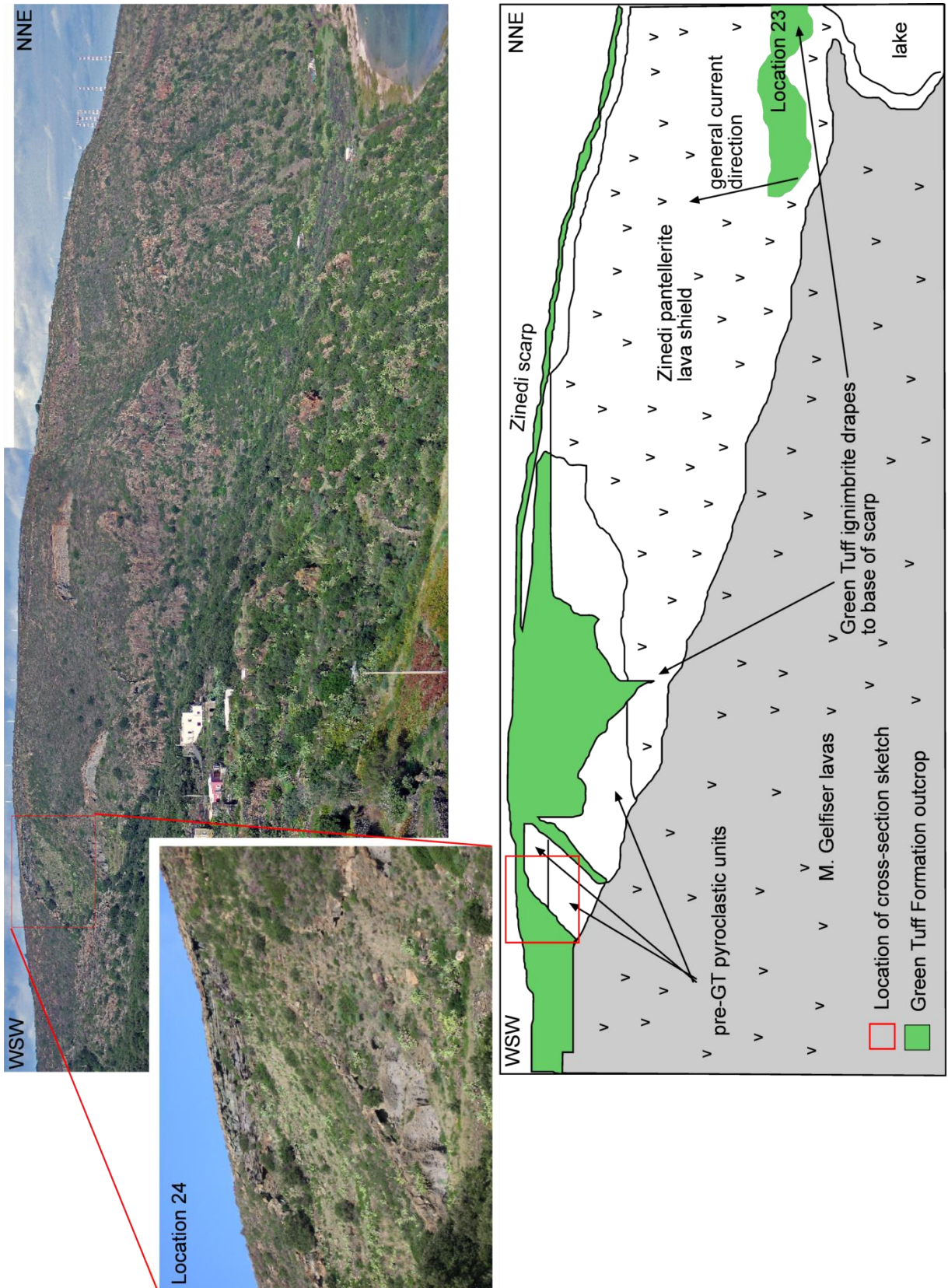


**Fig. 5-20:** View of the Zinedi scarp looking NNW. The Green Tuff ignimbrite outcrops along the top of this scarp and to the base at some locations. Location of cross-section sketch (Fig. 5-21) indicated. Green Tuff density current flowed to the NW.

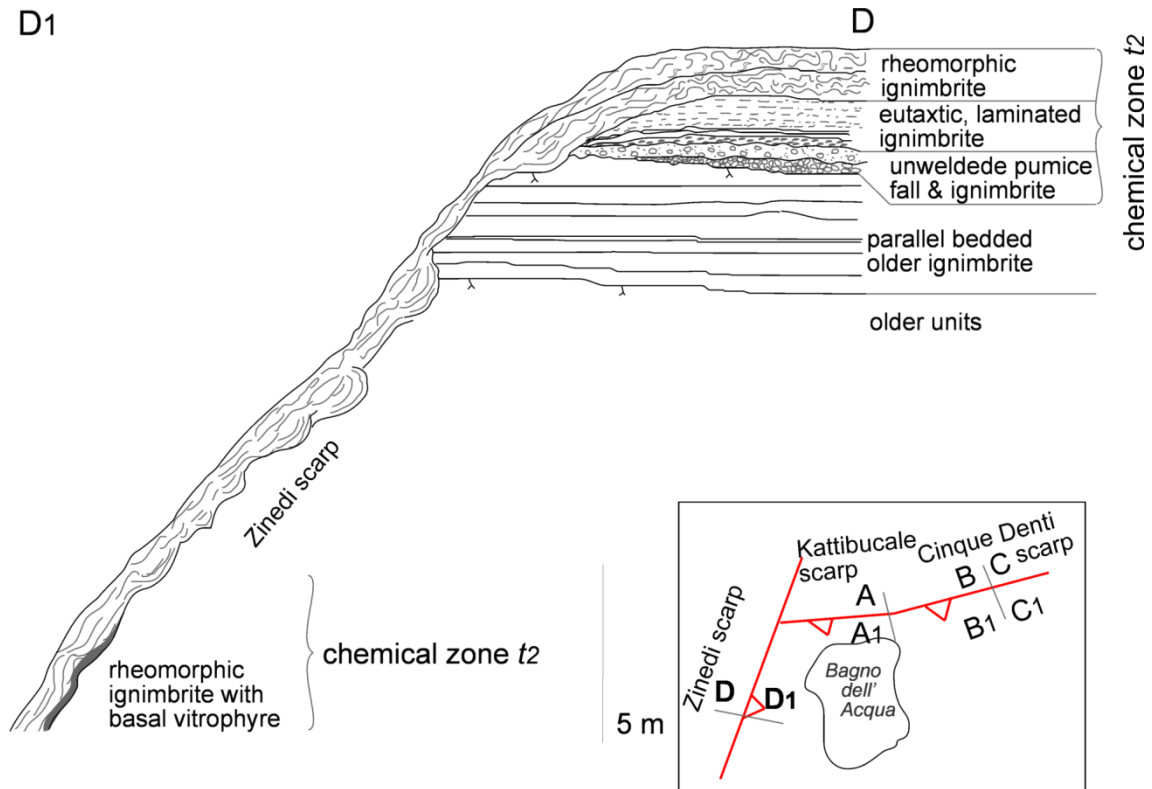


**Fig. 5-21:** Sketch of the Zinedi scarp viewed SW at location 24 (Fig. 5-16 and Fig. 5-20; UTM 32s, 0765752, 4078497). The lower half of the Green Tuff ignimbrite lies conformably with the underlying units (D). The upper, rheomorphic unit of the Green Tuff drapes down c.20 m at this location (D1), and to the base of the c. 200 m high scarp to the lake at location 23 (Fig. 5-20), which is in chemical zone  $t_2$ . This indicates that at least 200 m of this scarp was extant at the time of early ( $t_2$ ) stages of the Green Tuff ignimbrite.

implies that either the scarp was formed very early in the Green Tuff eruption (i.e. halfway through  $t_1$  or  $t_2$ ), or that the scarp already existed and that the loose and poorly welded lowermost parts of zone  $t_2$  were not able to be deposited upon the steep slope (c.  $60^\circ$ ). Given that the eruption during time-slices  $t_1$  and  $t_2$  appears to have been weak and sluggish, it seems unlikely that the caldera would have collapsed during these stages.

### **Does the lithic breccia represent a caldera-forming phase?**

Lithic breccias are most developed along the Monastero caldera scarp, but they do not occur in the same time-slice at all locations. A lithic-breccia commonly occurs in zone  $t_6$  just as at the type locality (location 44, Chapter 2) however, lithic breccias also occur within zones  $t_3$  to  $t_7$ . Therefore these lithic breccias do not provide a compelling evidence for a single caldera-forming phase during the Green Tuff eruption. In particular, the lithic breccia is not found in the first phases of the eruption ( $t_1$  or  $t_2$ ),

where one might be expected if a caldera-forming event caused the lower horizons (zone  $t_2$ ) on the Kattibucale and Zinedi scarps to be faulted.

Thus, the present study of the Green Tuff ignimbrite has yielded no compelling evidence of a caldera collapse episode, although a caldera collapse cannot be discounted. Along the Monastero scarp, the Green Tuff is clearly faulted and it does not drape this scarp. The best developed breccias also occur in this sector of the island. Therefore, it is possible that there was fault displacement along this scarp during the Green Tuff eruption. Faulting along the Zinedi, Kattibucale and Cinque Denti scarps during the eruption is less certain. The draping of the Green Tuff ignimbrite to the exposed base of these scarps suggests that they existed before the eruption of the Green Tuff. Reactivation of these faults at depths now buried however, cannot be discounted nor can the possibility of buried scarps inboard of these faults. If there was a caldera collapse during the Green Tuff eruption the diachronous nature of the lithic breccias suggests that movement along the faults may not have occurred during a distinct caldera-collapse phase. Instead, any collapse may have been progressive and incremental during the eruption. Far better developed, thick, coarse-grained lithic breccias are present in the pre-Green Tuff ignimbrites (Chapter 6) and probably record caldera collapse eruptions.

#### **5.4.5. Assumptions and potential problems**

The inference of diachronous emplacement over a topographic barrier and progressive inundation of barriers has relied on detailed mapping and geochemical sampling. Most useful were samples collected from the base of the Green Tuff ignimbrite where a contact with the underlying unit was clearly seen. Often, detailed sampling through sections particularly to the top of the Green Tuff ignimbrite was successful. But, the Green Tuff ignimbrite is not often covered by younger units so its top is commonly not preserved. Where possible, the upper vitrophyre was collected and interpreted to represent the final phase of the current. However, at several locations this upper vitrophyre was not preserved. Therefore interpretations made on the final stages of the sustained density current are more limited and subject to error. Similarly, very close (mm-cm) spaced sampling at all locations was not possible, and it is possible that some very thin compositional zones were overlooked.

## 5.5. Conclusions

This study, Chapter 5, has revealed that:

- The initial leading edge of the current did not surmount the topographic obstacles on initial impingement.
- Topographic barriers were progressively inundated during waxing phases of the current.
- Even small (c. 15 m high) barriers were sufficient to block, partly block or reflect the current.
- The initial stages of current,  $t_1$  and  $t_2$ , were likely to have been thin and low-velocity.
- The depositing current was deflected by barriers around the lower flanks of conical barriers and reflected back towards the general current direction.
- Thin ignimbrite on valley sides do not entirely represent a stratigraphically condensed equivalent of the valley fill: in some cases the initial encroachment of the current draped both valleys and interfluves followed by constrained deposit only in the valley axes-this indicates increasing channelization of an initially sheet-like current into topographically controlled thalwegs.
- Mass flux strongly controlled the currents ability to scale topographic barriers
- No support is documented for caldera collapse during the Green Tuff eruption. Any caldera collapse may have been progressive and incremental during the sustained eruption rather than during a distinct climactic phase.

---

# 6. Stratigraphy of the pre-Green Tuff welded ignimbrites of NE Pantelleria

---

## 6.1. Abstract

A revised stratigraphy for the welded ignimbrites of north-eastern Pantelleria is presented. The succession in the north eastern part of the island includes four extensive ignimbrite sheets with associated pumice fall deposits and lithic breccias. Predominantly trachyte in composition, the ignimbrites share similar characteristics such as pervasive welding, eutaxitic fabrics, rheomorphism, sheet and columnar jointing, and a dominantly feldspar phenocryst population. Compositional zoning within each ignimbrite makes correlations based on geochemistry difficult, so correlations presented here are primarily field based. Exposure is restricted to sea cliffs and caldera walls, hindering lateral tracing of individual units. Palaeosoils are used to demarcate 3 main pre-Green Tuff Formation eruption-units. This represents a reduction in the number of ignimbrite eruptions relative to previous studies but the eruptions were larger and more widespread. Identification of previously unrecognised co-ignimbrite breccias in the succession indicates that these large eruptions were likely to have been caldera-forming, and devastating on an island scale. We envisage that the caldera collapse history of the volcano is more complex than previously thought and involved a history of at least 4, overlapping calderas which cannot be physically distinguished.

## 6.2. Introduction

The volcanic activity predating and including the Green Tuff eruption is dominated by a series of welded ignimbrites, with inter-dispersed pumice fall deposits, basaltic lavas, and agglutinate shields. The welded ignimbrites have had a history of debate and reinterpretation in the literature. This study revisits the pre-Green Tuff Formation welded ignimbrite deposits and presents new field and geochemical data, focusing on the NE of the island where coastal exposures allows stratigraphic relations to be established. Preliminary results have led to a reduction in the number of units, indicating fewer but larger caldera-forming eruptions than previously thought.

### 6.2.1. Previous Work

Early descriptions of the pre-Green Tuff stratigraphy interpreted the intensely welded deposits as either lavas (Washington 1913-1914) or welded ignimbrites (Borsi *et al.* 1963; Korringa 1971; Villari 1970). However, these studies did not attempt to resolve a stratigraphy. Wright (1980) proposed the first stratigraphic scheme for the welded tuffs and interpreted them as welded fall deposits (Wolff & Wright 1981b, a). Evidence for this interpretation included grain size analysis (poorly sorted fall deposit), mantle bedding and deposition on steep slopes, and the presence of internal stratification (Wright 1980). However, it was being recognised at the time that these features could also occur in ignimbrites (Fisher & Schmincke 1984; Walker 1983) and despite working on similar features in the rheomorphic ignimbrites on Gran Canaria (Wolff & Wright 1981b), the authors did not recognise features that indicate deposition from pyroclastic density currents in the Pantescan ignimbrites, including imbricated fiamme which are particularly well developed in the Green Tuff ignimbrite. However, the stratigraphy produced by Wright (1980) was the first attempt at resolving the pre-Green Tuff pyroclastic stratigraphy, and provided a foundation for later workers to build on. Seven correlatable welded tuffs were recognised, with two pumice fall deposits. A further eight welded tuffs were identified, but not correlated beyond a single location. Later work reassessed the units and the evidence put forth by Wright (1980), and reinterpreted the deposits to be welded ignimbrites (Mahood & Hildreth 1986; Orsi *et al.* 1991). In light of this, Mahood & Hildreth (1986) established a new stratigraphy of the welded ignimbrites and inter-tuff deposits. Generalised vertical sections of the stratigraphy were not produced by either Wright (1980) or Mahood & Hildreth (1986) and are therefore not presented here.

#### Deposition from flow versus fall

The welded lapilli-tuff units are interpreted here as ignimbrites based upon the following field criteria: (1) very poor sorting with matrix-support (Fig. 6-1); (2) imbricated clasts, which are not just restricted to basal layers but prevalent throughout the deposits, including non-rheomorphic parts; (3) localised low-angle diffuse cross-bedding; (4) erosional features; (5) lateral changes in chemical composition and lithic populations; and (6) marked lateral and thickness variations. This has allowed us to correlate units previously interpreted as distinct units based on lateral variations.

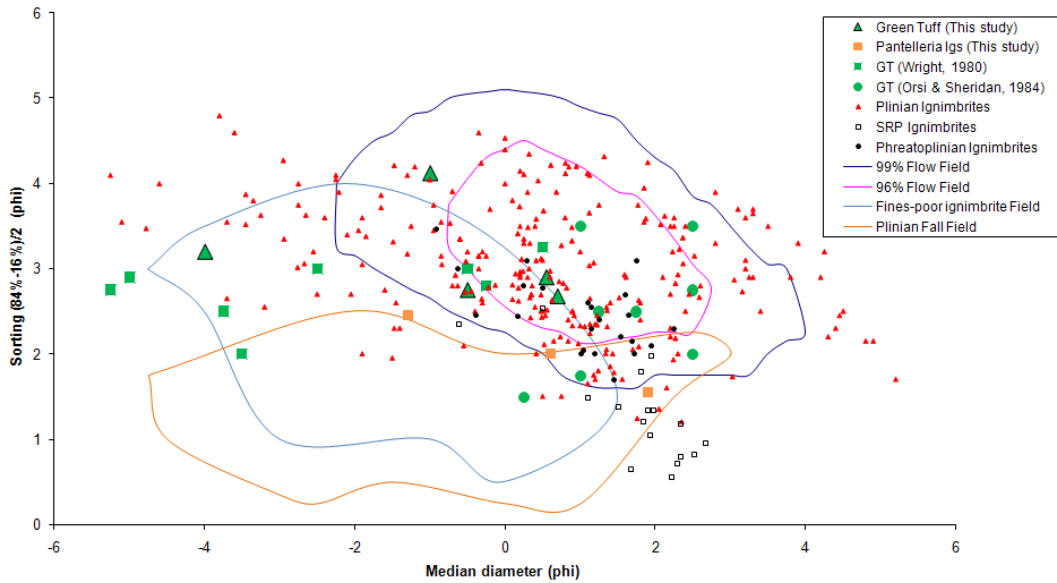


**Fig. 6-1: Granulometry of lapilli-tuff facies from Eruption-units 1, 2 and 3 (orange squares) compared to published data and the Green Tuff Formation. Size parameter plot of median diameter ( $\Phi$ ) vs. sorting ( $\sigma$ ) (parameters from Inman, 1952). Fields after Walker, (1971). Plinian and Snake River Plain (SRP) type volcanism data courtesy of B. Ellis (pers. comm.). The samples fall in the overlap area for pyroclastic density current, fines-poor current and plinian fall. They match more closely to the ‘flow fields’ suggesting that these samples are from a pyroclastic density current.**

### 6.3. Identification of three Eruption-units

#### 6.3.1. Field data

Mantling of the island by the Green Tuff Formation during the 50 ka eruption has covered the older stratigraphy leaving outcrops only in caldera scarps and sea cliffs. This hinders extensive correlations of the older units. This work is based on field work in the north eastern sector of the island and does not consider the Green Tuff further, as this is discussed in more detail in Chapters 2 through 5. Each unit was logged and laterally traced around the NE coast and in caldera scarp exposures along the Zinedi, Kattibucale and Cinque Denti scarp (Fig. 6-2). Key sections at Bagno dell Acqua, Bue Marino, and Punta Della Guardia (Fig. 6-2) were identified, logged and sampled in detail (Fig. 6-3). Three soil-bound eruption-units have been identified and are referred to as Eruption-units 1, 2 and 3; previous names for these units have not been retained.

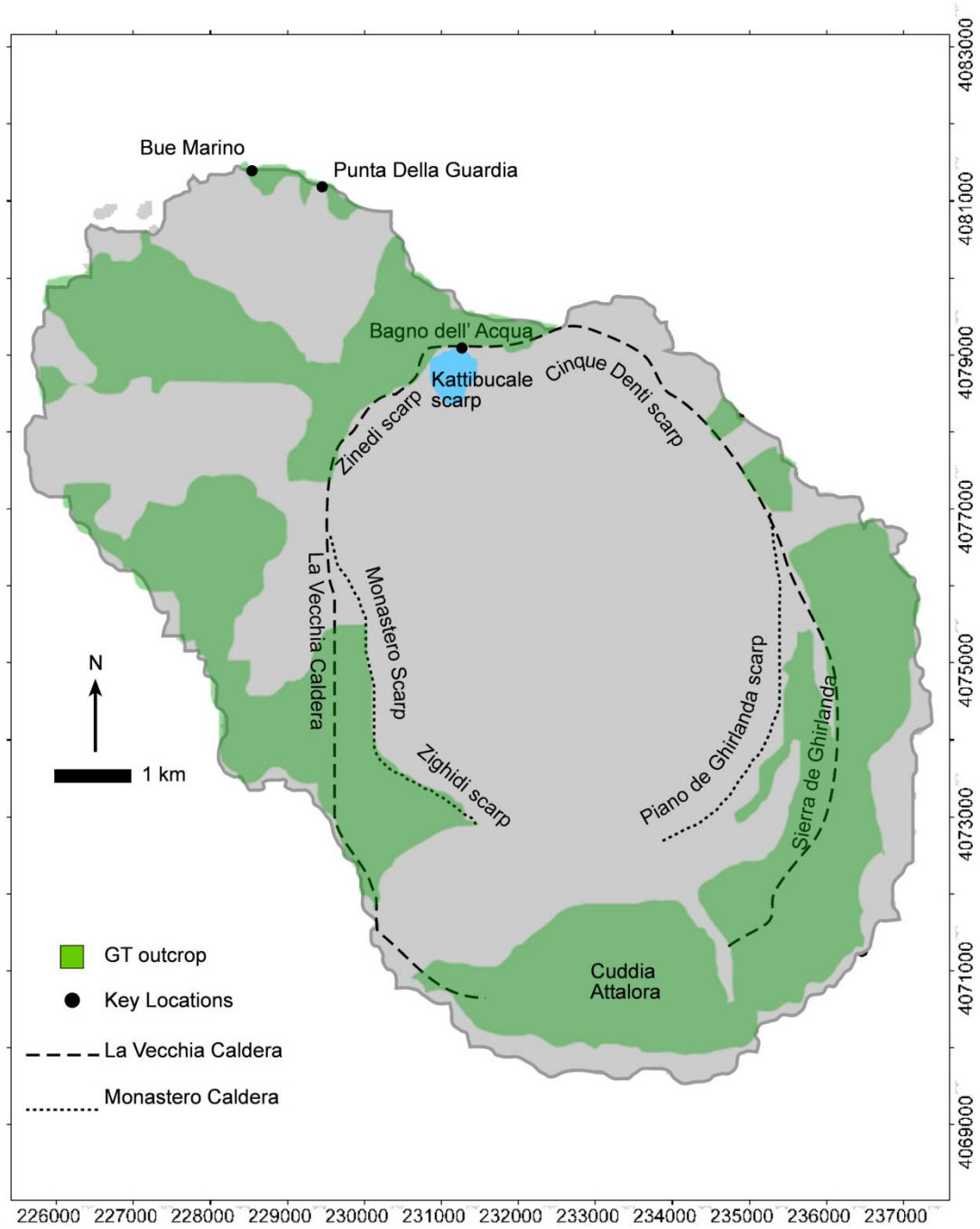


**Fig. 6-2: Location map of Pantelleria, Italy, showing three key locations: Bue Marino, Bagno Dell'Acqua and Punta Della Guardia. Coordinates are UTM zone 32N.**

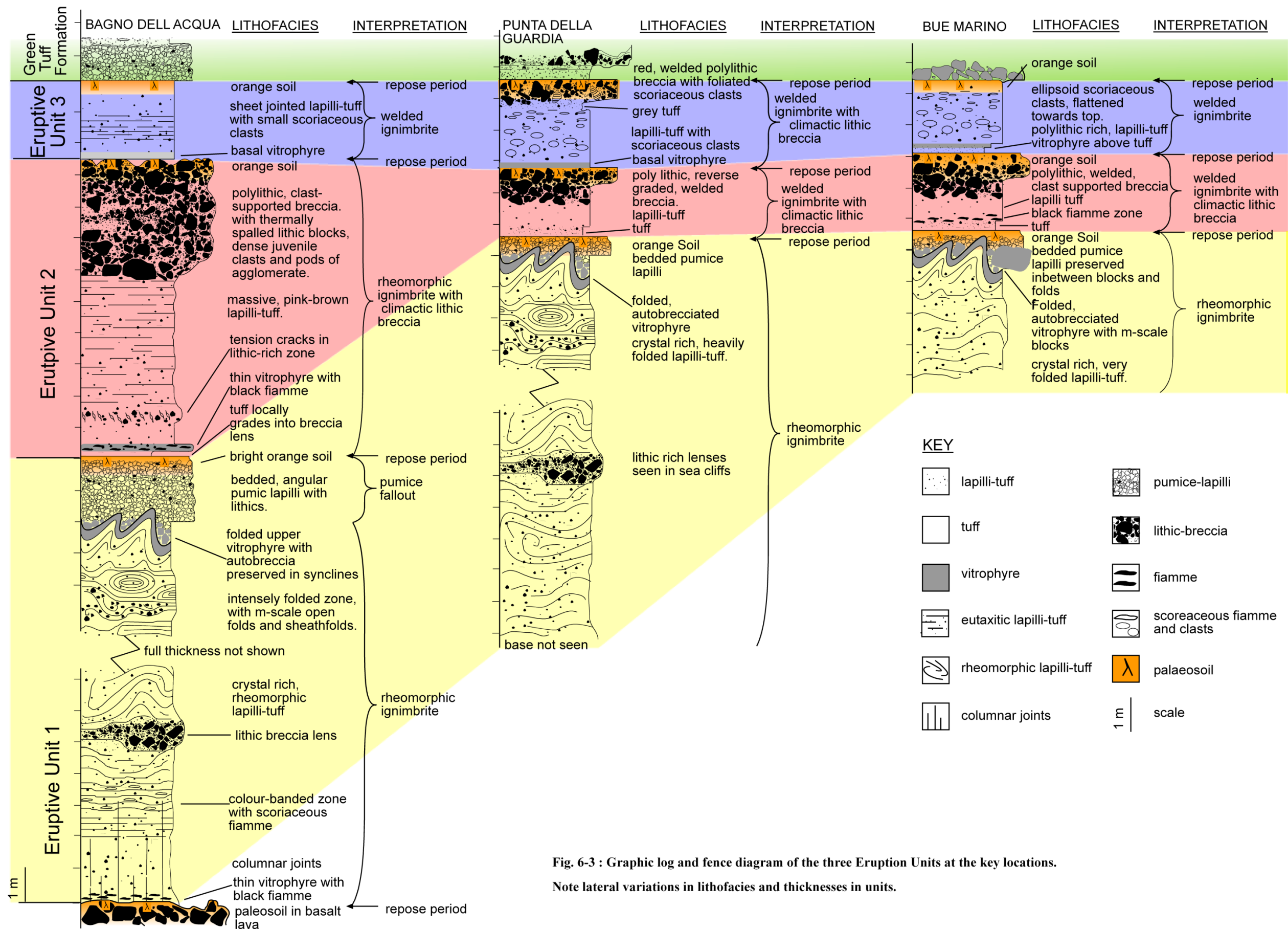


Fig. 6-3 : Graphic log and fence diagram of the three Eruption Units at the key locations.

Note lateral variations in lithofacies and thicknesses in units.

## **Eruption-unit 1**

### ***Description***

Eruption-unit 1 is best exposed in the Kattibucale caldera scarp at Bagno Del Acqua (Fig. 6-3) where it comprises a 25 m thick, trachytic eutaxitic lapilli-tuff overlain by a 2 m thick layer of parallel-bedded pumice lapilli. Both upper and basal contacts are exposed. The lapilli-tuff sits on top of a palaeosoil and has a poorly developed vitrophyre at its base, with small black, glassy fiamme. This passes up into lithoidal massive lapilli-tuff, characterized by its pink-brown colour, abundant large feldspar crystals (Fig.6-4E, up to 1 cm in size) and intense rheomorphic folding.

At Bagno dell Acqua, the lowermost 2 m has thick columnar joints (Fig. 6-3C) and above this is a zone of discontinuous flow banding with bands of beige and pink-brown tuff (Fig.6-4D). The upper 20 m of the lapilli-tuff is intensely folded, with metre-scale open folds and sheathfolds. It is topped by well developed vitrophyre which is heavily folded into asymmetric folds (Fig.6-4B). Remnants of an upper vitrophyre autobreccia are preserved in the rheomorphic synclines.

The tuff is overlain by a 2 m thick, bedded pumice lapilli deposit (Fig.6-4A). There is no soil or sediment at the base of the pumice lapilli deposit and some pumice lapilli have percolated into the cracks of the folded upper autobreccia of the underlying lapilli-tuff. It has a distinctive bright orange soil at its top.

### ***Interpretation***

The eutaxitic lapilli-tuff of Eruption-unit 1 is interpreted as an extremely high-grade, rheomorphic ignimbrite on the basis of a eutaxitic fabric at its base, extensive flow banding in its middle and metre-scale folding within its top. The absence of a basal breccia suggests it is not a lava flow (Henry & Wolff 1992). Rheomorphism in the upper zone may have been syn-depositional, but the upper vitrophyre autobreccia suggests that at least some of the rheomorphism was post-depositional, after the deposit had started to cool. The lack of a co-ignimbrite ash, sediment or a soil between the welded ignimbrite and the pumice fall deposit suggests that there was not a very long duration between deposition of these two layers, so that the eruption started with the emplacement of a hot, rheomorphic ignimbrite and ended with a sub-plinian phase.



**Fig.6-4: Field photos of Eruption-unit 1 at Bagno dell' Acqua. Large scale divisions are 10 cm**  
**A) Parallel-bedded pumice-lapilli (//bpL) deposit on top of folded, autobrecciated vitric lapilli-tuff (vLT). Note bright orange palaeosol. B) U shaped folds at top of tuff. C) Bottom half of unit at Bagno Dell Acqua showing vertical cooling joints, which end at the colour banded zone, approximately 2.5 m from base. D) Folded, colour banded zone. E) Large, abundant feldspar crystals in massive lapilli-tuff (mLT). Small scale divisions are 1 cm.**

## **Eruption-unit 2**

### ***Description***

Eruption-unit 2 is best exposed in the Kattibucale caldera scarp at Bagno Del Acqua (Fig. 6-2), where a 6 m thick welded lapilli-tuff is overlain by a 3.5 m thick lithic breccia (Fig. 6-3). Both upper and lower contacts are exposed. This unit thins considerably at the coastal locations (Fig. 6-3).

The trachytic to rhyolitic welded lapilli-tuff has a beige tuff layer at its base which locally grades into a lithic breccia lens. Above this is a poorly developed basal vitrophyre with black, glassy fiamme. It is predominantly a massive to diffusely-stratified, foliated, pink to purple-brown lapilli-tuff (Fig. 6-5A) with abundant feldspar crystals approximately 0.6 cm in size (Fig. 6-5D). It is generally lithic poor, but lithic abundance increases upwards.

The lapilli-tuff grades into a 3.5 m thick lithic breccia (Fig. 6-5B). The breccia is poly lithic and contains both fluidal-shaped juvenile bombs and lithic blocks up to 1 m in diameter with thermally spalled marginal flakes and juveniles with a cauliflower-texture (Fig. 6-5C). It includes patches of welded, matrix supported lapilli-tuff (Fig. 6-5E) but is predominantly clast supported, and is locally openwork.

### ***Interpretation***

The eutaxitic lapilli-tuff of Eruption-unit 2 is interpreted to be a high-grade welded ignimbrite. The tuff layer at the base may be a vent-derived ashfall deposit, subsequently overlain and fused by the ignimbrite. The breccia is interpreted as a proximal lithic breccia associated with the ignimbrite and not a fluvial breccia as previously described (Wright 1980). The thermal spalling and welded matrix suggest that it was emplaced hot, and the gradation from ignimbrite to breccia implies that deposition of the breccia was due to the same mechanism as the massive underlying ignimbrite, and without a repose period between the two events. The breccia represents a more energetic phase of the eruption, perhaps during a climatic, caldera collapse event. Fines would have been elutriated during rapid deposition.

A pumice fall deposit was not found within this eruption-unit. This may be because a plinian cloud was not developed and pumice lapilli not deposited, or it may have been subsequently eroded.

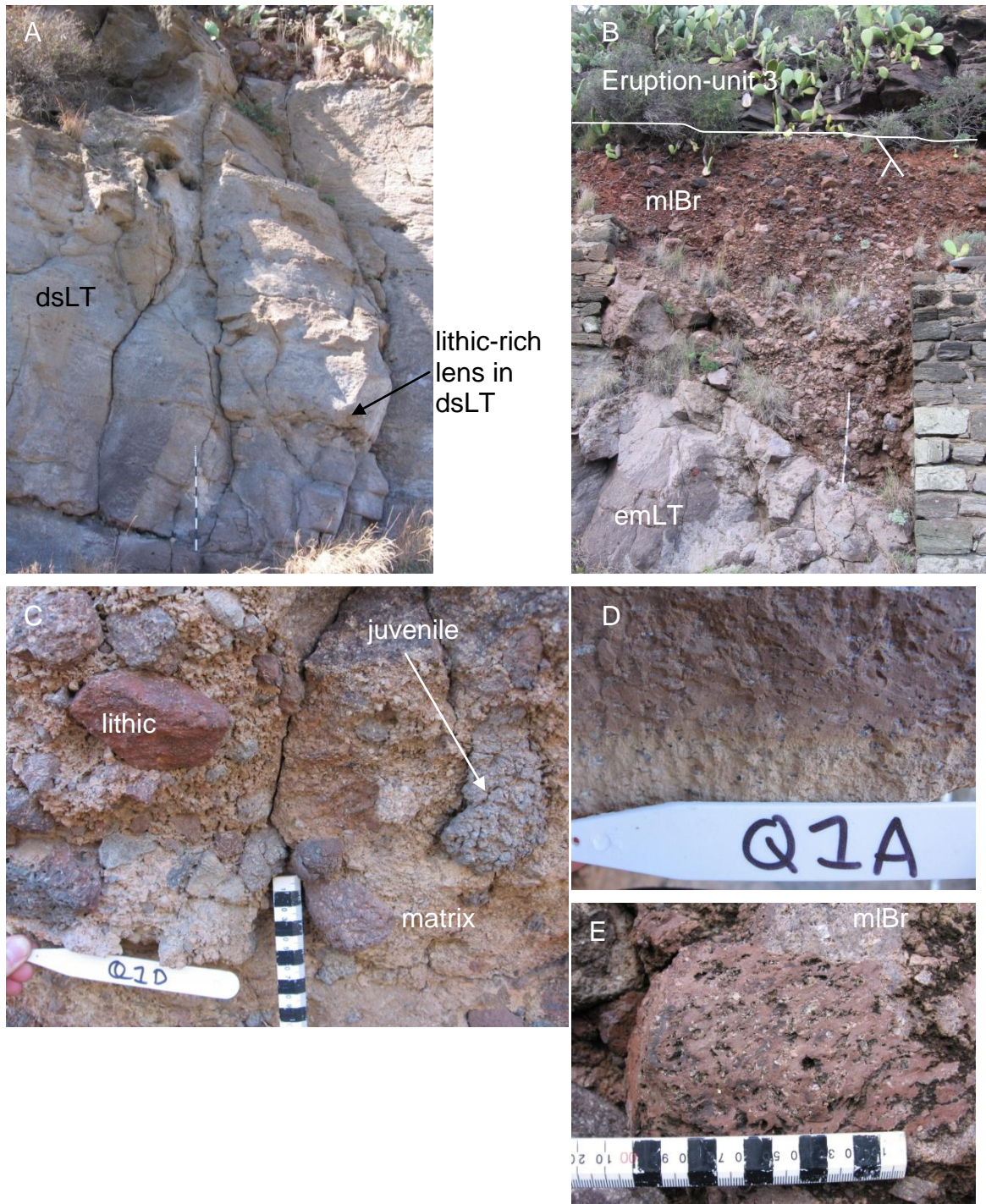


**Fig. 6-5:** Field photos of eruption-unit 2 at Bagno dell' Acqua. Large scale divisions are 10 cm. Small scale divisions are 1 cm. A) Diffusely stratified lapilli-tuff (dsLT) with lithic-rich lenses. B) Welded, clast supported breccia on top of eutaxitic massive lapilli-tuff (emLT). C) Close-up of the base of the breccia where it is welded and matrix-supported showing cauliflower textures on clasts, indicating hot emplacement. At the top of the breccia it is clast-supported. D) Abundant feldspar population of unit in massive tuff at the base of Eruption-unit 2. E) Area of welded tuff in the breccia.

### **Eruption-unit 3**

#### ***Description***

Eruption-unit 3 is defined at Punta Della Guardia (Fig. 6-3) where it comprises of a 2 m thick, eutaxitic lapilli-tuff overlain by a 0.5 m thick lithic breccia. Both its upper and lower contacts are exposed here. It is bound by palaeosoils (Fig.6-6A).

The trachytic lapilli-tuff is welded and has a well developed basal vitrophyre (Fig.6-6A). The lapilli-tuff is red-brown, contains abundant accidental lithic clasts and juvenile ellipsoid clasts that have a characteristic scoriaceous texture (Fig.6-6D) and occasionally imbricated (Fig.6-6C). Many of these have been eroded out, giving it a 'pockmarked' appearance (Fig.6-6C & D). These clasts become more flattened towards its top. A distinctive pale grey tuff layer occurs 2 m above the base (Fig.6-6B). This is laterally discontinuous. Above it lays a bright red, clast supported polyolithic breccia, which is variably welded and contains distinctive foliated juvenile clasts with a scoriaceous texture (Fig.6-6E).

This unit varies laterally and at Bagno Del Acqua, is quite different to the coastal locations. Here Unit 3 has a well developed basal vitrophyre that passes upwards into a sheet-jointed brown tuff with small juvenile clasts with a scoriaceous texture. The upper 1 m is massive tuff. Unit 3 at this location lacks the abundant accidental lithics, the lithic breccias but is correlated by the juvenile scoriaceous clasts.

#### ***Interpretation***

The tuff and lapilli-tuff of Eruption-unit 3 are interpreted as welded ignimbrite. It is unambiguously pyroclastic. The basal tuff layer may be a vent-derived ashfall deposit as it traces between localities. The basal vitrophyre of the ignimbrite above this layer at Bue Marino suggests that the ash was either emplaced cool, or had subsequently cooled so that the overlying welded lapilli-tuff could chill against it. This supports an ashfall interpretation, as falling through the atmosphere tends to cool pyroclasts. The overlying ignimbrite is laterally variable from lithic-rich lapilli tuff to sheeted tuff but all locations show distinctive scoriaceous juvenile clasts. These have sub-spherical vesicles, even when the clasts are flattened, suggesting that they vesiculated after welding-compaction. This is a common characteristic of peralkaline rheomorphic ignimbrites (Schminke, 1974). The lapilli-tuff and lithic breccia lithofacies are absent at Bagno Dell Acqua possibly because it was eroded or not deposited at the proximal location.

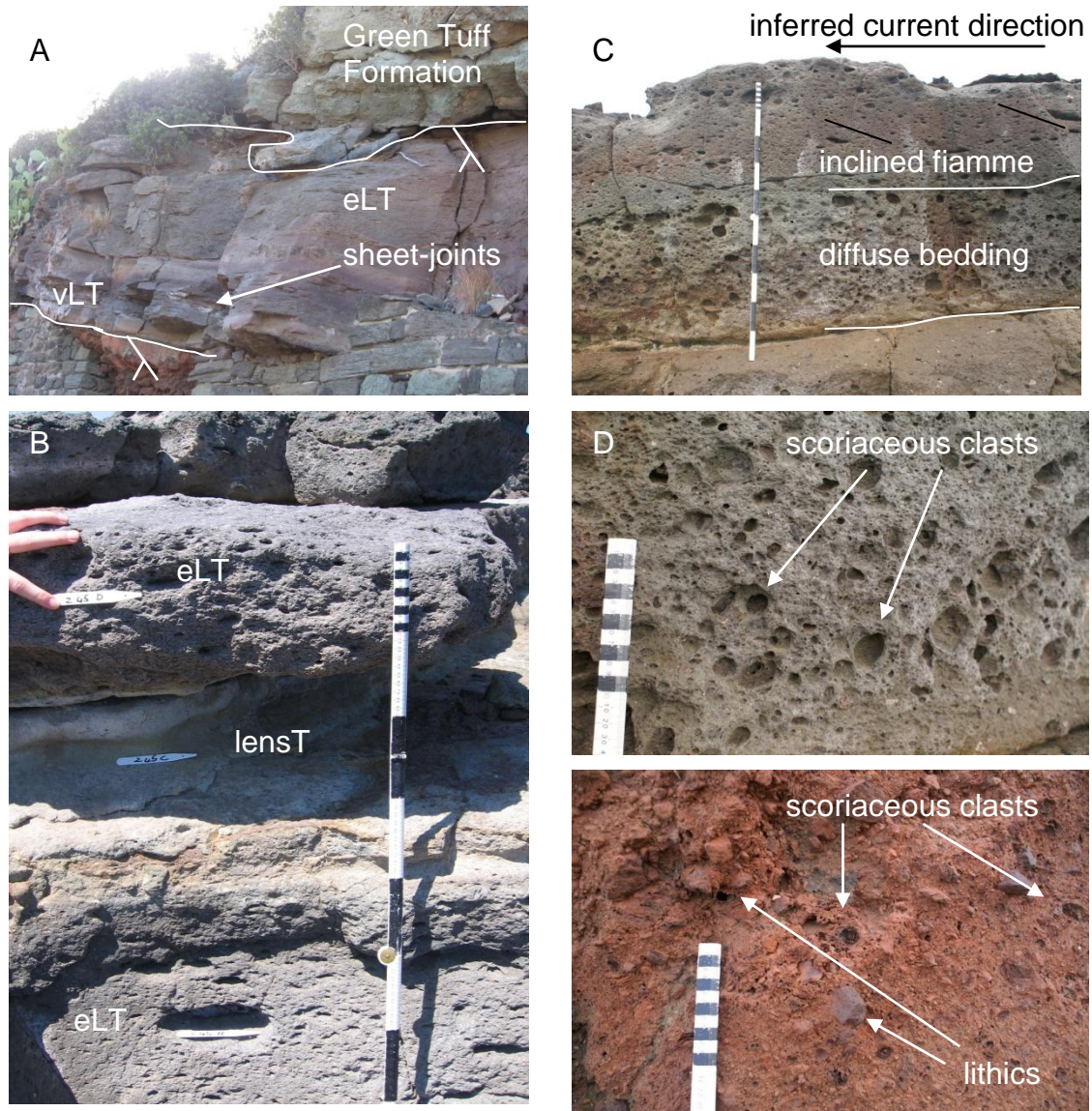


**Fig.6-6: Field photos of eruption-unit 3. A) Sheet-jointed, eutaxitic lapilli-tuff (eLT) at Bagno Dell Acqua with basal vitrophyre. B) Eutaxitic lapilli-tuff (eLT) at Punta Della Guardia with discontinuous lens of grey tuff (lensT). C) Diffusely-bedded lapilli-tuff at Punta Della Guardia showing gradation from circular to ellipsoid scoria clasts. Flattened clasts towards the top of the unit are imbricated indicating flow direction from right to left. D) Pockmarked texture characteristic of this unit at Punta della Guardia which is caused by scoriaceous juveniles, often weathered out. E) Red, welded lithic breccia at top of the unit at Punta Della Guardia, with scoriaceous clasts similar to lapilli-tuff. Large scale divisions are 10 cm, Small scale divisions are 1 cm.**

The pale grey tuff layer present at Punta Della Guardia may represent a fine-grained lithofacies of the ignimbrite, a vent-derived ashfall deposit, or alternatively a co-ignimbrite fallout deposit related to the underlying ignimbrite. The latter two interpretations would suggest a brief hiatus in ignimbrite deposition at this location. Directly above this tuff layer lays a welded, poly lithic breccia interpreted as a co-ignimbrite breccia. The grading from ignimbrite to breccia suggests a similar mechanism of deposition for both lithofacies without a repose period between them.

The breccia represents a higher velocity density current with a larger flow competence (Branney & Kokelaar 2002). However, with limited outcrop, it is not possible to tell whether this records local erosion and redeposition (Buesch 1992), deposition of larger clasts caused by local conditions, or whether it represents a larger event such as caldera collapse (Druitt & Bacon 1986).

No pumice lapilli fallout deposit was found associated with Eruption-unit 3 suggesting that either a plinian column was not established or that a fallout layer was subsequently eroded.

### **6.3.2. Chemical data**

Samples from the three eruption-units were processed for geochemical analysis and analysed by whole rock XRF following the methods outlined in Chapter 3. The three eruption-units all plot in the trachyte field on a TAS diagram (Fig.6-8A) and have a high Alkalic Index (molar  $\text{Na}_2\text{O} + \text{K}_2\text{O}/\text{Al}_2\text{O}_3$ ) of 0.9-1.4 (Fig.6-8B), making them mildly to strongly peralkaline (Mahood 1984). Each unit shows chemical zoning, which means that correlating on the basis of chemistry should be done with caution. However, it is possible to distinguish each eruption-unit on the basis of  $\text{TiO}_2$ , Ba, Zr and Nb concentrations which confirms the field correlations (Fig.6-9). Ba concentrations are particularly useful for distinguishing Eruption-unit 1 from the other two units (Fig.6-9B). This is likely due to its high feldspar population. Eruption-units 2 and 3 are less easy to distinguish from each other geochemically, although they do produce different Nb vs  $\text{TiO}_2$  patterns (Fig.6-9A).

## **6.4. A revised stratigraphy for the welded ignimbrites of Pantelleria, Italy.**

Palaeosoils in volcanic stratigraphy represent extended periods of repose and provide distinctive markers for correlations within subaerial volcanic successions. In this chapter we correlated three palaeosoil-bound eruption-units (Fig. 6-3). As this is preliminary work we have not given each unit a stratigraphic name but have abandoned names designated by Mahood and Hildreth (1984) and Wright (1980). Table 6-1 states how our Eruption Units 1, 2 and 3 correlate to original names.

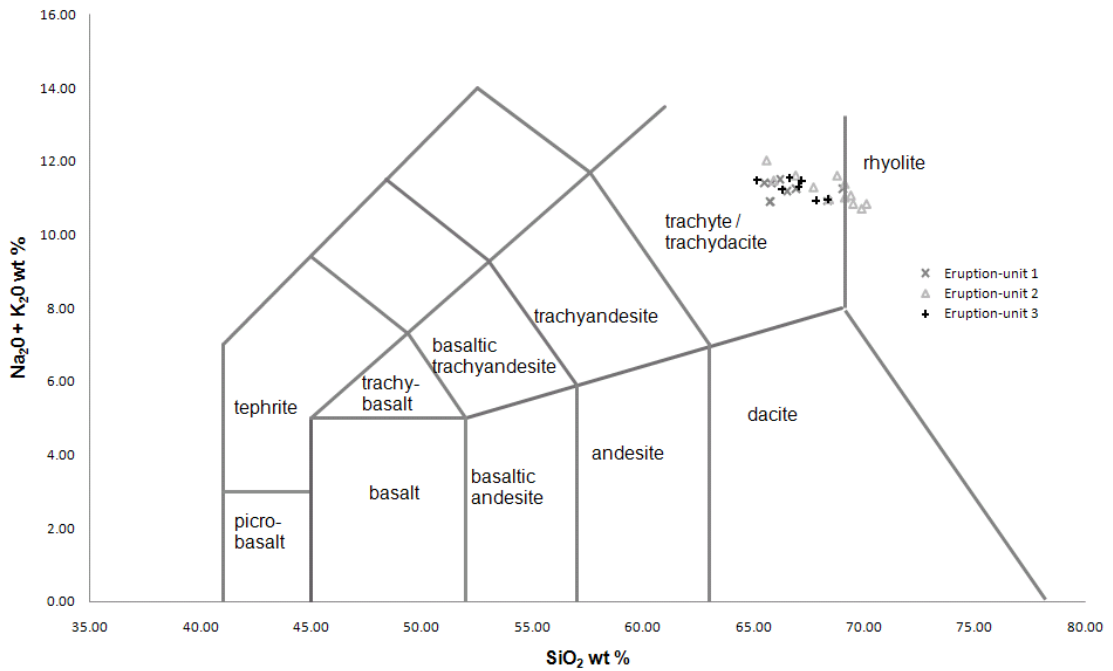


**Fig. 6-7: Total alkalis versus silica (TAS) plot for the three Eruption-units. Eruption-unit 2 is the most evolved and is rhyolitic to trachytic. Eruption-units 1 and 3 are trachytic.**

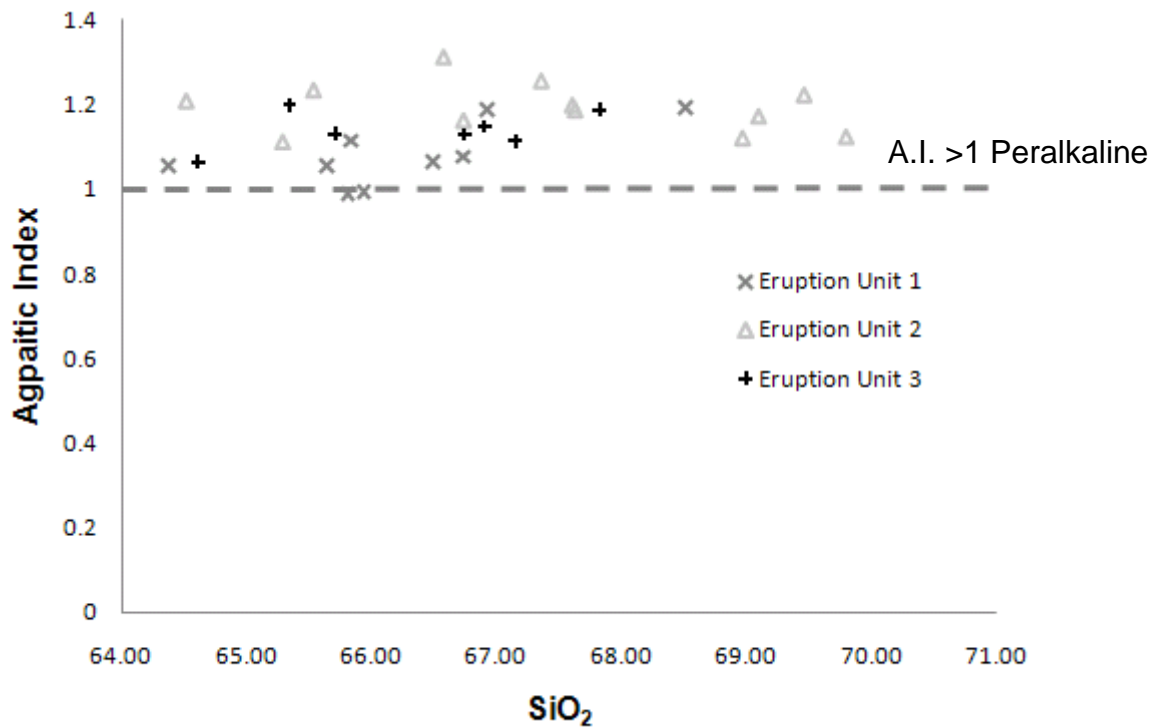


**Fig.6-8: Agpaitic Index (Molar [Na<sub>2</sub>O + K<sub>2</sub>O]/Al<sub>2</sub>O<sub>3</sub>) versus SiO<sub>2</sub> for Eruption-units 1, 2 and 3 showing mild to strongly peralkalinity. Eruption-unit 2 appears slightly more peralkaline than the others, and Eruption-unit 1 is the least peralkaline.**

**Table 6-1: Equivalence of stratigraphy reported here and that of Mahood and Hildreth, 1986 and Wright, 1980.**

<b>This Study</b>	<b>Mahood &amp; Hildreth</b>	<b>Wright 1980</b>
Green Tuff Formation	B (Green Tuff)	B
3	Z and D Reworked breccia	E of sections 1,2,3 C of 2,3,4,18 Reworked breccia
2	F and Q Reworked breccia	F of sections 1,2 E of 18 G of sections 1,2,3,5,7,9,10 Reworked breccia
1	P	G of sections 5, 8, 16, 18 G of 7,9

#### **6.4.1. Discussion and further work**

This study offers the possibility of a revised stratigraphy for the welded ignimbrites of Pantelleria, Italy. Three pre-Green Tuff soil bound eruption-units have been identified based on fieldwork and corroborated by geochemistry. This has simplified the stratigraphy in the north-eastern sector of the island in the post-La Vecchia caldera cycle to 4 welded ignimbrites from the 6 identified by Mahood and Hildreth (1986).

Wright (1980) identified seven correlatable welded, pumice-fall tuffs, two unwelded pumice-fall deposits and a further eight uncorrelated welded tuffs. Mahood and Hildreth (1984) revised this stratigraphy reducing the numerous units. They reinterpreted most of the units as welded ignimbrites, except units H and I, and this study concurs with this conclusion, as described previously. Reinterpretation of the units as ignimbrites has enabled correlations to be made despite considerable lateral variation in the lithofacies present at each location. Our correlations are based upon field observations of soil bound units, whereas Mahood and Hildreth largely relied upon Zr and Rb concentrations and K/Ar dates to support their field observations.

#### **Geochemical correlations**

The Green Tuff Formation (Chapters 2-5), the most extensively exposed and studied eruption unit on Pantelleria is a zoned deposit and shows remarkable variation particularly in Zr (500-2000 ppm), Rb (40-190 ppm), TiO<sub>2</sub> (0.4-0.8 wt %) and Ba (40-

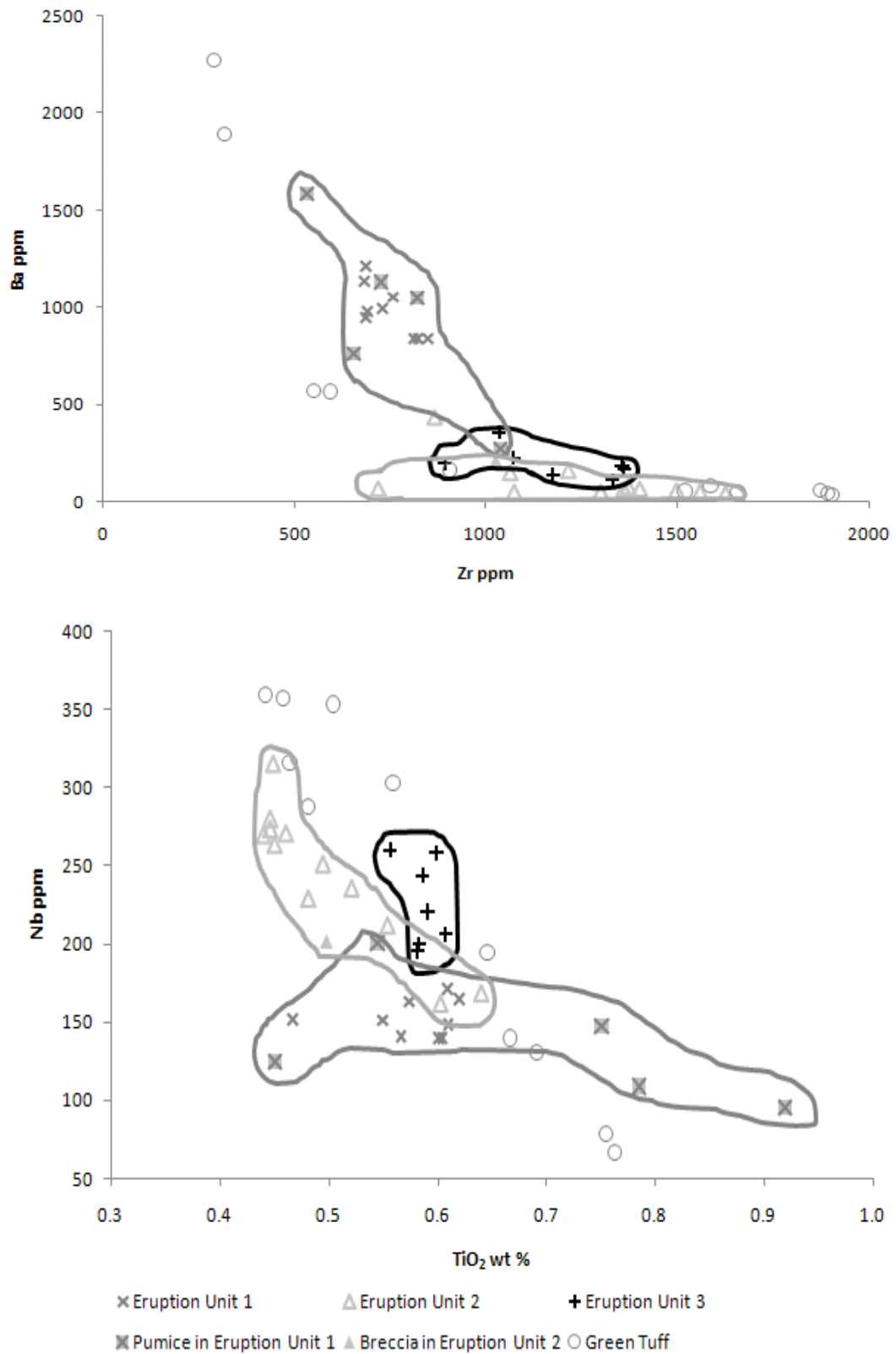


**Fig.6-9:** A) Ba vs Zr plots showing different fields for eruption-units 1, 2 and 3. B) Nb vs TiO<sub>2</sub> showing different fields for Eruption-units 1, 2 and 3. These fields overlap due to heterogeneity and zoning within single units. Note how the Green Tuff shows compositions covering all three fields, due to its strong vertical and sectoral zoning. This highlights how misleading geochemical correlations can be when dealing with zoned units.

2300 ppm). Its composition ranges from pantellerite (peralkaline trachyte) to trachyte and this makes distinguishing the Green Tuff Formation from other units difficult (Fig.6-9). With this in mind, the compositional variation of each unit at each location needs to be determined before it is possible to correlate on the basis of geochemistry. The limited whole rock analysis undertaken has shown that at each location, there is a significant variation in the key major and trace element concentrations and those fields defined for each unit overlap. Further studies to constrain the amount of variation are required to take these correlations further.

### K/Ar Ages Correlations

Previous field and geochemical correlations were supported by K/Ar ages (Mahood & Hildreth, 1986). Ages are published for the units at individual locations and then an average age given for each unit. This approach has some problems. When the individual ages are plotted with their error, considerable overlap is seen between the units (Fig.6-10). In particular, units F and Q have overlapping ages as do units D and Z. These overlaps in K/Ar ages are consistent with our conclusions that units F and Q are the same eruption-unit 2 and units D and Z are the same eruption-unit 3. These correlations would be further corroborated by high precision Ar/Ar dates.

Since this preliminary study was completed, new Ar/Ar dates for Eruption-unit 3 have been published (D =  $87 \pm 1.7$  ka and Z =  $87.5 \pm 1.3$  ka), confirming the correlation of D and Z as a single unit argued for here (La Felice *et al.* 2009).

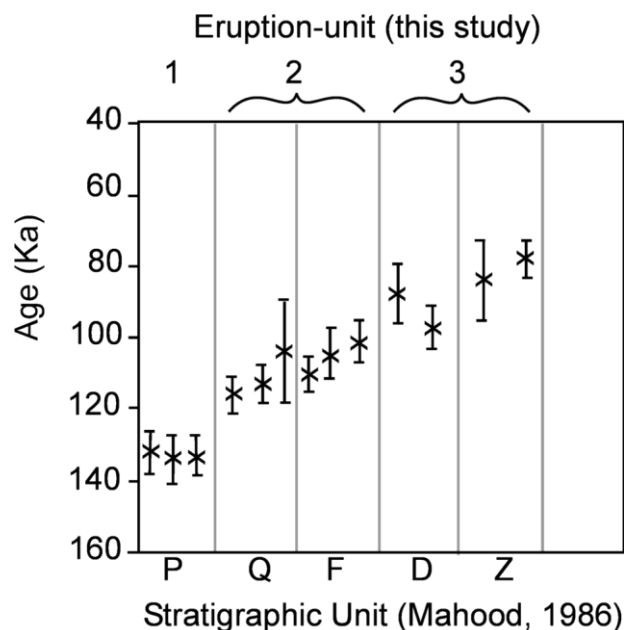


**Fig.6-10: Plot of ages published for units P, Q, F, D, Z (Mahood and Hildreth, 1986) at different locations. Individual K-Ar, with 1  $\sigma$  error represented by error bars. This shows clear overlap between the ages for units Q and F as well as D and Z. These units cannot be distinguished from each other by K/Ar dates.**

### **Implications for eruptive style**

The number of large, ignimbrite forming eruptions at Pantelleria during the last 140 ka is 4, rather than the 6 in previous accounts. We have identified extensive lithic breccias with two of these units (Eruption-units 2 and 3) and limited lithic breccias with Eruption-unit 1 and the Green Tuff Formation. A sub-plinian pumice fall is associated with Eruption unit 1 and a strombolian (to possible sub-plinian)-scale pumice-fall is associated with the Green Tuff. The four eruptions may be larger than previously thought: however, most of the tephra was deposited offshore and only proximal onshore deposits are seen. This means that volume estimates for the eruptions must be absolute minimum volumes. Recent work on Mediterranean tephra (Margari *et al.* 2007) has discovered Green Tuff Formation tephra in drill cores from Lesvos Island, Greece, suggesting a Santorini-scale eruption. The Green Tuff is not the thickest deposit in this succession and Eruption-unit 1 reaches thicknesses exceeding 25 m. Although thickness is not proportional to volume, some of the older eruptions could have been an equal size, or larger than the c.50 ka Green Tuff eruption. Further work on this older stratigraphy to extend correlations around the island, refine their geochemistry and produce radiometric ages is in progress (N. Jordan, PhD research, University of Leicester) and will enable better correlations with offshore tephras enabling better size estimates of these eruptions.

Identification of previously unrecognised large co-ignimbrite breccias in Eruption-units 2 and 3 and smaller scale breccias in Eruption-unit 1 and the Green Tuff indicate that these large eruptions may have been caldera forming, and devastating on an island scale. Only two main calderas are currently recognised on Pantelleria (see previous discussion in Chapter 5). Detailed field work investigating relationships of the ignimbrites and the caldera scarps are needed as it is likely that the caldera collapse history of the volcano is more complex than previously thought.

### **6.5. Conclusion**

This preliminary study (Chapter 6) has shown that:

- Reinterpretation of the pre-50 ka welded tuffs as ignimbrites has allowed for correlations of units that are laterally variable.

- In the NE of Pantelleria there are four palaeosoil-bound ignimbrites: Eruption-units 1, 2 and 3 and the Green Tuff Formation. This is a reduction in the number of ignimbrites from previous studies; however, each unit is considerably larger and more widespread than previously recognized.
- Each ignimbrite has an associated lithic breccia. Eruption-units 1 and 2 have well-developed, thick lithic breccias that almost certainly record a caldera collapse event. Eruption-unit 3 and the Green Tuff Formation have smaller lithic breccias, which typically occur as lenses or pods. These may record partial caldera collapse.
- The Eruption-units are chemically zoned, although the range of zoning is not as significant for Eruption-units 1-3 as in the Green Tuff Formation. This would hinder the correlation of units based upon whole rock chemical analysis.
- This preliminary study is now being continued by Nina Jordan (PhD student) at the University of Leicester. The stratigraphy presented here for the NE of Pantelleria is being traced around the island and extended further back into the volcano's history. Detailed field correlations will be combined with detailed whole rock analysis, phenocryst analysis and high-resolution radiometric dating.

---

# 7. Conclusions and further work

---

This thesis aimed to understand the emplacement of pyroclastic density currents by unravelling the internal architecture of an ignimbrite which comprised a single flow unit.

- Were low-aspect ratio ignimbrites with a circular distribution emplaced from currents that flowed radially, simultaneously in all directions from source?
- How do sustained pyroclastic density currents behave over topography?

A combination of detailed field work and closed spaced sampling for geochemical and petrological analysis revealed a linear trend in the geochemical zonation of the ignimbrite. This trend, the chemical stratigraphy, was then mapped for the entire deposit, so that its 3D internal architecture could be analysed. The internal chemical-architecture of the Green Tuff ignimbrite revealed that single, sustained, pyroclastic density currents have complex flow paths and are strongly affected by topography. This thesis documents the first detailed study of the internal chemical-architecture of an ignimbrite which comprises a single flow-unit. The main conclusions from each chapter are summarised below.

## 7.1. The Green Tuff Formation

- The Green Tuff Formation (new term) comprises the Kattibucale Member (new term), a strombolian (to possible sub-plinian)-scale pumice-fall deposit, and the Green Tuff ignimbrite Member (new term). A new type section is defined for the Green Tuff ignimbrite at Monastero and for the Kattibucale Member at Kattibucale.
- The low-aspect ratio Green Tuff ignimbrite, a single flow-unit, records a sustained, quasi-steady pyroclastic density current. It was deposited across the entire island of Pantelleria and up to 45 km offshore.
- The deposit welded instantly, as it progressively aggraded. Local rheomorphism occurred both syn-depositionally and post-depositionally as the ignimbrite started to cool. The rheomorphism does not significantly obscure primary textures such as bedding.

- There is no compelling evidence for a large caldera forming event during the eruption of the Green Tuff Formation.

## 7.2. The chemical stratigraphy of the Green Tuff Formation

- The Green Tuff Formation is chemically zoned. This is observed in the field by an increase in size and abundance of anorthoclase feldspar crystals.
- The Formation is markedly zoned in trace elements. Both the major elements, rare earth elements and phenocryst assemblage also show limited zoning. Zirconium ppm is used as a proxy for the chemical zonation.
- The chemical zonation observed in the ignimbrite records the progressive tapping of a single magma chamber which is zoned from pantellerite at its roof, to trachyte and into more basic magmas at depth.
- A linear decrease in zirconium ppm with height through the Green Tuff ignimbrite is defined and used as a ‘chemical stratigraphy’ or ‘chemical-architecture’ for the ignimbrite. This chemical stratigraphy was divided into eight successive zones, which are used as a proxy for time-slices through the sustained, brief history of the pyroclastic density current which deposited the ignimbrite.

### 7.2.1. Further work

- Much is still to be learned about the nature of the zoning of the magma chamber, which was outside the scope of this study. It is thought that the pantellerite is the result of extreme fractional crystallisation of a parental basalt. The large quantity of chemical data obtained during this research study could be used to test this concept. It may be possible to model whether the pantellerite is related to the trachyte through fractional crystallization alone.
- The large database on phenocryst and glass compositions could be used to investigate the partition coefficients for a variety of minerals in pantellerite liquid, as this is currently poorly understood, particularly for minerals such as aenigmatite.
- Zoned magma chambers often show marked variation in isotopic ratios, temperature and gas content. Obtaining this data was outside the scope of this study, however it could prove informative for understanding the petrogenetic story of the magma chamber. Furthermore, understanding the gas species and

temperature variations within the Green Tuff Formation could help understand the marked welding and rheomorphism variations observed in the ignimbrite.

### **7.3. Internal mapping of the chemical stratigraphy of the Green Tuff ignimbrite**

- Detailed field logging, mapping and sampling of the Green Tuff Formation revealed a complex 3D internal chemical-architecture of the deposit.
- The lithofacies in the Green Tuff ignimbrite are diachronous and cannot be identified as ‘members’ or used as ‘time-markers’ (Fig. 7-1).
- The internal chemical-architecture of the ignimbrite enabled reconstruction of ‘footprints’ of the pyroclastic density current through time.
- The pyroclastic density current did not flow radially for its entire duration. Rather, the leading edge progressively advanced during the waxing stage and then retreated as the current waned. The current also shifted laterally with time, inundating the entire island only during a peak, climactic phase of the eruption when mass flux was at its greatest.
- The flow-path of the pyroclastic density current was strongly controlled by topography. During the early time-slices of the current, the leading edge was initially blocked, reflected or deflected by even very small (c. 15 m) conical hills as well as transverse ridges. As the current waxed, and the mass flux of the eruption increased, the leading edge of the current progressively advanced over the barriers until it was able to overtop them. In the later time-slices, the current waned and was no longer able to pass over the largest barriers.
- The first phases and the final phase of the current were likely to have been weak, thin and low-velocity.
- The flow path of the pyroclastic density current was very complex and changed significantly during its brief duration. This has important implications for estimates of volume, mass flux and run-out distances, which impacts on the models that rely on these parameters to simulate pyroclastic density currents. The detailed study of the internal chemical-architecture of the single flow-unit has elucidated important information on the dynamics of the eruption and the behavior of the pyroclastic density current that deposited it. This complex internal architecture is cryptic and cannot be inferred from lithofacies variations.

Rather, lithofacies are diachronous and cannot be taken to represent a temporal history of the current.

### 7.3.1. Further work

- Pantelleria is a small island, c. 100 km<sup>2</sup>. The Green Tuff ignimbrite that outcrops today is relatively proximal to an inferred vent; it is likely that the majority of the ignimbrite was deposited in the sea. Therefore, it has not been possible to reconstruct the pyroclastic density current at its distal edges or to infer how the current behaved as it travelled far from source. Would the current behave the same in distal locations? An important extension of this research would be to apply the concept of an internal chemical-architecture to other ignimbrites. Of particular interest would be other large, low-aspect ratio ignimbrites which traverse a variety of topographic barriers and can be traced laterally around the vent as well as longitudinally from source such as Taupo, if it was chemically zoned. The chemical stratigraphy concept would be much more easily applied to unwelded ignimbrites, allowing for even closer spaced sampling, although these may not be as pristine, or be preserved on steep slopes.
- Further work could also involve applying this new concept to the models. For example, it was previously only possible to model the Green Tuff ignimbrite as a whole, assuming that it was emplaced instantaneously and radially. Now, it is possible to model each successive time-slice of the current, with each time slice having a different volume, run-out distance and ability to scale topographic barriers. This would allow for a more realistic simulation of the current.

## 7.4. The eruptive history of Pantelleria, Italy

- A new stratigraphy for the  $\geq 50$  ka deposits is proposed. Four large explosive eruptions are identified, at least two of which are inferred to record significant caldera-subsidence. These four eruption units (the Green Tuff Formation and Eruption-units 3, 2 and 1 in increasing age) are all broadly similar. Each comprises massive, diffusely bedded and cross-stratified ignimbrite and all include a lithic breccia. Eruption-units 1-3 are all more widespread and larger than previously thought and can be traced across the entire NE sector of the island.

#### **7.4.1. Further work**

- It is now thought that the newly correlated Eruption-units may have been deposited across the entire island and work is ongoing to identify them in sea cliffs and caldera scarp sections around the island. It would be important to characterize their detailed lithofacies, chemistry and phenocryst assemblage so that the stratigraphy can be refined and given proper stratigraphic names. Further work would also involve investigating the stratigraphy that lies beneath Eruption-unit 1 so that the volcanic history of the island can be better understood. This work is now being undertaken by Nina Jordan at the University of Leicester as a PhD research project.

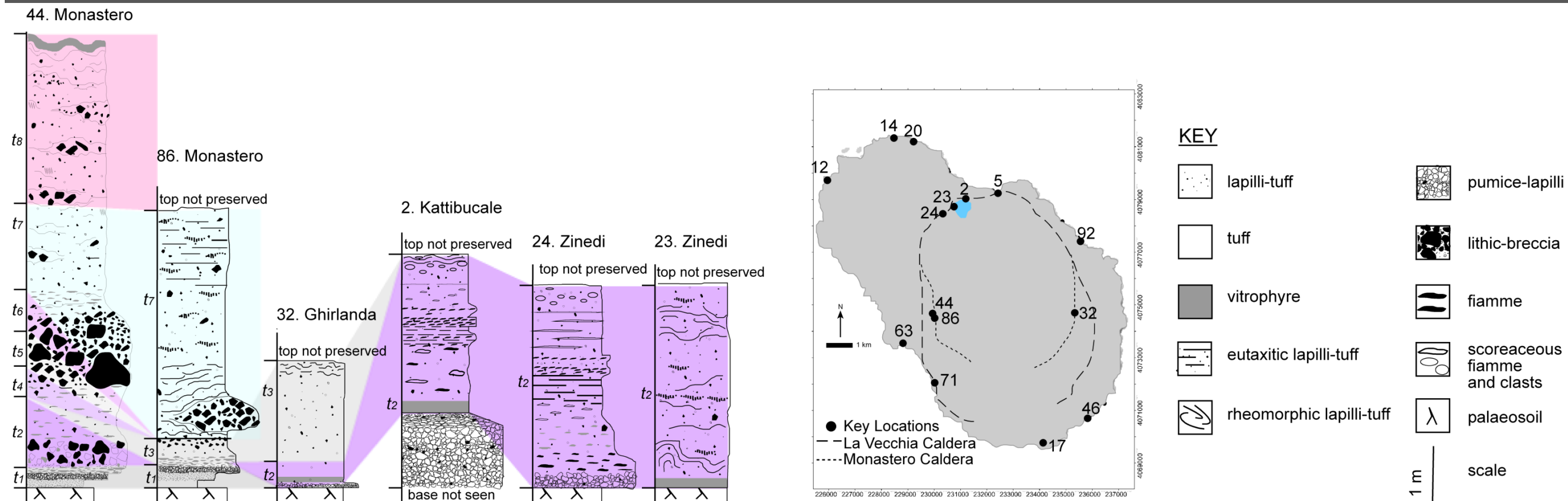


Fig. 7-1: Chemical stratigraphy super-imposed over simplified graphic logs of key locations along the caldera rim (top) and coast (bottom) of the Green Tuff Formation. This highlights how diachronous lithofacies are.

# 1. Appendix I

---

## 1.1. Artefacts in the footprint maps

# 2. Appendix II

---

## 2.1. Understanding geophysical density currents: internal chemical mapping of an ignimbrite provides snap-shots on pyroclastic density current behaviour

A paper prepared from Chapter 4 intended for Nature.

# 3. Appendix III

---

## 3.1. A CD of analytical data

### 3.1.1. XRF data

- All XRF data used in this thesis.
- Standard data including error.

### 3.1.2. LA ICP MS data

- All ICP MS data used in this thesis.
- Standard data

### 3.1.3. EMPA data

- All EMPA data used in this thesis

### 3.1.4. UTM coordinates of all field locations.

- UTM coordinates of field locations
- UTM coordinates for figures and photos
- List of field locations and type of sample taken.

---

# 1. Appendix I

---

## 1.1. Artefacts in the footprint maps

There is large potential for artefacts in the footprint maps as a result of sampling resolution. Firstly, there are areas of the island that were not sampled for geochemical analysis. This may be due to a lack of outcrop of the Green Tuff Formation, or lack of a suitable outcrop for analysis. For example, there are no data points in the area to the north-west of Montagne Grande as there were no suitable outcrops to sample (Fig. 1-1). Secondly, whilst the majority of locations sampled for geochemical analysis were complete sections exposed to the base of the Formation, this was not always possible. Fourteen locations where the base of the Green Tuff Formation was not exposed were included as part of the dataset used to create the footprint maps (Fig. 1-1). This creates an uncertainty in the footprint maps.

Here, the areas of uncertainty are identified in detail for each of the footprint maps (Figs 1-2 to 1-9). In these series of footprint maps, locations that are not exposed to the base are highlighted in yellow, to be distinguished from complete locations in black. For each footprint, key locations that are not exposed to the base are identified. However, these locations are only highlighted for footprints up to the first record of a geochemical zone. For example, a location that is not exposed to its base that records time-slice  $t_4$  is only highlighted for maps  $t_{1-3}$  as these time slices could be deposited here but are not exposed. The footprint map with the most uncertainty therefore is for time-slice  $t_1$  (Fig. 1-2). There are key locations near the airport and near the summit of Cuddia Attalora which are not exposed to the base. It is possible that the unexposed portions of the Formation at these locations record this time-slice, but were not sampled. This could extend this footprint to the summit of Cuddia Attalora and further across the plains to the north of the caldera. Similar gaps in the data set occur in time-slice  $t_2$  (Fig. 1-3). In time-slice  $t_3$ , key locations are again identified in the Cuddia Attalora area (Fig. 1-4). Here, outcrops were poor and there is a significant number of outcrops that are not exposed to the base of the Formation. It is possible that the inundation areas in this area are larger than those interpreted in Chapter 4. Time-slice  $t_4$  is much better constrained. Here, the largest artefact is due to a lack of exposure along the west coast and the base not being exposed at Grotto dello Storto (Fig. 1-5). It is possible that inundation by the

current is more complete along the western side of the island at this time. These same issues continue for time-slice  $t_5$  (Fig. 1-6) and partially during  $t_6$  (Fig. 1-7),  $t_7$  (Fig. 1-8) and  $t_8$  (Fig. 1-9). The area to the east of Cinque Denti remains an area of uncertainty throughout all of these time-slices.

These gaps in the data set are of concern regarding local inundation areas and extents. However, they do not change the key conclusions of a diachronous base to the Green Tuff ignimbrite which is supported by over 100 field locations.

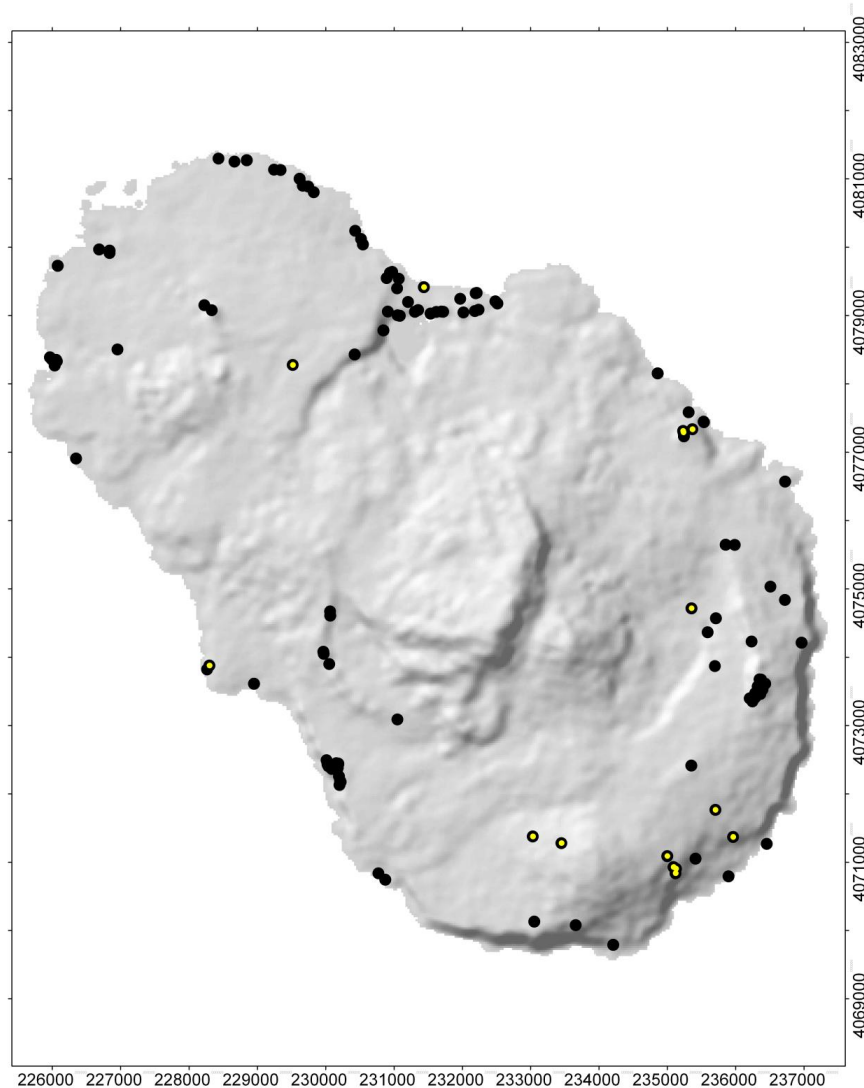


**Fig. 1-1:** Map showing the field locations sampled for geochemical analysis that were not exposed to the base (yellow circles). Black circles show field locations sampled for geochemical analysis that were exposed to the base.

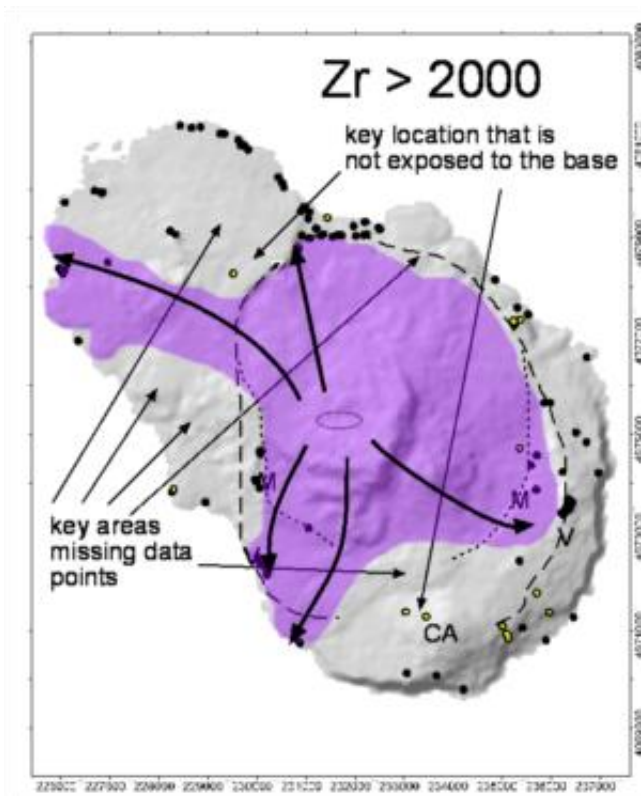


**Fig. 1-2:** Artefact map for footprint  $t_1$ . Locations that are not exposed to the base are highlighted in yellow. Of these, those that could impact interpretations as discussed in the text, are identified.

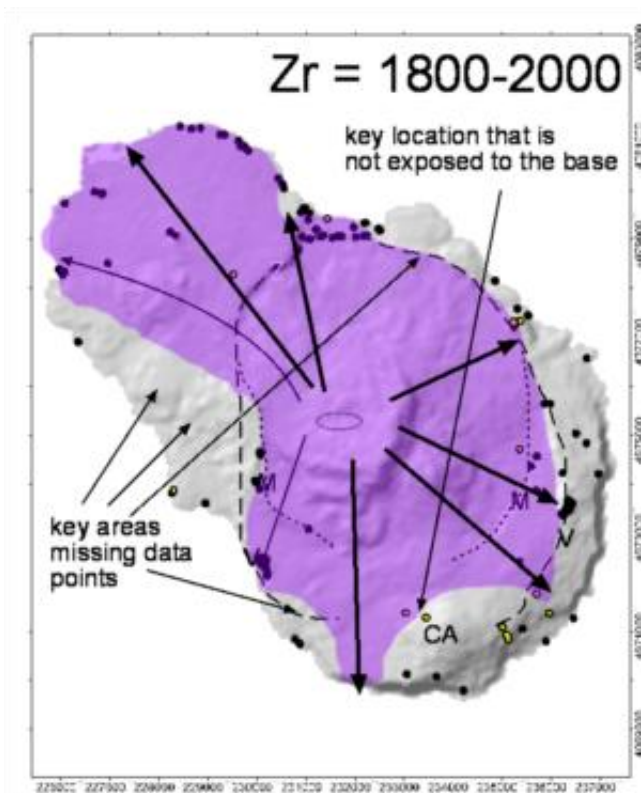


**Fig. 1-3:** Artefact map for footprint  $t_2$ . Locations that are not exposed to the base are highlighted in yellow. Of these, those that could impact interpretations as discussed in the text, are identified.

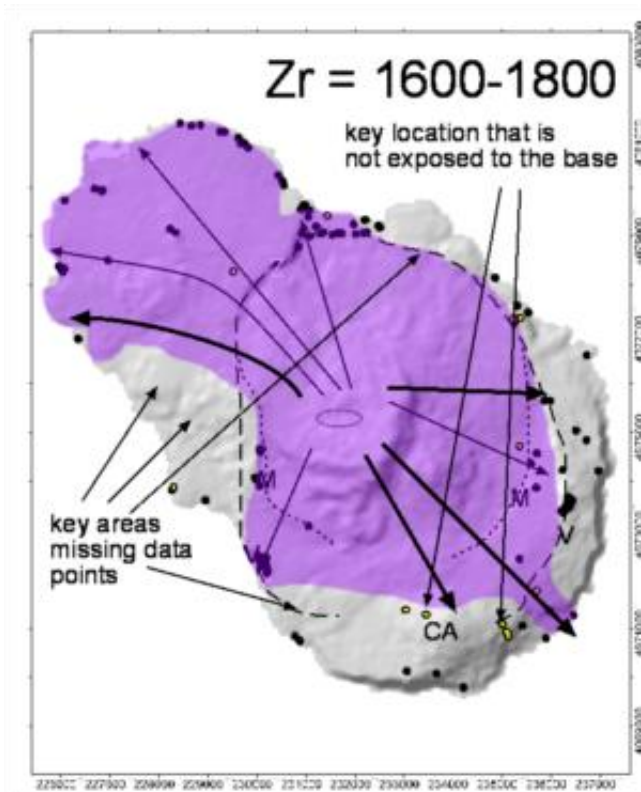


**Fig. 1-4: Artefact map for footprint  $t_3$ .** Locations that are not exposed to the base are highlighted in yellow. Of these, those that could impact interpretations as discussed in the text, are identified.

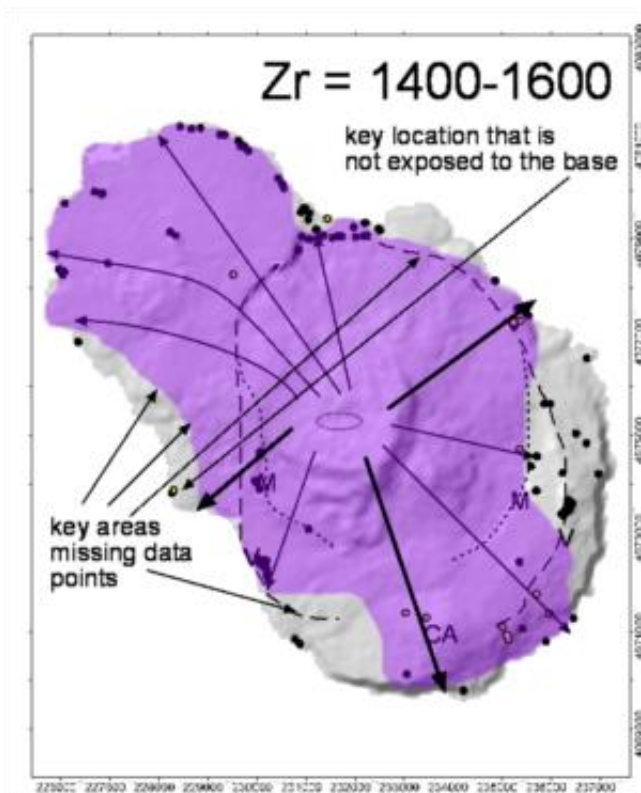


**Fig. 1-5: Artefact map for footprint  $t_4$ .** Locations that are not exposed to the base are highlighted in yellow. Of these, those that could impact interpretations as discussed in the text, are identified.

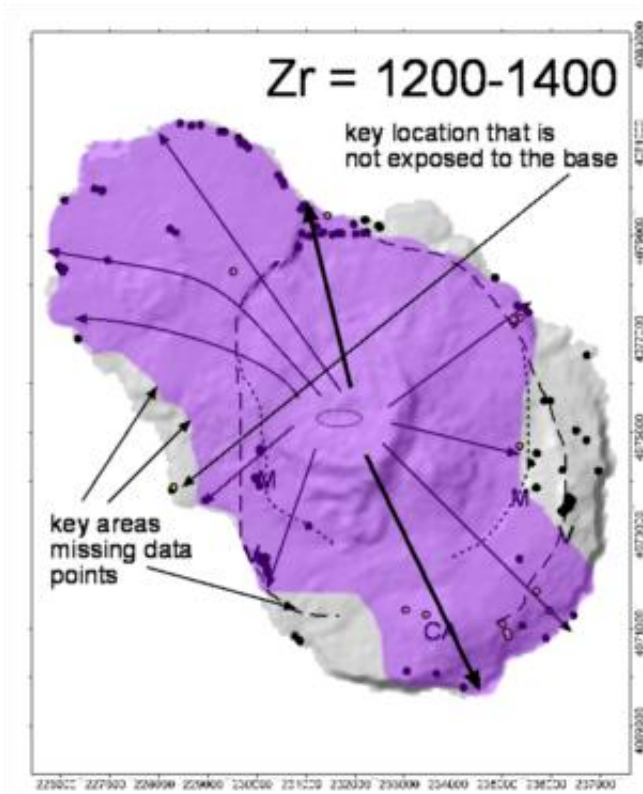


**Fig. 1-6: Artefact map for footprint  $t_5$ .** Locations that are not exposed to the base are highlighted in yellow. Of these, those that could impact interpretations as discussed in the text, are identified.

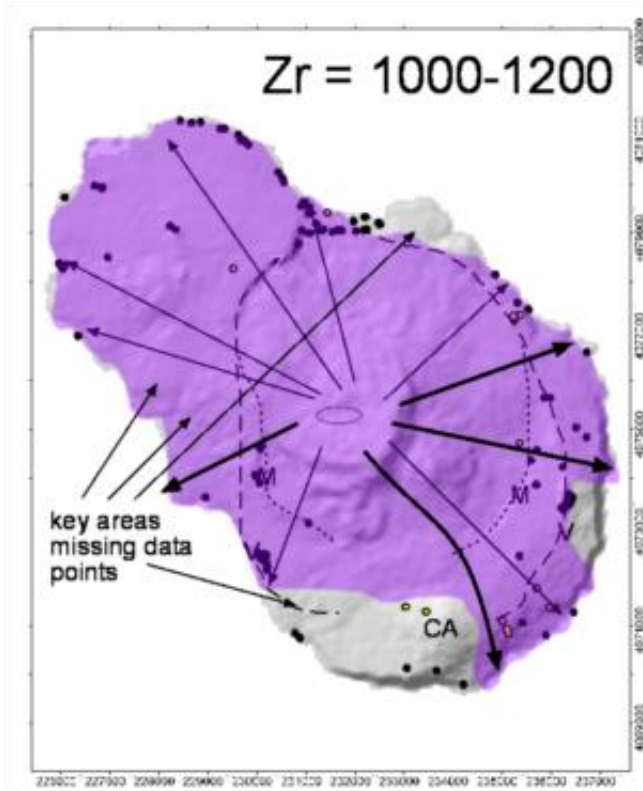


**Fig. 1-7: Artefact map for footprint  $t_6$ .** Locations that are not exposed to the base are highlighted in yellow. Of these, those that could impact interpretations as discussed in the text, are identified.

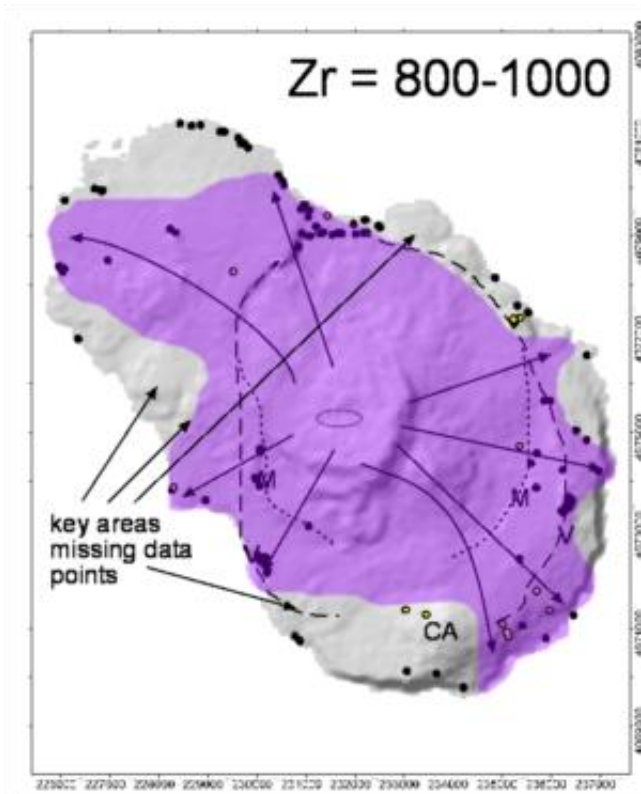


**Fig. 1-8: Artefact map for footprint  $t_7$ .** Locations that are not exposed to the base are highlighted in yellow. Of these, those that could impact interpretations as discussed in the text, are identified.

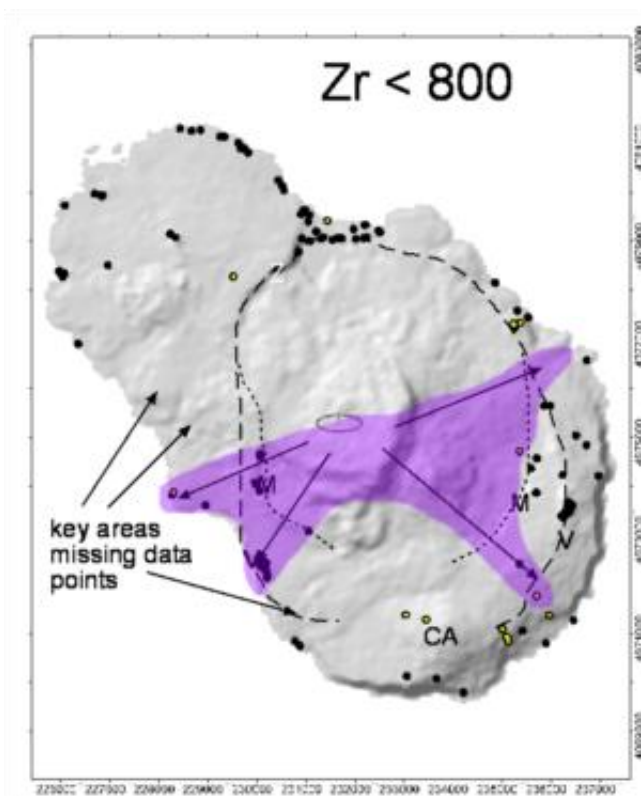


**Fig. 1-9: Artefact map for footprint  $t_8$ .** Locations that are not exposed to the base are highlighted in yellow. Of these, those that could impact interpretations as discussed in the text, are identified.

---

## **2.1. Understanding geophysical density currents: internal chemical mapping of an ignimbrite provides snap-shots on pyroclastic density current behaviour**

Rebecca Williams<sup>1</sup>, Michael J. Branney<sup>1</sup>, Tiffany L. Barry<sup>2</sup>.

<sup>1</sup> *University of Leicester, Geology Dept. University Road, Leicester, LE1 7RH, UK.*

<sup>2</sup> *Open University, Dept. of Earth & Environmental Sciences, Milton Keynes, MK7 6AA, UK.*

**Geophysical density currents are amongst the most catastrophic phenomenon on Earth [1, 2] Turbidity currents rapidly transport sediment thousands of kilometres across the ocean floor [3], and pyroclastic density currents are the most dangerous volcanic phenomenon faced by communities living near active volcanoes accounting for 26.8% of deaths caused by volcanic eruptions[4]. However, our understanding of density currents is hampered by the complete lack of any instrument or object that can withstand witnessing the emplacement of a density current. So how are we to understand how they evolve through time and space, how they react to topography and changes in source dynamics? The internal architecture of deposits from catastrophic density currents must be understood to provide a temporal history of the current.**

**Here, we study a low aspect-ratio ignimbrite, a product of particularly hazardous form of pyroclastic density current that erupts radially[5, 6] at high-velocity during caldera-forming eruptions. Using the pristine, welded Green Tuff ignimbrite on the island of Pantelleria, Italy, which is zoned from pantellerite at its base to trachyte at the top, we have chemically mapped the internal-architecture of the deposit to reconstruct how the current waxed and then waned during the**

**eruption and how the current encountered and overtopped topographic barriers, shifted direction with time, and at its climactic stage engulfed the entire island. These results show in detail that density currents can evolve significantly through the time of their emplacement, and have varying run-out distances, volumes, mass-fluxes and flow paths throughout their duration. This new knowledge impacts greatly on numerical models of geophysical mass flows.**

Low-aspect ratio ignimbrites are the deposits of particularly hazardous pyroclastic density currents which are thought to flow radially, simultaneously from source, overtopping all topographic barriers [5]. However, their behaviour is poorly understood. Field-based studies, as well as numerical and laboratory experiments, have shown that such currents are extremely mobile and can overwhelm topographic barriers at great distances from the source [6-9]. Yet other studies have shown that such currents can be reflected by obstacles [10, 11] or that deposition patterns can be affected by topography [12-15]. However, such features have yet to be documented in natural examples.

In this study we reveal the internal architecture of an ignimbrite sheet by using its well-defined chemical stratigraphy. Many ignimbrites exhibit some form of chemical zoning [16] and typically show an upward trend from more silicic compositions at their base to less evolved compositions at their top. This is commonly inferred to represent progressive tapping of a zoned magma chamber [17, 18] where the eruption taps into less dense, silicic portions of the magma chamber first, followed by progressive withdrawal from deeper depths of more mafic compositions. It follows that as a magma chamber is progressively tapped during an eruption, the aggrading ignimbrite sheet will similarly record the changing chemistry, but in reverse order; more silicic compositions at the base and least evolved at the top. There are several ignimbrites that are zoned, but

---

are compound; i.e. they are made up of several distinct flow units [19]. Here we examine a single flow unit which is dramatically zoned from pantellerite at its base to trachyte at its top. Using high resolution chemical variations within the ignimbrite we can establish chemical proxies for time and thereby examine slices or 'snap-shots' of the deposit at different stages of the eruption. This idea of using chemistry to demarcate time, otherwise called a chemical 'entrachron' (a line within an ignimbrite sheet that joins the first appearance of clasts or type of pumice that were entrained into the current at the same instant in time [20]) has been used to show how ignimbrites progressively aggrade during an eruption, through time using changing proportions of rhyolitic and andesitic pumices to define two or three zones within an ignimbrite [21, 22]. It has also been used to correlate co-ignimbrite lag breccias to their associated ignimbrites [23, 24].

The Green Tuff ignimbrite (50 ka [25], aspect ratio >1000), Pantelleria, was chosen as a case study for its excellently exposed outcrops both longitudinally from source and also laterally around the vent. Unfortunately, as with all ignimbrites, the outcrop is not 100% and the current is certain to have flowed into the surrounding sea. However, it is still an excellent example for this type of investigation for a number of reasons. (1) The deposit consists of a basal sub-plinian pumice and ash fall and an overlying ignimbrite, which is a single flow unit. The ignimbrite is not compound and represents a fluctuating quasi-steady current. (2) The deposit is welded almost entirely and the lack of a complex welding profile or internal vitrophyres supports the lithofacies interpretation that the ignimbrite is a single flow unit. (3) The viscous nature of the pyroclasts and their agglutination style of deposition mean that deposits were left on the entire landscape, including slopes up to 90°, which means that it is unlikely that the current was able to bypass without leaving evidence of its passing. (4) Most importantly, the Green Tuff ignimbrite shows linear, or gradational, zoning. A detailed geochemical study of a type

section reveals that the overall chemical zonation can be represented by variation within a single parameter (Fig. 1). A wide range of elements show a linear trend through the deposit, such as yttrium (Y) and neodymium (Nd), but zirconium (Zr) shows the widest range spanning over 1400 ppm, and is resistant to post-depositional weathering. To test whether whole rock Zr values reflect changing magma composition, as opposed to possible changes of phenocryst content, XRF whole rock data was compared to LA ICP-MS data for glass chemistry and it showed the same trend (Fig. 1). Therefore, we use whole rock Zr values as a proxy for all the chemical variations. As the deposit varies from pantellerite (peralkaline rhyolite) at its base to trachyte at its top, the whole rock Zr values decrease gradually from > 2000 ppm to < 800 ppm. This has enabled us to divide the deposit into eight different zones: the pantellerite end-member (>2000 ppm), the trachytic end-member (<800 ppm) and intervals of 200 ppm through the intervening deposit. Using over 80 field locations across the island of Pantelleria, and closely spaced vertical sampling ( $n > 400$ ) through sections with clearly defined upper and lower contacts, the zones (1-8) were mapped both regionally (longitudinally from source and laterally around the broadly circular sheet), and around topographic barriers draped by the ignimbrite. The study takes advantage of the young pristine deposit, superlative exposure, directional fabrics preserved in the deposit and topographic control.

The distribution of these zones across the island are interpreted to represent the ‘footprint’ of the pyroclastic density current during a short period of time during the eruption ( $t$ ). Therefore, studying the change in the footprint can shed light on how the current changed with time and how it responded to topographic features such as old caldera walls and scoria cones.

An initial phase of sub-plinian fallout was followed by pyroclastic fountaining. The first phase of the current ( $t_1$  of Fig. 2) was restricted to the north and east of the island by the old Zinedi scarp and Monastero caldera wall (Fig. 2). In the south the current overtopped the Monastero caldera wall but not the La Vecchia caldera wall outboard of this, except for a narrow breach west of the Cuddia Attalora shield. To the northwest, the current flowed unfettered across the low lying topography to the sea. During the next phase ( $t_2$  of Fig. 2) the current spread further northwards across the low lying area to the NNE, inundating the location of the modern town of Pantelleria and overtopping the Zinedi scarp. The footprint of the current also expanded eastwards overtopping parts of the Monastero caldera wall that were not reached in  $t_1$ . To the east of the Cuddia Attalora shield, a narrow breach of the La Vecchia caldera wall allowed the leading edge of the current to extend towards the sea. The breach of the La Vecchia caldera wall to the west of the Cuddia Attalora shield increased, and similarly the current reached the sea. As the current continued to wax ( $t_3$  of Fig. 2), its leading edge started to advance further up the Cuddia Attalora shield, but at this time it still failed to overtop the summit. However, to the east of this, the current reached the sea. There is further inundation of the Monastero caldera wall in the eastern sector; however the current was still constrained by the La Vecchia caldera wall outboard of this. During this time-slice the current's footprint extended in the northern sector as the leading edge of the current advanced NW. In the next phase ( $t_4$  of Fig. 2) the current continued to extend its runout path as it overtopped significant topographic barriers including wide sections of the La Vecchia caldera walls in the NE and WSW and notably, the summit region of the Cuddia Attalora shield. The northern sector of the island continued to be fully inundated. As the climactic phase of the eruption continued ( $t_5$  of Fig. 2), the current further inundated Cuddia Attalora and reached the sea beyond the shield. The large

Zinedi scarp in the north also became completely inundated. However, flow to the east and west remained restricted until the next phase. During  $t_6$  the current inundated the entire island, with only a few small exceptions, and reached the sea in all directions ( $t_6$  of Fig. 2). The La Vecchia caldera walls were overtopped both to the east and west. However, there are signs that the sustained current was starting to wane as its extent had retreated from the summit of the Cuddia Attalora shield, but rather was deflected around its eastern flank. In time-slice  $t_7$  (Fig. 2) the current waned and its footprint decreased significantly. The area over which it deposited reduced in size and the run-out distance for several sectors decreased. This is particularly evident in the northern sector. In the final phases of the current ( $t_8$  of Fig. 2), the current no longer travels to the north of the island and once again becomes restricted by the topographic barriers to the south. The current is mainly directed to the west and east.

The entrachron stratigraphy demonstrates that even though the deposit is thin and broadly circular, the current was not 'virtually instantaneous', i.e. in the first instances of the eruption the current did not flow out to the distal limit of the ignimbrite sheet in all directions. Rather, the leading edge of the rapid current slowly advanced with time, progressively inundating the island as the current gradually waxed, and then later it progressively retreated source-ward while the current slowly waned (Fig. 3). This demonstrates that the model for rapid radial flow as originally conceived for the Taupo ignimbrite [6, 26, 27] in which the initial current velocity was very high (driven by kinetic energy due to column collapse from >50 km) so that the current rapidly surmounted topographic hills to its distal limit, is not a tenable model for the Green Tuff ignimbrite. Rather, the run-out distance was probably a function of mass flux [20, 28] and as the mass flux slowly changed, so did the run-out distance. True radial flow was achieved (barring the effect of topographic obstacles) only during times of peak flow ( $t_4$ .

o). In this period, the ignimbrite underwent true progressive aggradation to form a layer-cake architecture. Shingling is observed in a couple of locations where the current shifted laterally with time (Fig. 3). During periods of initial waxing and post-climactic waning, shifting flow was most pronounced and the resultant internal architecture of the flow-unit is complex.

This complex, diachronous emplacement of the ignimbrite has implications for estimates of volume, mass flux and run-out distances and has implications for numerical models that rely on such parameters to simulate pyroclastic density currents and other geophysical mass flows. Firstly, the run-out distance increased and then decreased with time. This would invalidate the application of the energy line concept (H/L[29]) when total run-out distance is considered for an entire ignimbrite sheet. Secondly, volumes for the different time-slices of the Green Tuff ignimbrite have been calculated using the footprint area and an average thickness for each chemical zone. The ignimbrite volume erupted in successive time slices increased then decreased towards the end of the eruption (Fig. 4). The radial time-slices only account for less than 50% of the total volume of the ignimbrite. Thus, if volume is interpreted as a proxy for mass flux, it is clear that the assumption that the entire current was emplaced radially, immediately, would greatly over estimate the actual mass fluxes involved.

This study is the first integrated field and laboratory investigation to test long held hypotheses of the behaviour of pyroclastic density currents. We show that: (1) the current did not flow radially for its entire duration; (2) the leading edge of the current progressively advanced during the waxing stage of the current and then retreated as the current waned; (3) the current shifted laterally with time, resulting in a broadly circular sheet; and (4) the current was not able to overtop topographic barriers at all stages during the eruption.

**Methods**

XRF analyses were carried out at the University of Leicester using a Philips PW1400 X-Ray Fluorescence spectrometer which operates 3Kw Rhodium (Rh) anode side window X-Ray tubes powered by standard Philips PW 1730 series generators.

Operating conditions are optimised for sensitivity and resolution.

Laser ablation analysis was performed on polished 100 µm sections at the Open University on an Agilent 7500A quadrupole ICP-MS coupled with a New Wave UP213 Nd:Yag deep UV (213 nm) laser system.

**Acknowledgements**

We thank N. Marsh for XRF analysis, Dr S. Hammond for assistance with LA ICP-MS analysis and acknowledge NERC studentship to R Williams.

**Author contribution**

M.J.B conceived and designed the research program; R.W. conducted the field work, the sample preparation and geochemical analysis and analysed the data; T.L.B advised on the use of the geochemistry.

Reprints and permissions information is available at [npg.nature.com/reprintsandpermissions](http://npg.nature.com/reprintsandpermissions)

The authors declare no competing financial interests.

Correspondence and requests for materials should be addressed to [rw89@le.ac.uk](mailto:rw89@le.ac.uk)

1. Heezen, B.C. and W.M. Ewing, *Turbidity currents and submarine slumps, and the 1929 Grand Banks [Newfoundland] earthquake*. American Journal of Science, 1954. **250**(12): p. 849-873.
2. Voight, B., *The 1985 Nevado-Del-Ruiz Volcano Catastrophe - Anatomy and Retrospection*. Journal of Volcanology and Geothermal Research, 1990. **42**(1-2): p. 151-188.
3. Talling, P.J., L.A. Amy, and R.B. Wynn, *New insight into the evolution of large-volume turbidity currents: comparison of turbidite shape and previous modelling results*. Sedimentology, 2007. **54**(4): p. 737-769.
4. Tanguy, J.C., et al., *Victims from volcanic eruptions: a revised database*. Bulletin of Volcanology, 1998. **60**(2): p. 137-144.
5. Walker, G.P.L., R.F. Heming, and C.J.N. Wilson, *Low-Aspect Ratio Ignimbrites*. Nature, 1980. **283**(5744): p. 286-287.
6. Wilson, C.J.N., *The Taupo Eruption, New-Zealand .2. The Taupo Ignimbrite*. Philosophical Transactions of the Royal Society of London Series a-Mathematical Physical and Engineering Sciences, 1985. **314**(1529): p. 229-&.
7. Aramaki, S. and T. Ui, *The Aira and Ata pyroclastic flows and related caldera and depressions in southern Kyushu, Japan*. Bulletin of Volcanology, 1966. **29**: p. 29-47.
8. Fisher, R.V., et al., *Mobility of a Large-Volume Pyroclastic Flow - Emplacement of the Campanian Ignimbrite, Italy*. Journal of Volcanology and Geothermal Research, 1993. **56**(3): p. 205-220.
9. Miller, T.P. and R.L. Smith, *Spectacular Mobility of Ash Flows around Aniakchak and Fisher Calderas, Alaska*. Geology, 1977. **5**(3): p. 173-176.
10. Edwards, D.A., et al., *On Experimental Reflected Density Currents and the Interpretation of Certain Turbidites*. Sedimentology, 1994. **41**(3): p. 437-461.
11. Kneller, B., et al., *Oblique Reflection of Turbidity Currents*. Geology, 1991. **19**(3): p. 250-252.
12. Alexander, J. and S. Morris, *Observations on Experimental, Nonchannelized High-Concentration Turbidity Currents and Variations in Deposits around Obstacles*. Journal of Sedimentary Research Section a-Sedimentary Petrology and Processes, 1994. **64**(4): p. 899-909.
13. Kubo, Y., *Experimental and numerical study of topographic effects on deposition from two-dimensional, particle-driven density currents*. Sedimentary Geology, 2004. **164**(3-4): p. 311-326.
14. Bursik, M.I. and A.W. Woods, *The effects of topography on sedimentation from particle-laden turbulent density currents*. Journal of Sedimentary Research, 2000. **70**(1): p. 53-63.
15. Woods, A.W., M.I. Bursik, and A.V. Kurbatov, *The interaction of ash flows with ridges*. Bulletin of Volcanology, 1998. **60**(1): p. 38-51.
16. Bachmann, O. and G.W. Bergantz, *Deciphering magma chamber dynamics from styles of compositional zoning in large silicic ash flow sheets*. Reviews in Mineralogy and Geochemistry, 2008. **69**(1): p. 651-674.
17. Macdonald, R., et al., *STRONG COMPOSITIONAL ZONATION IN PERALKALINE MAGMA - MENENGAI, KENYA RIFT-VALLEY*. Journal of Volcanology and Geothermal Research, 1994. **60**(3-4): p. 301-325.
18. Leat, P.T., R. Macdonald, and R.L. Smith, *GEOCHEMICAL EVOLUTION OF THE MENENGAI CALDERA VOLCANO, KENYA*. Journal of Geophysical Research, 1984. **89**(NB10): p. 8571-8592.
19. Fierstein, J. and C.J.N. Wilson, *Assembling an ignimbrite: Compositionally defined eruptive packages in the 1912 Valley of Ten Thousand Smokes ignimbrite, Alaska*. Geological Society of America Bulletin, 2005. **117**(7-8): p. 1094-1107.
20. Branney, M.J. and B.P. Kokelaar, *Pyroclastic density currents and the sedimentation of ignimbrites*. Memoir / Geological Society of London ; no.27. 2002, London: The Geological Society. 143.

21. Branney, M.J. and P. Kokelaar, *Giant bed from a sustained catastrophic density current flowing over topography: Acatlan ignimbrite, Mexico*. *Geology*, 1997. **25**(2): p. 115-118.
22. Carrasco-Nunez, G. and M.J. Branney, *Progressive assembly of a massive layer of ignimbrite with a normal-to-reverse compositional zoning: the Zaragoza ignimbrite of central Mexico*. *Bulletin of Volcanology*, 2005. **68**(1): p. 3-20.
23. Druitt, T.H. and C.R. Bacon, *Lithic Breccia and Ignimbrite Erupted during the Collapse of Crater Lake Caldera, Oregon*. *Journal of Volcanology and Geothermal Research*, 1986. **29**(1-4): p. 1-32.
24. Wright, J.V. and G.P.L. Walker, *Eruption, Transport and Deposition of Ignimbrite - a Case-Study from Mexico*. *Journal of Volcanology and Geothermal Research*, 1981. **9**(2-3): p. 111-131.
25. Mahood, G.A. and W. Hildreth, *Geology of the peralkaline volcano at Pantelleria, Strait of Sicily*. *Bulletin of Volcanology*, 1986. **48**(2-3): p. 143-172.
26. Wilson, C.J.N. and W. Hildreth, *The Bishop Tuff: New insights from eruptive stratigraphy*. *Journal of Geology*, 1997. **105**(4): p. 407-439.
27. Wilson, C.J.N. and G.P.L. Walker, *The Taupo Eruption, New-Zealand .1. General-Aspects*. *Philosophical Transactions of the Royal Society of London Series a-Mathematical Physical and Engineering Sciences*, 1985. **314**(1529): p. 199-&.
28. Bursik, M.I. and A.W. Woods, *The dynamics and thermodynamics of large ash flows*. *Bulletin of Volcanology*, 1996. **58**(2-3): p. 175-193.
29. Sheridan, M.F., *Emplacement of pyroclastic flows: A review*, in *Ash-flow tuffs*, C.E. Chapin and W.E. Elston, Editors. 1979, *Geol. Soc. Am., Special Papers*. p. 125-136.

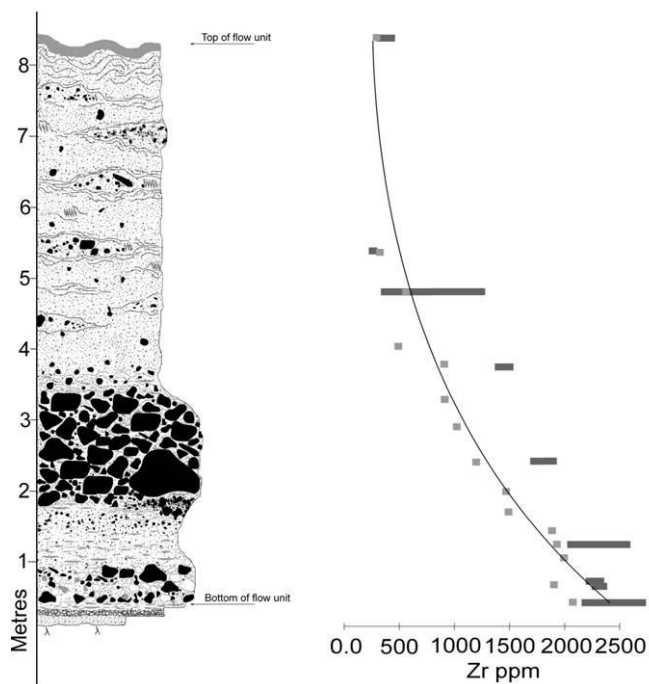


**Figure 1: Graphic log of the Green Tuff ignimbrite type section showing the linear grading of Zr values through the deposit. Pale grey squares show values from XRF whole rock analyses and dark grey shaded area shows range of values obtained for LA ICP MS spot analyses of matrix. Polynomial trend-line used. Note large gap due to inaccessible cliff: this part of the unit has been sampled extensively at other locations.**

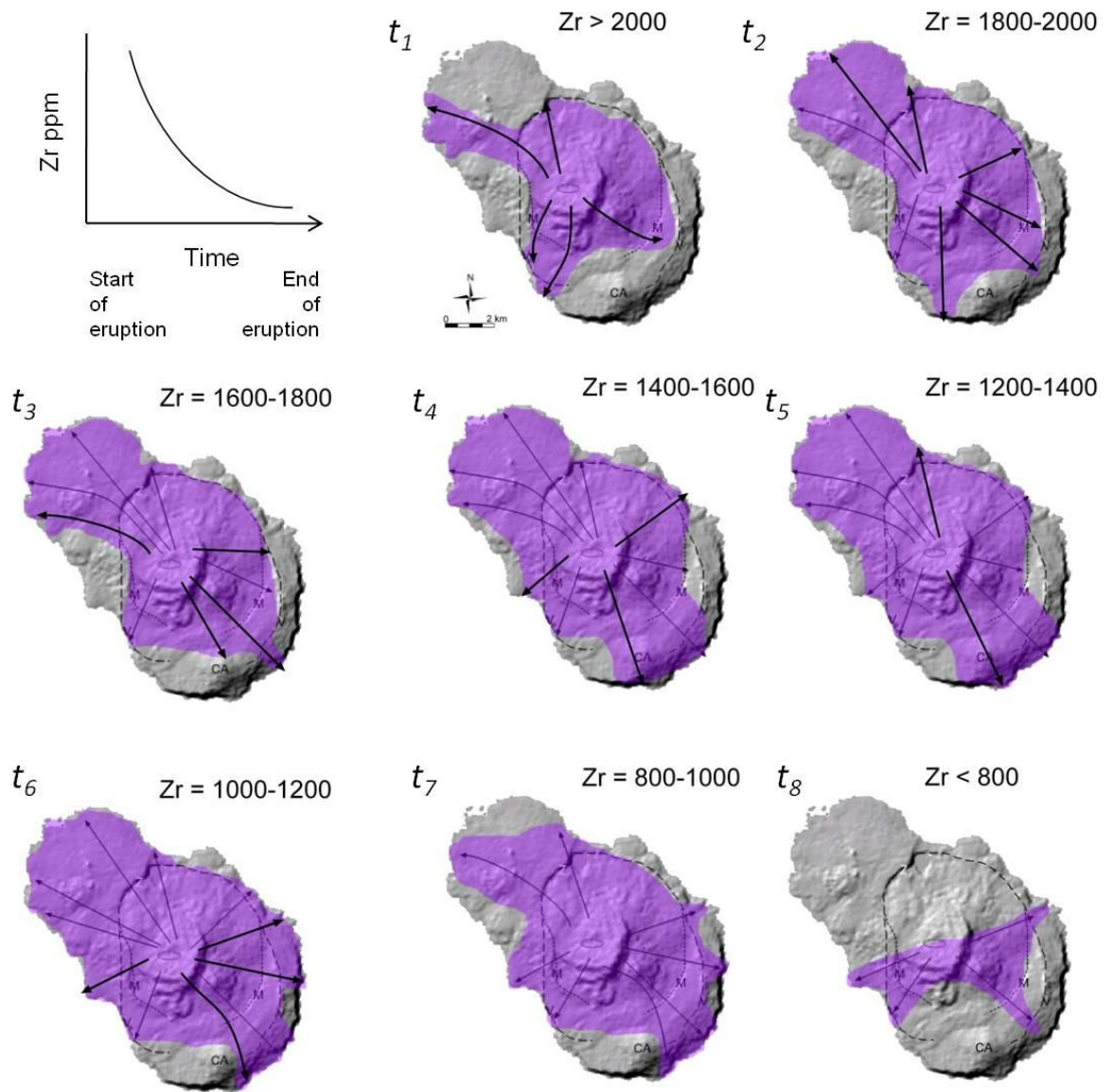


**Figure 2.** Evolving footprint of the density current shown at different time-slices through the current's duration from start ( $t_1$ ) to finish ( $t_8$ ) using Zr ppm as a proxy for glass and mineralogy changes. Arrows indicate inferred current directions from source. The area of inundation increases as the current waxes to a climactic phase ( $t_{4,5}$ ) and then decreases as the current wanes. For example, during phase  $t_7$ , the footprint area has decreased although the eruption is still continuing showing that the area that is being deposited on land is decreasing as the current is waning. Heavy arrows indicate changes in current inundation from previous time-slice (pale arrows). M - Monastero caldera wall, V - La Vecchia caldera wall, Z - Zinedi scarp, CA - Cuddia Attalora shield.

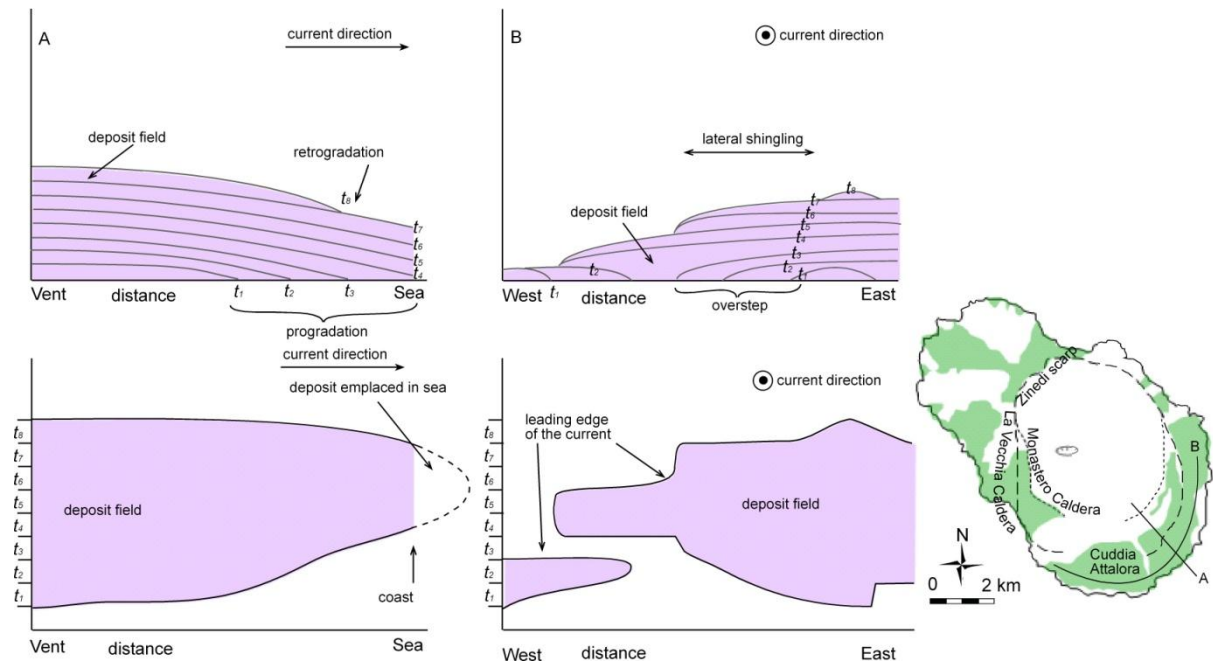


**Figure 3.** Schematic cross-sections through the deposit field showing entrachron architecture at three locations. Cross sections are not to scale. **A:** Significant progradation is seen in the south as the current waxed through its initial stages ( $t_{1-4}$ ). During the climactic phase of the current, layer-cake stratigraphy is seen when the current is truly radial ( $t_{5-7}$ ). During the final phase of the current the leading edge retrogrades ( $t_8$ ). **B:** Lateral shingling is seen in the south of the island. During the first phase of the current the leading edge of the current is limited to narrow fingers ( $t_{1-2}$ ). As the current waxed, the current shifted laterally to over step its own deposit from east to west ( $t_{2-4}$ ). As the current waned, the current again shifted eastward ( $t_{5-7}$ ) until only a narrow finger of the current remained ( $t_8$ ).

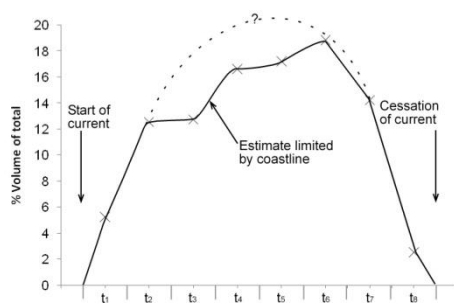


**Figure 4.** Volume of the ignimbrite per time slice, represented as a % of the total volume. The dashed line represents uncertainty where total volume would only be recorded offshore.

- Aines, R. D. & Lowenstein, J. B. 1990. Evidence for CO<sub>2</sub> rich vapor in pantellerite magma chambers. *Eos Transactions*, **43**, 1700.
- Alexander, J. & Morris, S. 1994. Observations on Experimental, Nonchannelized High-Concentration Turbidity Currents and Variations in Deposits around Obstacles. *Journal of Sedimentary Research Section a-Sedimentary Petrology and Processes*, **64**, 899-909.
- Anastasakis, G. & Pe-Piper, G. 2006. An 18 m thick volcanoclastic interval in Pantelleria Trough, Sicily Channel, deposited from a large gravitative flow during the Green Tuff eruption. *Marine Geology*, **231**, 201-219.
- Andrews, G. & Branney, M. J. 2010. Emplacement and rheomorphic deformation of a large, lava-like rhyolitic ignimbrite: Grey's Landing, southern Idaho. *GSA Bulletin*, **In press**.
- Andrews, G. D. M. & Branney, M. J. 2005. Folds, fabrics, and kinematic criteria in rheomorphic ignimbrites of the Snake River Plain, Idaho: insights into emplacement and flow. *In: Pederson J, D. C. (ed.) Interior Western United States: GSA Field Guide* **6**, 310-328.
- Andrews, G. D. M., Branney, M. J., Bonnicksen, B. & McCurry, M. 2008. Rhyolitic ignimbrites in the Rogerson Graben, southern Snake River Plain volcanic province: volcanic stratigraphy, eruption history and basin evolution. *Bulletin of Volcanology*, **70**, 269-291.
- Aramaki, S. & Ui, T. 1966. The Aira and Ata pyroclastic flows and related caldera and depressions in southern Kyushu, Japan. *Bulletin of Volcanology*, **29**, 29-47.
- Avanzinelli, R., Bindi, L., Menchetti, S. & Conticelli, S. 2004. Crystallisation and genesis of peralkaline magmas from Pantelleria Volcano, Italy: an integrated petrological and crystal-chemical study. *Lithos*, **73**, 41-69.
- Bachmann, O. & Bergantz, G. W. 2008. Deciphering magma chamber dynamics from styles of compositional zoning in large silicic ash flow sheets. *Reviews in Mineralogy and Geochemistry*, **69**, 651-674.
- Bacon, C. R. 1983. Eruptive history of Mount Mazama and Crater Lake Caldera, Cascade Range, USA. *Journal of Volcanology and Geothermal Research*, **18**, 57-115.
- Baer, E. M., Fisher, R. V., Fuller, M. & Valentine, G. 1997. Turbulent transport and deposition of the Ito pyroclastic flow; determinations using anisotropy of magnetic susceptibility. *Journal of Geophysical Research*, **102**, 22.
- Bailey, D. K., Weaver, S. D. & Sutherland, D. S. 1975. Eburru Volcano - Re-Appraisal of Previous Sample Population. *Contributions to Mineralogy and Petrology*, **50**, 47-48.

- Baker, D. H. & Vaillancourt, J. 1994. The viscosity of F + H<sub>2</sub>O-bearing peralkaline and peraluminous rhyolitic melts. *Mineralogical Magazine*, **58A**, 40-41.
- Barberi, F., Ghigliotti, M., Macedonio, G., Orellana, H., Pareschi, M. T. & Rosi, M. 1992. Volcanic Hazard Assessment of Guagua Pichincha (Ecuador) Based on Past Behavior and Numerical-Models. *Journal of Volcanology and Geothermal Research*, **49**, 53-68.
- Barberi, F., Innocenti, F., Lirer, L., Munno, R., Pescatore, T. & Santacroce, R. 1978. The Campanian ignimbrite; a major prehistoric eruption in the Neapolitan area (Italy). *Bulletin Volcanologique*, **41**, 10-29.
- Barclay, J., Carroll, M. R., Houghton, B. F. & Wilson, C. J. N. 1996. Pre-eruptive volatile content and degassing history of an evolving peralkaline volcano. *Journal of Volcanology and Geothermal Research*, **74**, 75-87.
- Battaglia, M. 1993. On pyroclastic flow emplacement. *Journal of Geophysical Research*, **98**, 22.
- Beresford, S. W. & Cole, J. W. 2000. Kaingaroa Ignimbrite, Taupo Volcanic Zone, New Zealand: evidence for asymmetric caldera subsidence of the Reporoa Caldera. *New Zealand Journal of Geology and Geophysics*, **43**, 471-481.
- Bindeman, I. 2008. Oxygen isotopes in mantle and crustal magmas as revealed by single crystal analysis. *Reviews in Mineralogy and Geochemistry*, **69**, 445-478.
- Black, S., Macdonald, R. & Kelly, M. R. 1997. Crustal origin for peralkaline rhyolites from Kenya: Evidence from U-series disequilibria and Th-isotopes. *Journal of Petrology*, **38**, 277-297.
- Blake, S. 1981. Eruptions from Zoned Magma Chambers. *Journal of the Geological Society*, **138**, 281-287.
- Borsi, S., Marinelli, G., Mazzoncini, F., Mittempergher, M. & Tedesco, C. 1963. Reconnaissance of some ignimbrites at Pantelleria and Eolian islands. *Bulletin of Volcanology*, **25**, 359-363.
- Bouma, A. H. 1962. *Sedimentology of some Flysch deposits; a graphic approach to facies interpretation*. ed.) Elsevier, Amsterdam,
- Bourdier, J. L. & Abdurachman, E. K. 2001. Decoupling of small-volume pyroclastic flows and related hazards at Merapi volcano, Indonesia. *Bulletin of Volcanology*, **63**, 309-325.
- Branney, M. J., Barry, T. L. & Godchaux, M. 2004. Sheathfolds in rheomorphic ignimbrites. *Bulletin of Volcanology*, **66**, 485-491.
- Branney, M. J., Bonnicksen, B., Andrews, G. D. M., Ellis, B., Barry, T. L. & McCurry, M. 2008. 'Snake River (SR)-type' volcanism at the Yellowstone hotspot track:

- distinctive products from unusual, high-temperature silicic super-eruptions. *Bulletin of Volcanology*, **70**, 293-314.
- Branney, M. J. & Kokelaar, B. P. 2002. Pyroclastic density currents and the sedimentation of ignimbrites. *Memoir / Geological Society of London ; no.27*, 143.
- Branney, M. J. & Kokelaar, P. 1992. A Reappraisal of Ignimbrite Emplacement - Progressive Aggradation and Changes from Particulate to Nonparticulate Flow during Emplacement of High-Grade Ignimbrite. *Bulletin of Volcanology*, **54**, 504-520.
- Branney, M. J. & Kokelaar, P. 1997. Giant bed from a sustained catastrophic density current flowing over topography: Acatlan ignimbrite, Mexico. *Geology*, **25**, 115-118.
- Brown, R. J. 2001. *Eruption history and depositional processes of the Poris ignimbrite of Tenerife and the Glaramara Tuff of the English Lake District*. PhD thesis, University of Leicester.
- Brown, R. J., Barry, T. L., Branney, M. J., Pringle, M. S. & Bryan, S. E. 2003. The Quaternary pyroclastic succession of southeast Tenerife, Canary Islands: explosive eruptions, related caldera subsidence, and sector collapse. *Geological Magazine*, **140**, 265-288.
- Brown, R. J. & Branney, M. 2004. Bypassing and diachronous deposition from density currents: Evidence from a giant regressive bed form in the Poris ignimbrite, Tenerife, Canary Islands. *Geology*, **32**, 445-448.
- Brown, R. J. & Branney, M. J. 2004. Event-stratigraphy of a caldera-forming ignimbrite eruption on Tenerife: the 273 ka Poris Formation. *Bulletin of Volcanology*, **66**, 392-416.
- Bryan, S. E., Cas, R. A. F. & Marti, J. 1998. Lithic breccias in intermediate volume phonolitic ignimbrites, Tenerife (Canary Islands); constraints on pyroclastic flow depositional processes. *Journal of Volcanology and Geothermal Research*, **81**, 269-296.
- Buddington, A. F. & Lindsley, D. H. 1964. Iron-titanium oxide minerals and synthetic equivalents. *Journal of Petrology*, **5**, 310-357.
- Buesch, D. C. 1992. Incorporation and Redistribution of Locally Derived Lithic Fragments within a Pyroclastic Flow. *Geological Society of America Bulletin*, **104**, 1193-1207.
- Burgisser, A. 2005. Physical volcanology of the 2,050 BP caldera-forming eruption of Okmok volcano, Alaska. *Bulletin of Volcanology*, **67**, 497-525.
- Bursik, M. I. & Woods, A. W. 1996. The dynamics and thermodynamics of large ash flows. *Bulletin of Volcanology*, **58**, 175-193.

- Bursik, M. I. & Woods, A. W. 2000. The effects of topography on sedimentation from particle-laden turbulent density currents. *Journal of Sedimentary Research*, **70**, 53-63.
- Butler, G. W. & Perry, G. H. 1892. On the Matter Thrown up During the Submarine Eruption North-West of Pantelleria, October 1891. *Nature*, **45**, 251-252.
- Calder, E. S., Cole, P. D., Dade, W. B., Druitt, T. H., Hoblitt, R. P., Huppert, H. E., Ritchie, L., Sparks, R. S. J. & Young, S. R. 1999. Mobility of pyroclastic flows and surges at the Soufriere Hills Volcano, Montserrat. *Geophysical Research Letters*, **26**, 537-540.
- Capaccioni, B. & Cuccoli, F. 2005. Spatter and welded air fall deposits generated by fire-fountaining eruptions: Cooling of pyroclasts during transport and deposition. *Journal of Volcanology and Geothermal Research*, **145**, 263-280.
- Capaccioni, B., Nappi, G. & Valentini, L. 2001. Directional fabric measurements: an investigative approach to transport and depositional mechanisms in pyroclastic flows. *Journal of Volcanology and Geothermal Research*, **107**, 275-292.
- Carey, S. N., Sigurdsson, H. & Sparks, R. S. J. 1988. Experimental studies of particle-laden plumes. *J. Geophys. Res.*, **93**, 15314-15328.
- Carmichael, I. S. E. 1967. The iron-titanium oxides of salic volcanic rocks and their associated ferromagnesian silicates. *Contributions to Mineralogy and Petrology*, **14**, 36-64.
- Carmichael, I. S. E. & MacKenzie, W. S. 1963. Feldspar-liquid equilibria in pantellerites; an experimental study. *Am J Sci*, **261**, 382-396.
- Carrasco-Nunez, G. & Branney, M. J. 2005. Progressive assembly of a massive layer of ignimbrite with a normal-to-reverse compositional zoning: the Zaragoza ignimbrite of central Mexico. *Bulletin of Volcanology*, **68**, 3-20.
- Carroll, M. R. 2005. Chlorine solubility in evolved alkaline magmas. *Annals of Geophysics*, **48**, 619-631.
- Cas, R. A. F. & Wright, J. V. 1987. *Volcanic successions, modern and ancient; a geological approach to processes, products and successions*. ed.). Allen & Unwin London, United Kingdom,
- Catalano, S. G., G.; Lanzafame, G.; Tortorici, L. 2007. Fenomeni di reomorfismo nell'Ignimbrite Verdi di Pantelleria: strutture di flusso primario o secondario? *Rendiconti Società Geologica Italiana, Nuova Serie*, **4**, 174-176.
- Chapin, C. E. & Lowell, G. R. 1979. Primary and secondary flow structures in ash-flow tuffs of the Gribbles Run paleovalley, central Colorado. *Special Paper - Geological Society of America*, 137-154.

- Choux, C., Druitt, T. & Thomas, N. 2004. Stratification and particle segregation in flowing polydisperse suspensions, with applications to the transport and sedimentation of pyroclastic density currents. *Journal of Volcanology and Geothermal Research*, **138**, 223-241.
- Civetta, L., Cornette, Y., Gillot, P. Y. & Orsi, G. 1988. The Eruptive History of Pantelleria (Sicily Channel) in the Last 50 Ka. *Bulletin of Volcanology*, **50**, 47-57.
- Civetta, L., D'Antonio, M., Orsi, G. & Tilton, G. R. 1998. The geochemistry of volcanic rocks from Pantelleria island, Sicily channel: Petrogenesis and characteristics of the mantle source region. *Journal of Petrology*, **39**, 1453-1491.
- Civile, D., Lodolo, E., Accettella, D., Geletti, R., Ben-Avraham, Z., Deponte, M., Facchin, L., Ramella, R. & Romeo, R. 2010. The Pantelleria graben (Sicily Channel, Central Mediterranean): An example of intraplate 'passive' rift. *Tectonophysics*, **490**, 173-183.
- Civile, D., Lodolo, E., Tortorici, L., Lanzafame, G. & Brancolini, G. 2008. Relationships between magmatism and tectonics in a continental rift: The Pantelleria Island region (Sicily Channel, Italy). *Marine Geology*, **251**, 32-46.
- Cleary, P. W. & Campbell, C. S. 1993. Self-lubrication for long runout landslides; examination by computer simulation. *Journal of Geophysical Research*, **98**, 21.
- Cornette, Y., Crisci, G. M., Gillot, P. Y. & Orsi, G. 1983. Recent volcanic history of pantelleria: A new interpretation. *Journal of Volcanology and Geothermal Research*, **17**, 361-373.
- Dade, W. B. & Huppert, H. E. 1996. Emplacement of the Taupo ignimbrite by a dilute turbulent flow. *Nature*, **381**, 509-512.
- De Rita, D., Giordano, G. & Milli, S. 1998. Forestepping-backstepping stacking pattern of volcanoclastic successions: Roccamonfina volcano, Italy (vol 78, pg 267, 1997). *Journal of Volcanology and Geothermal Research*, **80**, 155-+.
- Dellino, P., Zimanowski, B., Büttner, R., La Volpe, L., Mele, D. & Sulpizio, R. 2007. Large-scale experiments on the mechanics of pyroclastic flows: Design, engineering, and first results. *J. Geophys. Res.*, **112**, B04202.
- Denlinger, R. P. 1987. A model for generation of ash clouds by pyroclastic flows, with application to the 1980 eruptions at Mount St. Helens, Washington. *Journal of Geophysical Research*, **92**, 10.
- Dingwell, D. B., Hess, K. U. & Romano, C. 1998. Extremely fluid behavior of hydrous peralkaline rhyolites. *Earth and Planetary Science Letters*, **158**, 31-38.
- Dolan, J., Beck, C. & Ogawa, Y. 1989. Upslope Deposition of Extremely Distal Turbidites - an Example from the Tiburon Rise, West-Central Atlantic. *Geology*, **17**, 990-994.

- Doyle, E. E., Hogg, A. J., Mader, H. M. & Sparks, R. S. J. 2010. A two-layer model for the evolution and propagation of dense and dilute regions of pyroclastic currents. *Journal of Volcanology and Geothermal Research*, **190**, 365-378.
- Druitt, T. H. 1985. Vent evolution and lag breccia formation during the Cape Riva eruption of Santorini, Greece. *Journal of Geology*, **93**, 439-454.
- Druitt, T. H. 1992. Emplacement of the 18 May 1980 Lateral Blast Deposit Ene of Mount St-Helens, Washington. *Bulletin of Volcanology*, **54**, 554-572.
- Druitt, T. H. 1995. Settling behaviour of concentrated dispersions and some volcanological applications. *Journal of Volcanology and Geothermal Research*, **65**, 27-39.
- Druitt, T. H. 1998. Pyroclastic density currents. In: Gilbert, J. S. a. S., R.S.J. (ed.) *The Physics of Explosive Volcanic Eruptions*. Geological Society, Special Publications, London, **145**, 145-182.
- Druitt, T. H. & Bacon, C. R. 1986. Lithic Breccia and Ignimbrite Erupted during the Collapse of Crater Lake Caldera, Oregon. *Journal of Volcanology and Geothermal Research*, **29**, 1-32.
- Duller, R. A., Mountney, N. P., Russell, A. J. & Cassidy, N. C. 2008. Architectural analysis of a volcanoclastic jokulhlaup deposit, southern Iceland: sedimentary evidence for supercritical flow. *Sedimentology*, **55**, 939-964.
- Edgar, C. J., Wolff, J. A., Nichols, H. J., Cas, R. A. F. & Marti, J. 2002. A complex quaternary ignimbrite-forming phonolitic eruption: the poris member of the Diego Hernandez Formation (Tenerife, Canary Islands). *Journal of Volcanology and Geothermal Research*, **118**, 99-130.
- Edwards, D. A., Leeder, M. R., Best, J. L. & Pantin, H. M. 1994. On Experimental Reflected Density Currents and the Interpretation of Certain Turbidites. *Sedimentology*, **41**, 437-461.
- Ellis, B. 2009. *Rhyolitic explosive eruptions of the central Snake River Plain, Idaho: Investigations of the Lower Cassia Mountains succession and surrounding areas*. PhD thesis, University of Leicester.
- Esperanca, S. & Crisci, G. M. 1995. The island of Pantelleria: A case for the development of DMM-HIMU isotopic compositions in a long-lived extensional setting. *Earth and Planetary Science Letters*, **136**, 167-182.
- Ferriz, H. & Mahood, G. A. 1984. Eruption Rates and Compositional Trends at Los-Humeros-Volcanic-Center, Puebla, Mexico. *Journal of Geophysical Research*, **89**, 8511-8524.
- Fierstein, J. & Wilson, C. J. N. 2005. Assembling an ignimbrite: Compositionally defined eruptive packages in the 1912 Valley of Ten Thousand Smokes ignimbrite, Alaska. *Geological Society of America Bulletin*, **117**, 1094-1107.

- Finetti, I. 1984. Geophysical study of the Sicily Channel rift zone. *Bollettino di Geofisica Teorica ed Applicata*, **26**, 3-28.
- Fisher, R. V. 1966. Mechanism of deposition from pyroclastic flows. *Am J Sci*, **264**, 350-363.
- Fisher, R. V. 1990. Transport and Deposition of a Pyroclastic Surge across an Area of High Relief - the 18 May 1980 Eruption of Mount St-Helens, Washington. *Geological Society of America Bulletin*, **102**, 1038-1054.
- Fisher, R. V., Orsi, G., Ort, M. & Heiken, G. 1993. Mobility of a Large-Volume Pyroclastic Flow - Emplacement of the Campanian Ignimbrite, Italy. *Journal of Volcanology and Geothermal Research*, **56**, 205-220.
- Fisher, R. V. & Schmincke, H.-U. 1984. *Pyroclastic rocks*. ed.).Springer-Verlag : Berlin, Federal Republic of Germany, Federal Republic of Germany,
- Freundt, A. 1998. The formation of high-grade ignimbrites, I: Experiments on high- and low-concentration transport systems containing sticky particles. *Bulletin of Volcanology*, **59**, 414-435.
- Freundt, A. 1999. Formation of high-grade ignimbrites - Part II. A pyroclastic suspension current model with implications also for low-grade ignimbrites. *Bulletin of Volcanology*, **60**, 545-567.
- Freundt, A. & Schmincke, H. U. 1992. Mixing of rhyolite, trachyte, and basalt magma erupted from a vertically and laterally zoned reservoir, composite flow P1, Gran Canaria. *Contributions to Mineralogy and Petrology*, **112**, 1-19.
- Gardner, J. E., Burgisser, A. & Stelling, P. 2007. Eruption and deposition of the Fisher Tuff (Alaska): Evidence for the evolution of pyroclastic flows. *Journal of Geology*, **115**, 417-435.
- Gibson, I. L. 1794. A review of the geology, petrology and geochemistry of the Volcano Fantale. *Bulletin of Volcanology*, **38**, 791-802.
- Gibson, I. L. 1970. A Pantelleritic Welded Ash-Flow Tuff from Ethiopian Rift Valley. *Contributions to Mineralogy and Petrology*, **28**, 89-&.
- Gioncada, A. & Landi, P. 2010. The pre-eruptive volatile contents of recent basaltic and pantelleritic magmas at Pantelleria (Italy). *Journal of Volcanology and Geothermal Research*, **189**, 191-201.
- Giordano, D., Nichols, A. R. L. & Dingwell, D. B. 2005. Glass transition temperatures of natural hydrous melts: a relationship with shear viscosity and implications for the welding process. *Journal of Volcanology and Geothermal Research*, **142**, 105-118.

- Giordano, G. 1998. The effect of paleotopography on lithic distribution and facies associations of small volume ignimbrites: the WTT Cupa (Roccamonfina volcano, Italy). *Journal of Volcanology and Geothermal Research*, **87**, 255-273.
- Giordano, G., De Rita, D., Cas, R. & Rodani, S. 2002. Valley pond and ignimbrite veneer deposits in the small-volume phreatomagmatic 'Peperino Albano' basic ignimbrite, Lago Albano maar, Colli Albani volcano, Italy: influence of topography. *Journal of Volcanology and Geothermal Research*, **118**, 131-144.
- Giordano, G., Porreca, M., Musacchio, P. & Mattei, M. 2008. The Holocene Secche di Lazzaro phreatomagmatic succession (Stromboli, Italy): evidence of pyroclastic density current origin deduced by facies analysis and AMS flow directions. *Bulletin of Volcanology*, **70**, 1221-1236.
- Girolami, L., Druitt, T. H., Roche, O. & Khrabrykh, Z. 2008. Propagation and hindered settling of laboratory ash flows. *Journal of Geophysical Research-Solid Earth*, **113**.
- Girolami, L., Roche, O., Druitt, T. H. & Corpetti, T. 2010. Particle velocity fields and depositional processes in laboratory ash flows, with implications for the sedimentation of dense pyroclastic flows. *Bulletin of Volcanology*, **72**, 747-759.
- Gladstone, C., Ritchie, L. J., Sparks, R. S. J. & Woods, A. W. 2004. An experimental investigation of density-stratified inertial gravity currents. *Sedimentology*, **51**, 767-789.
- Hargrove, H. R. & Sheridan, M. F. 1984. Welded Tuffs Deformed into Megarhomorphic Folds during Collapse of the Mcdermitt Caldera, Nevada-Oregon. *Journal of Geophysical Research*, **89**, 8629-8638.
- Hayashi, J. N. & Self, S. 1992. A Comparison of Pyroclastic Flow and Debris Avalanche Mobility. *Journal of Geophysical Research-Solid Earth*, **97**, 9063-9071.
- Henry, C. D. & Wolff, J. A. 1992. Distinguishing Strongly Rheomorphic Tuffs from Extensive Silicic Lavas. *Bulletin of Volcanology*, **54**, 171-186.
- Hildreth, W. 1981. Gradients in Silicic Magma Chambers - Implications for Lithospheric Magmatism. *Journal of Geophysical Research*, **86**, 153-192.
- Hoblitt, R. P., Miller, C. D. & Vallance, J. W. 1981. Origin and stratigraphy of the deposit produced by the May 18 directed blast. In: Lipman, P. W. & Mullineaux, D. R. (eds.) *The 1980 eruptions of Mount St. Helens, Washington; U. S. Geological Survey Professional Paper 1250*. U. S. Geological Survey : Reston, VA, United States, United States, 401-419.
- Hoblitt, R. P., Wolfe, E. W., Scott, W. E., Couchman, M. R., Pallister, J. S. & Javier, D. 1996. The preclimactic eruptions of Mount Pinatubo, June 1991. *Fire and mud: Eruptions and Lahars of Mount Pinatubo, Philippines* Philippine Institute of

- Volcanology and Seismology : University of Washington Press, United States, Quezon City, Philippines, 457-511.
- Houghton, B. F., Wilson, C. J. N., Fierstein, J. & Hildreth, W. 2004. Complex proximal deposition during the Plinian eruptions of 1912 at Novarupta, Alaska. *Bulletin of Volcanology*, **66**, 95-133.
- Hughes, S. R. & Druitt, T. H. 1998. Particle fabric in a small, type-2 ignimbrite flow unit (Laacher See, Germany) and implications for emplacement dynamics. *Bulletin of Volcanology*, **60**, 125-136.
- Kamata, H., Suzuki-Kamata, K. & Bacon, C. R. 1993. Deformation of the Wineglass Welded Tuff and the timing of caldera collapse at Crater Lake, Oregon. *Journal of Volcanology and Geothermal Research*, **56**, 253-265.
- Keller, J., Ryan, W. B. F., Ninkovich, D. & Altherr, R. 1978. Explosive Volcanic Activity in Mediterranean over Past 200,000 Yr as Recorded in Deep-Sea Sediments. *Geological Society of America Bulletin*, **89**, 591-604.
- Kneller, B., Edwards, D., Mccaffrey, W. & Moore, R. 1991. Oblique Reflection of Turbidity Currents. *Geology*, **19**, 250-252.
- Kneller, B. C. & Branney, M. J. 1995. Sustained high-density turbidity currents and the deposition of thick massive sands. *Sedimentology*, **42**, 607-616.
- Kobberger, G. & Schmincke, H. U. 1999. Deposition of rheomorphic ignimbrite D (Mogan Formation), Gran Canaria, Canary Islands, Spain. *Bulletin of Volcanology*, **60**, 465-485.
- Korringa, M. K. 1971. Steeply-dipping welded tuff mantling the walls of the Pantelleria Caldera. *Peralkaline Acid Volcanism*. Catania.
- Korringa, M. K. & Noble, D. C. 1972. Genetic significance of chemical, isotopic, and petrographic features of some peralkaline salic rocks from Island of Pantelleria. *Earth and Planetary Science Letters*, **17**, 258-262.
- Kovalenko, V. I., Naumov, V. B., Solovova, I. P., Giris, A. V., Khervig, R. L. & Boriani, A. 1994. Volatile components, composition, and crystallization conditions of the Pantelleria basalt–pantellerite association magmas, inferred from the melt and fluid inclusion data. *Petrology*, **2**, 19-34.
- Kover, T. P. 1995. *Application of a digital terrain model for the modeling of volcanic flows; a tool for volcanic hazard determination*. PhD thesis, SUNY at Buffalo, Buffalo, NY (Master's).
- Kubo, Y. 2004. Experimental and numerical study of topographic effects on deposition from two-dimensional, particle-driven density currents. *Sedimentary Geology*, **164**, 311-326.

- La Felice, S., Rotolo, S. G., Scaillet, S. & Vita, G. 2009. Tephrostratigraphy, petrochemistry and  $^{40}\text{Ar}$ - $^{39}\text{Ar}$  age data on Pre-Green Tuff sequences, Pantelleria. *Congresso Fist Geitalia 2009*, Rimini, 9-11 settembre 2009
- Lagmay, M. A., Pyle, D. M., Dade, B. & Oppenheimer, C. 1999. Control of crater morphology on flow path direction of Soufriere-type pyroclastic flows. *Journal of Geophysical Research-Solid Earth*, **104**, 7169-7181.
- Leat, P. T., Macdonald, R. & Smith, R. L. 1984. Geochemical evolution of the Menengai Caldera Volcano, Kenya. *Journal of Geophysical Research*, **89**, 8571-8592.
- Leat, P. T. & Schmincke, H. U. 1993. Large-Scale Rheomorphic Shear Deformation in Miocene Peralkaline Ignimbrite-E, Gran-Canaria. *Bulletin of Volcanology*, **55**, 155-165.
- Legros, F. & Kelfoun, K. 2000. On the ability of pyroclastic flows to scale topographic obstacles. *Journal of Volcanology and Geothermal Research*, **98**, 235-241.
- Lirer, L., Petrosino, P. & Alberico, I. 2001. Hazard assessment at volcanic fields: the Campi Flegrei case history. *Journal of Volcanology and Geothermal Research*, **112**, 53-73.
- Lowe, D. R. 1982. Sediment gravity flows; II, Depositional models with special reference to the deposits of high-density turbidity currents. *Journal of Sedimentary Petrology*, **52**, 279-297.
- Lowenstein, J. B. 1994. Chlorine, fluid immiscibility and degassing in peralkaline magmas from Pantelleria, Italy. *American Mineralogist*, **79**, 353-369.
- Lowenstein, J. B. 1994. Chlorine, Fluid Immiscibility, and Degassing in Peralkaline Magmas from Pantelleria, Italy. *American Mineralogist*, **79**, 353-369.
- Lowenstein, J. B. & Mahood, G. A. 1991. New Data on Magmatic H<sub>2</sub>O Contents of Pantellerites, with Implications for Petrogenesis and Eruptive Dynamics at Pantelleria. *Bulletin of Volcanology*, **54**, 78-83.
- Lowenstein, J. B., Mahood, G. A., Hervig, R. L. & Sparks, J. 1993. The Occurrence and Distribution of Mo and Molybdenite in Unaltered Peralkaline Rhyolites from Pantelleria, Italy. *Contributions to Mineralogy and Petrology*, **114**, 119-129.
- Macdonald, R. 1974. Nomenclature and petrochemistry of the peralkaline oversaturated extrusive rocks. *Bulletin Volcanologique*, **38**, 498-516.
- Macdonald, R., Navarro, J. M., Upton, B. G. J. & Davies, G. R. 1994. Strong compositional zonation in peralkaline magma - Menengai, Kenya Rift-Valley. *Journal of Volcanology and Geothermal Research*, **60**, 301-325.

- Mahood, G., Halliday, A. N. & Hildreth, W. 1990. Isotopic evidence for the origin of pantellerites in a rift related alkalic suite: Pantelleria, Italy. . *International Volcanological Congress*. Mainz, Germany: IAVCEI Abstracts.
- Mahood, G. & Hildreth, W. 1983. Nested Calderas and Trapdoor Uplift at Pantelleria, Strait of Sicily. *Geology*, **11**, 722-726.
- Mahood, G. A. 1984. Pyroclastic Rocks and Calderas Associated with Strongly Peralkaline Magmatism. *Journal of Geophysical Research*, **89**, 8540-8552.
- Mahood, G. A. & Hildreth, W. 1986. Geology of the peralkaline volcano at Pantelleria, Strait of Sicily. *Bulletin of Volcanology*, **48**, 143-172.
- Malin, M. C. & Sheridan, M. F. 1982. Computer-Assisted Mapping of Pyroclastic Surges. *Science*, **217**, 637-640.
- Margari, V., Pyle, D. M., Bryant, C. & Gibbard, P. L. 2007. Mediterranean tephra stratigraphy revisited; results from a long terrestrial sequence on Lesbos Island, Greece. *Journal of Volcanology and Geothermal Research*, **163**, 34-54.
- Mattia, M., Bonaccorso, A. & Guglielmino, F. 2007. Ground deformations in the Island of Pantelleria (Italy): Insights into the dynamic of the current intereruptive period. *J. Geophys. Res.*, **112**, B11406.
- McCaffrey, W. D., Choux, C. M., Baas, J. H. & Haughton, P. D. W. 2003. Spatio-temporal evolution of velocity structure, concentration and grainsize stratification within experimental particulate gravity currents. *Marine and Petroleum Geology*, **20**, 851-860.
- Middleton, G. V. 1967. Experiments on density and turbidity currents; [Part] 3, Deposition of sediment. *Canadian Jour. Earth Sci.*, **4**, 475-505.
- Miller, T. P. & Smith, R. L. 1977. Spectacular Mobility of Ash Flows around Aniakchak and Fisher Calderas, Alaska. *Geology*, **5**, 173-176.
- Moore, I. & Kokelaar, P. 1998. Tectonically controlled piecemeal caldera collapse: A case study of Glencoe volcano, Scotland. *Geological Society of America Bulletin*, **110**, 1448-1466.
- Muck, M. T. & Underwood, M. B. 1990. Upslope Flow of Turbidity Currents - a Comparison among Field Observations, Theory, and Laboratory Models. *Geology*, **18**, 54-57.
- Nichols, G. 1999. *Sedimentology and stratigraphy*. ed.).Blackwell Science Oxford, United Kingdom,
- Ono, K. & Watanabe, K. 1974. Secondary Flowage in Aso-2 Pyroclastic Flow Deposit around the West Rim of the Aso Caldera, Central Kyushu. *Bulletin of the Volcanological Society of Japan*, **19**, 93-110.

- Orsi, G., Ruvo, L. & Scarpati, C. 1991. The recent explosive volcanism at Pantelleria. *Geologische Rundschau*, **80**, 187-200.
- Orsi, G. & Sheridan, M. F. 1984. The Green Tuff of Pantelleria: Rheoignimbrite or rheomorphic fall? *Bulletin of Volcanology*, **47**, 611-626.
- Pabst, S., Wörner, G., Civetta, L. & Tesoro, R. 2008. Magma chamber evolution prior to the Campanian Ignimbrite and Neapolitan Yellow Tuff eruptions (Campi Flegrei, Italy). *Bulletin of Volcanology*, **70**, 961-976.
- Palladino, D. M. & Simei, S. 2002. Three types of pyroclastic currents and their deposits: examples from the Vulsini Volcanoes, Italy. *Journal of Volcanology and Geothermal Research*, **116**, 97-118.
- Palladino, D. M. & Taddeucci, J. 1998. The basal ash deposit of the Sovana Eruption (Vulsini Volcanoes, central Italy): the product of a dilute pyroclastic density current. *Journal of Volcanology and Geothermal Research*, **87**, 233-254.
- Parello, F., Allard, P., D'Alessandro, W., Federico, C., Jean-Baptiste, P. & Catani, O. 2000. Isotope geochemistry of Pantelleria volcanic fluids, Sicily Channel rift: a mantle volatile end-member for volcanism in southern Europe. *Earth and Planetary Science Letters*, **180**, 325-339.
- Parker, D. & White, J. 2008. Large-scale silicic alkalic magmatism associated with the Buckhorn Caldera, Trans-Pecos Texas, USA: comparison with Pantelleria, Italy. *Bulletin of Volcanology*, **70**, 403-415.
- Passchier, C. W. & Trouw, R. A. J. 2005. *Microtectonics*. ed.).Springer : Berlin, Federal Republic of Germany, Federal Republic of Germany,
- Peterson, D. W. 1979. Significance of the flattening of pumice fragments in ash-flow tuffs. *Special Paper - Geological Society of America*, 195-204.
- Pickering, K. T., Underwood, M. B. & Taira, A. 1992. Open-Ocean to Trench Turbidity-Current Flow in the Nankai Trough - Flow Collapse and Reflection. *Geology*, **20**, 1099-1102.
- Pioli, L. & Rosi, M. 2005. Rheomorphic structures in a high-grade ignimbrite: the Nuraxi tuff, Sulcis volcanic district (SW Sardinia, Italy). *Journal of Volcanology and Geothermal Research*, **142**, 11-28.
- Piper, D. J. W. & Normark, W. R. 1983. Turbidite Depositional Patterns and Flow Characteristics, Navy Submarine Fan, California Borderland. *Sedimentology*, **30**, 681-694.
- Pittari, A., Cas, R. A. F., Edgar, C. J., Nichols, H. J., Wolff, J. A. & Marti, J. 2006. The influence of palaeotopography on facies architecture and pyroclastic flow processes of a lithic-rich ignimbrite in a high gradient setting: The Abrigo Ignimbrite, Tenerife, Canary Islands. *Journal of Volcanology and Geothermal Research*, **152**, 273-315.

- Pittari, A., Cas, R. A. F. & Marti, J. 2005. The occurrence and origin of prominent massive, pumice-rich ignimbrite lobes within the Late Pleistocene Abrigo Ignimbrite, Tenerife, Canary Islands. *Journal of Volcanology and Geothermal Research*, **139**, 271-293.
- Powell, M. & Powell, R. 1974. An Olivine-Clinopyroxene Geothermometer. *Contributions to Mineralogy and Petrology*, **48**, 249-263.
- Powell, R. & Powell, M. 1977. Geothermometry and oxygen barometry using coexisting iron-titanium oxides; a reappraisal. *Mineralogical Magazine and Journal of the Mineralogical Society*, **41**, 257-263.
- Quane, S. L. & Russell, J. K. 2005. Welding: insights from high-temperature analogue experiments. *Journal of Volcanology and Geothermal Research*, **142**, 67-87.
- Ragan, D. M. & Sheridan, M. F. 1972. Compaction of Bishop Tuff, California. *Geological Society of America Bulletin*, **83**, 95-&.
- Riehle, J. R. 1973. Calculated Compaction Profiles of Rhyolitic Ash-Flow Tuffs. *Geological Society of America Bulletin*, **84**, 2193-2216.
- Rivas, D., Fuentes, O. U. V. & Ochoa, J. 2005. Topographic effects on the dynamics of gravity currents in a rotating system. *Dynamics of Atmospheres and Oceans*, **39**, 227-249.
- Roche, O., Gilbertson, M. A., Phillips, J. C. & Sparks, R. S. J. 2004. Experimental study of gas-fluidized granular flows with implications for pyroclastic flow emplacement. *Journal of Geophysical Research-Solid Earth*, **109**.
- Roche, O., Gilbertson, M. A., Phillips, J. C. & Sparks, R. S. J. 2005. Inviscid behaviour of fines-rich pyroclastic flows inferred from experiments on gas-particle mixtures. *Earth and Planetary Science Letters*, **240**, 401-414.
- Roche, O., Montserrat, S., Nino, Y. & Tamburrino, A. 2008. Experimental observations of water-like behavior of initially fluidized, dam break granular flows and their relevance for the propagation of ash-rich pyroclastic flows. *Journal of Geophysical Research-Solid Earth*, **113**.
- Rollinson, H. R. 1993. *Using geochemical data; evaluation, presentation, interpretation*. ed.). Longman Scientific & Technical :, Harlow, United Kingdom,
- Ross, C. S. & Smith, R. L. 1961. Ash-flow tuffs; their origin, geologic relations, and identification. *U. S. Geological Survey Professional Paper*.
- Rotolo, S. G., La Felice, S., Mangalaviti, A. & Landi, P. 2007. Geology and petrochemistry of the recent (< 25 ka) silicic volcanism at Pantelleria Island. *Bollettino Della Societa Geologica Italiana*, **126**, 191-208.

- Rowley, P. J., Waltham, D., Menzies, M., Kokelaar, P. 2010. Ignimbrite reworking: experimental and field observations of remobilisation, shear instabilities and recumbent flames. *VMSG Glasgow*.
- Russell, J. K., Giordano, D. & Dingwell, D. B. 2003. High-temperature limits on viscosity of non-Arrhenian silicate melts. *American Mineralogist*, **88**, 1390-1394.
- Russell, J. K. & Quane, S. L. 2005. Rheology of welding: inversion of field constraints. *Journal of Volcanology and Geothermal Research*, **142**, 173-191.
- Scaillet, B. & Macdonald, R. A. Y. 2003. Experimental Constraints on the Relationships between Peralkaline Rhyolites of the Kenya Rift Valley. *J. Petrology*, **44**, 1867-1894.
- Schmincke, H. 1974. Volcanological aspects of peralkaline silicic welded ash-flow tuffs. *Bulletin of Volcanology*, **38**, 594-636.
- Schmincke, H. U. & Swanson, D. A. 1967. Laminar viscous flowage structures in ash-flow tuffs from Gran Canaria, Canary islands. *Journal of Geology*, **75**, 641-664.
- Schumacher, R. & Schmincke, H. U. 1990. The Lateral Facies of Ignimbrites at Laacher See Volcano. *Bulletin of Volcanology*, **52**, 271-285.
- Self, S., Goff, F., Gardner, J. N., Wright, J. V. & Kite, W. M. 1986. Explosive Rhyolitic Volcanism in the Jemez Mountains - Vent Locations, Caldera Development and Relation to Regional Structure. *Journal of Geophysical Research-Solid Earth and Planets*, **91**, 1779-1798.
- Sheridan, M. F. 1979. Emplacement of pyroclastic flows: A review. *In: Chapin & Elston (eds.) Ash-flow tuffs. Geol. Soc. Am., Special Papers*, **180**, 125-136.
- Sheridan, M. F. & Malin, M. C. 1983. Application of Computer-Assisted Mapping to Volcanic Hazard Evaluation of Surge Eruptions - Vulcano, Lipari, and Vesuvius. *Journal of Volcanology and Geothermal Research*, **17**, 187-202.
- Sheridan, M. F., Stinton, A. J., Patra, A., Pitman, E. B., Bauer, A. & Nichita, C. C. 2005. Evaluating Titan2D mass-flow model using the 1963 Little Tahoma Peak avalanches, Mount Rainier, Washington. *Journal of Volcanology and Geothermal Research*, **139**, 89-102.
- Sheridan, M. F. a. R. D. M. 1976. Compaction of Ash-Flow Tuffs. *In: K.H., C. G. V. a. W. (ed.) Compaction of coarse-grained sediments. Elsevier Scientific Pub. Co., , Amsterdam ; New York*.
- Smith, R. L. 1960. Ash flows. *Geological Society of America Bulletin*, **71**, 795-841.
- Southard, J. B. 2006. *An Introduction to Fluid Motions, Sediment Transport, and Current-Generated Sedimentary Structures*. ed.).Massachusetts Institute of Technology, Cambridge, Massachusetts, 552.

- Sparks, R. S. J. 1976. Grain-Size Variations in Ignimbrites and Implications for Transport of Pyroclastic Flows. *Sedimentology*, **23**, 147-188.
- Sparks, R. S. J., Bursik, M. I., Carey, S. N., Gilbert, J. S., Glaze, L. S., Sigurdsson, H. & Woods, A. W. 1997. *Volcanic plumes*. ed.) John Wiley and Sons : , Chichester, United Kingdom,
- Sparks, R. S. J., Self, S. & Walker, G. P. L. 1973. Products of Ignimbrite Eruptions. *Geology*, **1**, 115-118.
- Steven, T. A. & Lipman, P. W. 1976. Calderas of the San Juan volcanic field, southwestern Colorado. *U. S. Geological Survey Professional Paper*.
- Stevenson, R. J. & Wilson, L. 1997. Physical volcanology and eruption dynamics of peralkaline agglutinates from Pantelleria. *Journal of Volcanology and Geothermal Research*, **79**, 97-122.
- Storey, M., Wolff, J. A., Norry, M. J. & Marriner, G. F. 1989. Origin of hybrid lavas from Agua de Pau volcano, Sao Miguel, Azores. *Geological Society, London, Special Publications*, **42**, 161-180.
- Straub, S. 1996. Self-organization in the rapid flow of granular material: evidence for a major flow mechanism. *Geologische Rundschau*, **85**, 85-91.
- Sulpizio, R., De Rosa, R. & Donato, P. 2008. The influence of variable topography on the depositional behaviour of pyroclastic density currents: The examples of the Upper Pollara eruption (Salina Island, southern Italy). *Journal of Volcanology and Geothermal Research*, **175**, 367-385.
- Sulpizio, R., Dellino, P., Joachim, G. & Joan, M. 2008. Chapter 2 Sedimentology, Depositional Mechanisms and Pulsating Behaviour of Pyroclastic Density Currents. *Developments in Volcanology*. Volume 10 ed. Elsevier, 57-96.
- Sulpizio, R., Dellino, P., Mele, D. & La Volpe, L. 2008. Generation of pyroclastic density currents from pyroclastic fountaining or transient explosions: insights from large scale experiments. *Collapse Calderas Workshop*. IOP Publishing.
- Sumner, E. J., Amy, L. A. & Talling, P. J. 2008. Deposit structure and processes of sand deposition from decelerating sediment suspensions. *Journal of Sedimentary Research*, **78**, 529-547.
- Sumner, J. M. & Branney, M. J. 2002. The emplacement history of a remarkable heterogeneous, chemically zoned, rheomorphic and locally lava-like ignimbrite: 'TL' on Gran Canaria. *Journal of Volcanology and Geothermal Research*, **115**, 109-138.
- Suzuki, K. & Ui, T. 1982. Grain-Orientation and Depositional Ramps as Flow Direction Indicators of a Large-Scale Pyroclastic Flow Deposit in Japan. *Geology*, **10**, 429-432.

- Suzuki, K. & Ui, T. 1983. Factors governing the flow lineation of a large-scale pyroclastic flow; an example in the Ata pyroclastic flow deposit, Japan. *Bulletin Volcanologique*, **46**, 71-81.
- Tanguy, J. C., Ribiere, C., Scarth, A. & Tjetjep, W. S. 1998. Victims from volcanic eruptions: a revised database. *Bulletin of Volcanology*, **60**, 137-144.
- Troll, V. R. & Schmincke, H. U. 2002. Magma mixing and crustal recycling recorded in ternary feldspar from compositionally zoned peralkaline Ignimbrite 'A', Gran Canaria, Canary Islands. *Journal of Petrology*, **43**, 243-270.
- Trua, T., Deniel, C. & Mazzuoli, R. 1999. Crustal control in the genesis of Plio-Quaternary bimodal magmatism of the Main Ethiopian Rift (MER): geochemical and isotopic (Sr, Nd, Pb) evidence. *Chemical Geology*, **155**, 201-231.
- Turner, J. S. 1966. Jets and plumes with negative or reversing buoyancy. *Journal of Fluid Mechanics*, **26**, 779-792.
- Ui, T., Suzukikamata, K., Matsusue, R., Fujita, K., Metsugi, H. & Araki, M. 1989. Flow Behavior of Large-Scale Pyroclastic Flows - Evidence Obtained from Petrofabric Analysis. *Bulletin of Volcanology*, **51**, 115-122.
- Valentine, G. A. 1987. Stratified flow in pyroclastic surges. *Bulletin of Volcanology*, **49**, 616-630.
- Valentine, G. A. & Giannetti, B. 1995. Single pyroclastic beds deposited by simultaneous fallout and surge processes; Roccamonfina Volcano, Italy. *Journal of Volcanology and Geothermal Research*, **64**, 129-137.
- Valentine, G. A. & Wohletz, K. H. 1989. Environmental Hazards of Pyroclastic Flows Determined by Numerical-Models. *Geology*, **17**, 641-644.
- Valentine, G. A. & Wohletz, K. H. 1989. Numerical-Models of Plinian Eruption Columns and Pyroclastic Flows. *Journal of Geophysical Research-Solid Earth and Planets*, **94**, 1867-1887.
- Valentine, G. A., Wohletz, K. H. & Kieffer, S. W. 1992. Effects of Topography on Facies and Compositional Zonation in Caldera-Related Ignimbrites. *Geological Society of America Bulletin*, **104**, 154-165.
- van Achterbergh, E., Ryan, C. G., Jackson, S. E. & Griffin, W. L. 2001. Data reduction software for LA-ICP-MS. *Short Course Handbook*, **29**, 239-243.
- Villari, L. 1970. On particular ignimbrites of the island of Pantelleria (channel of Sicily). *Bulletin of Volcanology*, **33**, 828-839.
- Villari, L. 1974. The island of Pantelleria. *Bulletin Volcanologique*, **38**, 680-724.
- Vrolijk, P. J. & Southard, J. B. 1997. Experiments on rapid deposition of sand from high-velocity flows. *Geoscience Canada*, **24**, 45-54.

- Wadge, G., Jackson, P., Bower, S. M., Woods, A. W. & Calder, E. 1998. Computer simulations of pyroclastic flows from dome collapse. *Geophysical Research Letters*, **25**, 3677-3680.
- Walker, G. P. L. 1971. Grain-size characteristics of pyroclastic deposits. *Journal of Geology*, **79**, 696-714.
- Walker, G. P. L. 1983. Ignimbrite types and ignimbrite problems. *Journal of Volcanology and Geothermal Research*, **17**, 65-88.
- Walker, G. P. L. 1985. Origin of coarse lithic breccias near ignimbrite source vents. *Journal of Volcanology and Geothermal Research*, **25**, 157-171.
- Walker, G. P. L., Hayashi, J. N. & Self, S. 1995. Travel of Pyroclastic Flows as Transient Waves - Implications for the Energy Line Concept and Particle-Concentration Assessment. *Journal of Volcanology and Geothermal Research*, **66**, 265-282.
- Walker, G. P. L., Heming, R. F. & Wilson, C. J. N. 1980. Low-Aspect Ratio Ignimbrites. *Nature*, **283**, 286-287.
- Walker, G. P. L., Self, S. & Froggatt, P. C. 1981. The ground layer of the Taupo ignimbrite; a striking example of sedimentation from a pyroclastic flow. *Journal of Volcanology and Geothermal Research*, **10**, 1-11.
- Walker, G. P. L., Wilson, C. J. N. & Froggatt, P. C. 1981. An Ignimbrite Veneer Deposit - the Trail-Marker of a Pyroclastic Flow. *Journal of Volcanology and Geothermal Research*, **9**, 409-421.
- Wallace, A. B., Drexler, J. W., Grant, N. K. & Noble, D. C. 1980. Icelandite and Aenigmatite-Bearing Pantellerite from the Mcdermitt Caldera Complex, Nevada-Oregon. *Geology*, **8**, 380-384.
- Washington, H. S. 1909. Submarine eruptions of 1831 and 1891 near Pantelleria. *American Journal of Science*, **s4-27**, 131-150.
- Washington, H. S. 1913-1914. The volcanoes and rocks of Pantelleria: I, II and III. *Journal of Geology*, **21-22**, 653-670, 683-713, 22: 16-27.
- Watanabe, K., Ono, K. & Okumura, K. 1983. Pull-apart structures and squeeze-out of essential lens found in the Aso pyroclastic flow deposits, Japan. *Bulletin of the Volcanological Society of Japan*, **28**, 87-99.
- Webster, J., Taylor, R. P. & Bean, C. 1993. Pre-eruptive melt composition and constraints on degassing of a water-rich pantellerite magma, Fantale volcano, Ethiopia *Contributions to Mineralogy and Petrology*, **114**.

- White, J. C., Parker, D. F. & Ren, M. 2009. The origin of trachyte and pantellerite from Pantelleria, Italy: Insights from major element, trace element, and thermodynamic modelling. *Journal of Volcanology and Geothermal Research*, **179**, 33-55.
- Wilson, C. J. N. 1985. The Taupo Eruption, New-Zealand .2. The Taupo Ignimbrite. *Philosophical Transactions of the Royal Society of London Series a-Mathematical Physical and Engineering Sciences*, **314**, 229.
- Wilson, C. J. N. 1997. Emplacement of Taupo ignimbrite. *Nature*, **385**, 306-307.
- Wilson, C. J. N. & Hildreth, W. 1997. The Bishop Tuff: New insights from eruptive stratigraphy. *Journal of Geology*, **105**, 407-439.
- Wilson, C. J. N. & Hildreth, W. 1998. Hybrid fall deposits in the Bishop Tuff, California: A novel pyroclastic depositional mechanism. *Geology*, **26**, 7-10.
- Wilson, C. J. N. & Hildreth, W. 2003. Assembling an ignimbrite: Mechanical and thermal building blocks in the Bishop Tuff, California. *Journal of Geology*, **111**, 653-670.
- Wilson, C. J. N., Houghton, B. F., Kamp, P. J. J. & McWilliams, M. O. 1995. An Exceptionally Widespread Ignimbrite with Implications for Pyroclastic Flow Emplacement. *Nature*, **378**, 605-607.
- Wilson, C. J. N. & Walker, G. P. L. 1982. Ignimbrite Depositional Facies - the Anatomy of a Pyroclastic Flow. *Journal of the Geological Society*, **139**, 581-592.
- Wilson, C. J. N. & Walker, G. P. L. 1985. The Taupo Eruption, New-Zealand .1. General-Aspects. *Philosophical Transactions of the Royal Society of London Series a-Mathematical Physical and Engineering Sciences*, **314**, 199.
- Wolff, J. A. & Wright, J. V. 1981. Formation of the green tuff, Pantelleria. *Bulletin Volcanologique*, **44**, 681-690.
- Wolff, J. A. & Wright, J. V. 1981. Rheomorphism of welded tuffs. *Journal of Volcanology and Geothermal Research*, **10**, 13-34.
- Woods, A. W., Bursik, M. I. & Kurbatov, A. V. 1998. The interaction of ash flows with ridges. *Bulletin of Volcanology*, **60**, 38-51.
- Woods, A. W. & Caulfield, C. C. P. 1992. A Laboratory Study of Explosive Volcanic-Eruptions. *Journal of Geophysical Research-Solid Earth*, **97**, 6699-6712.
- Wright, J. V. 1980. Stratigraphy and geology of the welded air-fall tuffs of Pantelleria, Italy. *Geologische Rundschau*, **69**, 263-291.
- Wright, J. V., Self, S. & Fisher, R. V. 1981. Towards a facies model for ignimbrite-forming eruptions *NATO advanced study institutes series; Series C, Mathematical and physical sciences*, 433-439.

- Wright, J. V. & Walker, G. P. L. 1981. Eruption, Transport and Deposition of Ignimbrite - a Case-Study from Mexico. *Journal of Volcanology and Geothermal Research*, **9**, 111-131.
- Yokoyama, S. 1974. *Mode of Movement and Emplacement of Ito Pyroclastic Flow from Aira Caldera, Japan*. University of Tsukuba, Institute of Geoscience : Ibaraki, Japan, Japan, 17-62.